IN-07
9983
P-198

NASA Contractor Report 189106 - VOL-II

Stratified Charge Rotary Engine Critical Technology Enablement
Volume II - Appendixes

C.E. Irion and R.E. Mount
Rotary Power International, Inc.
Wood-Ridge, New Jersey

(NASA-CR-189106-Vol-2) STRATIFIED CHARGE ROTARY ENGINE CRITICAL TECHNOLOGY ENABLEMENT. VOLUME 2: APPENDIXES Final Report (Rotary Power International) 198 p
N94-34233
Unclas
G3/07 0009983

August 1992

Prepared for
Lewis Research Center
Under Contract NAS3-25945

National Aeronautics and
Space Administration

Table of Contents

APPENDIX A: NEW IMPROVED COMPUTATIONAL FLUID DYNAMICS (CFD) CODES/DETAILED ILLUSTRATIONS

APPENDIX B: FEASIBILITY ANALYSIS-ROTATING VALVE HIGH PRESSURE COMMON RAIL SYSTEM

APPENDIX C: TURBOMACHINERY SYSTEM ANALYSIS FOR STRATIFIED CHARGE ROTARY ENGINE CRITICAL TECHNOLOGY ENABLEMENT; REPORT NO. AER 3485, SUNDSTRAND AEROSPACE CORPORATION, 4 OCTOBER 91

APPENDIX A

NEW/IMPROVED COMPUTATIONAL FLUID DYNAMICS (CFD) CODES

DETAILED ILLUSTRATIONS

(Refer to Volume I, NASA CR 189106 for Supporting Text)

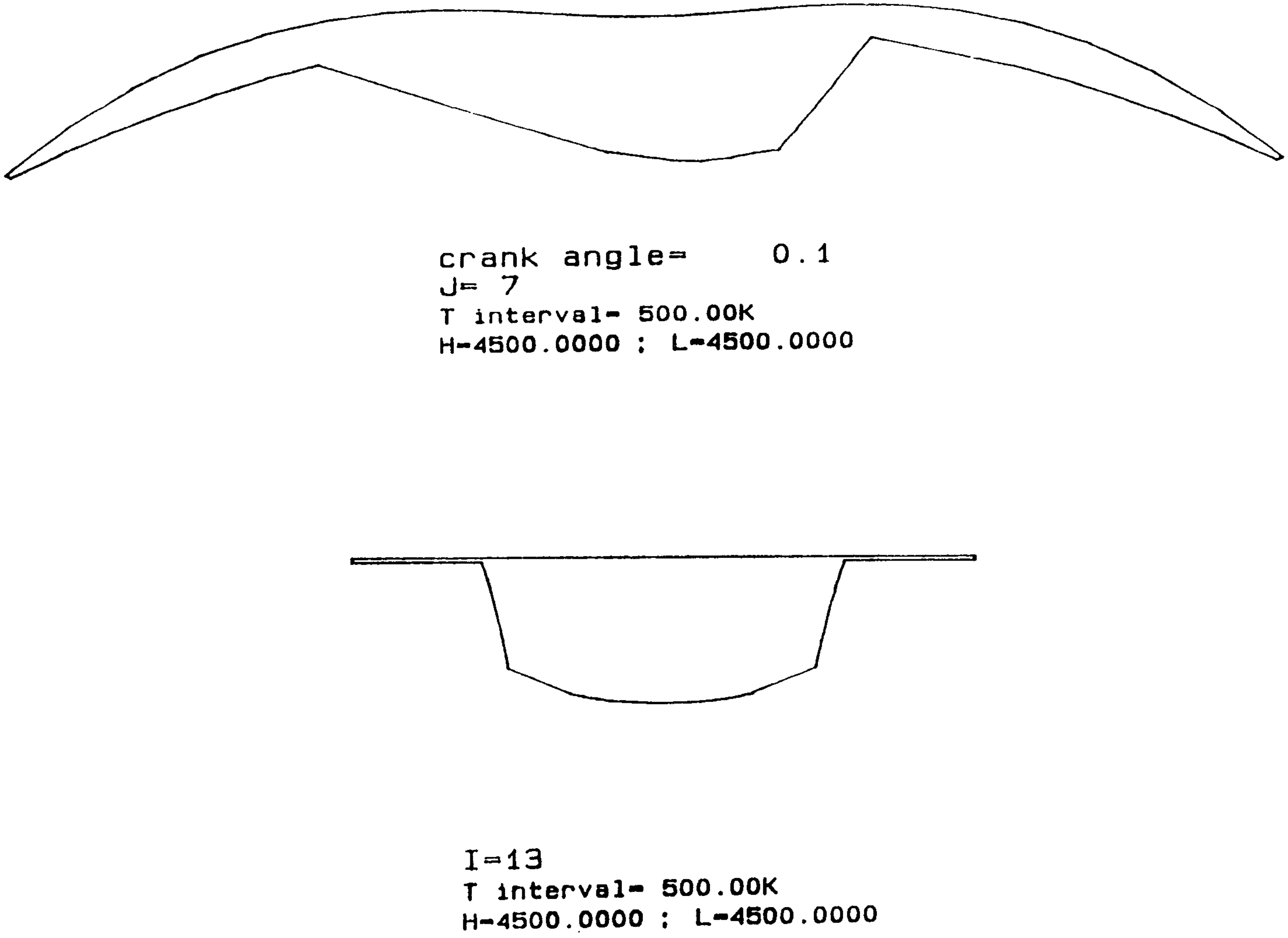
crank angle= 0.1
J= 7
T interval= 500.00K
H=4500.0000 ; L=4500.0000
I=13
T interval= 500.00K
H=4500.0000 ; L=4500.0000

Fig.1 (a) Cross-sections of standard pocket geometry

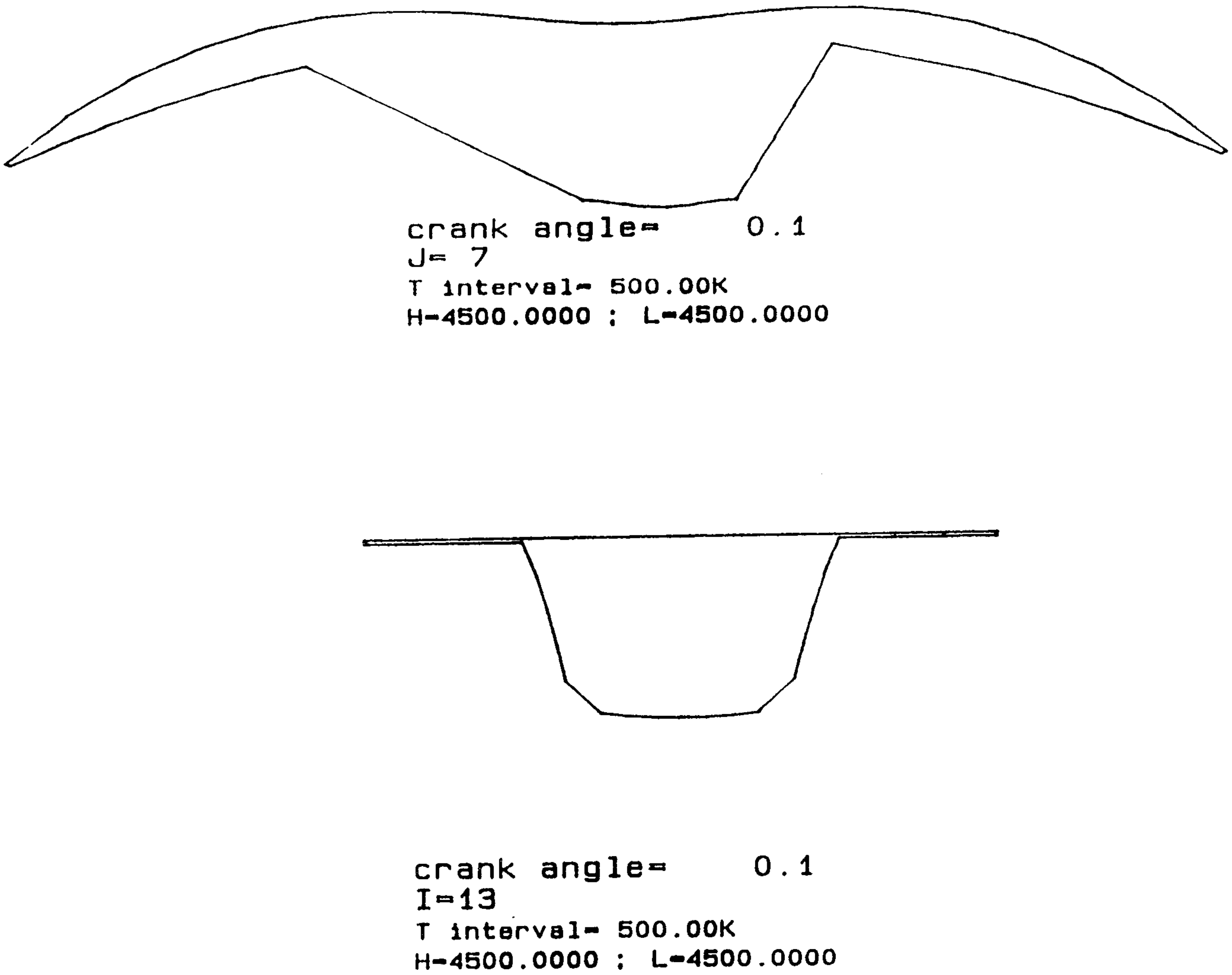
crank angle= 0.1
J= 7
T interval= 500.00K
H=4500.0000 ; L=4500.0000
crank angle= 0.1
I=13
T interval= 500.00K
H=4500.0000 ; L=4500.0000

Fig.1 (b) Cross-sections of deep pocket geometry

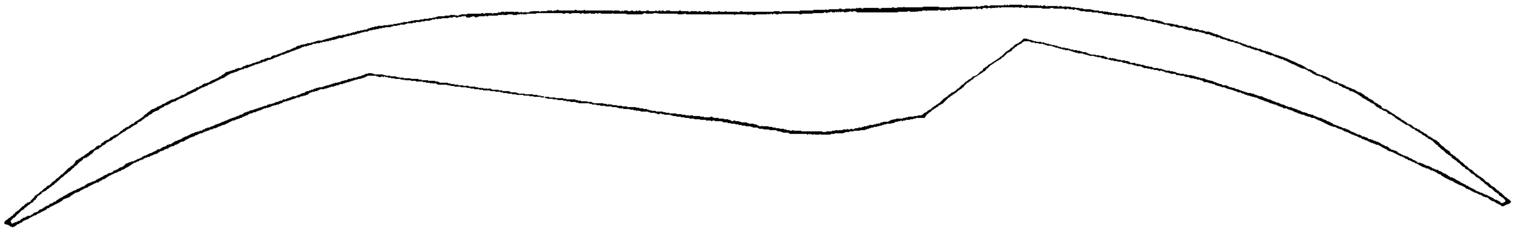

crank angle= 0.1
J= 7
T interval= 500.00K
H=4500.0000 ; L=4500.0000

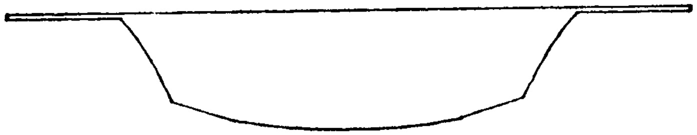

crank angle= 0.1
I=13
T interval= 500.00K
H=4500.0000 ; L=4500.0000

Fig.1 (c) Cross-sections of shallow pocket geometry

Fig.2 Computed pressure as a function of crank angle for the pockets of varying depths

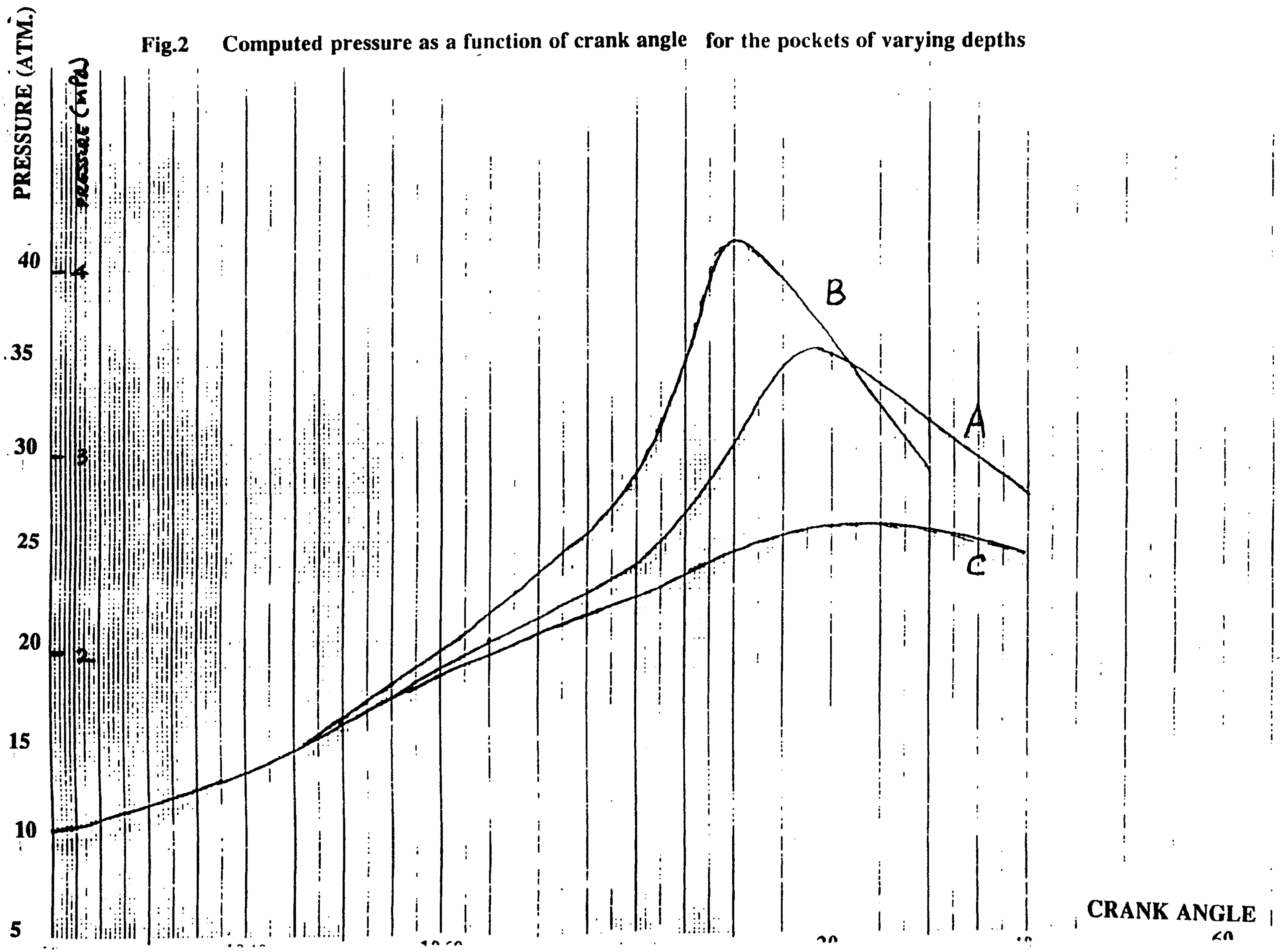

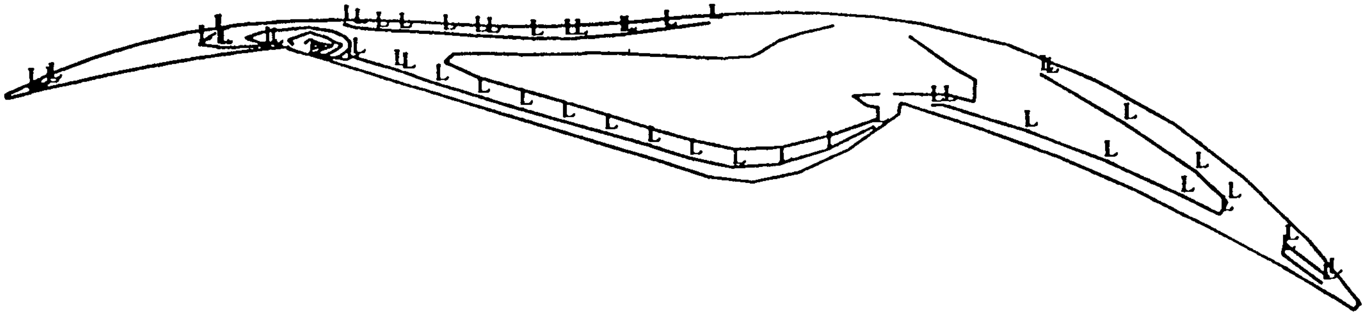

DIFFUSIVITY, interval = 20.00 cm2/s
H = 200.0 ; L = 20.00
J = 7
crank angle = 1140.0

Fig. 3(a): Cross-section of combustion chamber along symmetry plane showing diffusivity contours at 1140 CA. for standard pocket rotor.

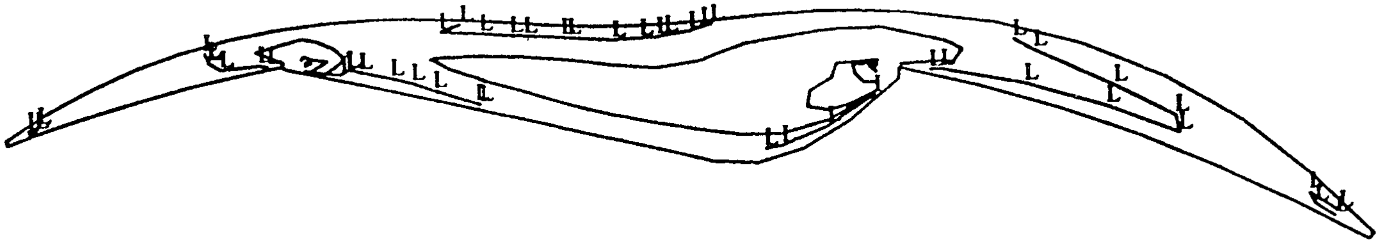

DIFFUSIVITY, interval = 20.00 cm2/s
H = 200.0 ; L = 20.00
J = 7
crank angle = 1155.0

Fig. 3(b): Cross-section of combustion chamber along symmetry plane showing diffusivity contours at 1155 CA. for standard pocket rotor.

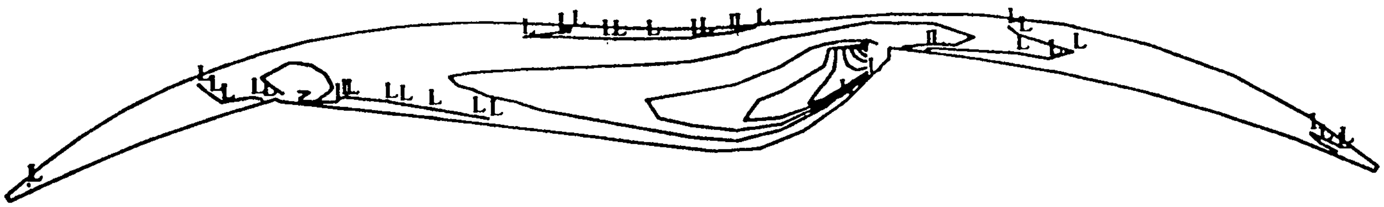

DIFFUSIVITY, interval = 20.00 cm2/s
H = 200.0 ; L = 20.00
J = 7
crank angle = 1170.0

Fig. 3(c): Cross-section of combustion chamber along symmetry plane showing diffusivity contours at 1170 CA. for standard pocket rotor.

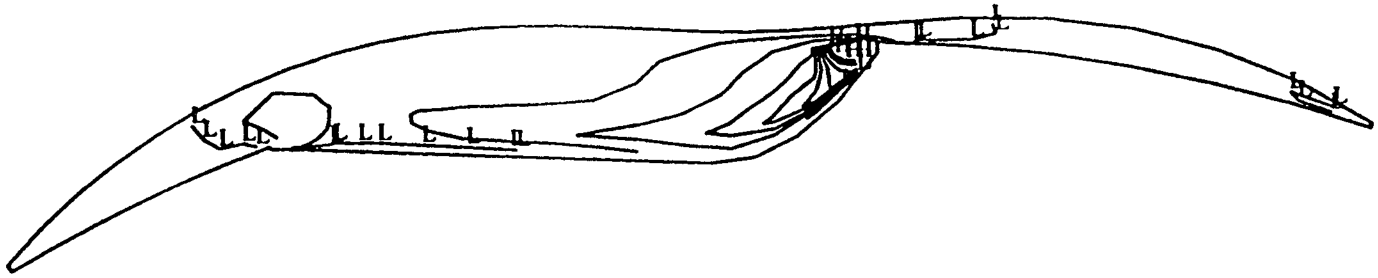

DIFFUSIVITY, interval = 20.00 cm2/s
H = 200.0 ; L = 20.00
J = 7
crank angle = 1185.0

Fig. 3(d): Cross-section of combustion chamber along symmetry plane showing diffusivity contours at 1185 CA. for standard pocket rotor.

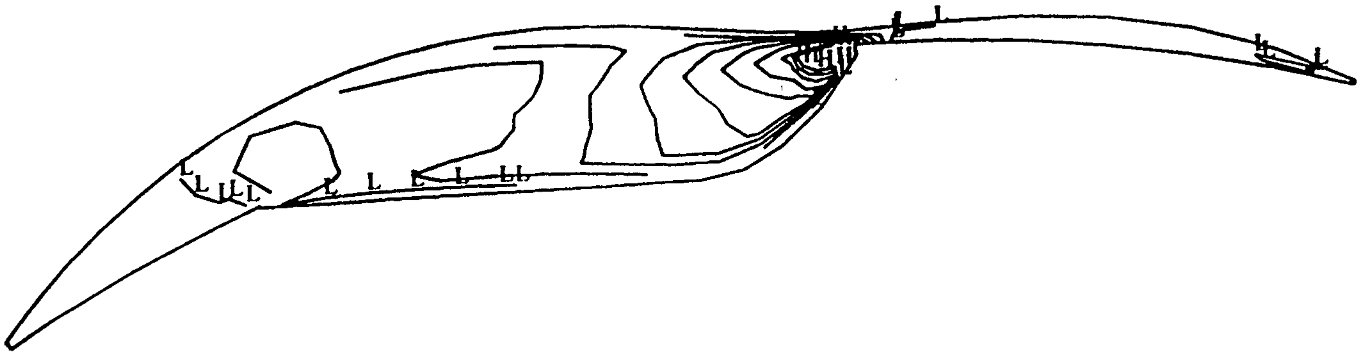

DIFFUSIVITY, interval = 20.00 cm2/s

H = 200.0 ; L = 20.00

J = 7

crank angle = 1200.0

Fig. 3(e): Cross-section of combustion chamber along symmetry plane showing diffusivity contours at 1200 CA. for standard pocket rotor.

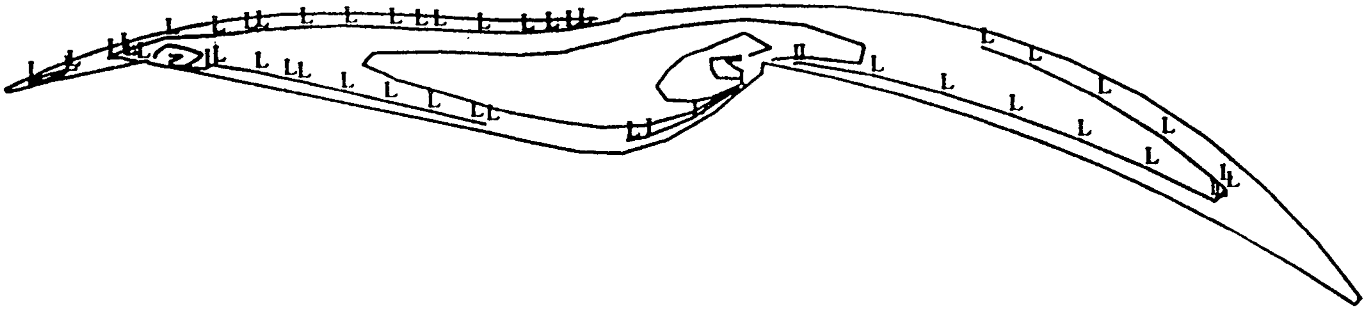

DIFFUSIVITY, interval = 20.00 cm2/s
H = 200.0 ; L = 20.00
J = 7
crank angle = 1140.0

Fig. 4(a): Cross-section of combustion chamber along symmetry plane showing diffusivity contours at 1140 CA. for leading pocket rotor.

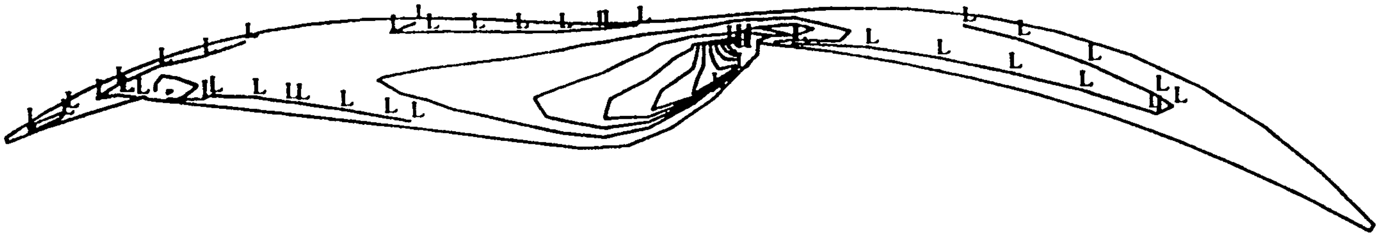

DIFFUSIVITY, interval = 20.00 cm2/s
H = 200.0 ; L = 20.00
J = 7
crank angle = 1155.0

Fig. 4(b): Cross-section of combustion chamber along symmetry plane showing diffusivity contours at 1155° CA. for leading pocket rotor.

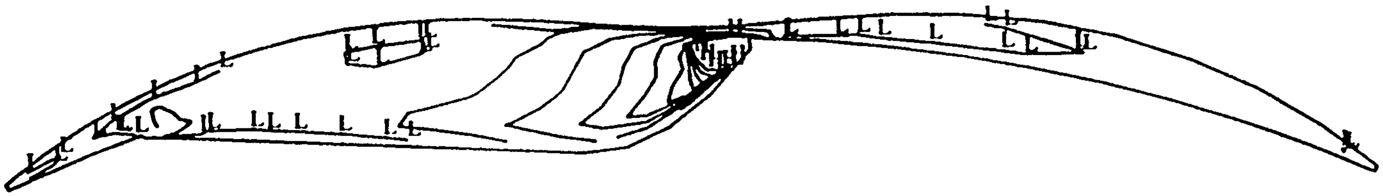

DIFFUSIVITY, interval = 20.00 cm2/s
H = 200.0 ; L = 20.00
J = 7
crank angle = 1170.0

Fig. 4(c): Cross-section of combustion chamber along symmetry plane showing diffusivity contours at 1170 CA. for leading pocket rotor.

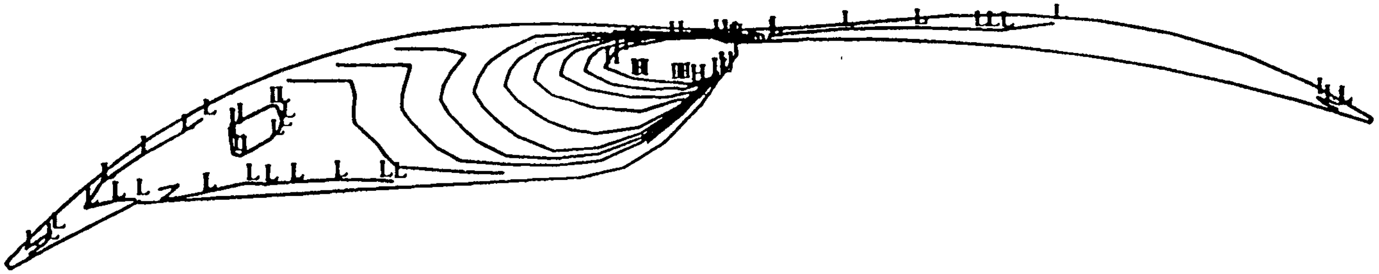

DIFFUSIVITY, interval = 20.00 cm2/s
H = 200.0 ; L = 20.00
J = 7
crank angle = 1185.0

Fig. 4(d): Cross-section of combustion chamber along symmetry plane showing diffusivity contours at 1185 CA. for leading pocket rotor.

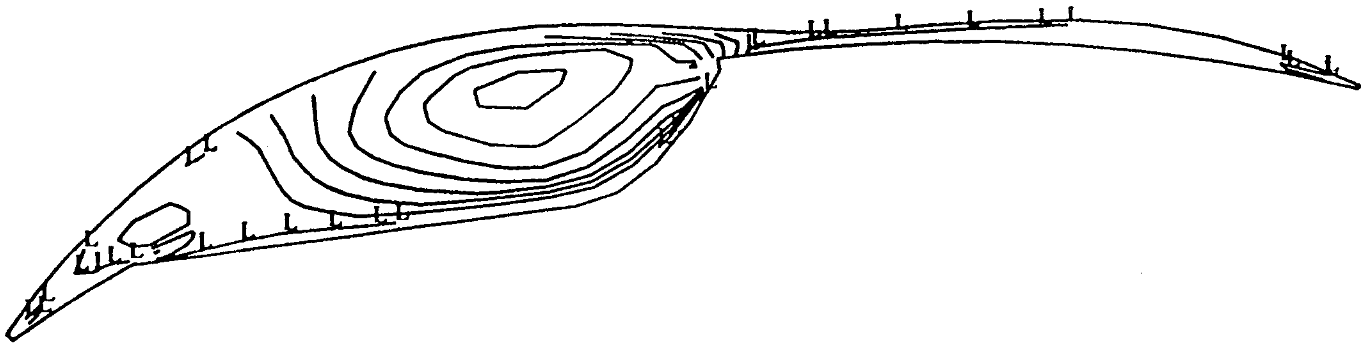

DIFFUSIVITY, interval = 20.00 cm2/s
H = 200.0 ; L = 20.00
J = 7
crank angle = 1200.0

Fig. 4(e): Cross-section of combustion chamber along symmetry plane showing diffusivity contours at 1200 CA. for leading pocket rotor.

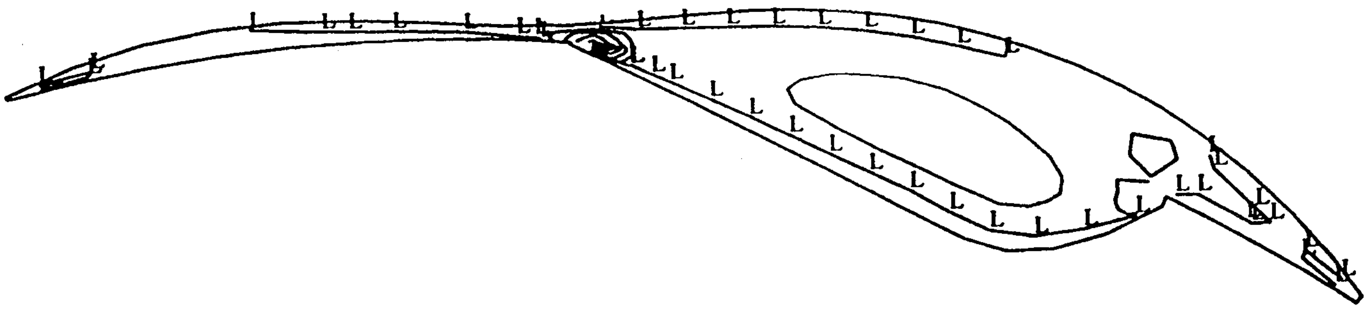

DIFFUSIVITY, interval = 20.00 cm2/s
H = 200.0 ; L = 20.00
J = 7
crank angle = 1140.0

Fig. 5(a): Cross-section of combustion chamber along symmetry plane showing diffusivity contours at 1140 CA. for trailing pocket rotor.

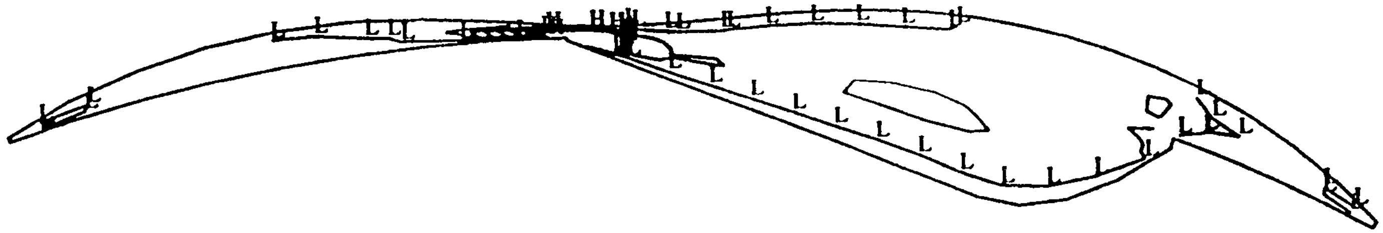

DIFFUSIVITY, interval = 20.00 cm2/s
H = 200.0 ; L = 20.00
J = 7
crank angle = 1155.0

Fig. 5(b): Cross-section of combustion chamber along symmetry plane showing diffusivity contours at 1155 CA. for trailing pocket rotor.

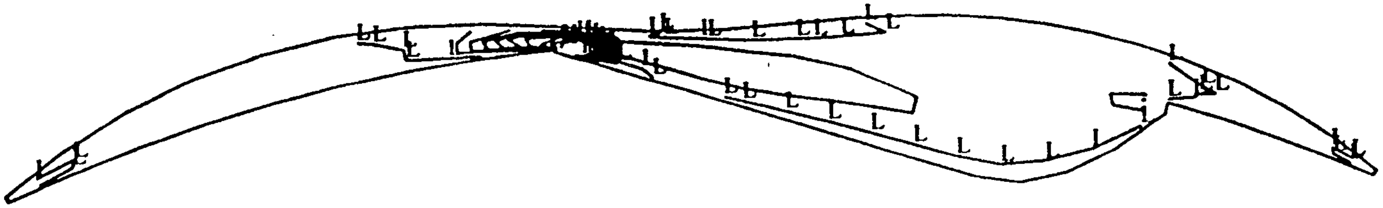

Fig. 5(c): Cross-section of combustion chamber along symmetry plane showing diffusivity contours at 1170 CA. for trailing pocket rotor.

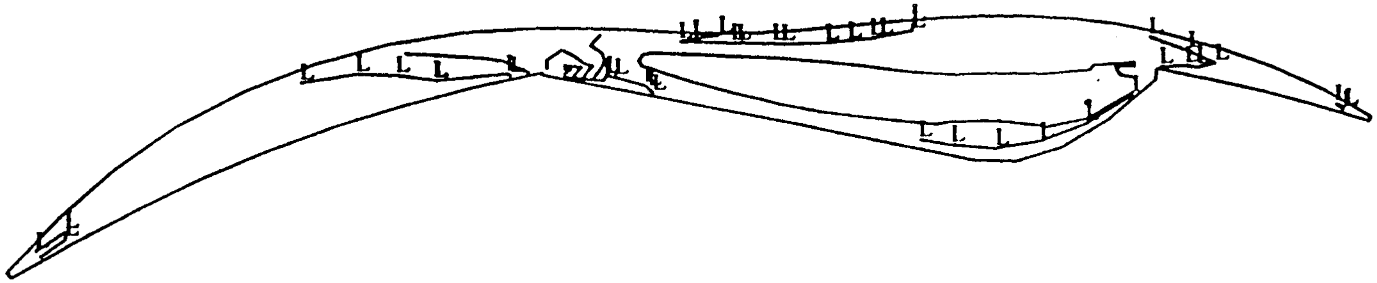

DIFFUSIVITY, interval = 20.00 cm2/s
H = 200.0 ; L = 20.00
J = 7
crank angle = 1185.0

Fig. 5(d): Cross-section of combustion chamber along symmetry plane showing diffusivity contours at 1185 CA. for trailing pocket rotor.

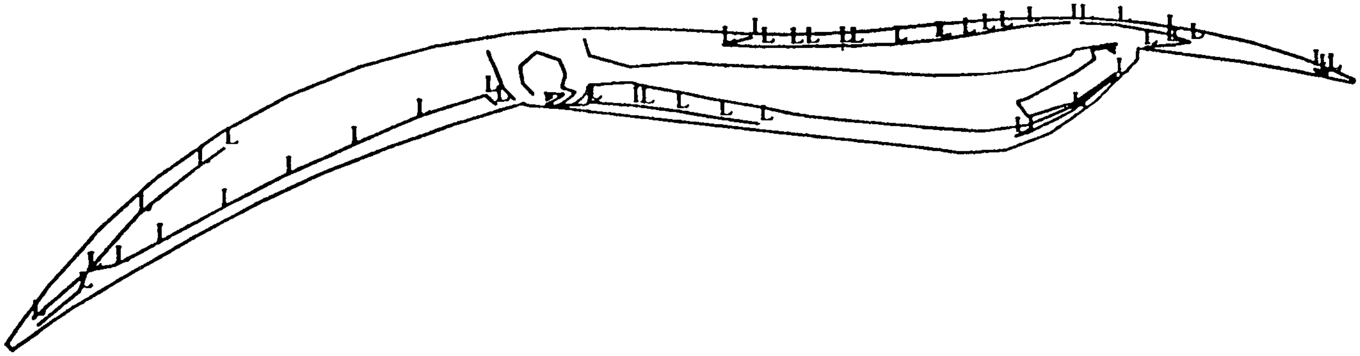

DIFFUSIVITY, interval = 20.00 cm2/s
H = 200.0 ; L = 20.00
J = 7
crank angle = 1200.0

Fig. 5(e): Cross-section of combustion chamber along symmetry plane showing diffusivity contours at 1200 CA. for trailing pocket rotor.

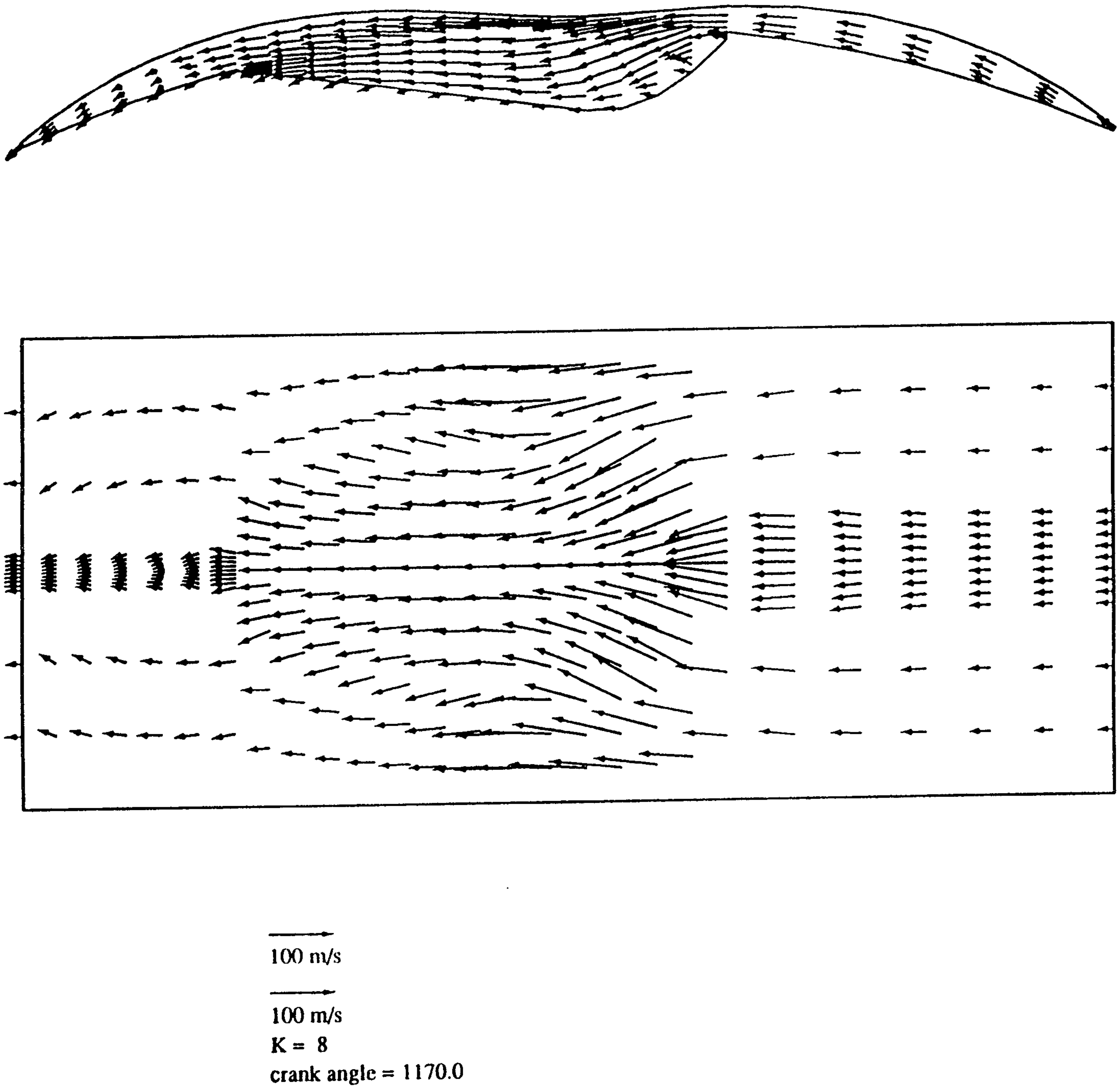

Fig. 3(f): Top view and cross-section view of combustion chamber along symmetry plane showing velocity vectors at 1170 CA. for standard pocket rotor.

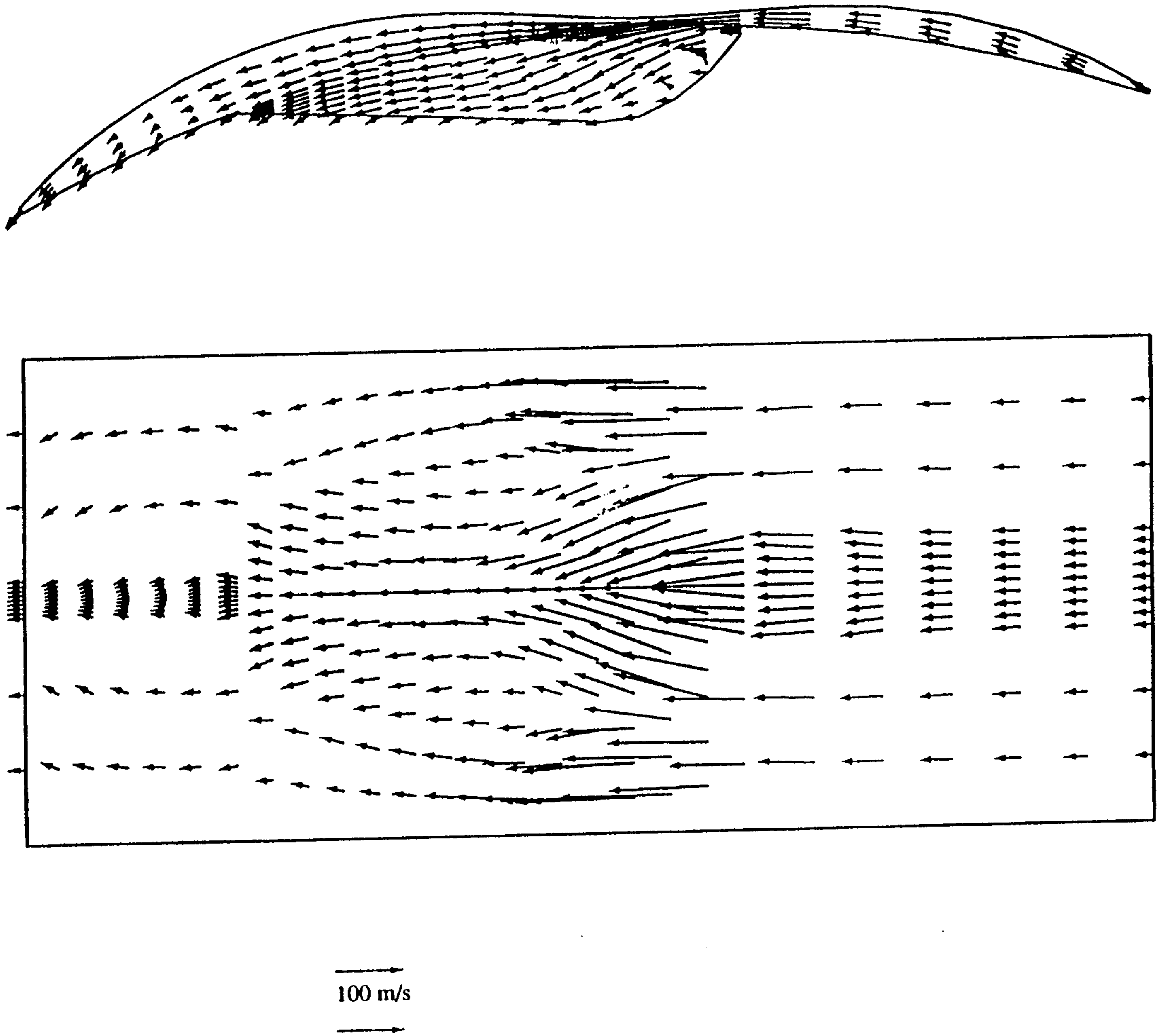

Fig. 3(g): Top view and cross-section view of combustion chamber along symmetry plane showing velocity vectors at 1185 CA. for standard pocket rotor.

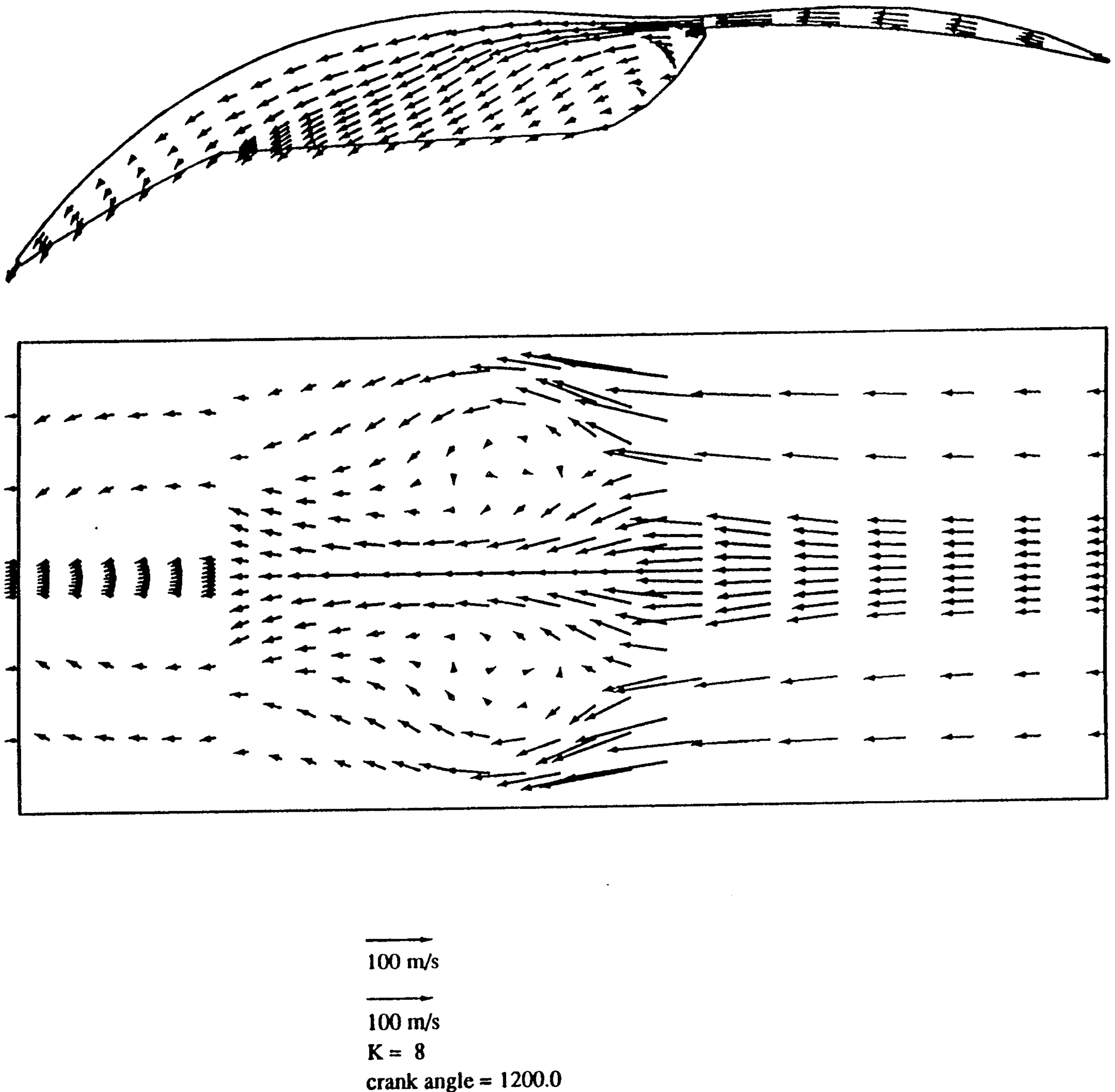

Fig. 3(h): Top view and cross-section view of combustion chamber along symmetry plane showing velocity vectors at 1200 CA. for standard pocket rotor.

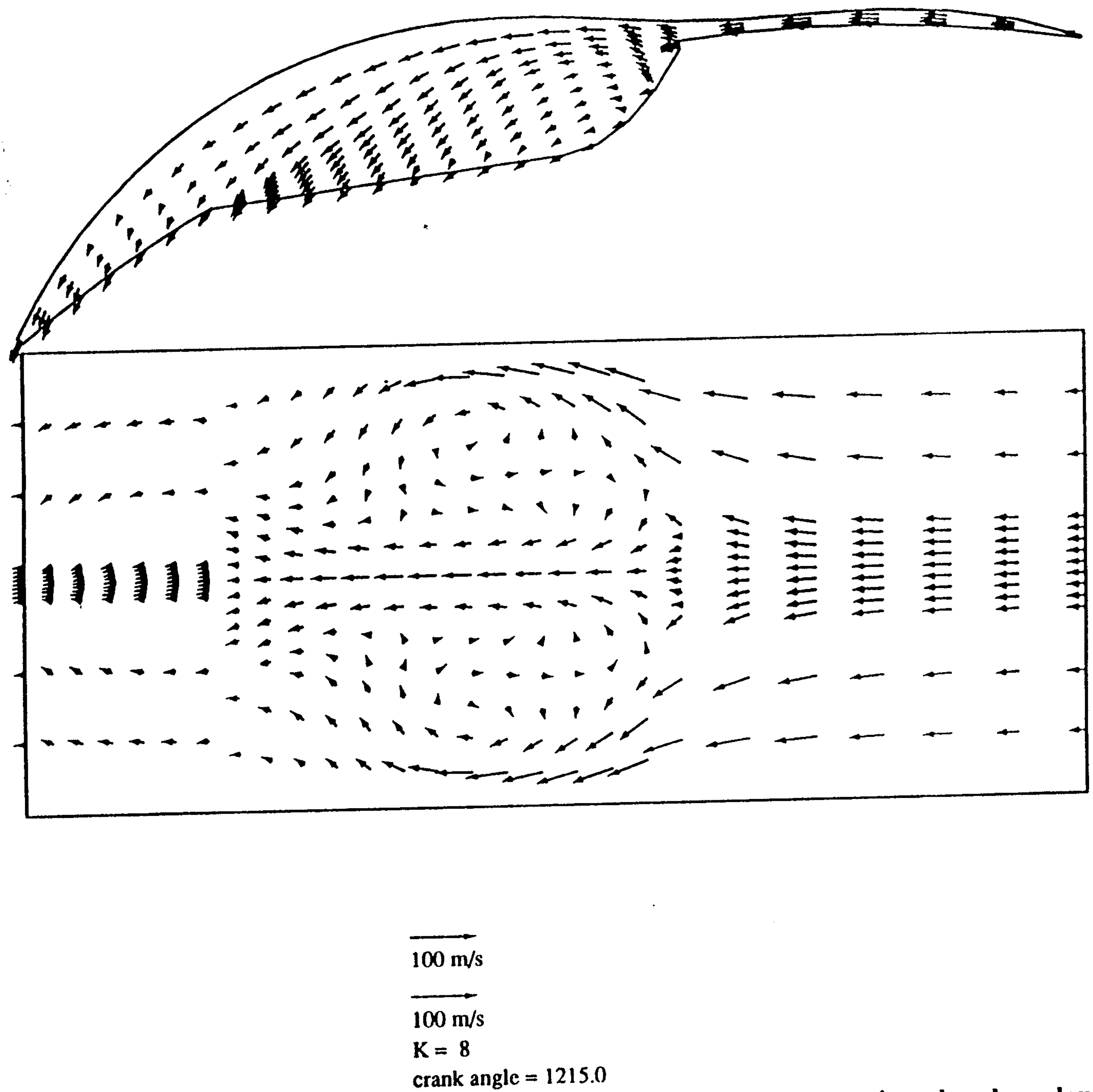
100 m/s
100 m/s
K = 8
crank angle = 1215.0

Fig. 3(i): Top view and cross-section view of combustion chamber along symmetry plane showing velocity vectors at 1215 CA. for standard pocket rotor.

Figure 1(j)

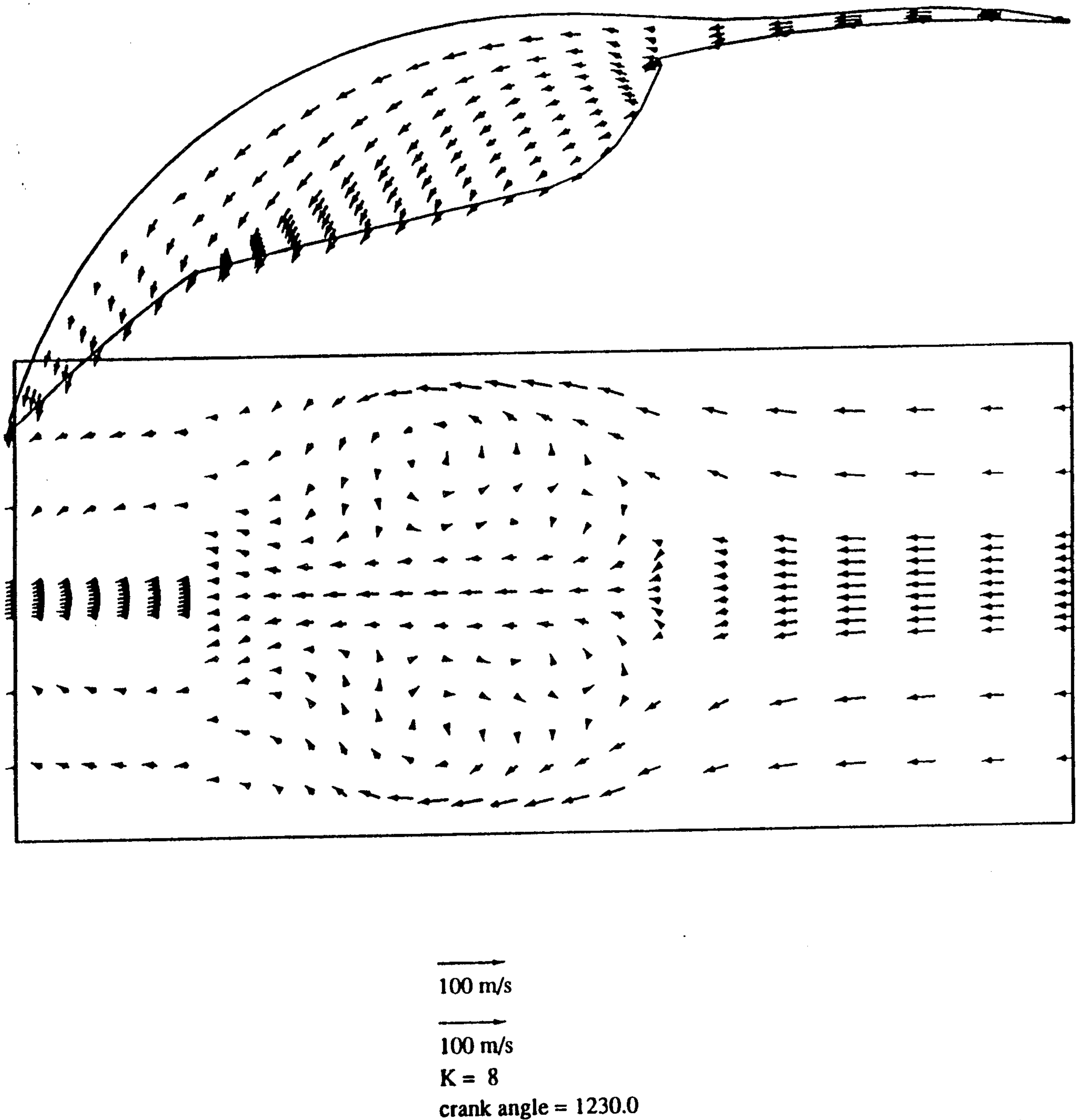

Fig. 3(j): Top view and cross-section view of combustion chamber along symmetry plane showing velocity vectors at 1230 CA. for standard pocket rotor.

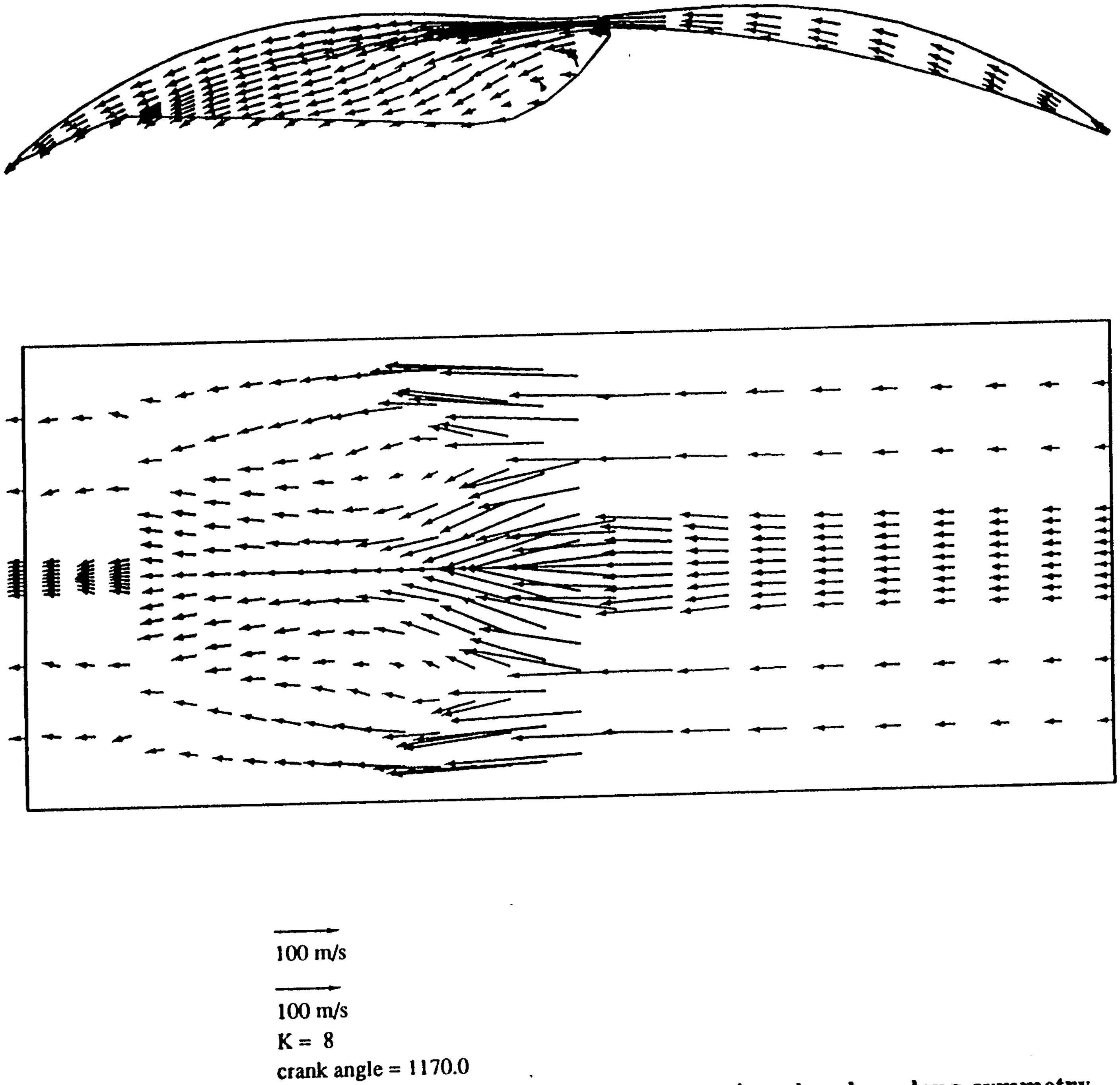

Fig. 4(f): Top view and cross-section view of combustion chamber along symmetry plane showing velocity vectors at 1170 CA. for leading pocket rotor.

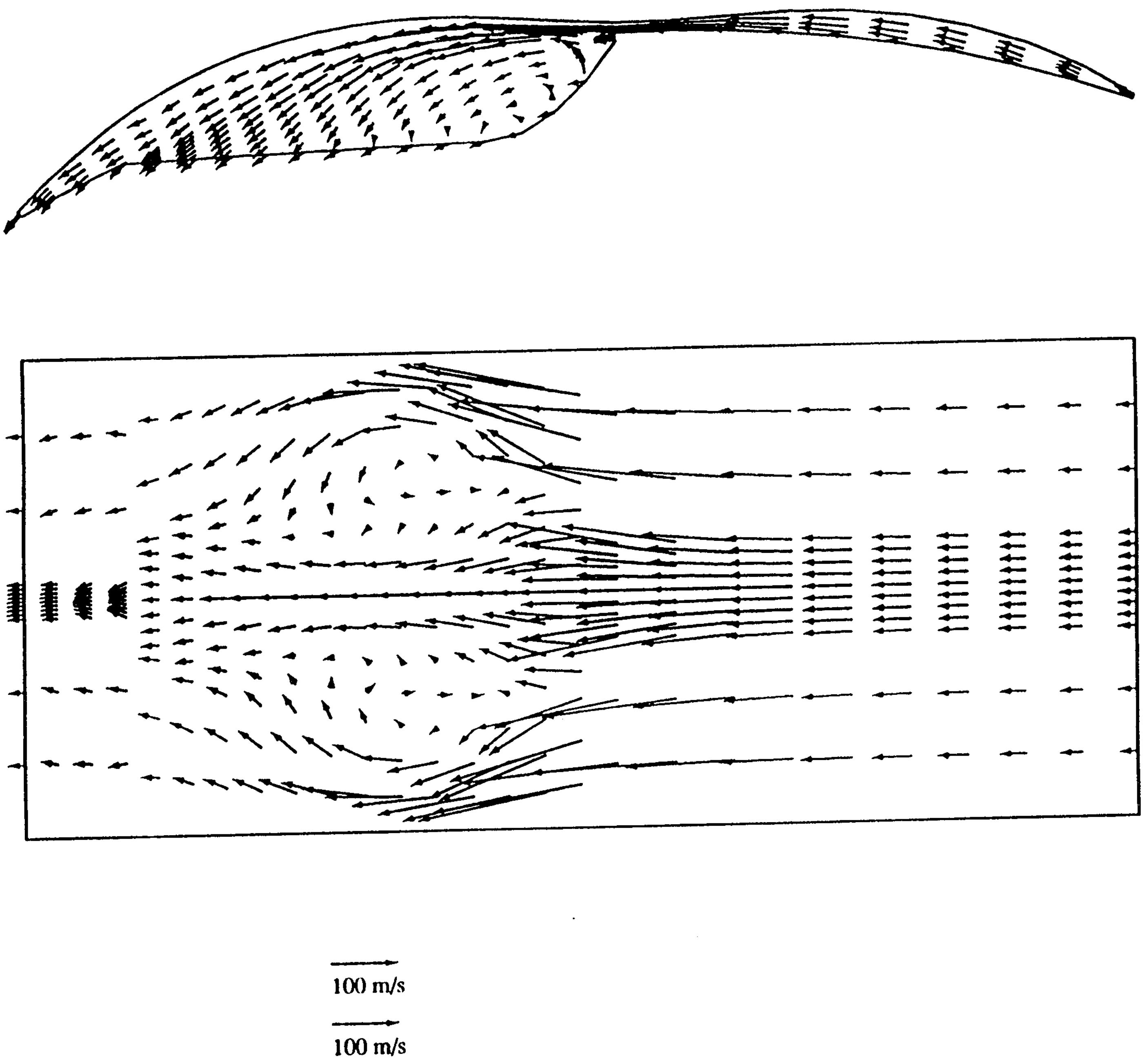

Fig. 4(g): Top view and cross-section view of combustion chamber along symmetry plane showing velocity vectors at 1185 CA. for leading pocket rotor.

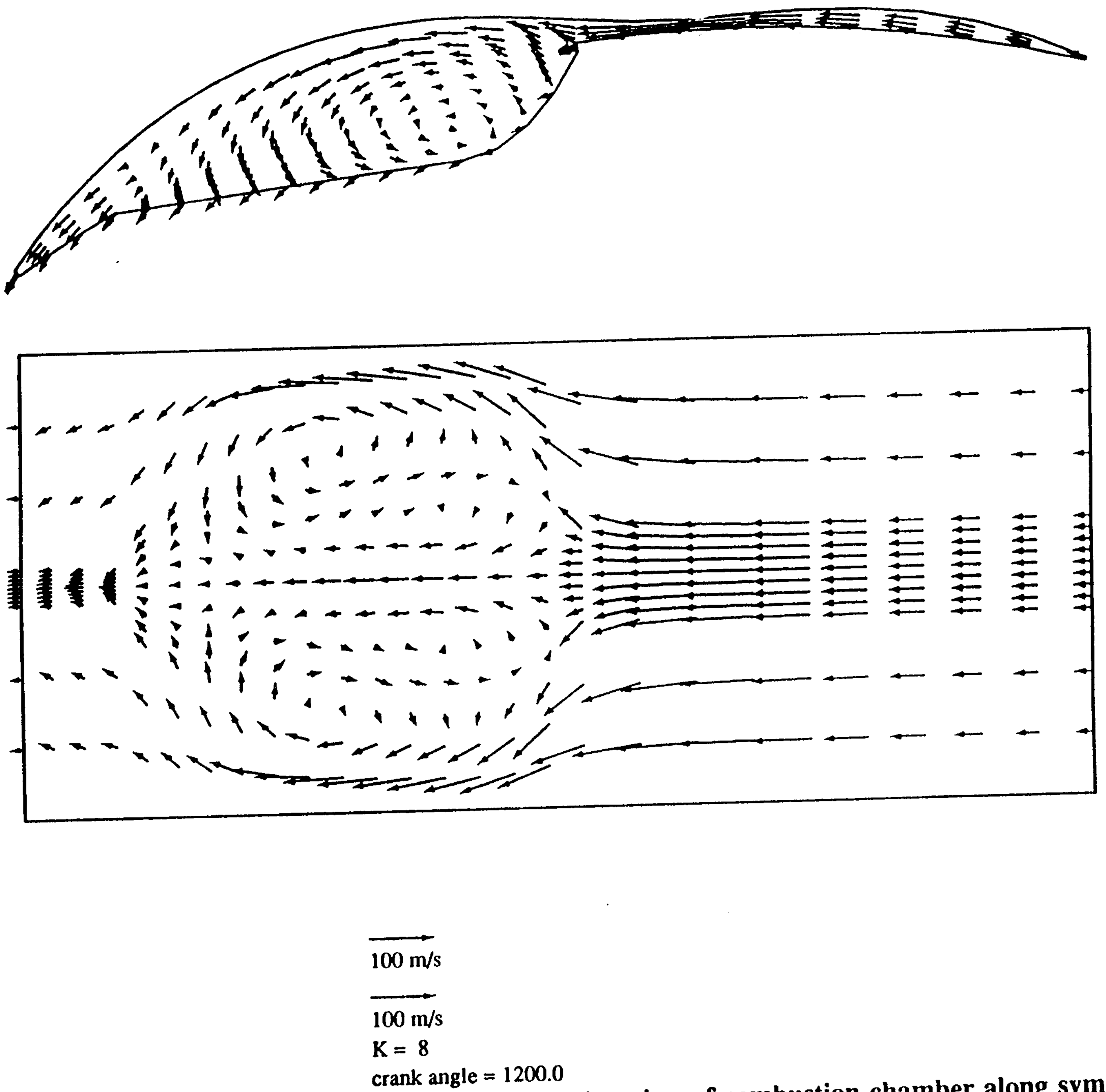

Fig. 4(h): Top view and cross-section view of combustion chamber along symmetry plane showing velocity vectors at 1200 CA. for leading pocket rotor.

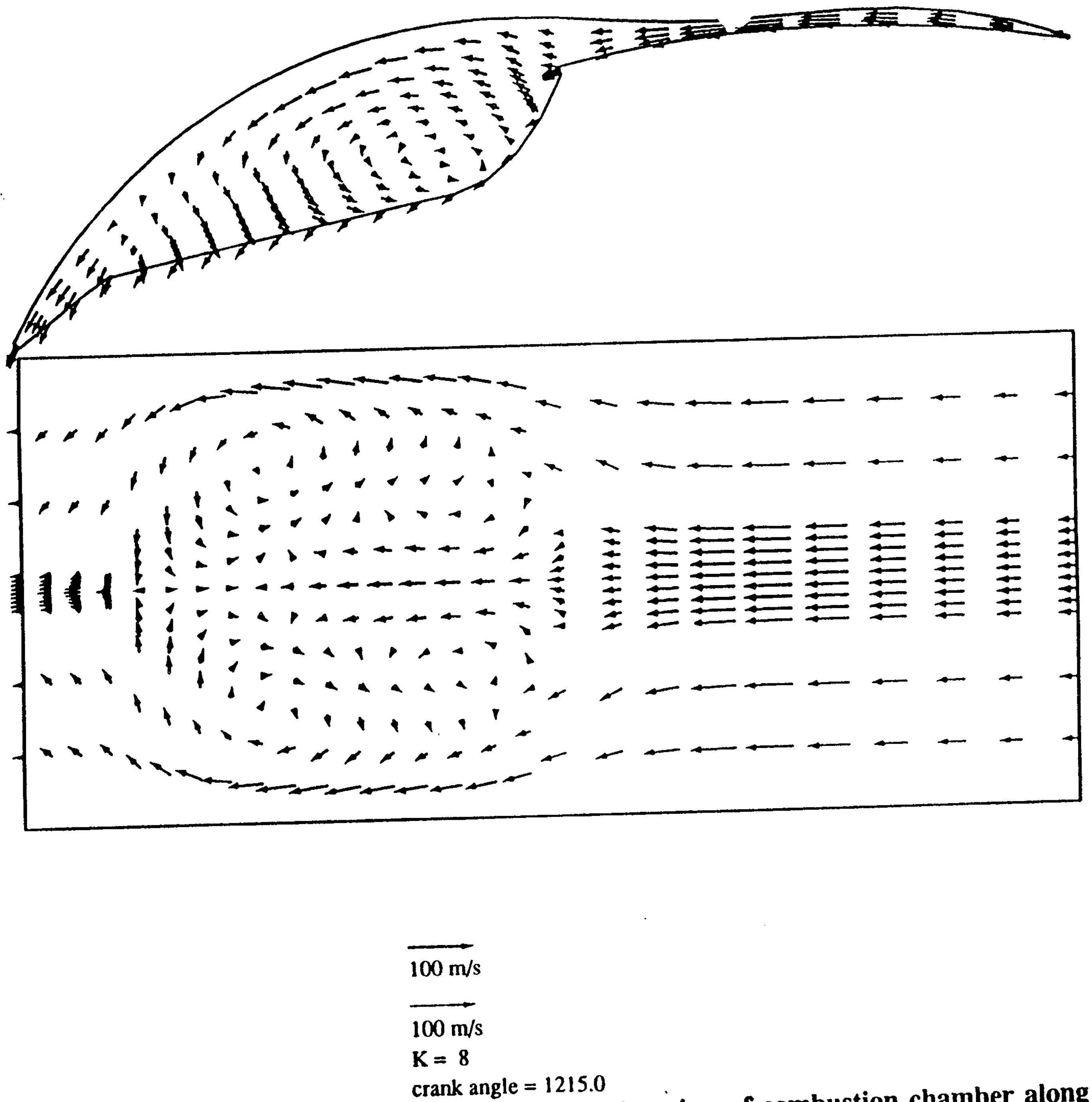

Fig. 4(i): Top view and cross-section view of combustion chamber along symmetry plane showing velocity vectors at 1215 CA. for leading pocket rotor.

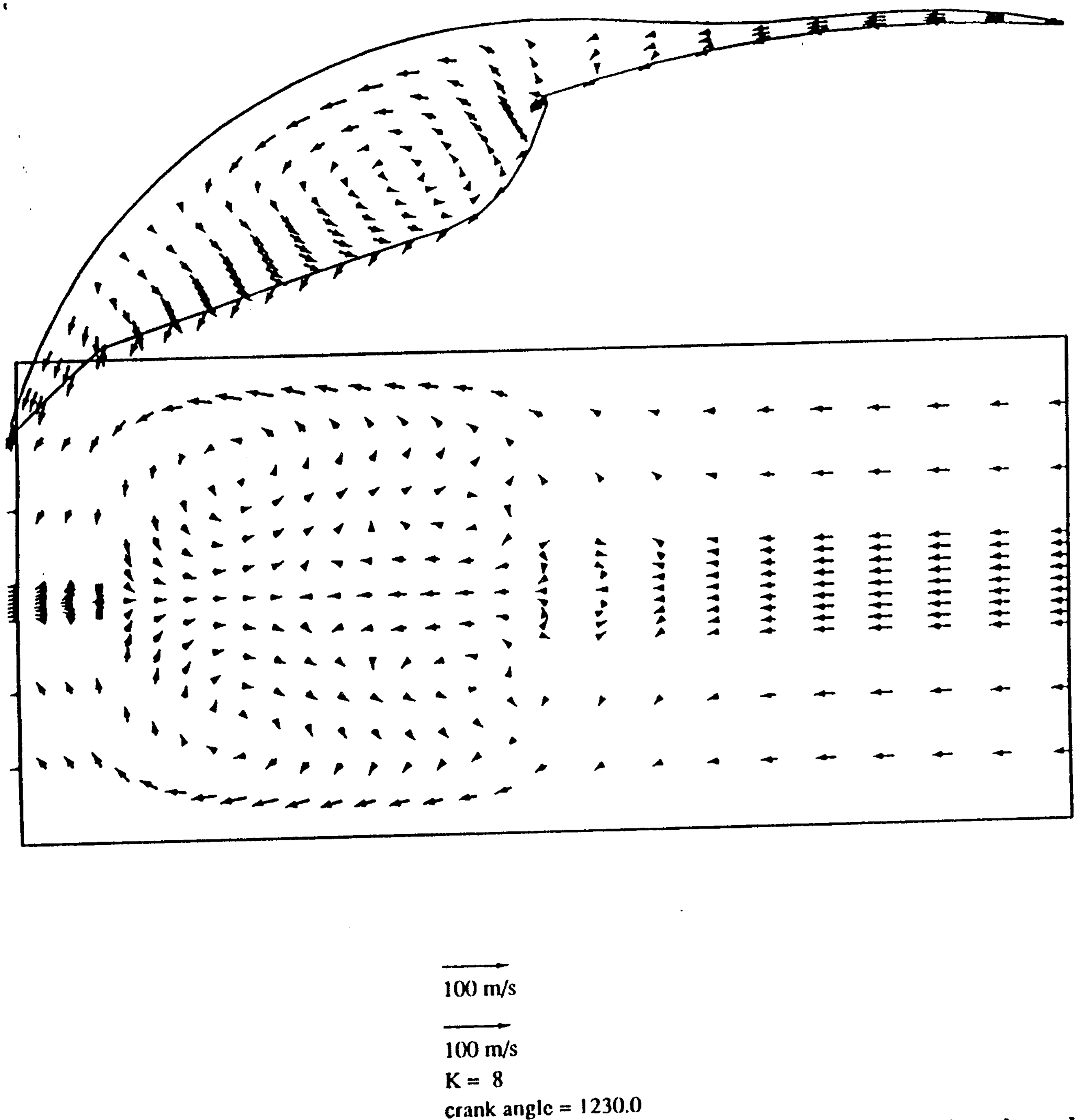

Fig. 4(j): Top view and cross-section view of combustion chamber along symmetry plane showing velocity vectors at 1230 CA. for leading pocket rotor.

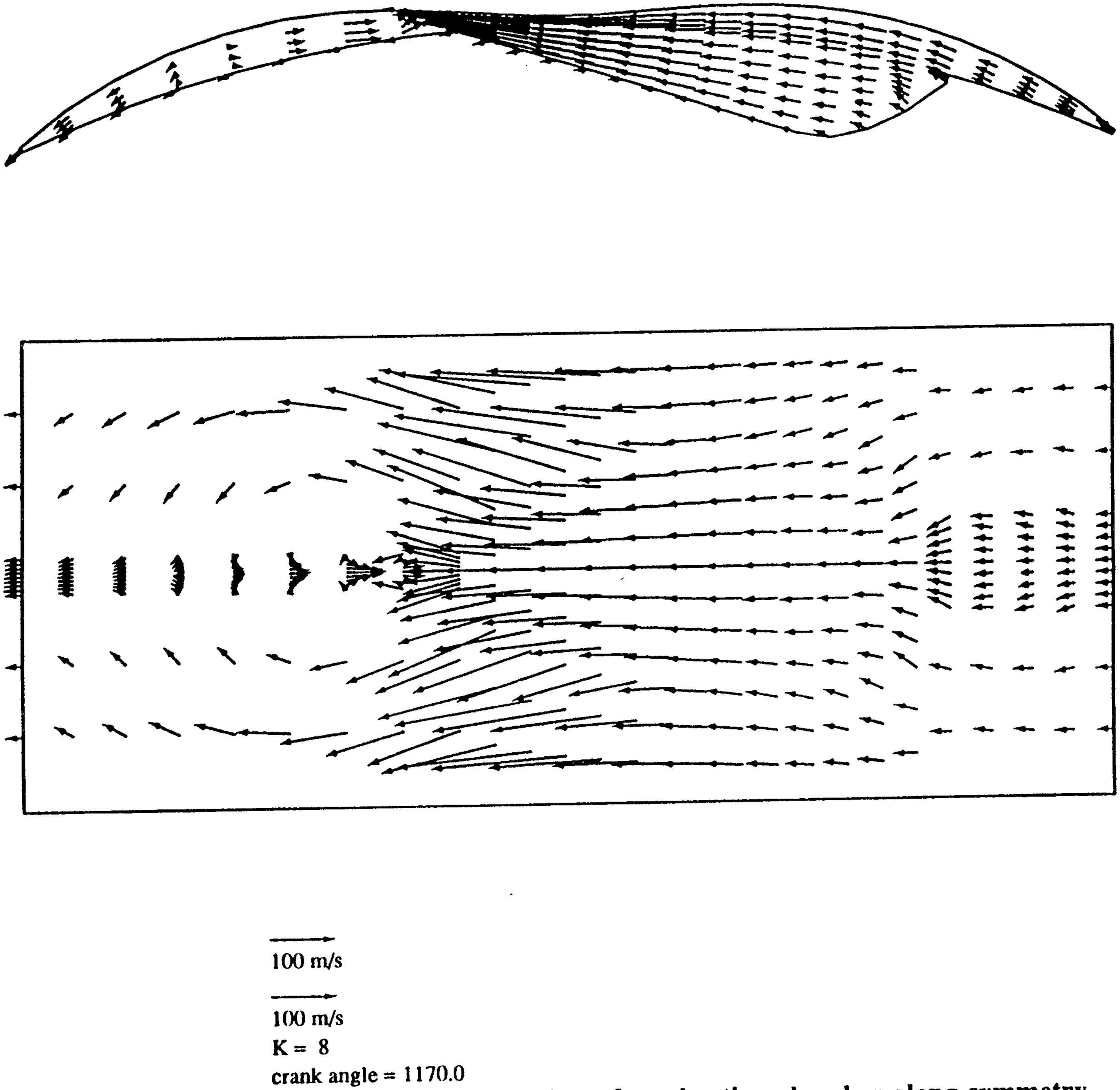

Fig. 5(f): Top view and cross-section view of combustion chamber along symmetry plane showing velocity vectors at 1170 CA. for trailing pocket rotor.

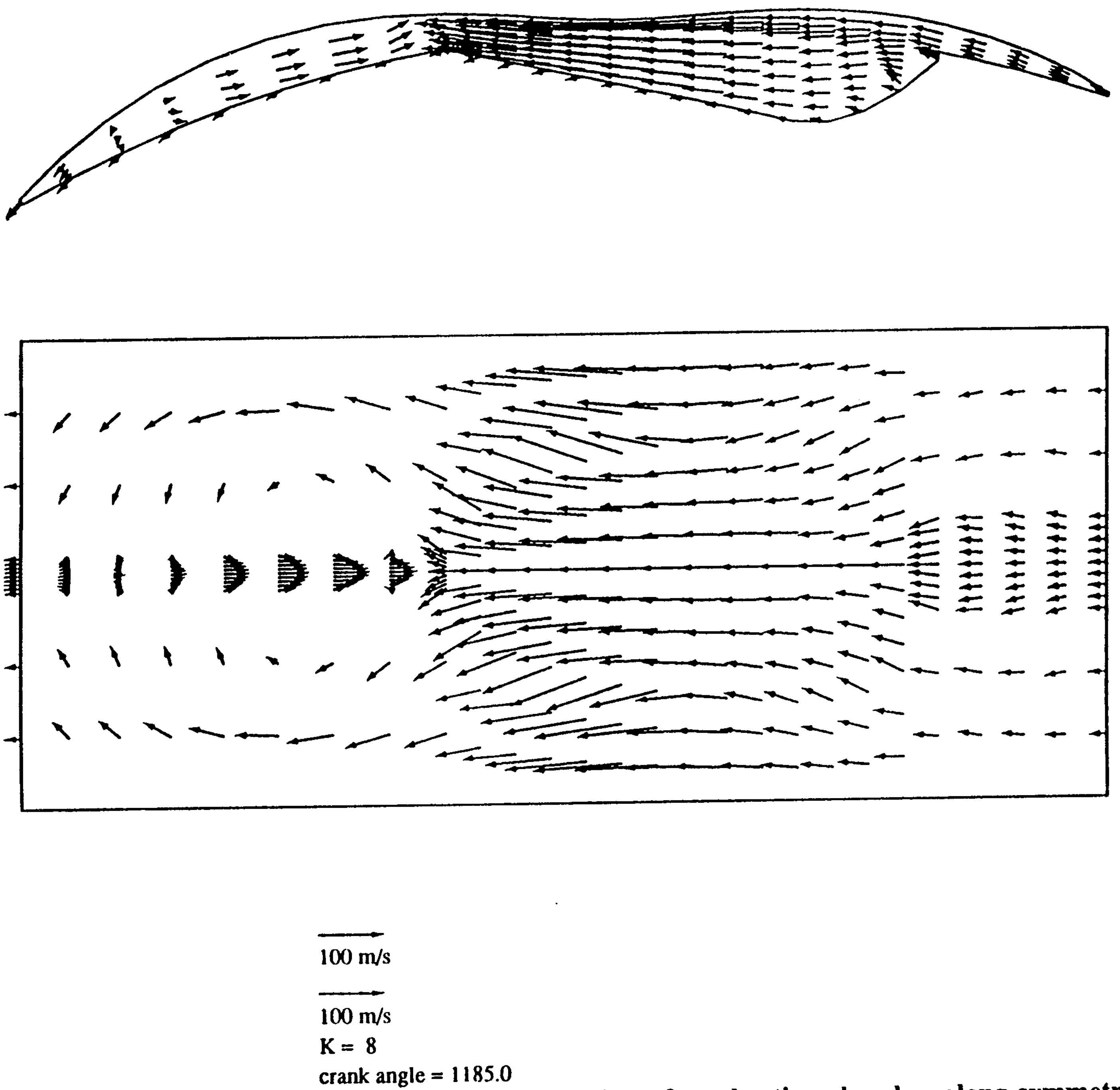

Fig. 5(g): Top view and cross-section view of combustion chamber along symmetry plane showing velocity vectors at 1185 CA. for trailing pocket rotor.

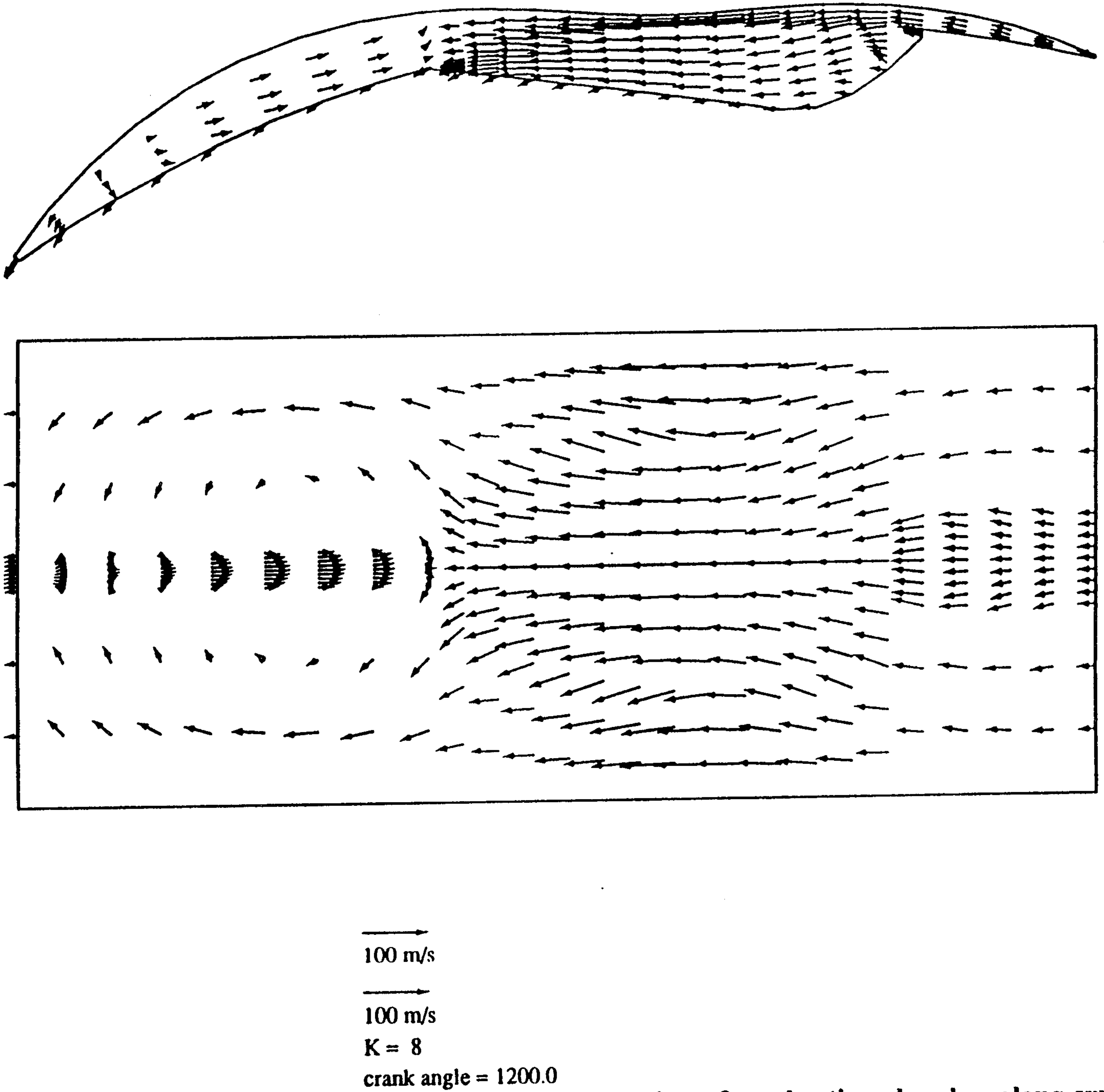

Fig. 5(h): Top view and cross-section view of combustion chamber along symmetry plane showing velocity vectors at 1200 CA. for trailing pocket rotor.

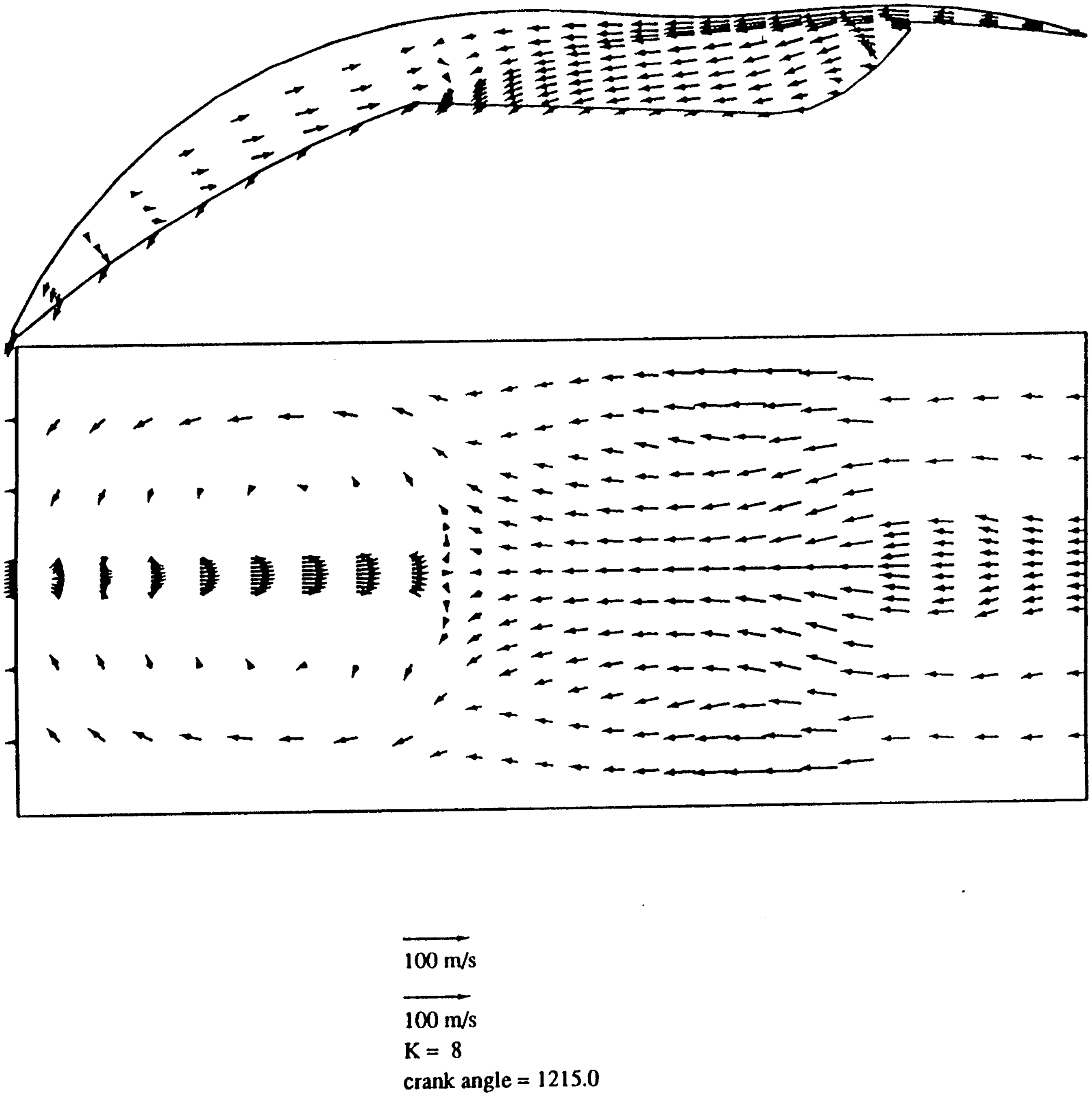

Fig. 5(i): Top view and cross-section view of combustion chamber along symmetry plane showing velocity vectors at 1215 CA. for trailing pocket rotor.

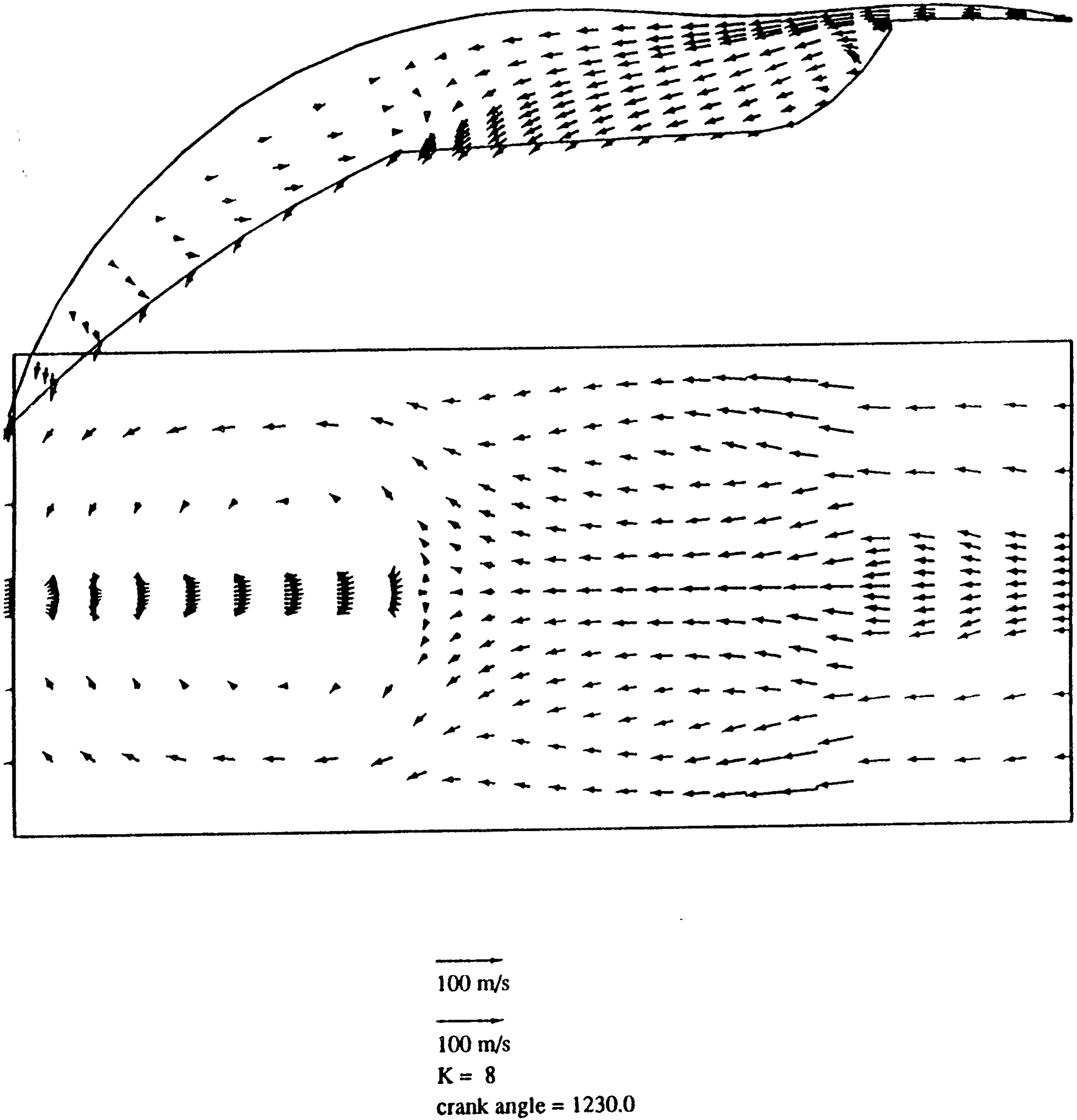

Fig. 5(j): Top view and cross-section view of combustion chamber along symmetry plane showing velocity vectors at 1230 CA. for trailing pocket rotor.

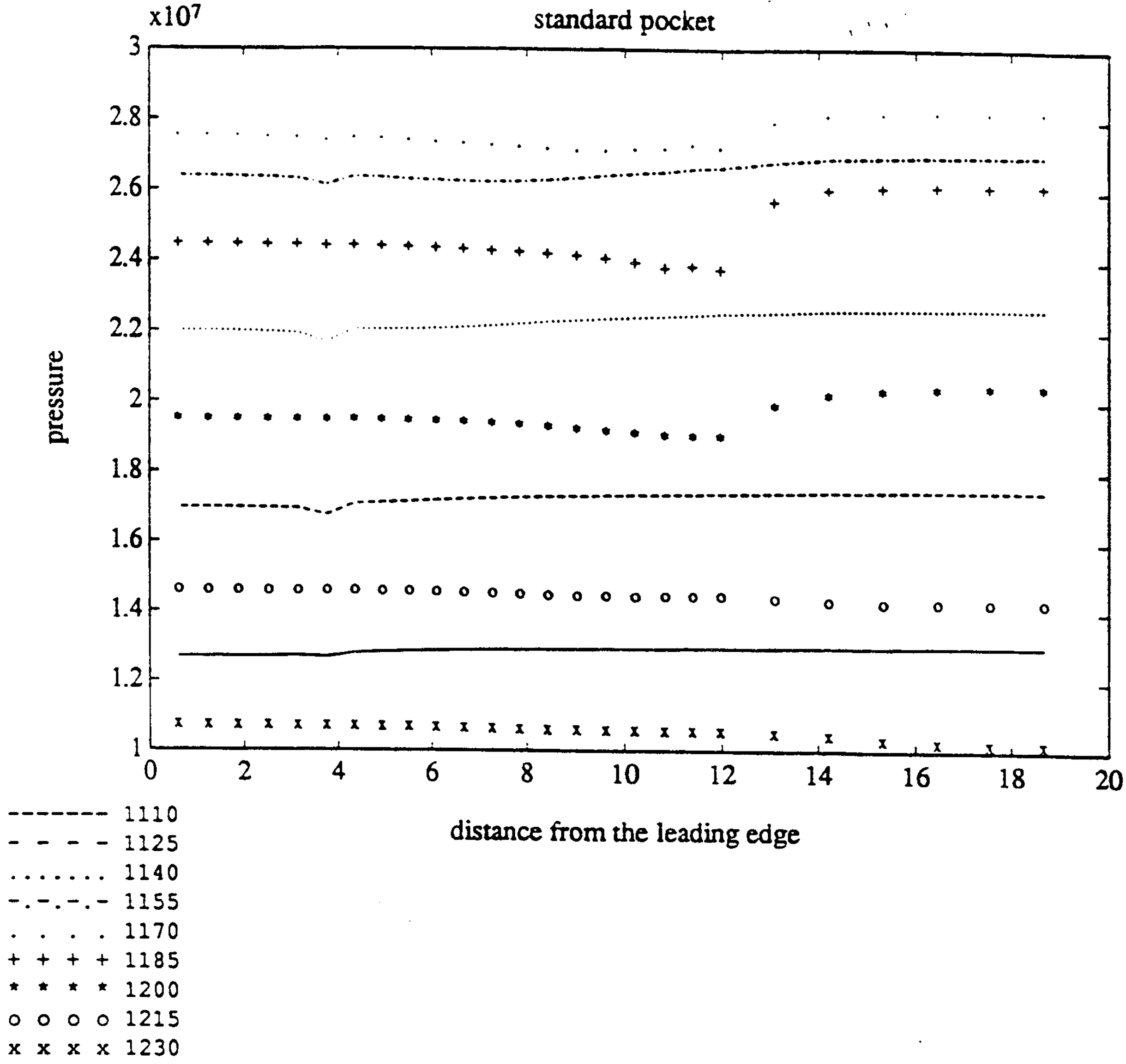

Fig. 3(k): Pressure along the rotor at different crank angles

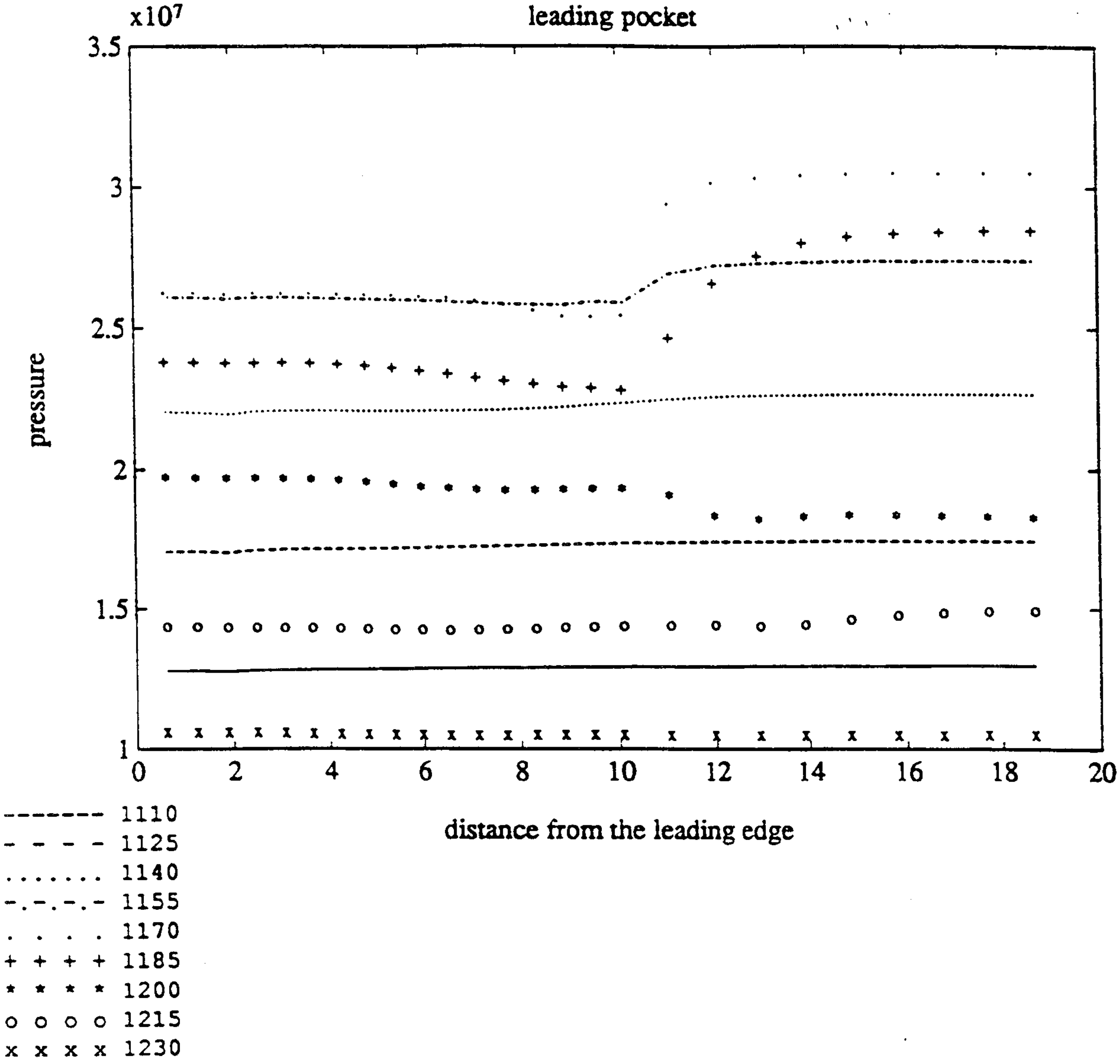

Fig. 4(k): Pressure along the rotor at different crank angles

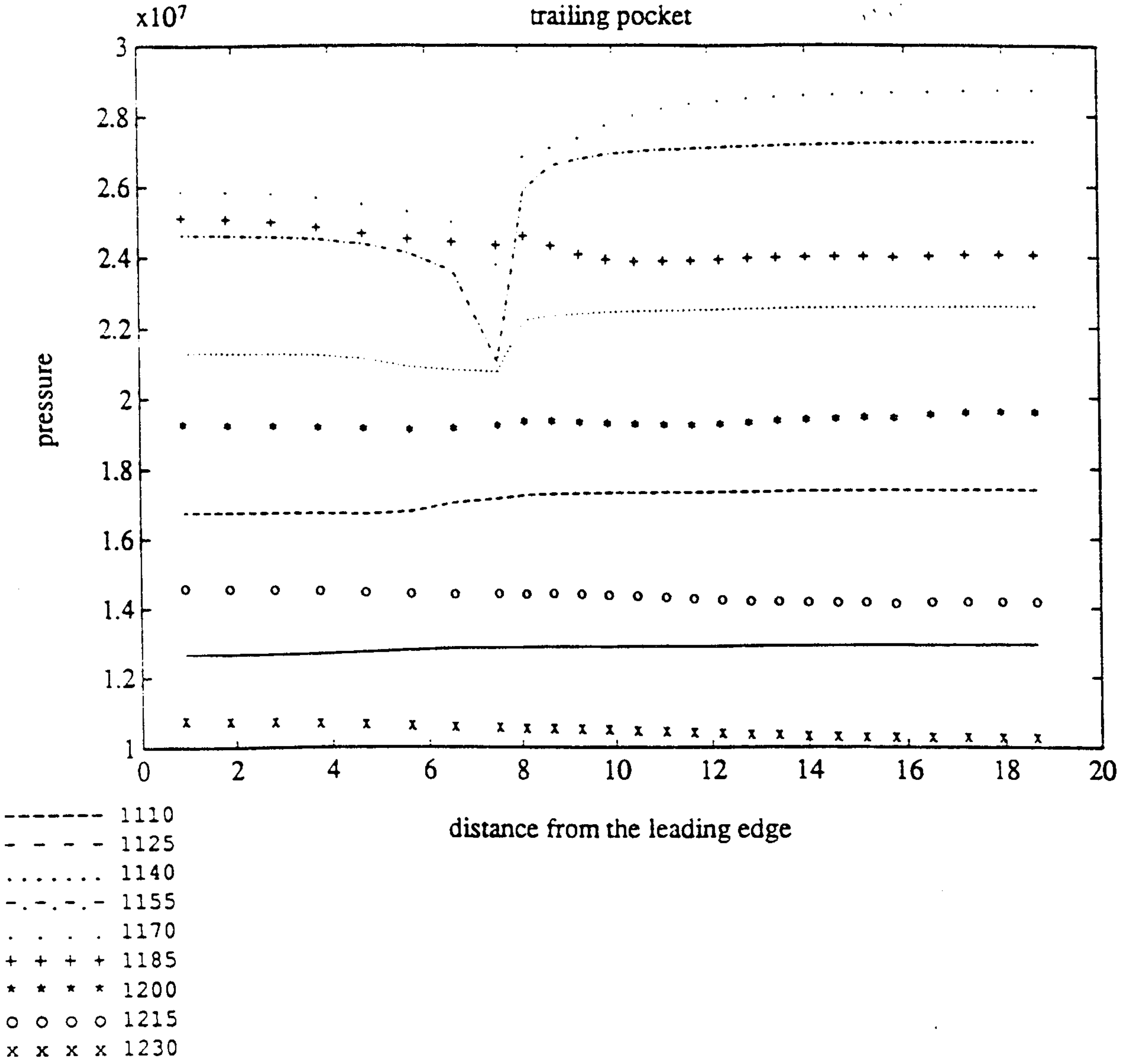

Fig. 5(k): Pressure along the rotor at different crank angles

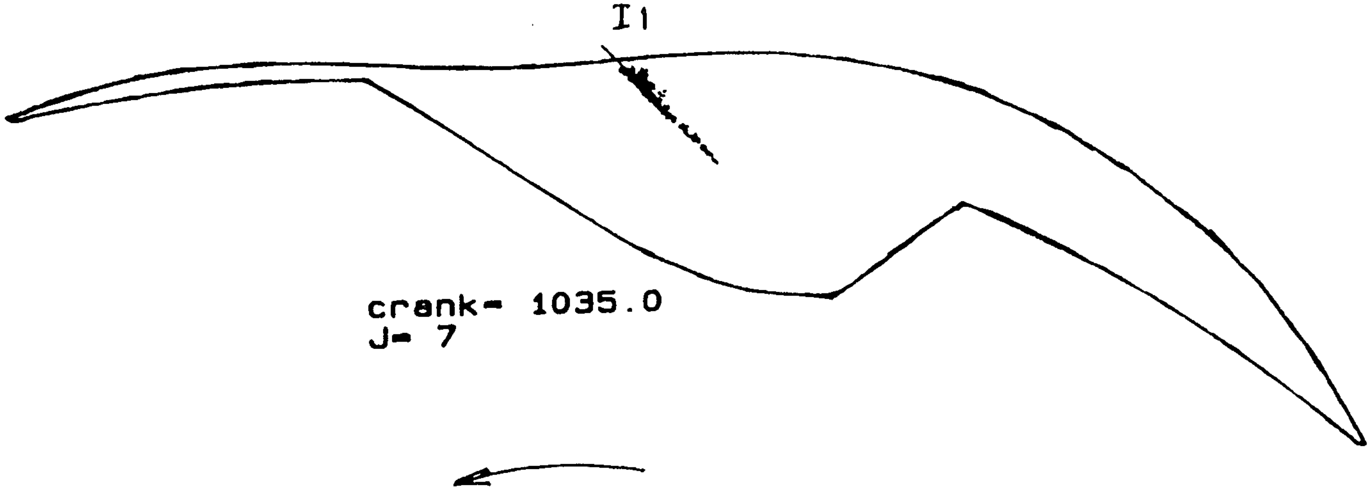
I1
crank= 1035.0
J= 7

Fig. 6: Cross-section view of combustion chamber along symmetry plane showing liquid fuel distribution at 1035 CA (1080 is TC).

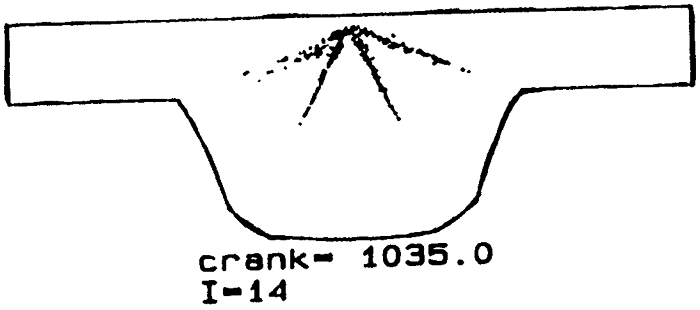
crank= 1035.0
I=14

Fig. 7: Cross-section of combustion chamber showing liquid fuel distribution at 1035 CA. Injector has a 4-hole pattern.

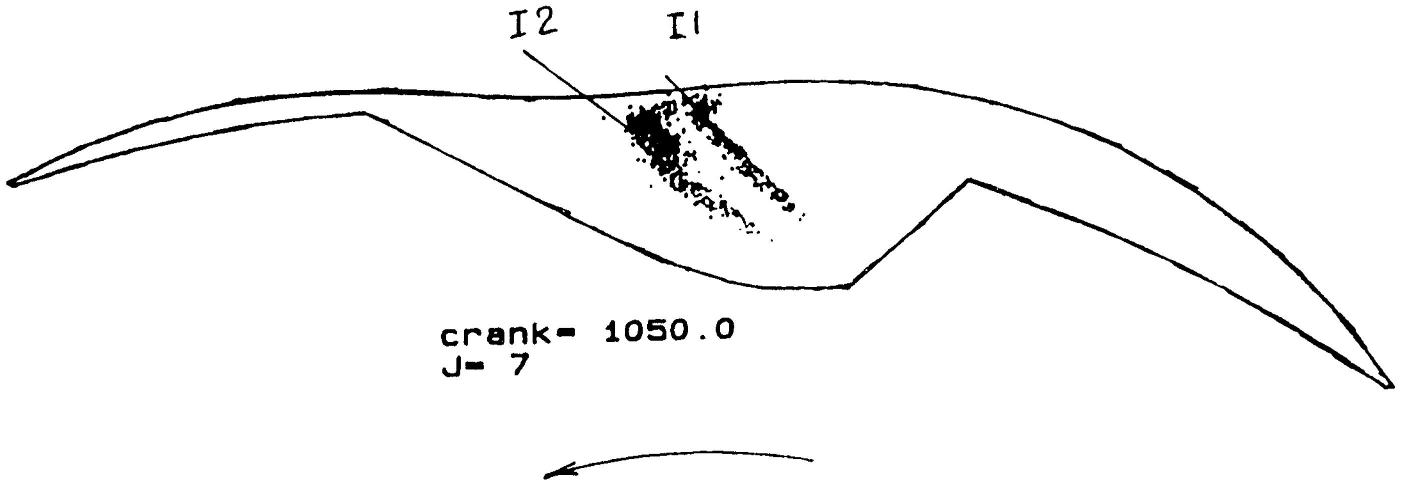
I2
I1
crank= 1050.0
J= 7

Fig. 8: Cross-section view of combustion chamber along symmetry plane showing liquid fuel distribution at 1050 CA.

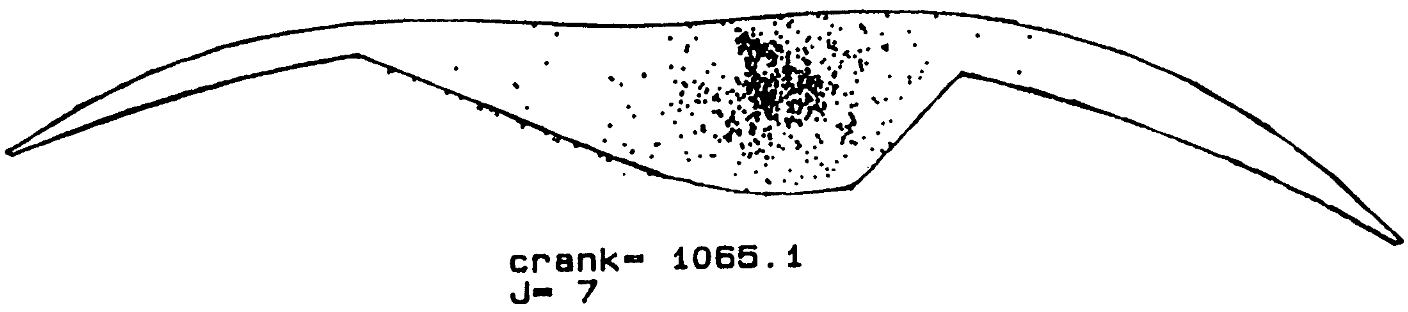

Fig. 9: Cross-section view of combustion chamber along symmetry plane showing liquid fuel distribution at 1065 CA.

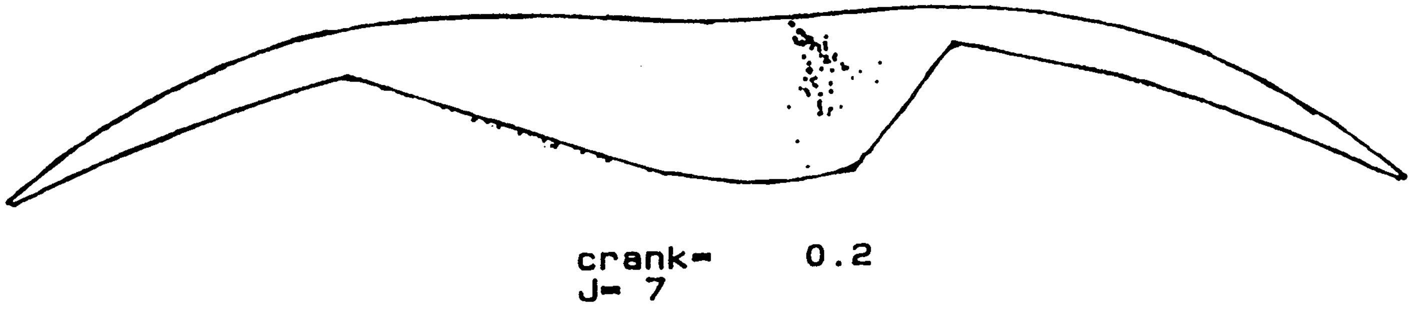

Fig. 10: Cross-section view of combustion chamber along symmetry plane showing liquid fuel distribution at TC.

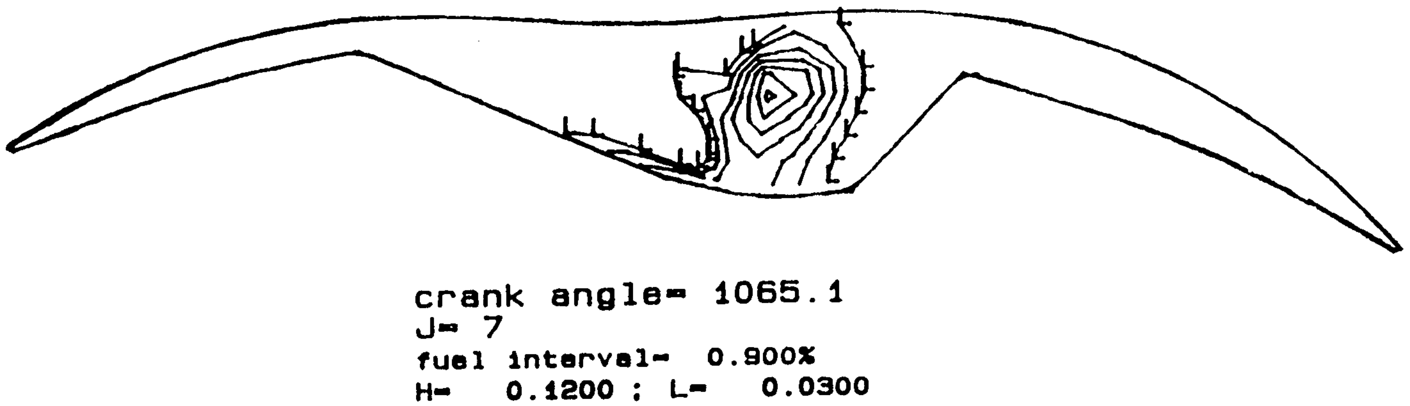

Fig. 11: Cross-section view of combustion chamber along symmetry plane showing vaporized fuel distribution at 1065.1 CA.

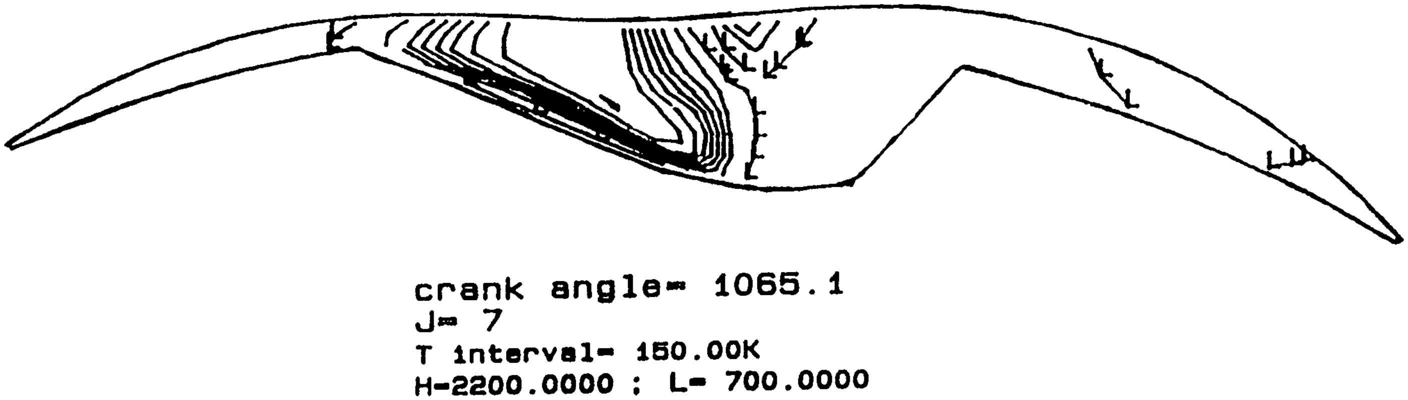

Fig. 12: Cross-section view of combustion chamber along symmetry plane showing temperature contours at 1065 CA.

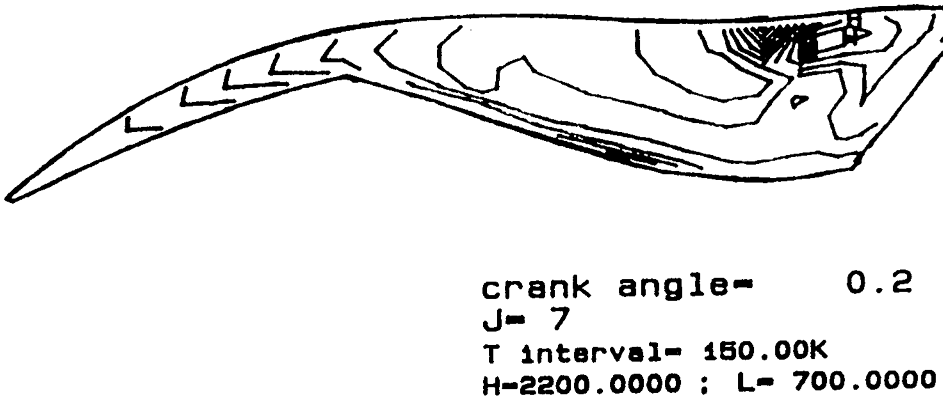

Fig. 13: Cross-section view of combustion chamber along symmetry plane showing temperature contours at TC.

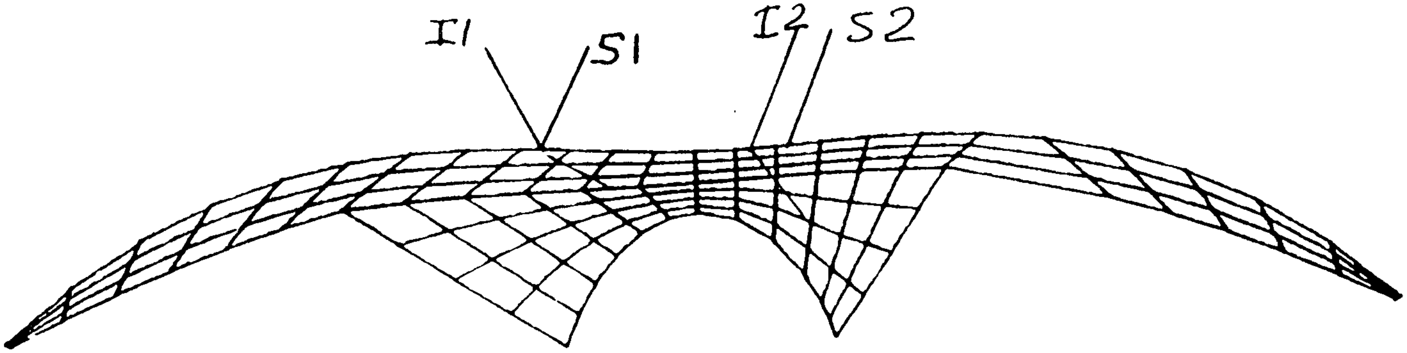

Fig. 14 (a): Cross-section view of combustion chamber along symmetry plane showing grid layout and locations of injectors and spark plugs.

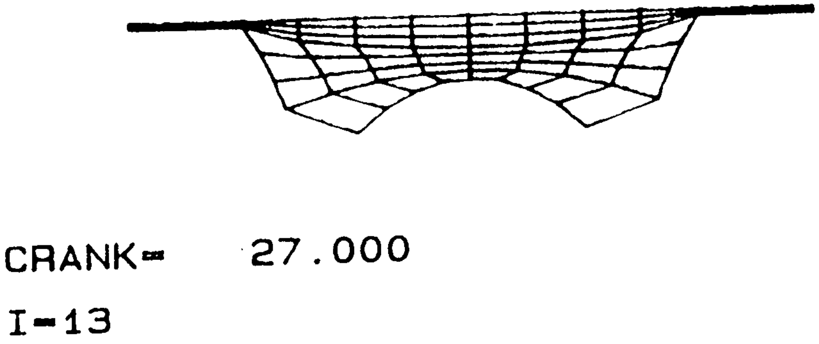
CRANK= 27.000
I=13

Fig. 14 (b): Cross-section view of combustion chamber showing grid layout.

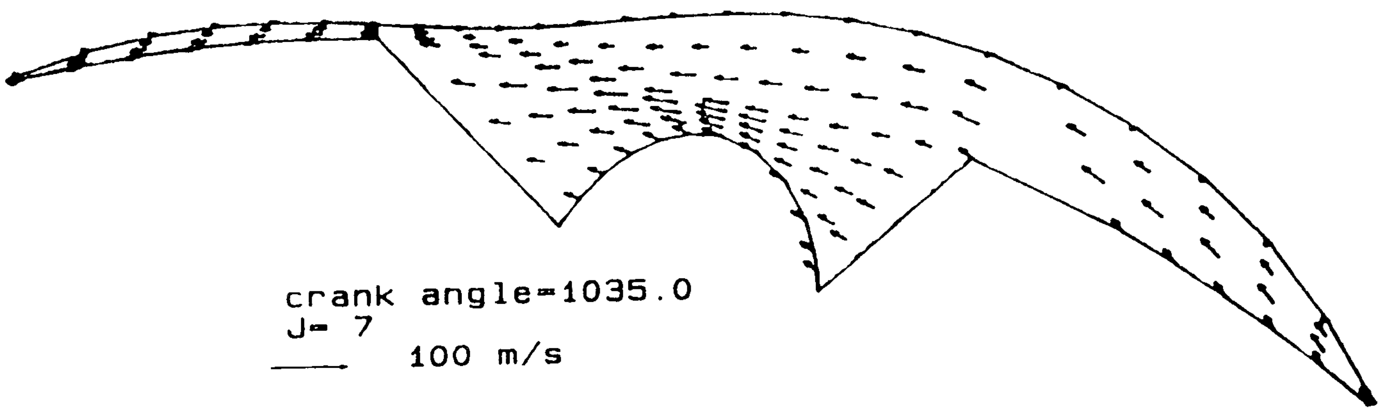

Fig. 15 (a): Cross-section view of combustion chamber along symmetry plane showing velocity vectors at 1035 CA.

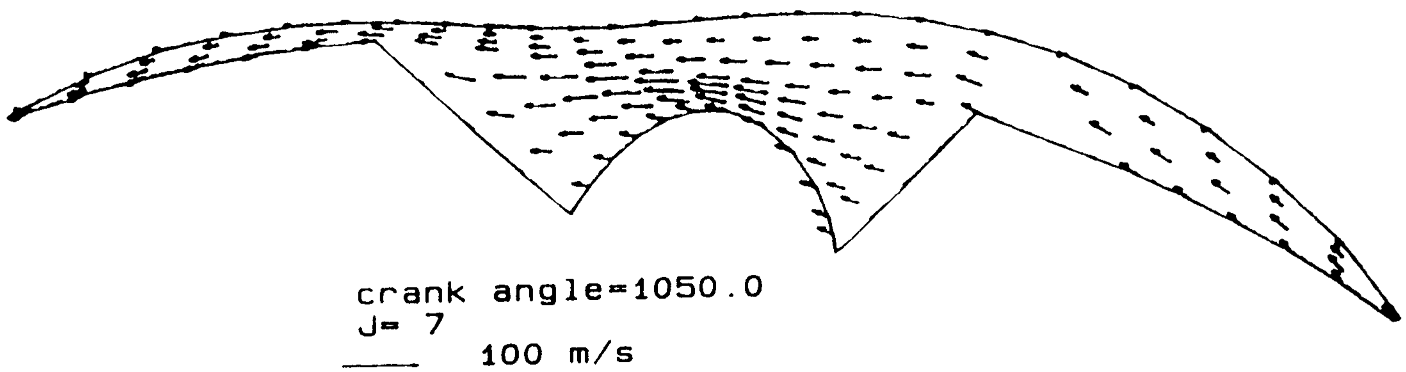

Fig. 15 (b): Cross-section view of combustion chamber along symmetry plane showing velocity vectors at 1050 CA.

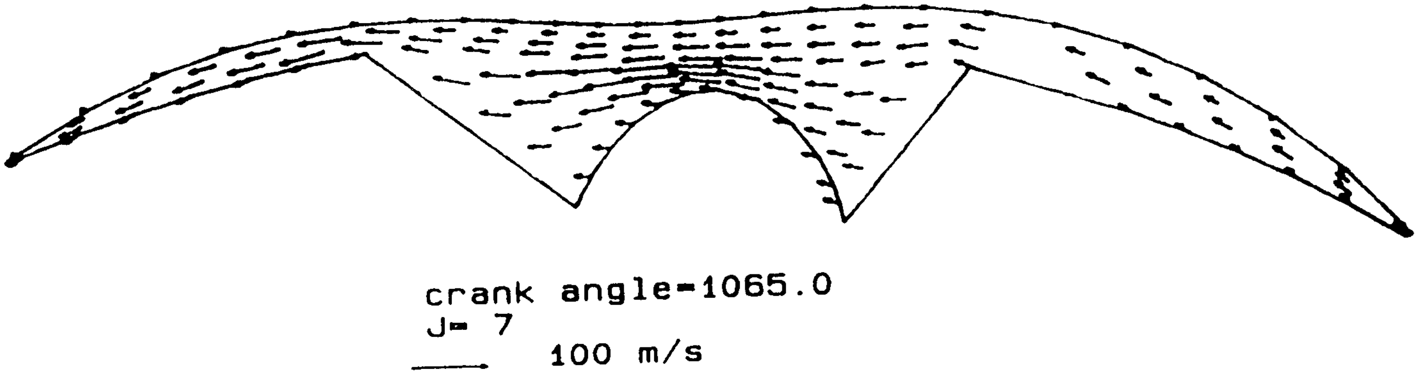

Fig. 15 (c): Cross-section view of combustion chamber along symmetry plane showing velocity vectors at 1065 CA.

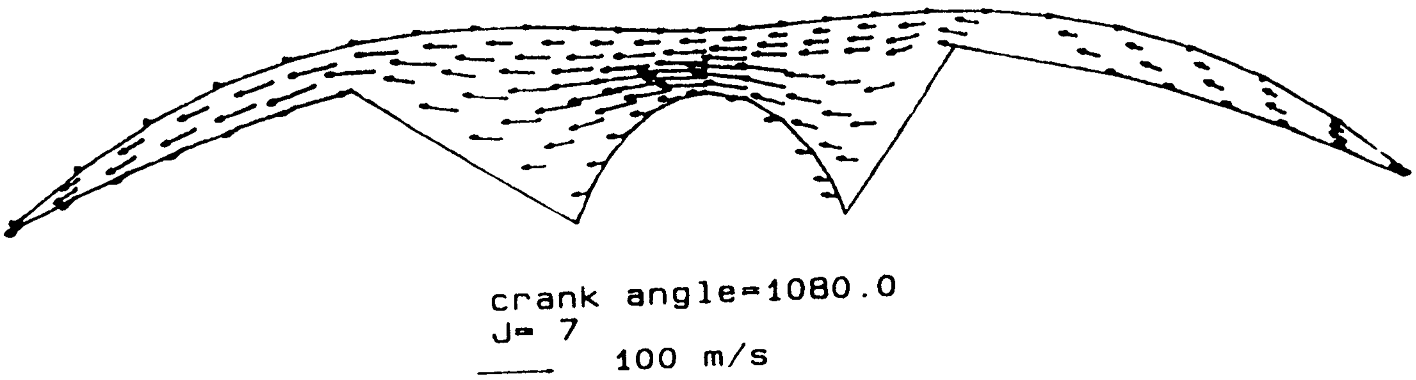

Fig. 15 (d): Cross-section view of combustion chamber along symmetry plane showing velocity vectors at TC.

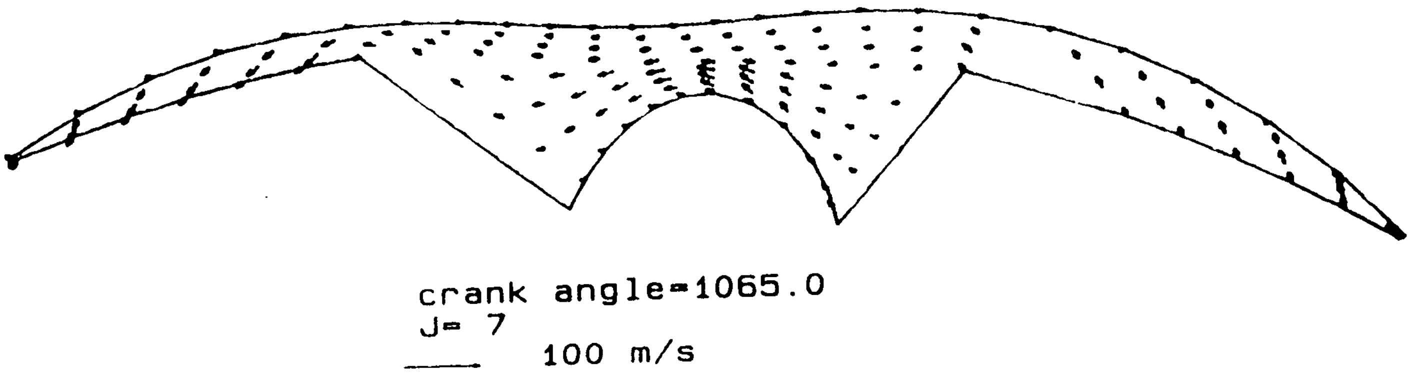

Fig. 15 (e): Cross-section view of combustion chamber along symmetry plane showing velocity vectors with respect to the rotor at 1065 CA.

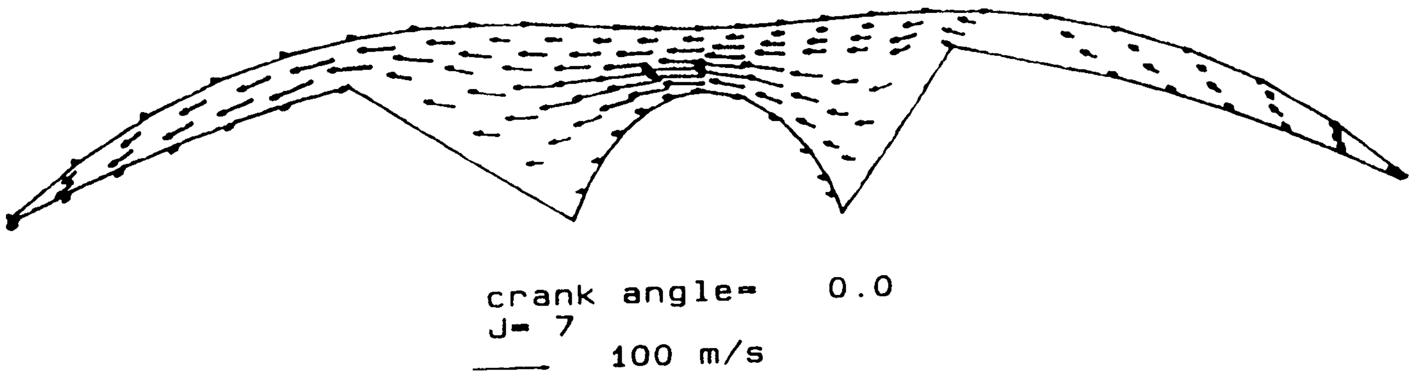

Fig. 15 (f): Cross-section view of combustion chamber along symmetry plane showing velocity vectors with respect to the rotor at TC.

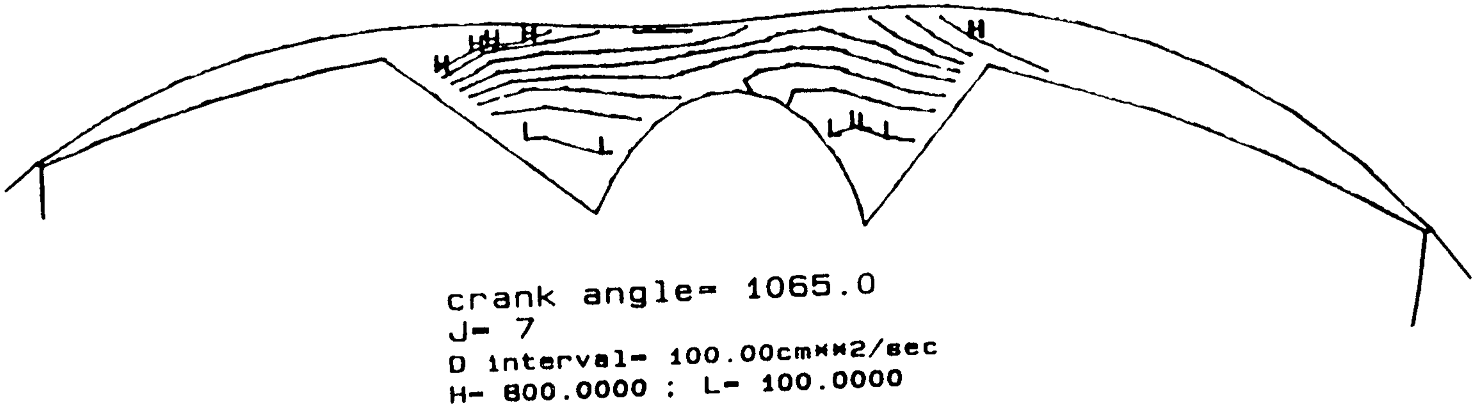

Fig. 16 (a): Cross-section view of combustion chamber along symmetry plane showing diffusivity at 1065 CA.

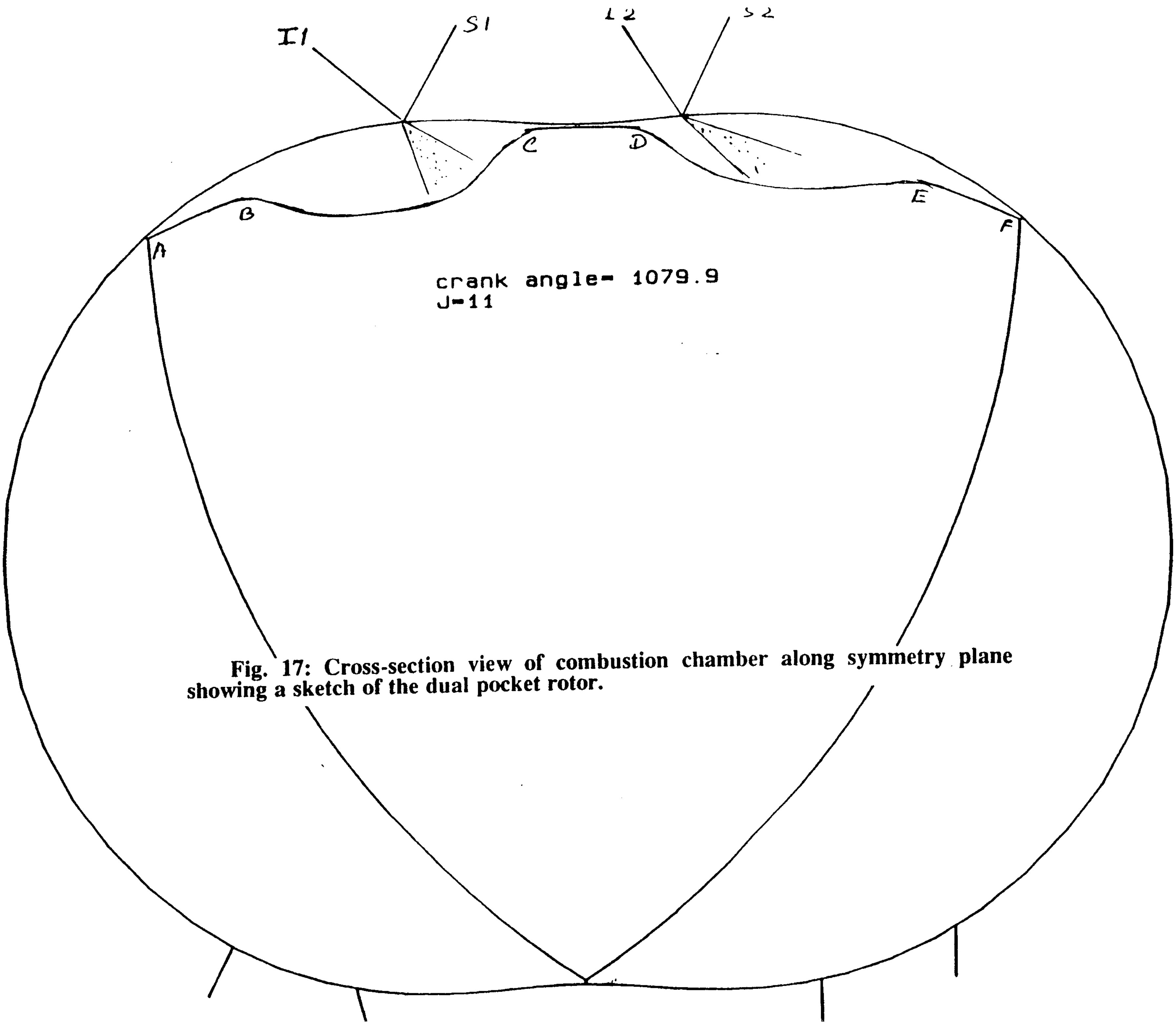
I1
S1
I2
S2
A
B
C
D
E
F
crank angle= 1079.9
J=11

Fig. 17: Cross-section view of combustion chamber along symmetry plane showing a sketch of the dual pocket rotor.

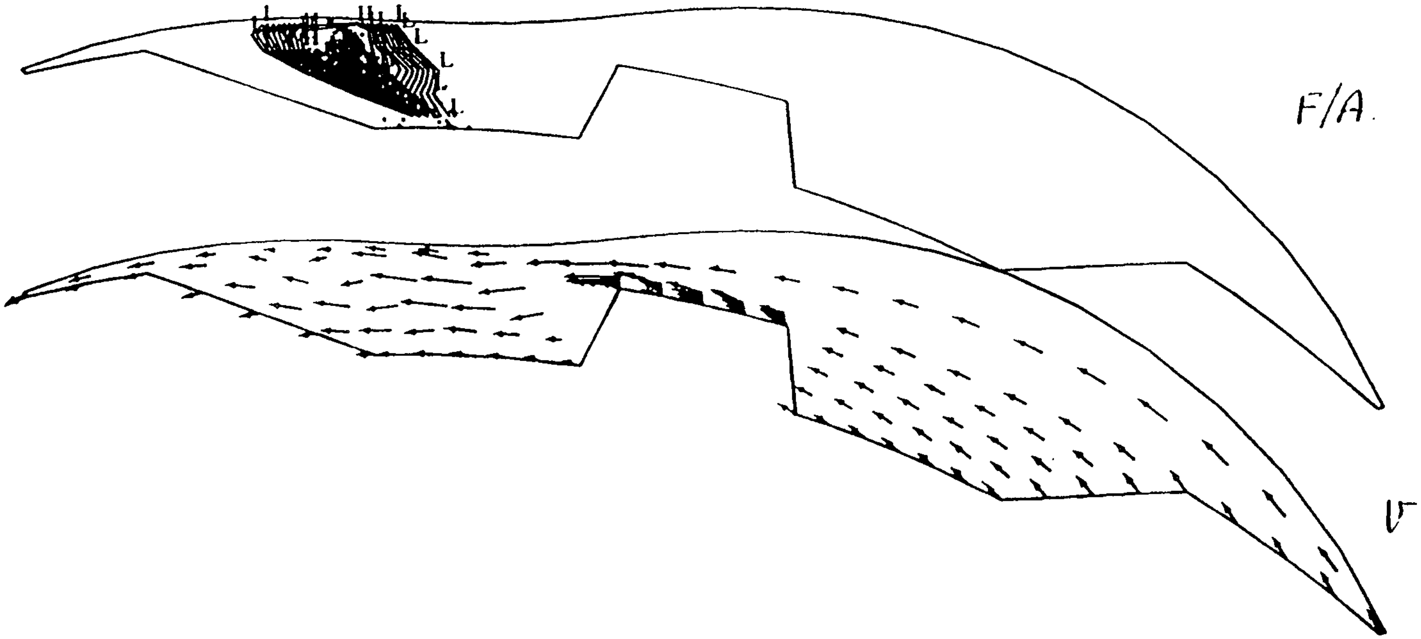

FUEL/AIR RATIO, interval = 0.1000E-01

H = .1200 ; L = .3000E-01

100 m/s

J = 7

Fig. 18(a): Cross-section view of combustion chamber along symmetry plane showing liquid fuel and vaporized fuel distribution and velocity vectors at 1035 CA.

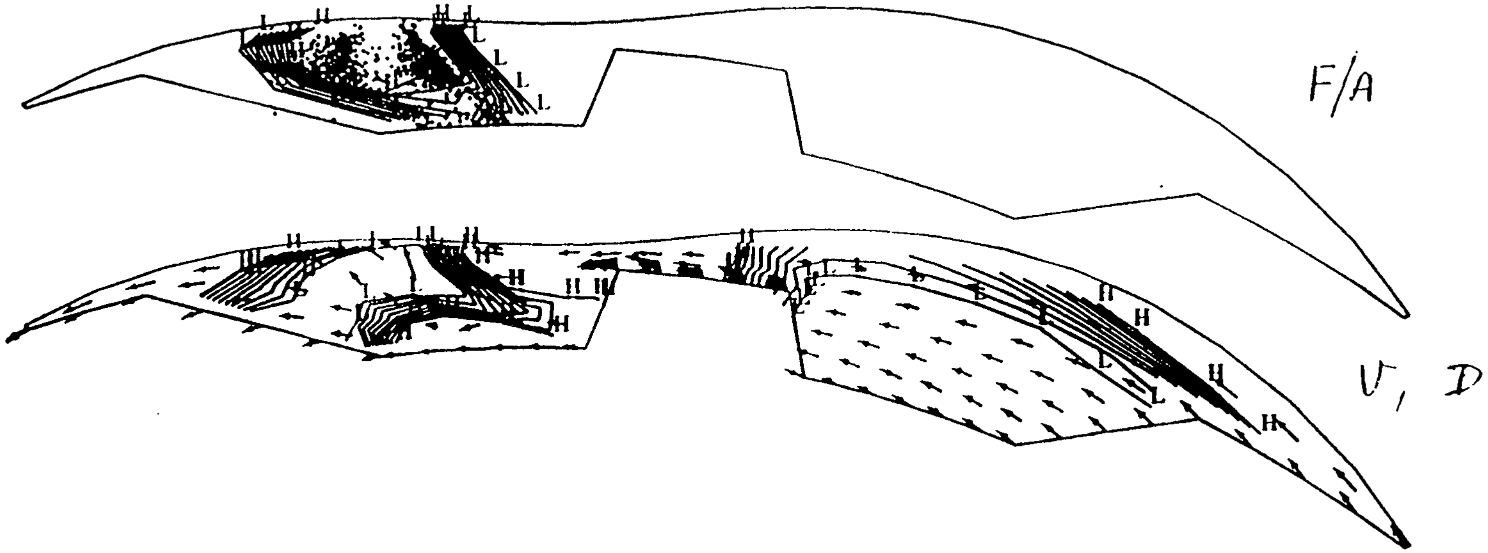

Fig. 18(b): Cross-section view of combustion chamber along symmetry plane showing liquid fuel and vaporized fuel distribution ,velocity vectors and diffusivity contours at 1050 CA.

FUEL/AIR RATIO, interval = 0.1000E-01
H = .1200 ; L = .3000E-01
TEMPERATURE, interval = 155.6 K
H = 2100. ; L = 700.0
DIFFUSIVITY, interval = 55.56 cm2/s
H = 600.0 ; L = 100.0

⟶
100 m/s
I = 7

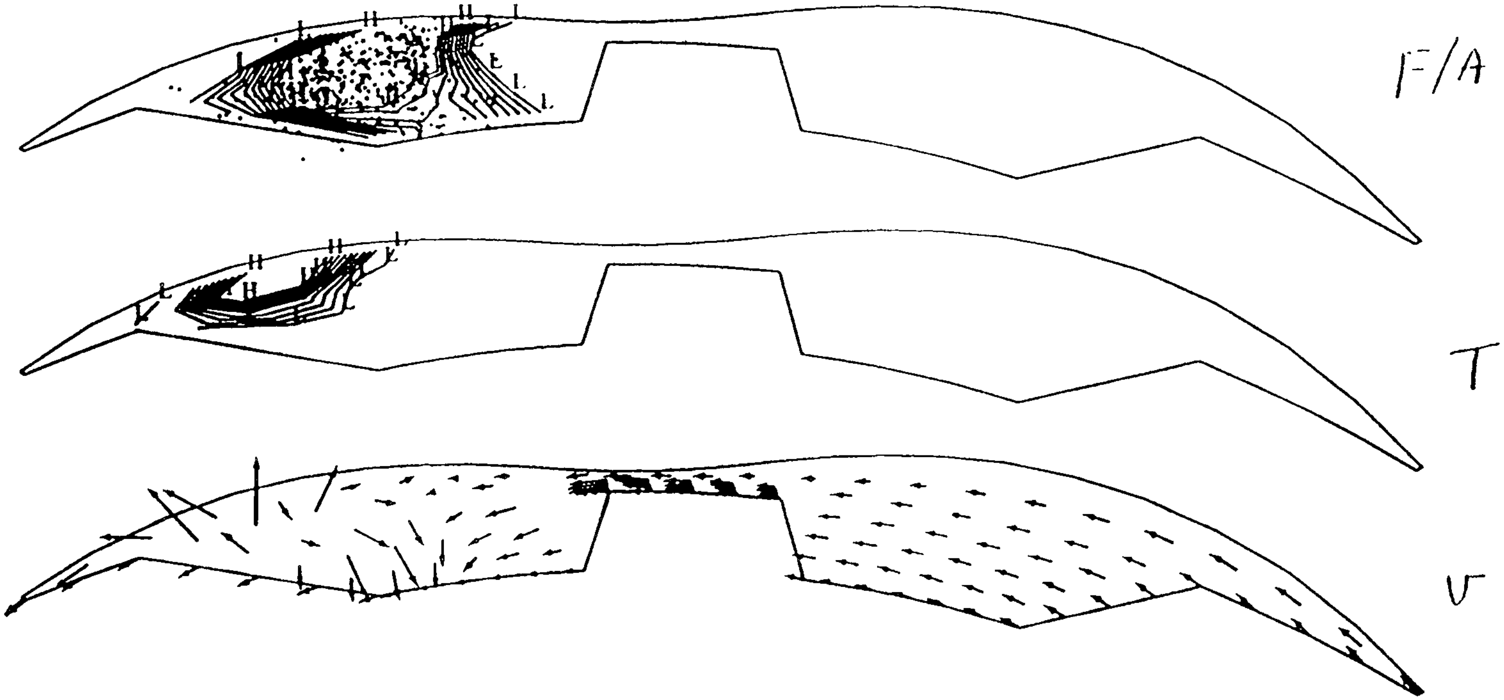

FUEL/AIR RATIO, interval = 0.1000E-01
H = .1200 ; L = .3000E-01
TEMPERATURE, interval = 155.6 K
H = 2100. ; L = 700.0

100 m/s
J = 7

Fig. 18(c): Cross-section view of combustion chamber along symmetry plane showing liquid fuel and vaporized fuel distribution,temperature contours and velocity

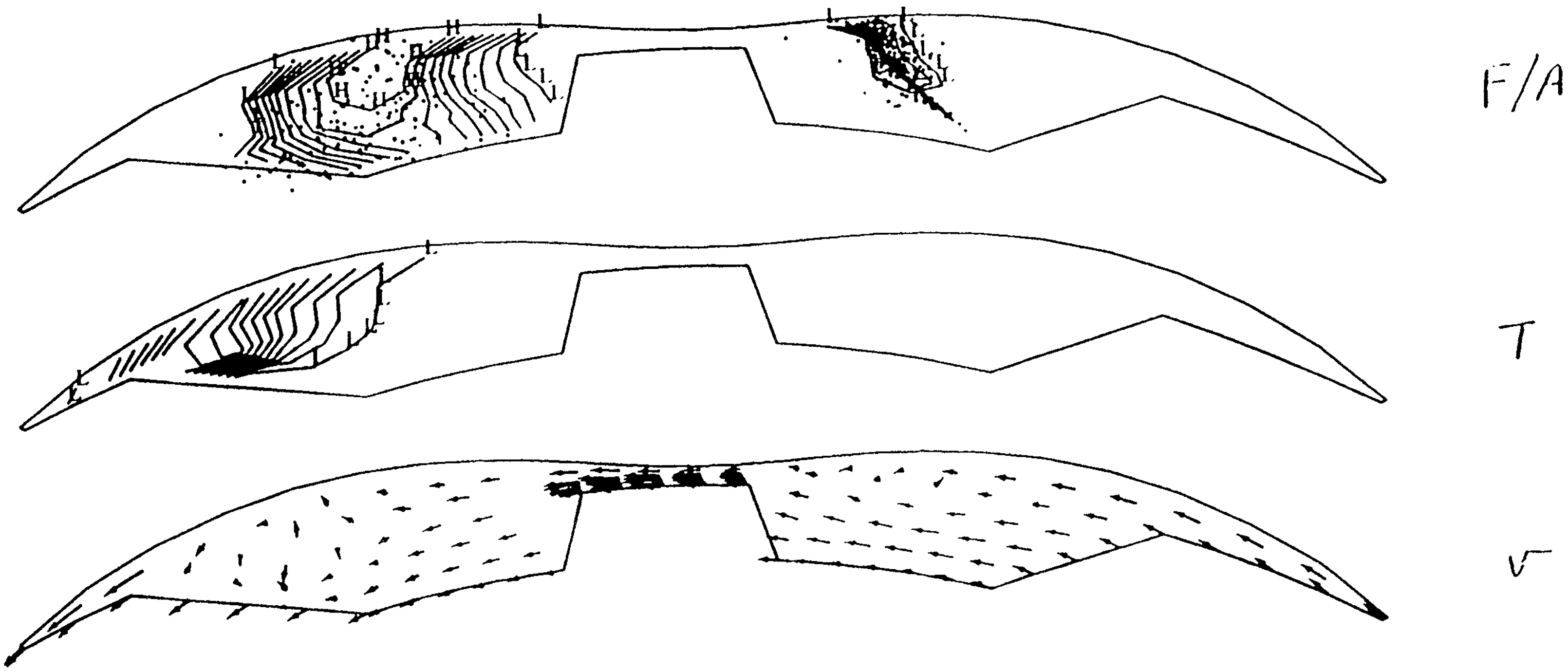

FUEL/AIR RATIO, interval = 0.1000E-01
H = .1200 ; L = .3000E-01
TEMPERATURE, interval = 155.6 K
H = 2100. ; L = 700.0

100 m/s
J = 7

Fig. 18(d): Cross-section view of combustion chamber along symmetry plane showing liquid fuel and vaporized fuel distribution,temperature contours and velocity

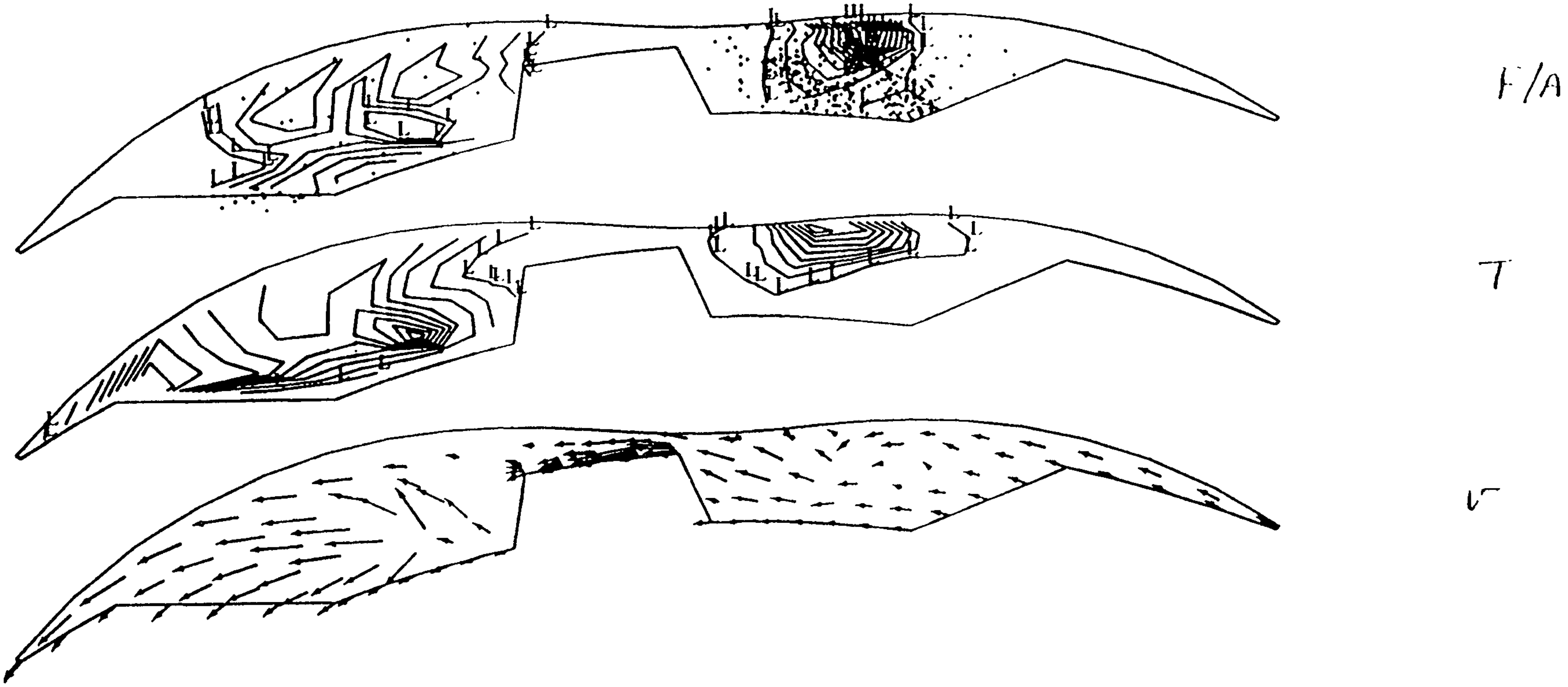

FUEL/AIR RATIO, interval = 0.1000E-01
H = .1200 ; L = .3000E-01
TEMPERATURE, interval = 155.6 K
H = 2100. ; L = 700.0

100 m/s
J = 7

Fig. 18(e): Cross-section view of combustion chamber along symmetry plane showing liquid fuel and vaporized fuel distribution,temperature contours and velocity

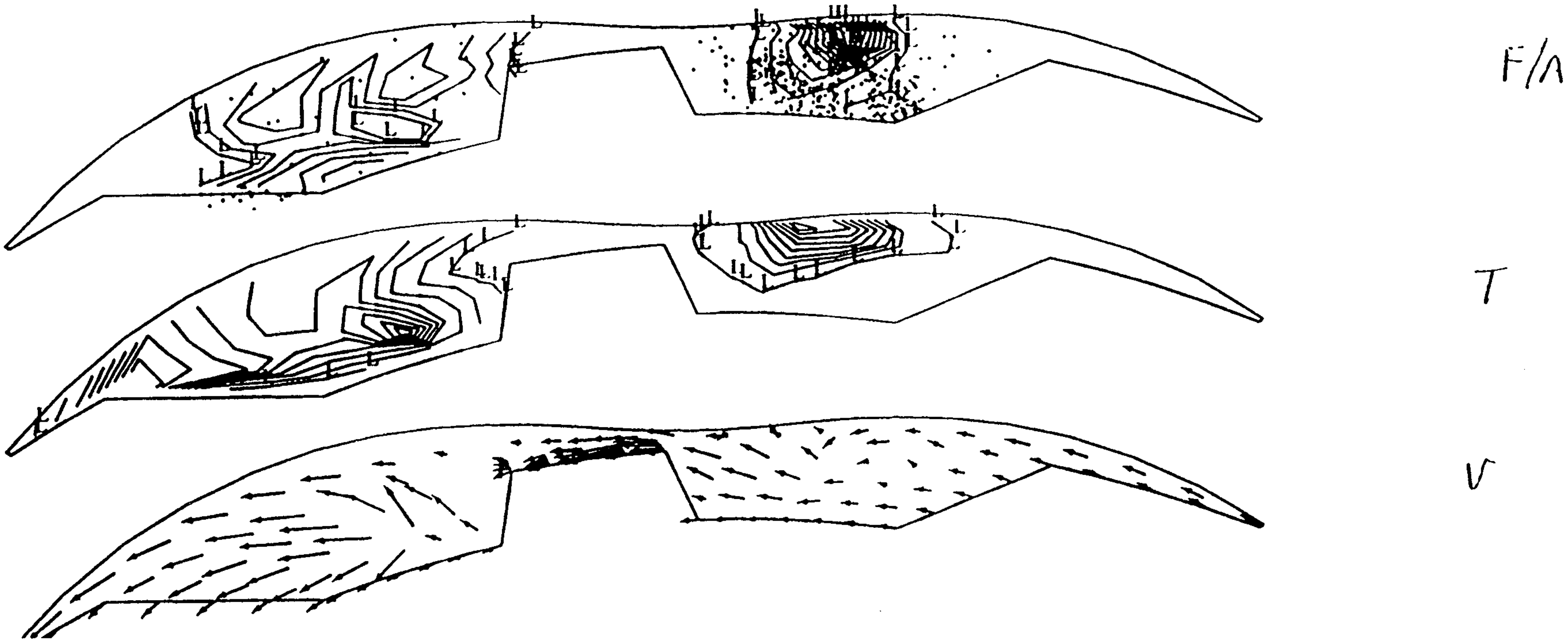

Fig. 18(f): Cross-section view of combustion chamber along symmetry plane showing liquid fuel and vaporized fuel distribution,temperature contours and velocity vectors at 30 CA ATC.

FUEL/AIR RATIO, interval = 0.1000E-01
H = .1200 ; L = .3000E-01
TEMPERATURE, interval = 155.6 K
H = 2100. ; L = 700.0

100 m/s
TEMPERATURE, interval = 155.6 K
H = 2100. ; L = 700.0

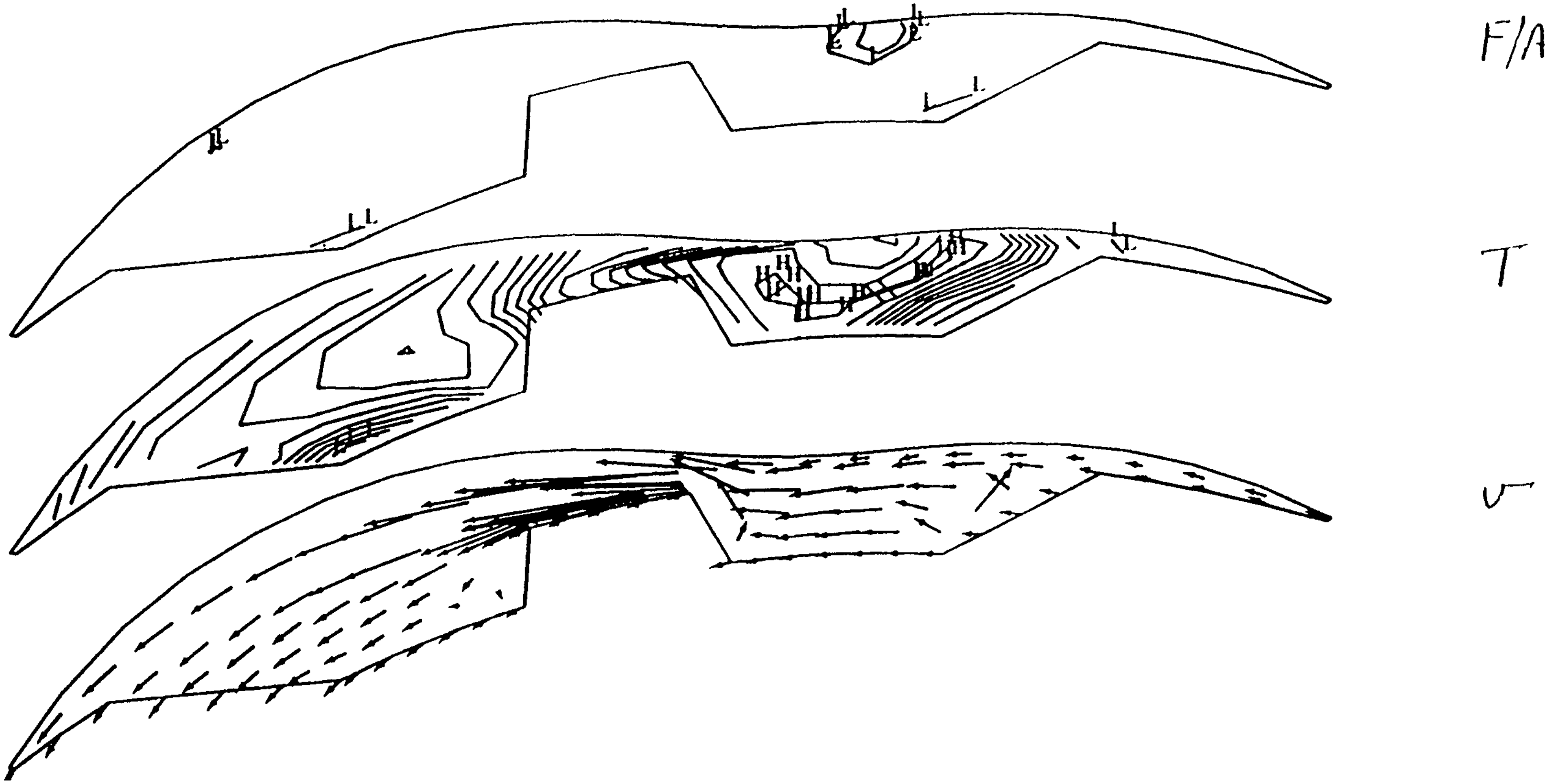

Fig. 18(g): Cross-section view of combustion chamber along symmetry plane showing liquid fuel and vaporized fuel distribution,temperature contours and velocity vectors at 45 CA ATC.

TEMPERATURE, interval = 0.1000E-01K
H = .1200 ; L = .3000E-01
FUEL/AIR RATIO, interval = 0.1000E-01
H = .1200 ; L = .3000E-01
TEMPERATURE, interval = 155.6 K
H = 2100. ; L = 700.0

100 m/s

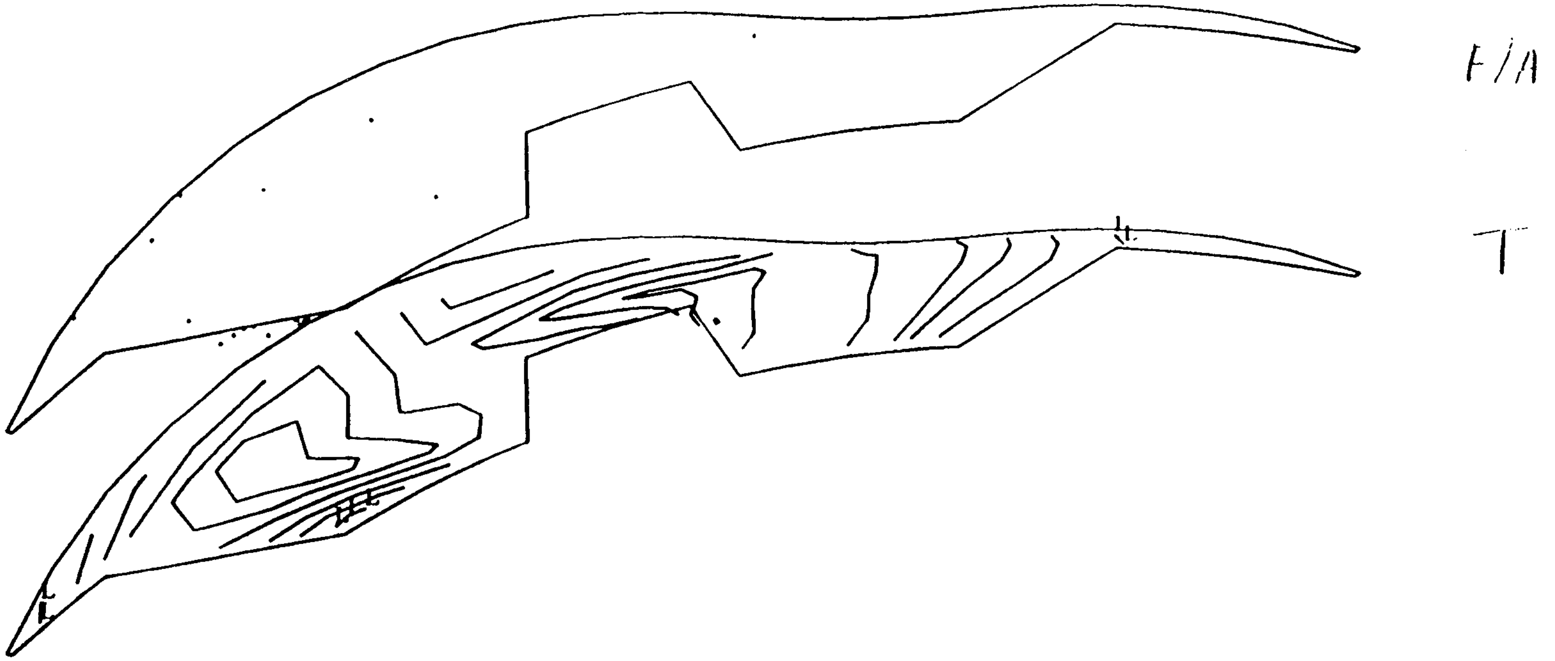

Fig. 18(h): Cross-section view of combustion chamber along symmetry plane showing liquid fuel and vaporized fuel distribution and temperature contours at 60 CA ATC.

FUEL/AIR RATIO, interval = 0.1000E-01
H = .1200 ; L = .3000E-01
TEMPERATURE, interval = 155.6 K
H = 2100. ; L = 700.0
TEMPERATURE, interval = 22.22 K
H = 2300. ; L = 2100.
TEMPERATURE, interval = 11.11 K
H = 2200. ; L = 2100.

Fig. 19: DUAL CHAMBER PRESSURES WITH AND WITHOUT COMBUSTION

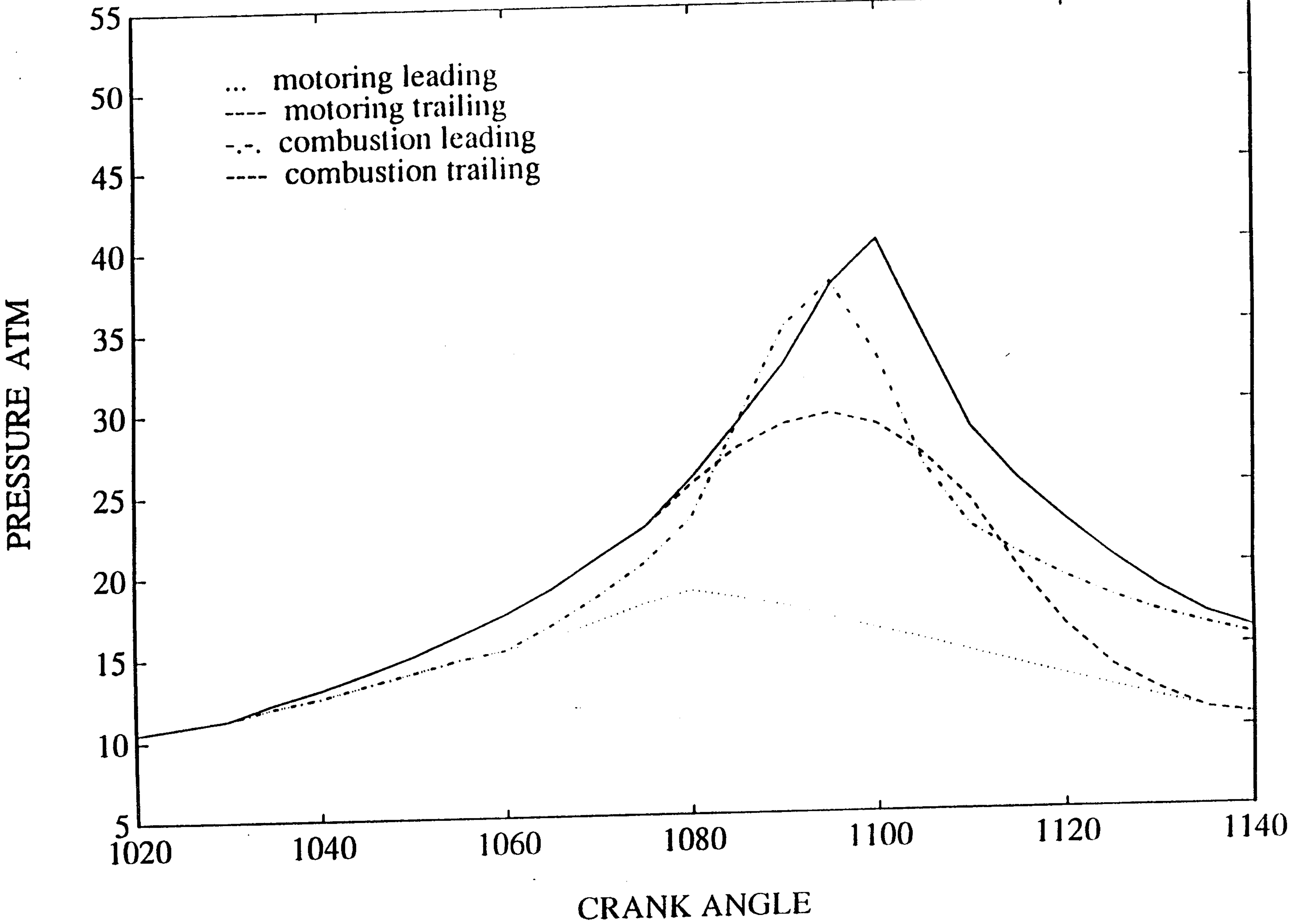

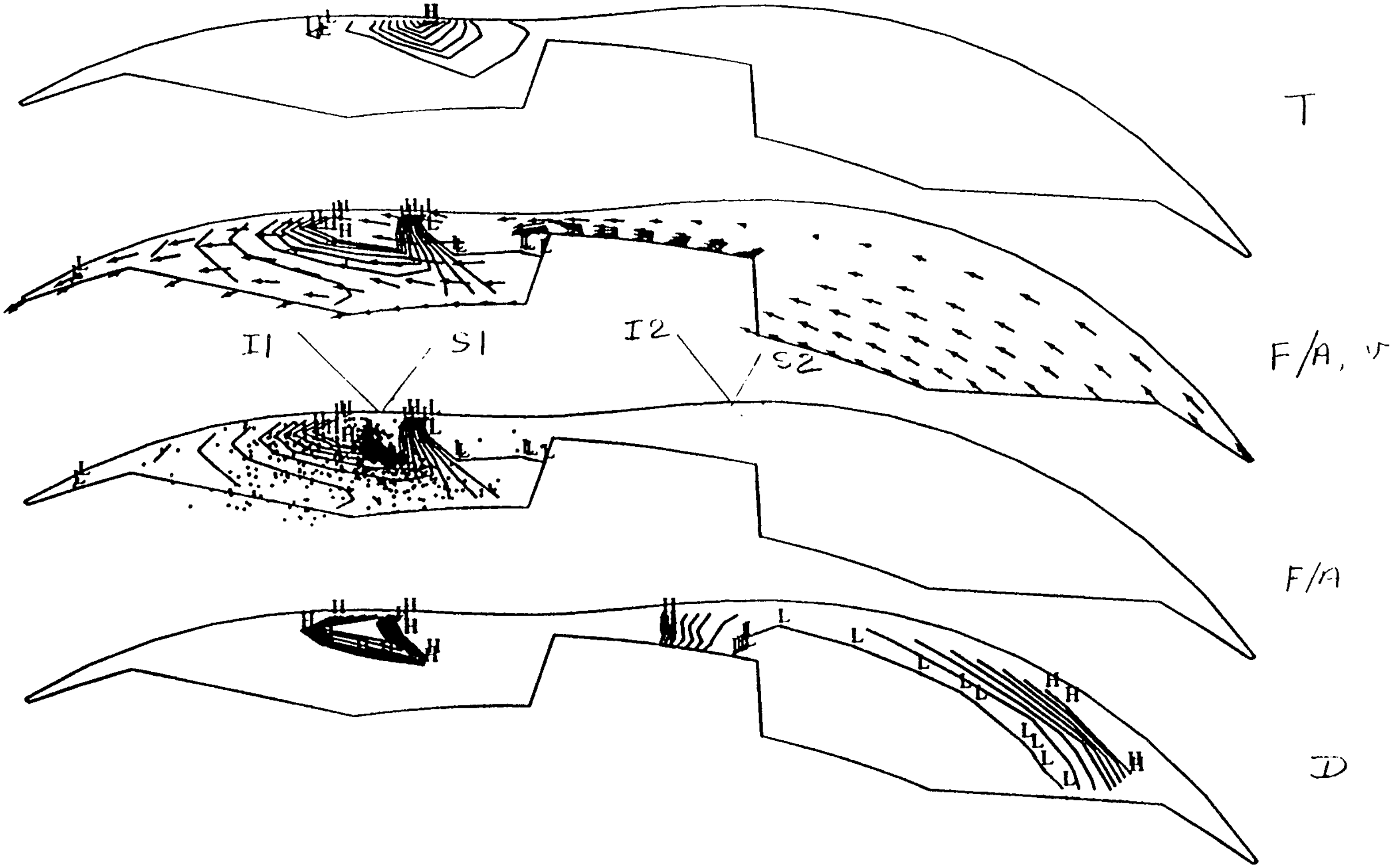

Fig. 20(a): Cross-section view of combustion chamber along symmetry plane showing temperature, vaporized fuel distribution and velocity vectors, vaporized and liquid fuel distribution, and diffusivity contours at 1050 CA.

TEMPERATURE, interval = 177.8 K
H = 2100. ; L = 500.0
FUEL/AIR RATIO, interval = 0.2122E-01
H = .2000 ; L = .9000E-02

100 m/s
FUEL/AIR RATIO, interval = 0.2122E-01
H = .2000 ; L = .9000E-02
DIFFUSIVITY, interval = 71.43 cm2/s

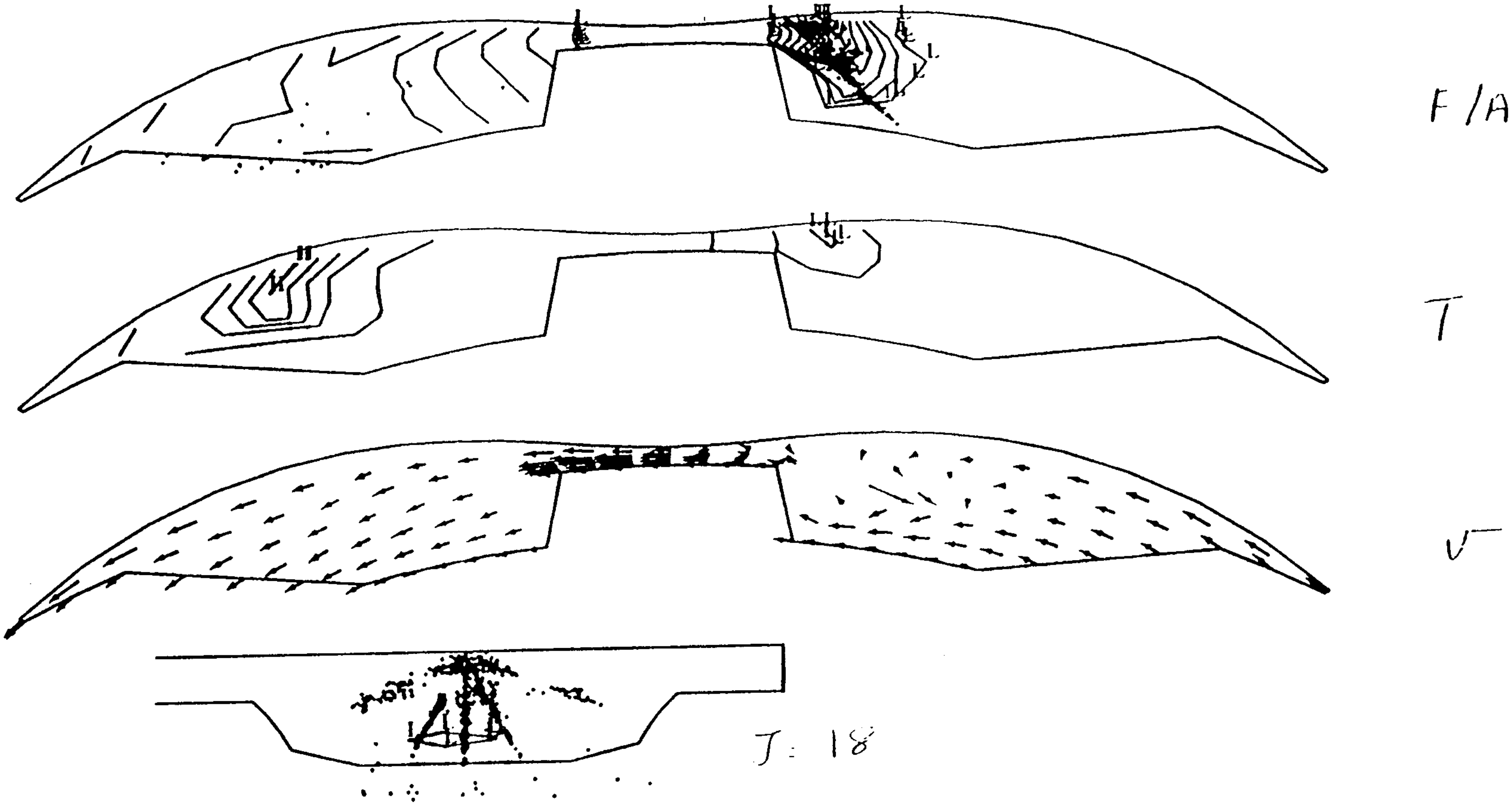

Fig. 20(b): Cross-section view of combustion chamber along symmetry plane showing liquid fuel and vaporized fuel distribution ,temperature and velocity vectors at 1080 CA (top center).

FUEL/AIR RATIO, interval = 0.1122E-01
H = .1100 ; L = .9000E-02
TEMPERATURE, interval = 91.00 K
H = 980.0 ; L = 525.0

——→
100 m/s
FUEL/AIR RATIO, interval = 0.1122E-01
H = .1100 ; L = .9000E-02

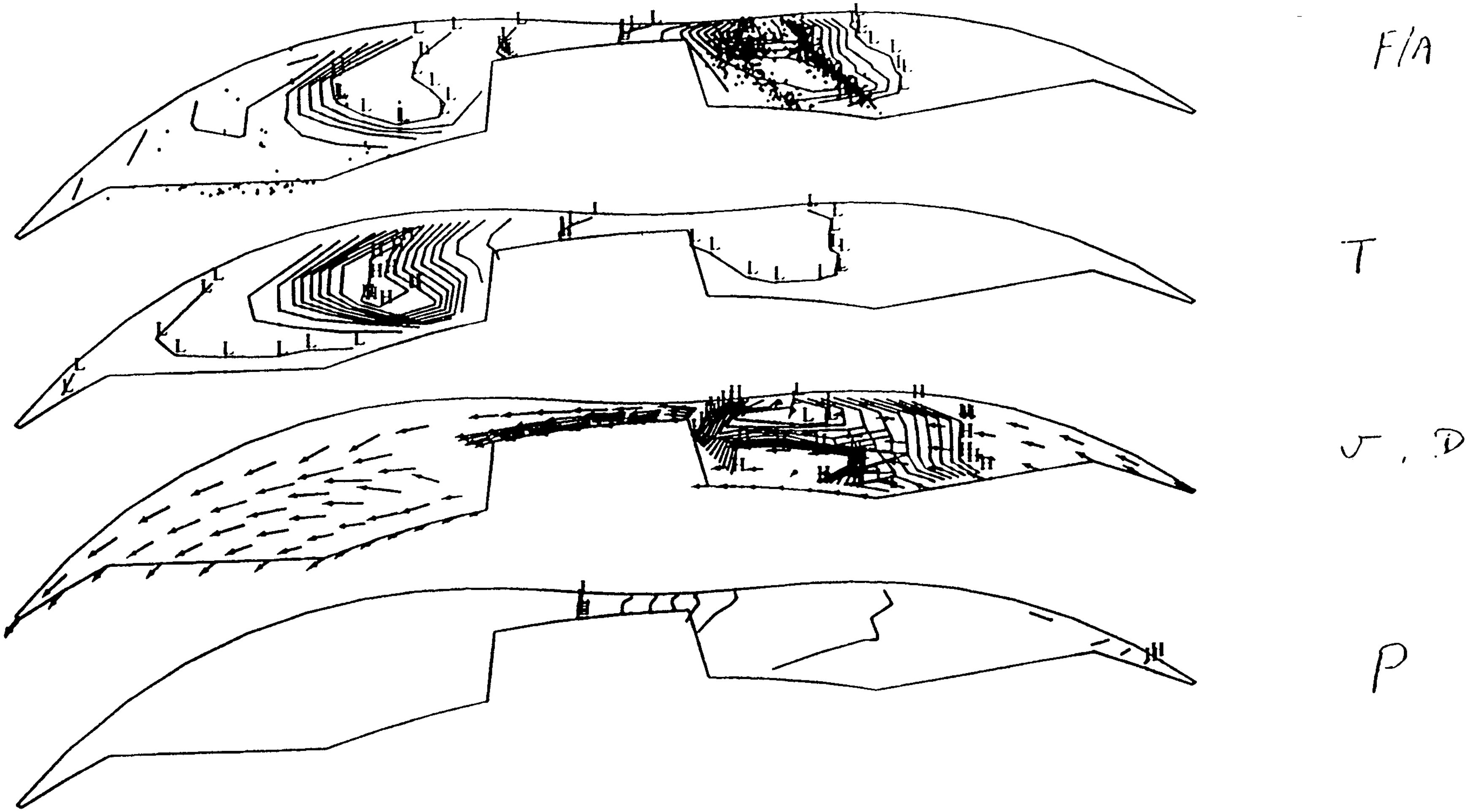

Fig. 20(c): Cross-section view of combustion chamber along symmetry plane showing liquid fuel and vaporized fuel distribution,temperature contours, velocity vectors and pressure contours at 15 CA ATC.

FUEL/AIR RATIO, interval = 0.1456E-01

H = .1400 ; L = .9000E-02

TEMPERATURE, interval = 166.7 K

H = 2100. ; L = 600.0

⟶

100 m/s

DIFFUSIVITY, interval = 77.78 cm2/s

H = 800.0 ; L = 100.0

PRESSURE, interval = 0.3889E+07dyne/cm2

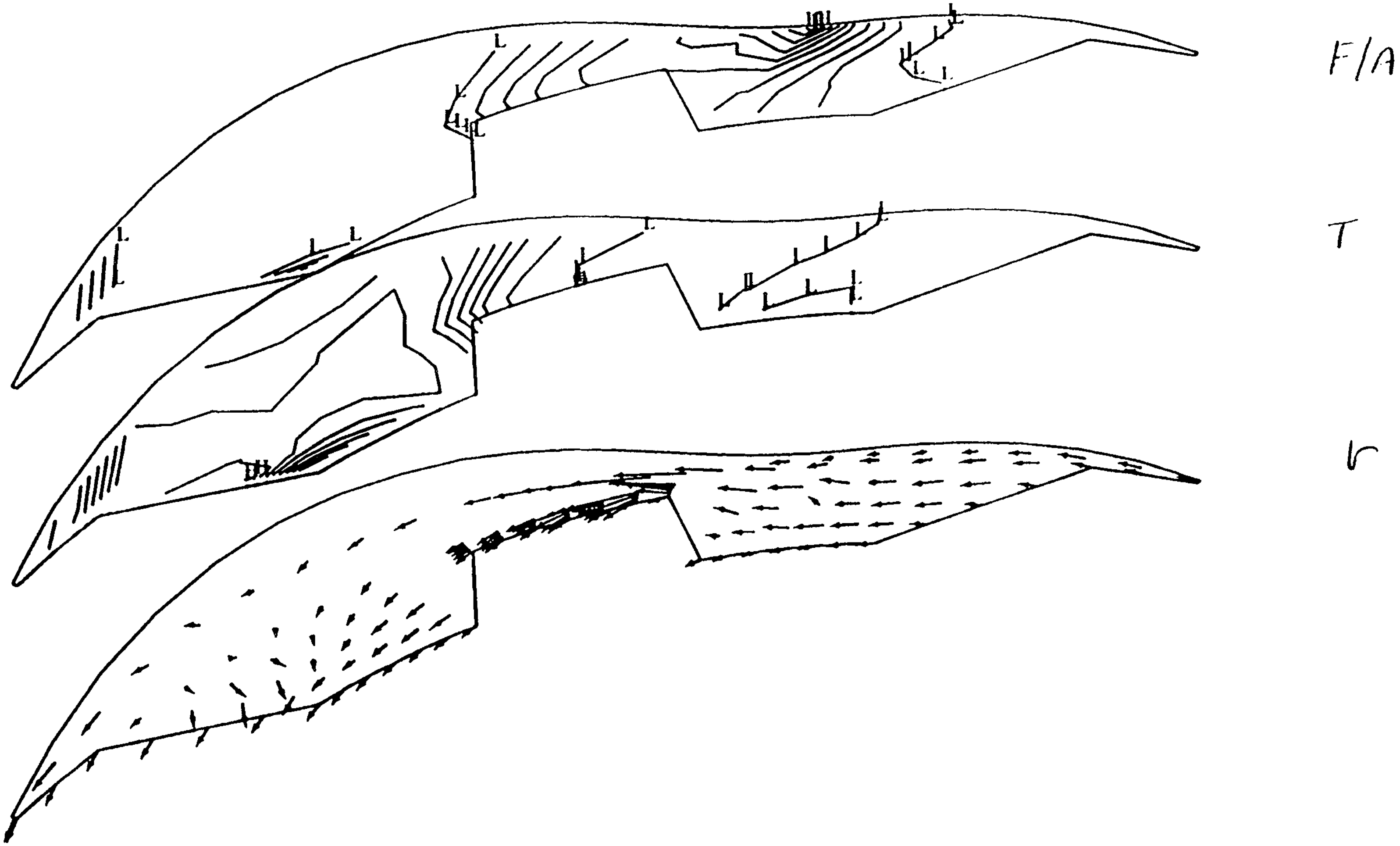

Fig. 20(d): Cross-section view of combustion chamber along symmetry plane showing liquid fuel and vaporized fuel distribution,temperature contours and velocity vectors at 45 CA ATC.

FUEL/AIR RATIO, interval = 0.1233E-01
H = .1200 ; L = .9000E-02
TEMPERATURE, interval = 166.7 K
H = 2100. ; L = 600.0

100 m/s
J = 7
crank angle = 44.8

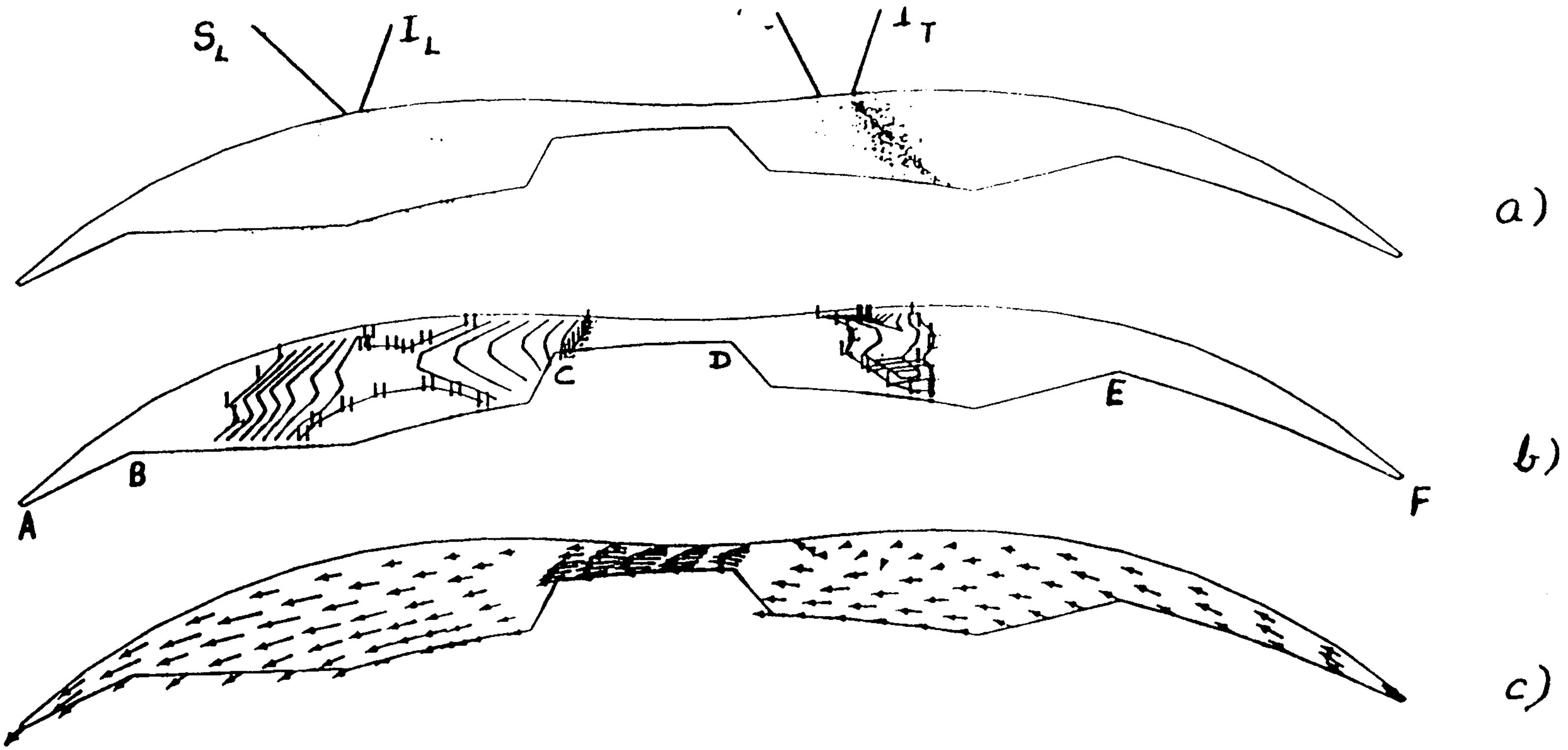

Fig. 21: Computed liquid particle distribution (a), vaporized fuel-air distribution (b) and velocity flowfield for the dual-pocket rotor at TDC.

MASS FRACTION OF FUEL, interval = 0.1286E-01
H = .1200 ; L = .3000E-01

100 m/s
vertex limits of the region: (1, 7, 1) to (25, 7, 8)

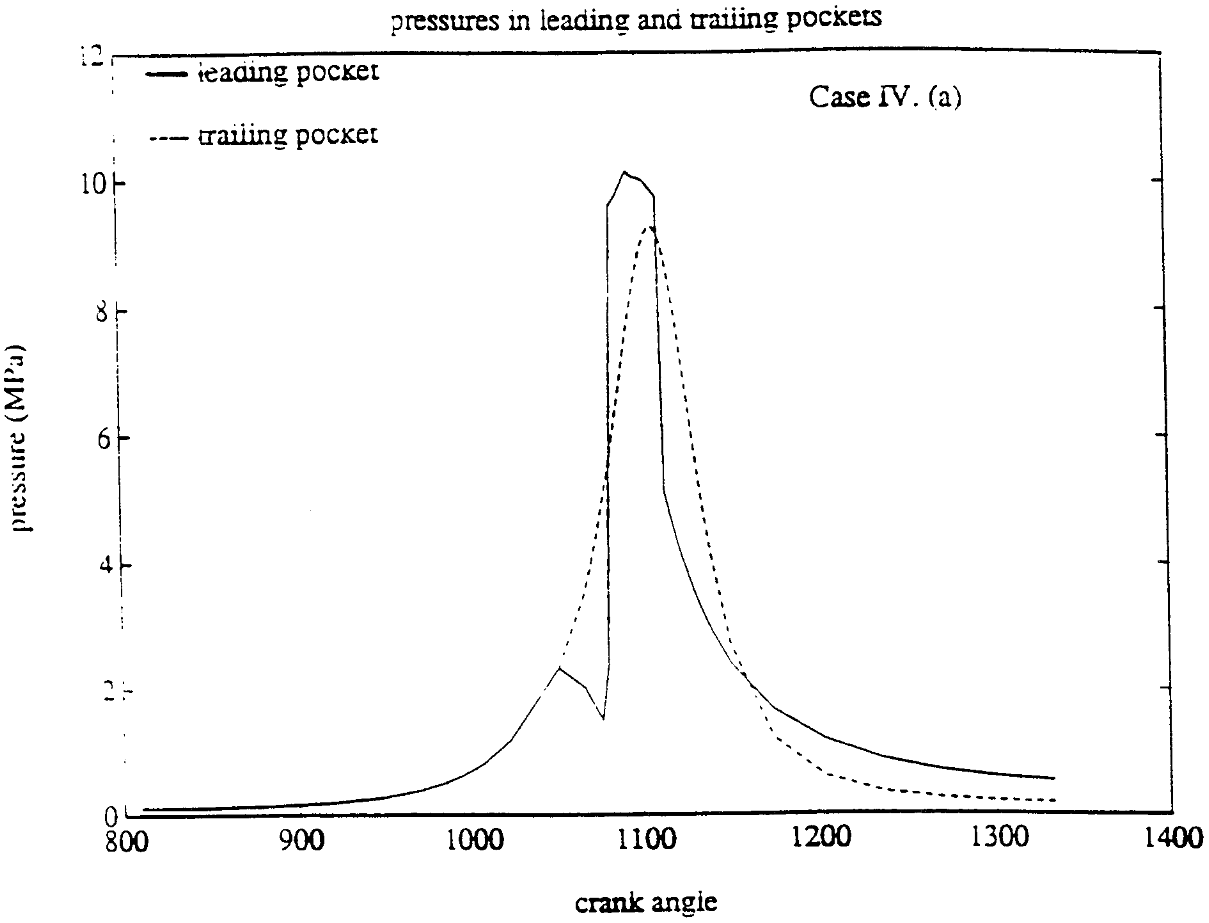

Fig. 22 (a): Computed pressures in the leading and the trailing pockets at high load (about 200 PSI IMEP) with 25% of fuel injected into trailing pocket and 75% of fuel injected into the leading pocket - Case (a)

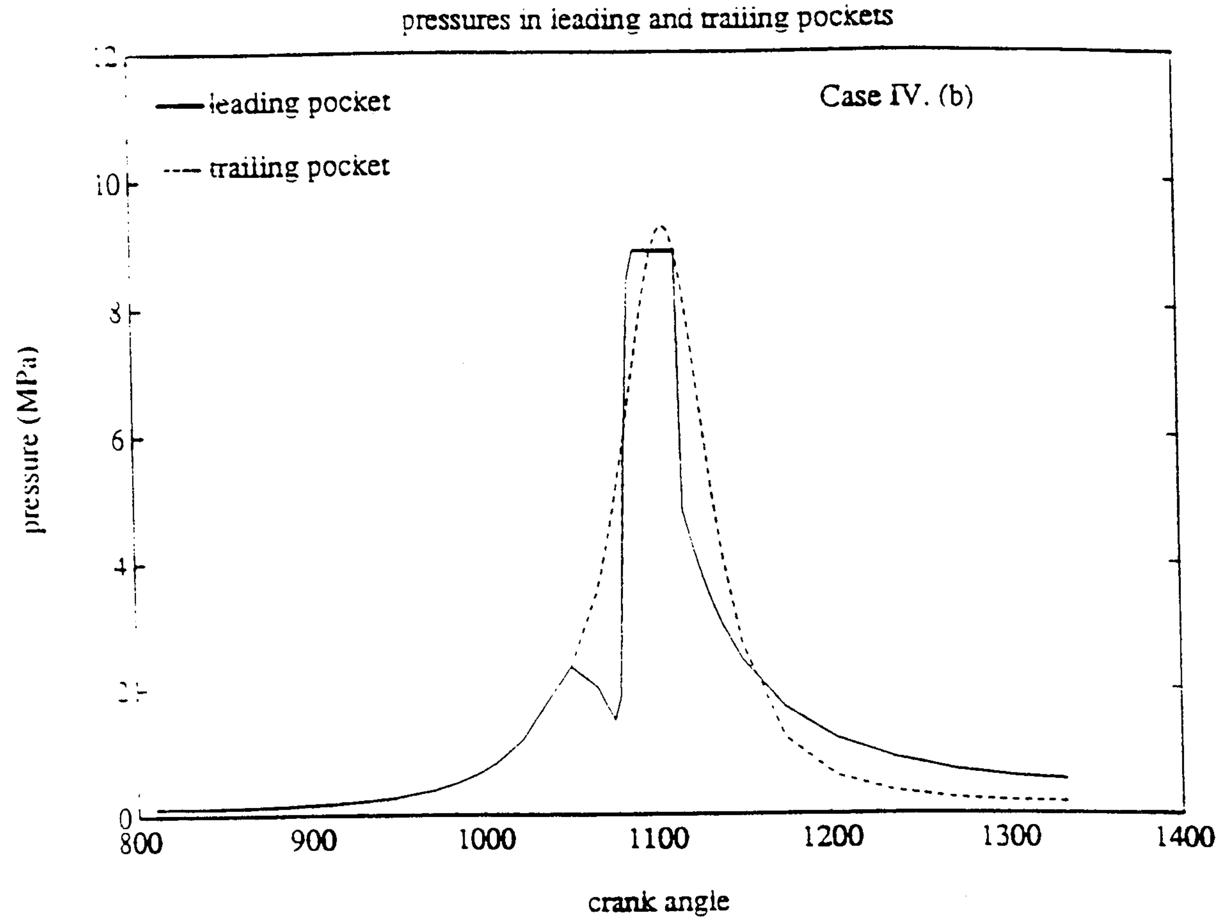

Fig. 22 (b): Computed pressures in the leading and trailing pockets with 25% of high load fuel (i.e. quantity in Case a) injected into trailing pocket and 50% of high load quantity of fuel injected into leading pocket - Case (b)

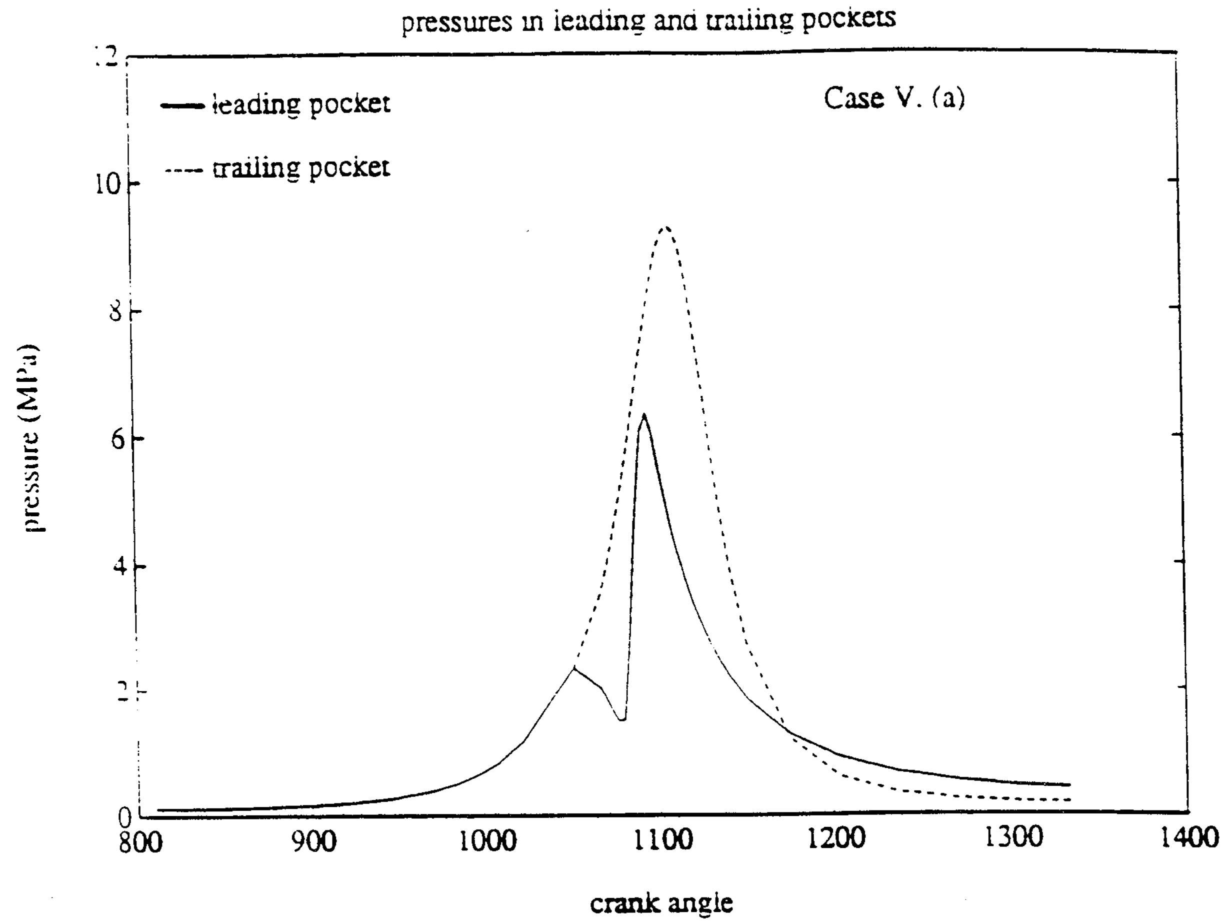

Fig. 22 (c): Computed pressures in the leading and trailing pockets with 25% of high load fuel (i.e. quantity in Case a) injected into trailing pocket and 25% of high load quantity of fuel injected into leading pocket - Case (c)

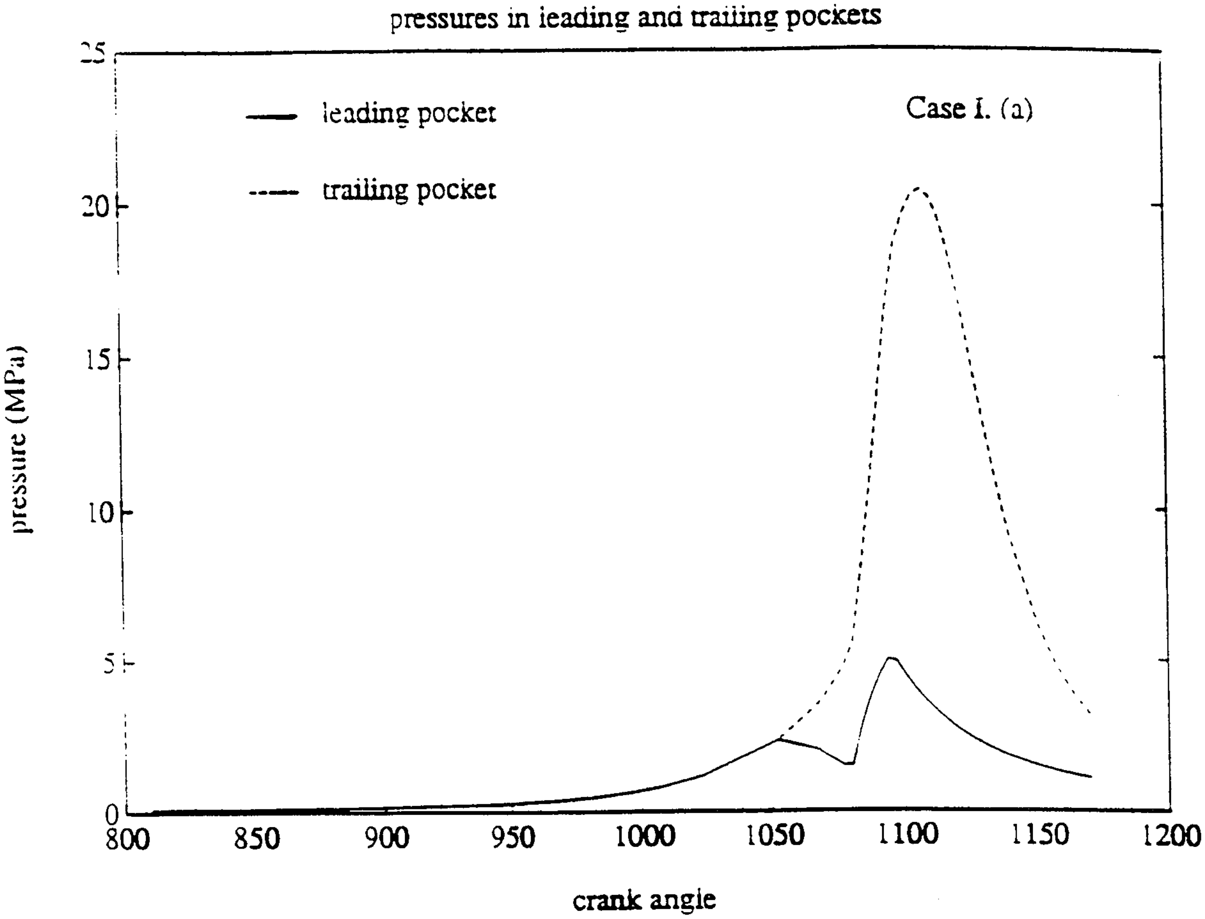

Fig. 23 (a): Computed pressures in the leading and trailing pockets when injection and spark timings for trailing pocket are adjusted to obtain 5% to 95% of mass fraction burned between 0 and 30 CA ATC.

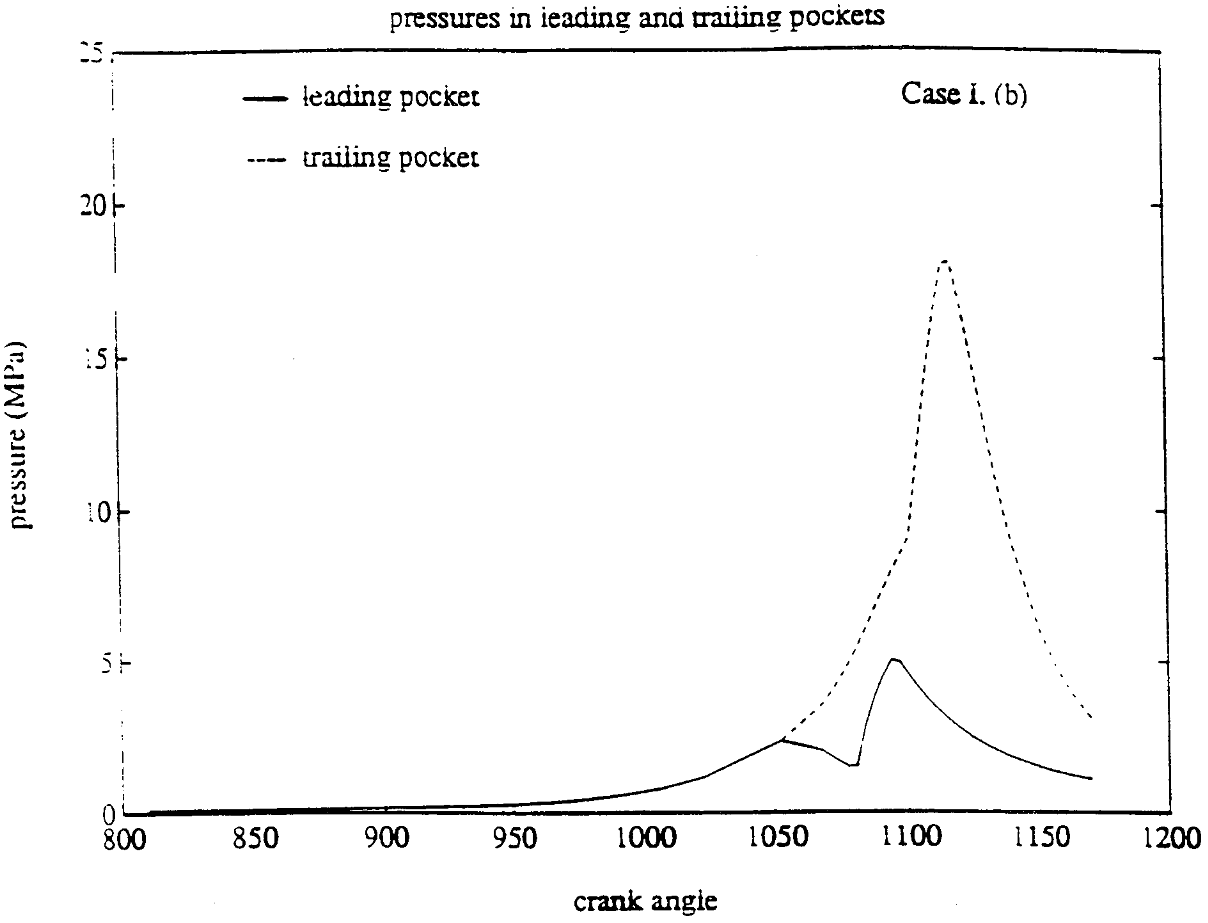

Fig. 23 (b): Computed pressures in the leading and trailing pockets when injection and spark timings for trailing pocket are adjusted to obtain 5% to 95% of mass fraction burned between 20 and 55 CA ATC.

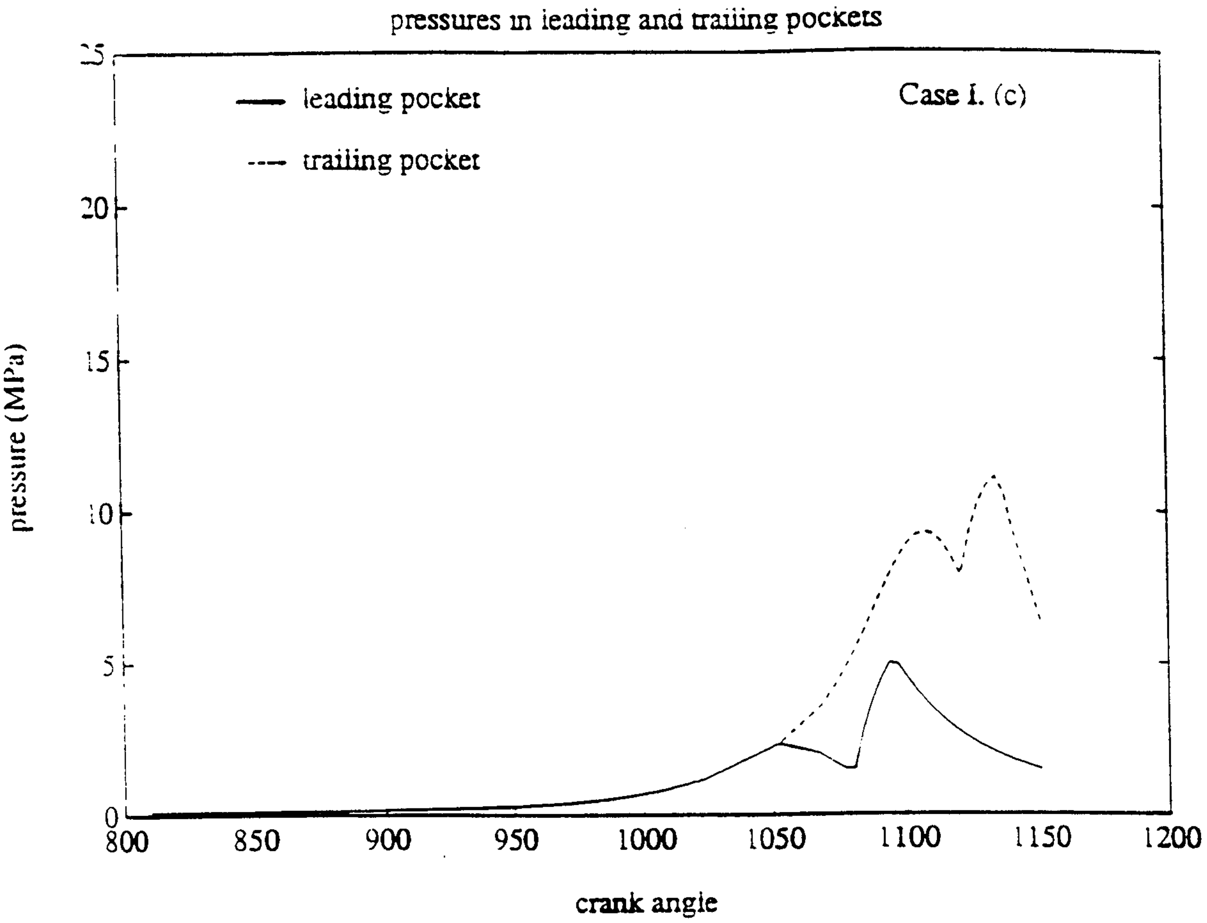

Fig. 23 (c): Computed pressures in the leading and trailing pockets when injection and spark timings for trailing pocket are adjusted to obtain 5% to 95% of mass fraction burned between 50 and 75 CA ATC.

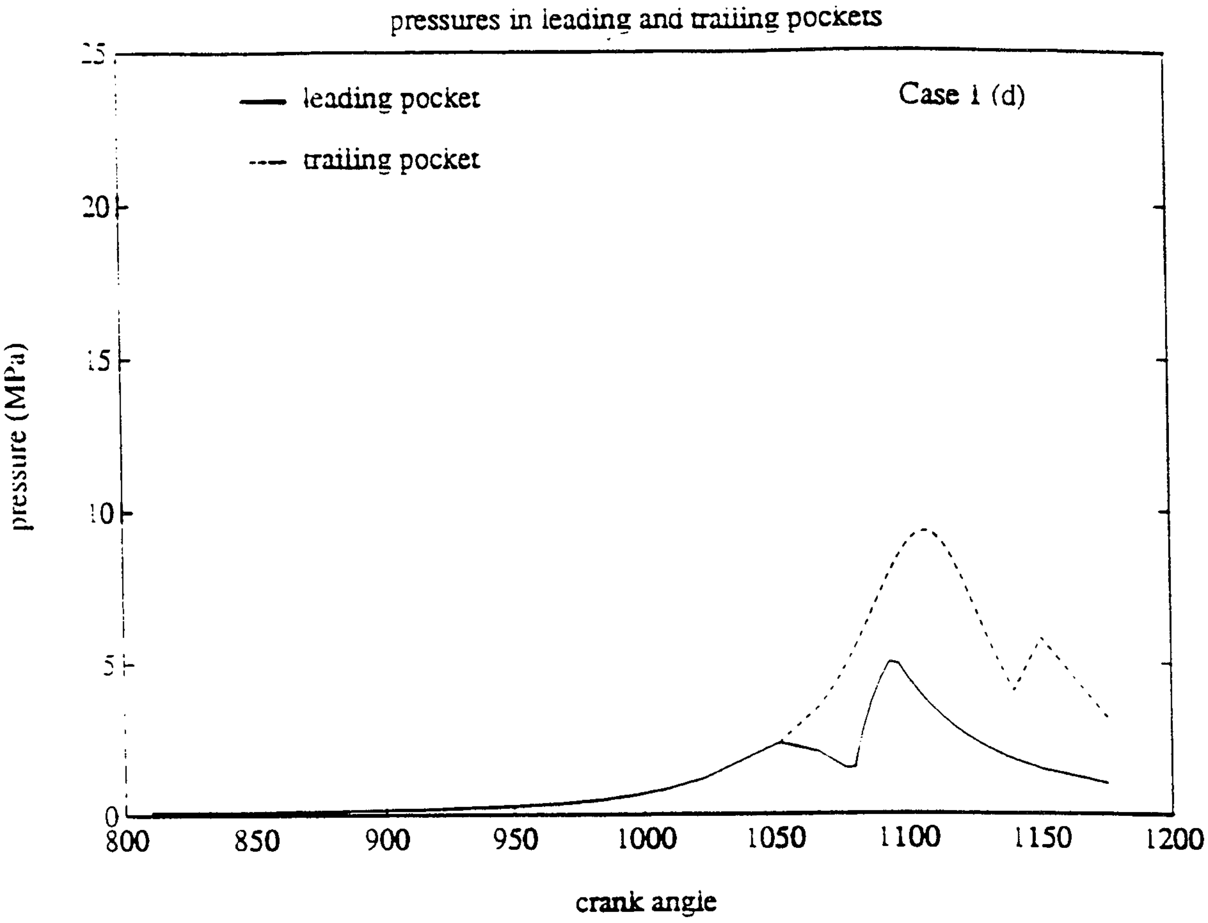

Fig. 23 (d): Computed pressures in the leading and trailing pockets when injection and spark timings for trailing pocket are adjusted to obtain 5% to 95% of mass fraction burned between 60 and 95 CA ATC.

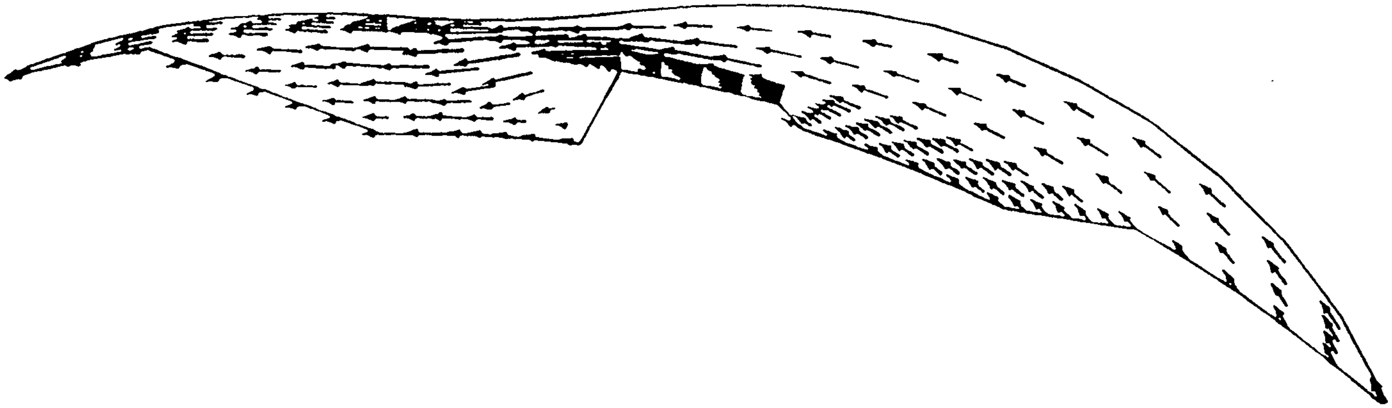

100 m/s
vertex limits of the region: (1, 7, 1) to (25, 7,11)

Fig. 24 (a): Velocity flowfield in the symmetry plane at 1135 CA

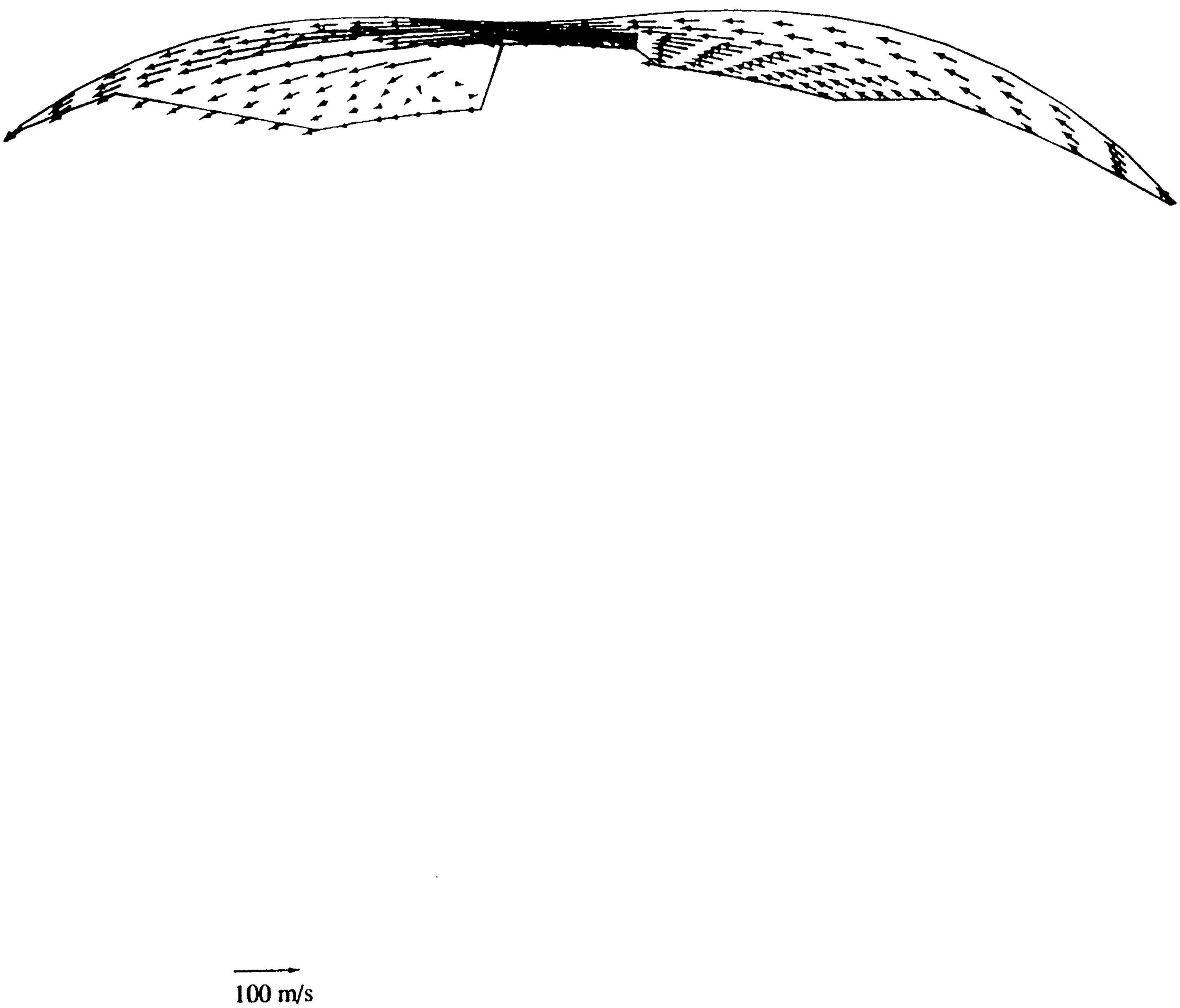

vertex limits of the region: (1, 7, 1) to (25, 7,11)

Fig. 24(b): Velocity flowfield in the symmetry plane at 1165 CA

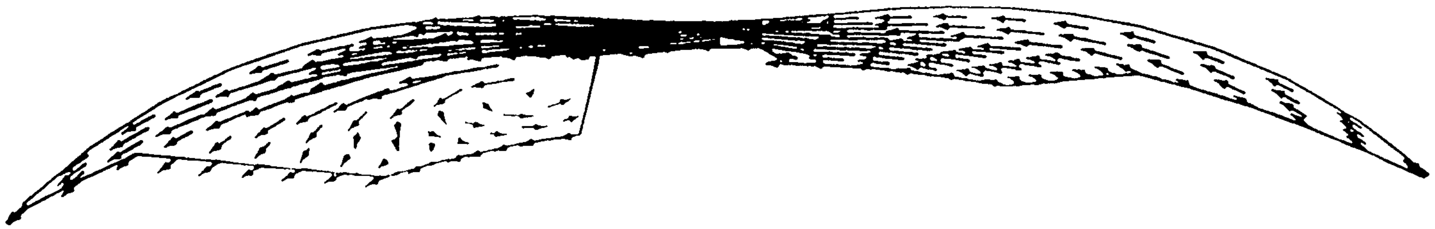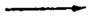

100 m/s

vertex limits of the region: (1, 7, 1) to (25, 7,11)

[illegible]

Fig.24(c): Velocity flowfield in the symmetry plane at 1170CA

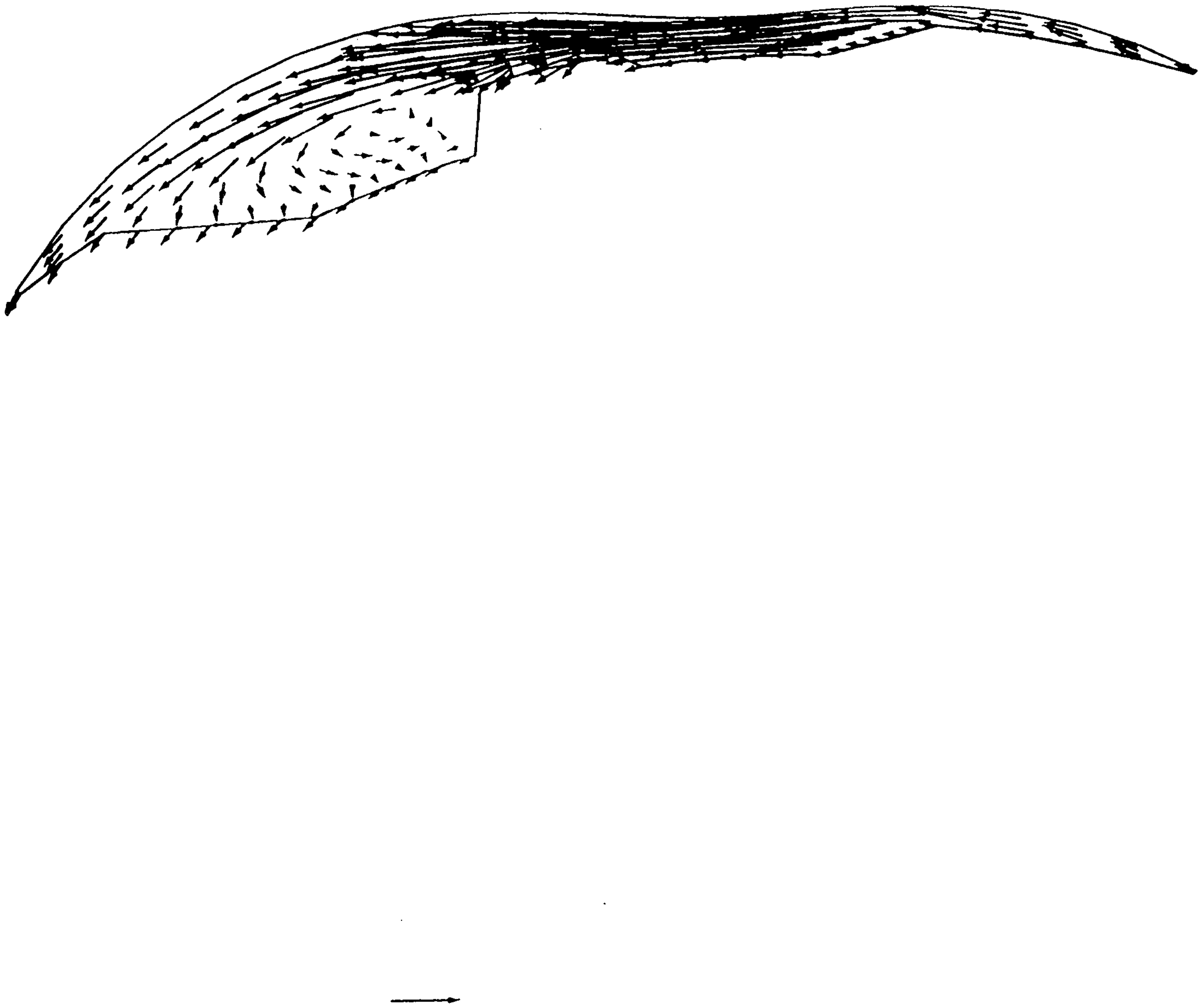

vertex limits of the region: (1, 7, 1) to (25, 7,11)

Fig.24(d): Velocity flowfield in the symmetry plane at 30 CA

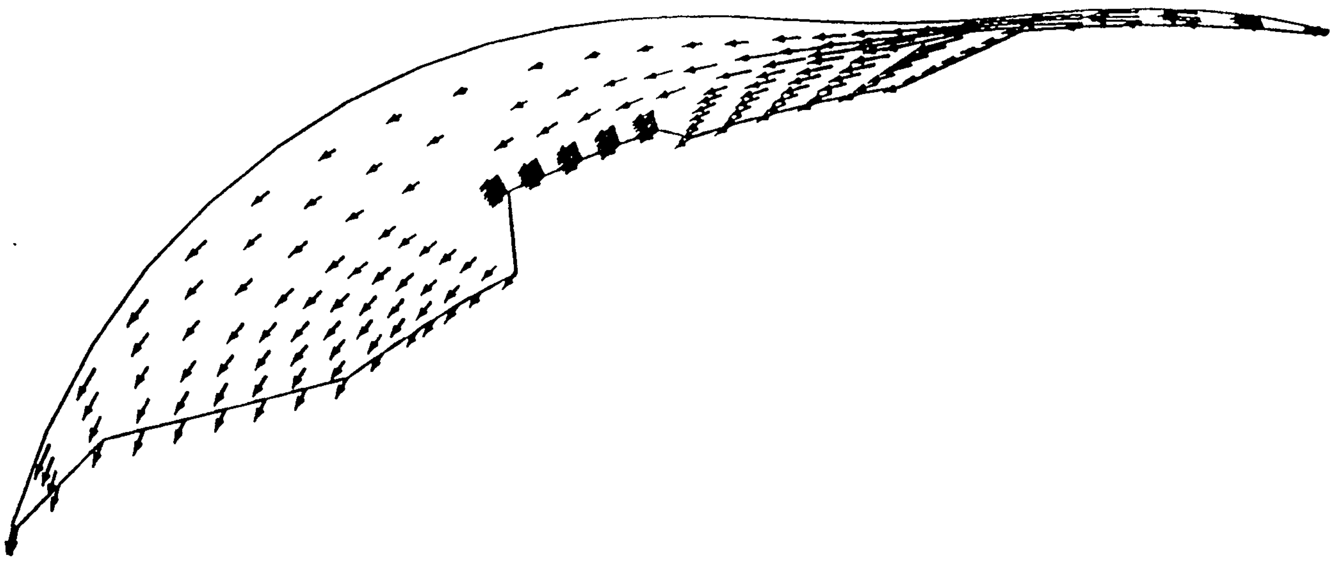

100 m/s

vertex limits of the region: (1, 7, 1) to (25, 7,11)

Fig.24(e): Velocity flowfield in the symmetry plane at 60 CA

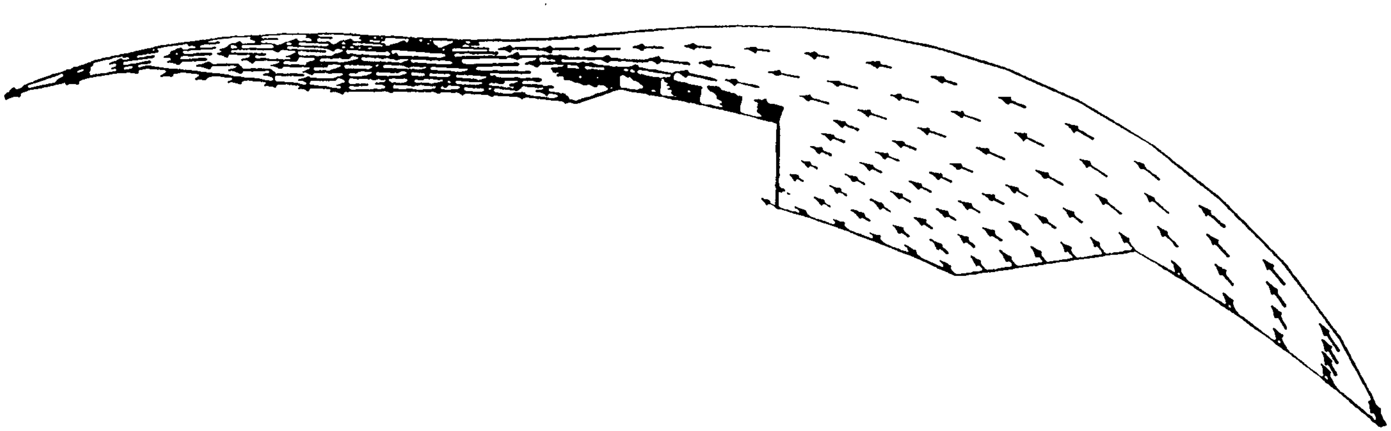

100 m/s

vertex limits of the region: (1, 7, 1) to (25, 7,11)

Fig. 25(a): Velocity flowfield in the symmetry plane at 1135CA

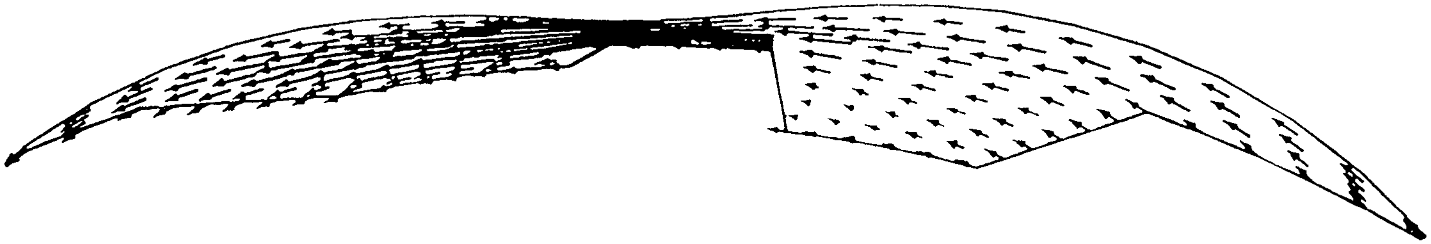

100 m/s

vertex limits of the region: (1, 7, 1) to (25, 7,11)

Fig. 25(b): Velocity flowfield in the symmetry plane at 1165CA

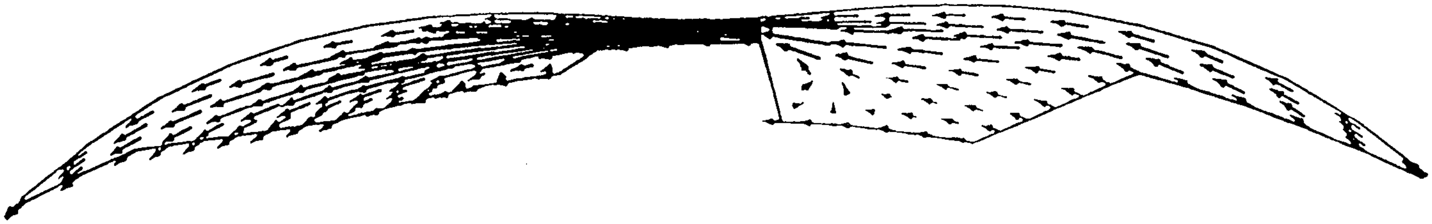

100 m/s

vertex limits of the region: (1, 7, 1) to (25, 7,11)

Fig.25(c): Velocity flowfield in the symmetry plane at 1170 CA

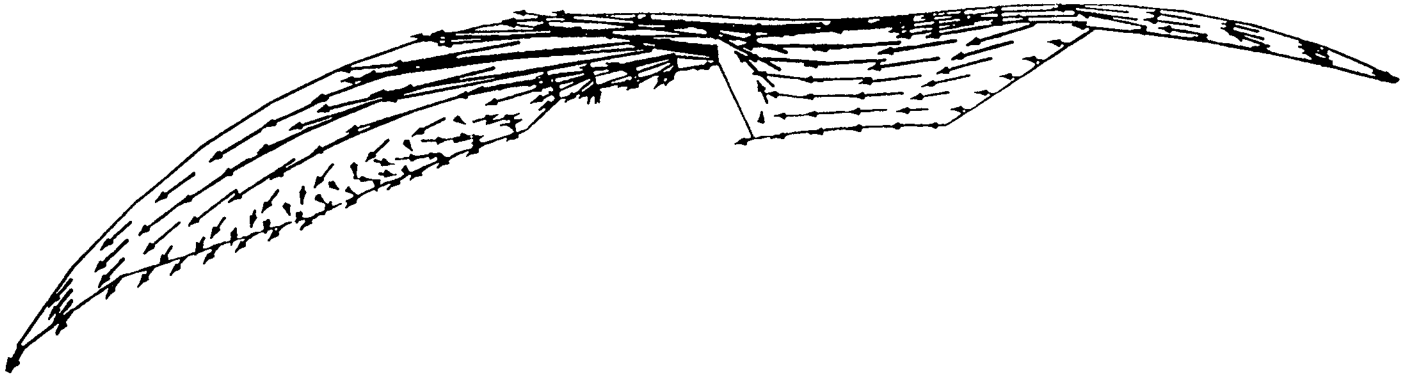

100 m/s
vertex limits of the region: (1, 7, 1) to (25, 7,11)

Fig.25(d): Velocity flowfield in the symmetry plane at 30 CA

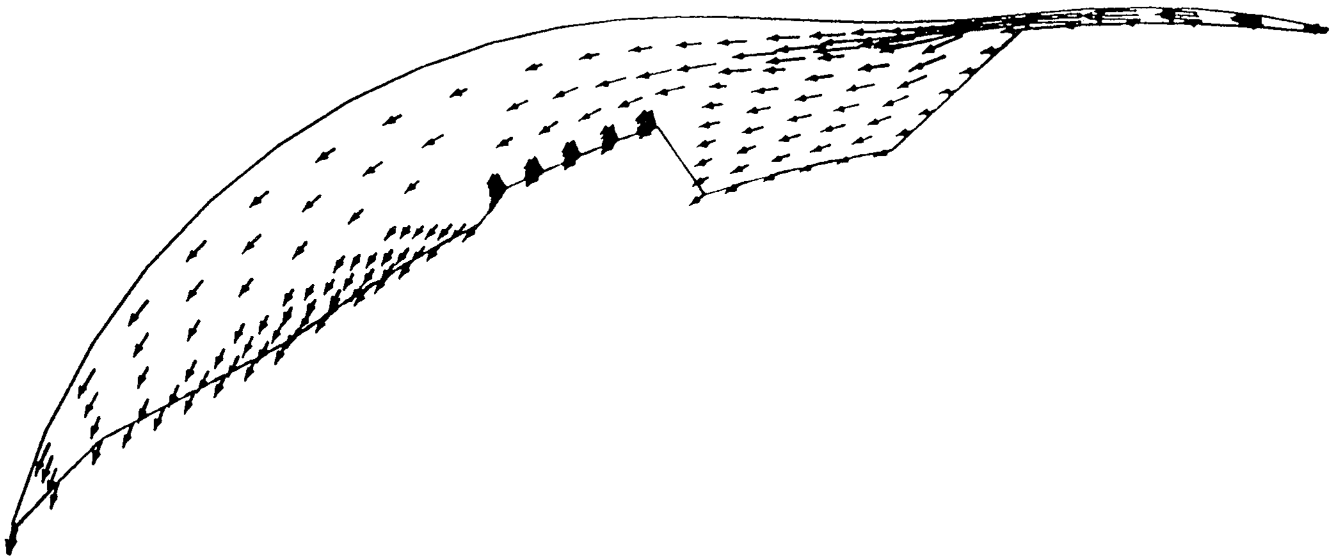

100 m/s
vertex limits of the region: (1, 7, 1) to (25, 7,11)

Fig.25(e): Velocity flowfield in the symmetry plane at 60CA

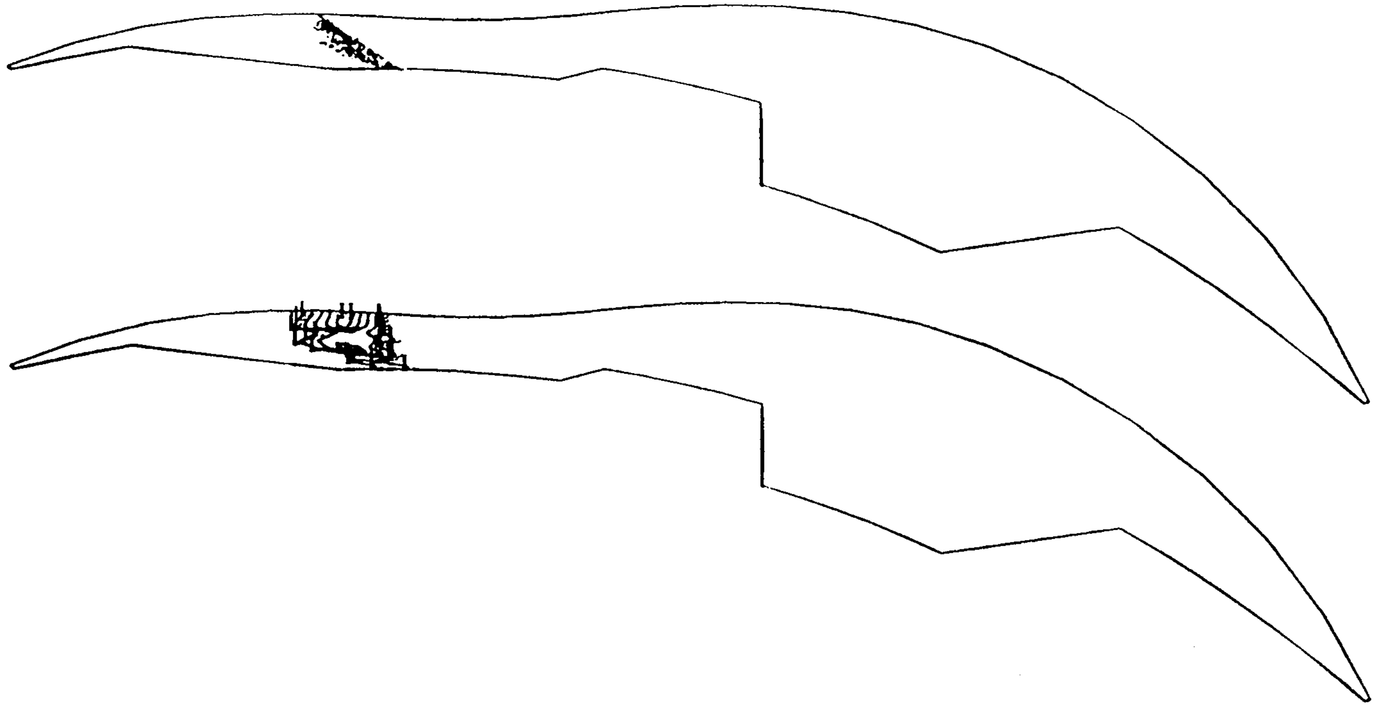

MASS FRACTION OF FUEL, interval = 0.18000E-01
H = 0.12000 ; L = 0.30000E-01
vertex limits of the region: (1, 7, 1) to (25, 7,11)
crank angle = 15.0

Fig.26(a): Particle at fuel/air distribution in chamber at 1135 CA

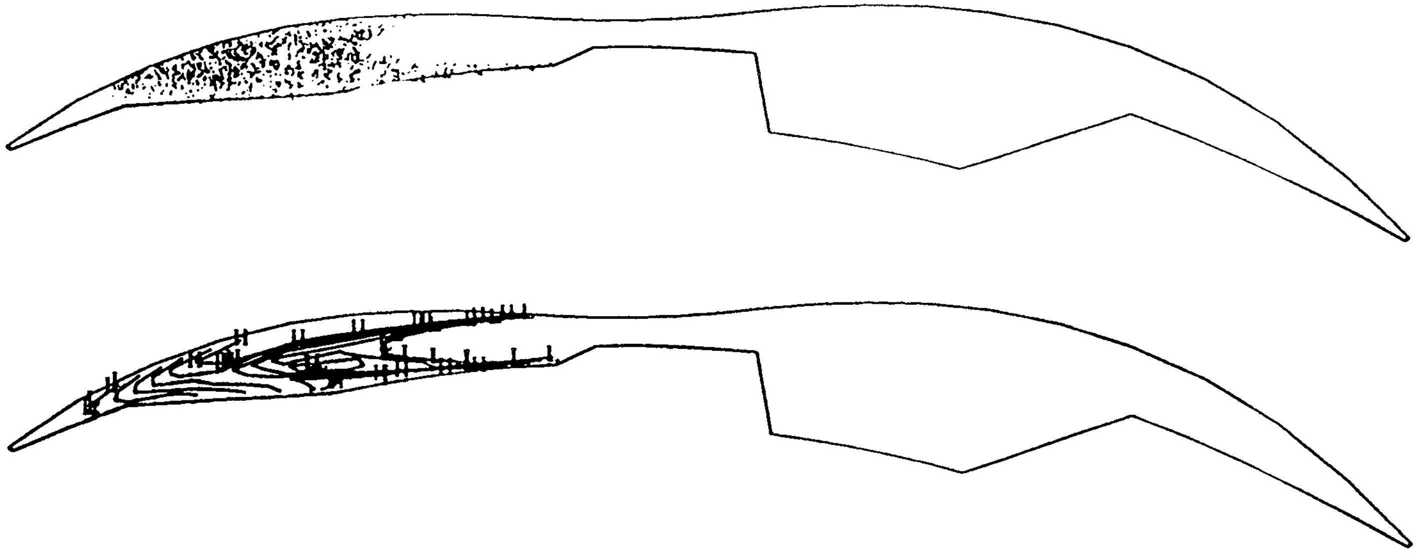

MASS FRACTION OF FUEL, interval = 0.18000E-01
H = 0.12000 ; L = 0.30000E-01
vertex limits of the region: (1, 7, 1) to (25, 7,11)
crank angle = 25.0

Fig.26(b): Particle and fuel/air distribution in the chamber at 1165 CA

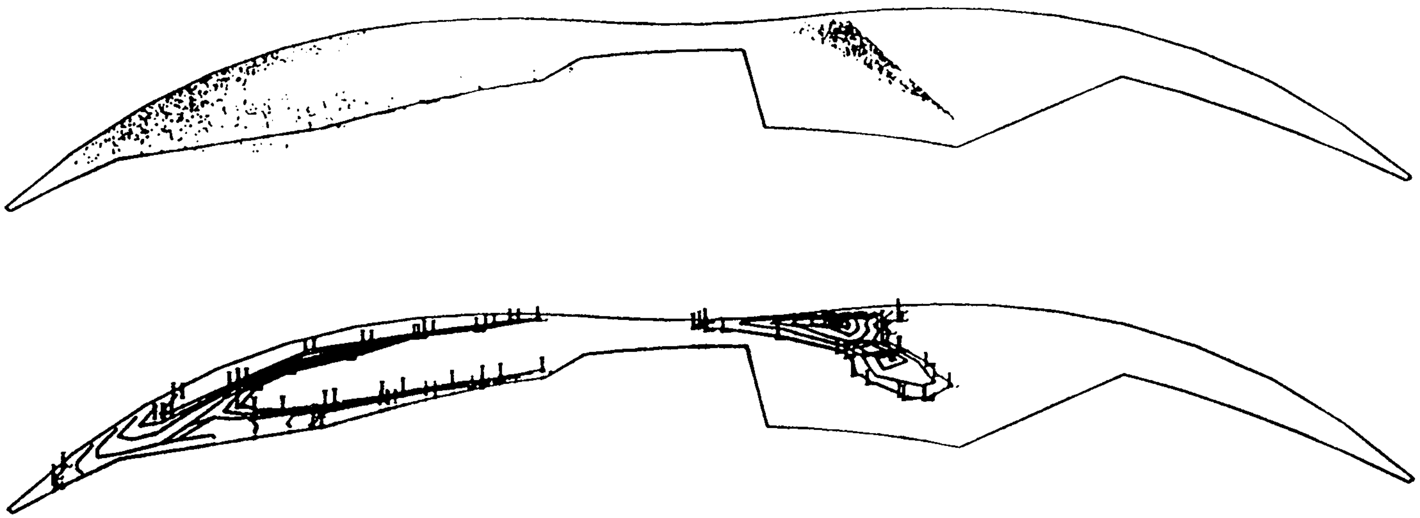

MASS FRACTION OF FUEL, interval = 0.18000E-01
H = 0.12000 ; L = 0.30000E-01
vertex limits of the region: (1, 7, 1) to (25, 7,11)
crank angle = 30.1

Fig.26(c): Particle and fuel/air distribution in the chamber at 1170CA

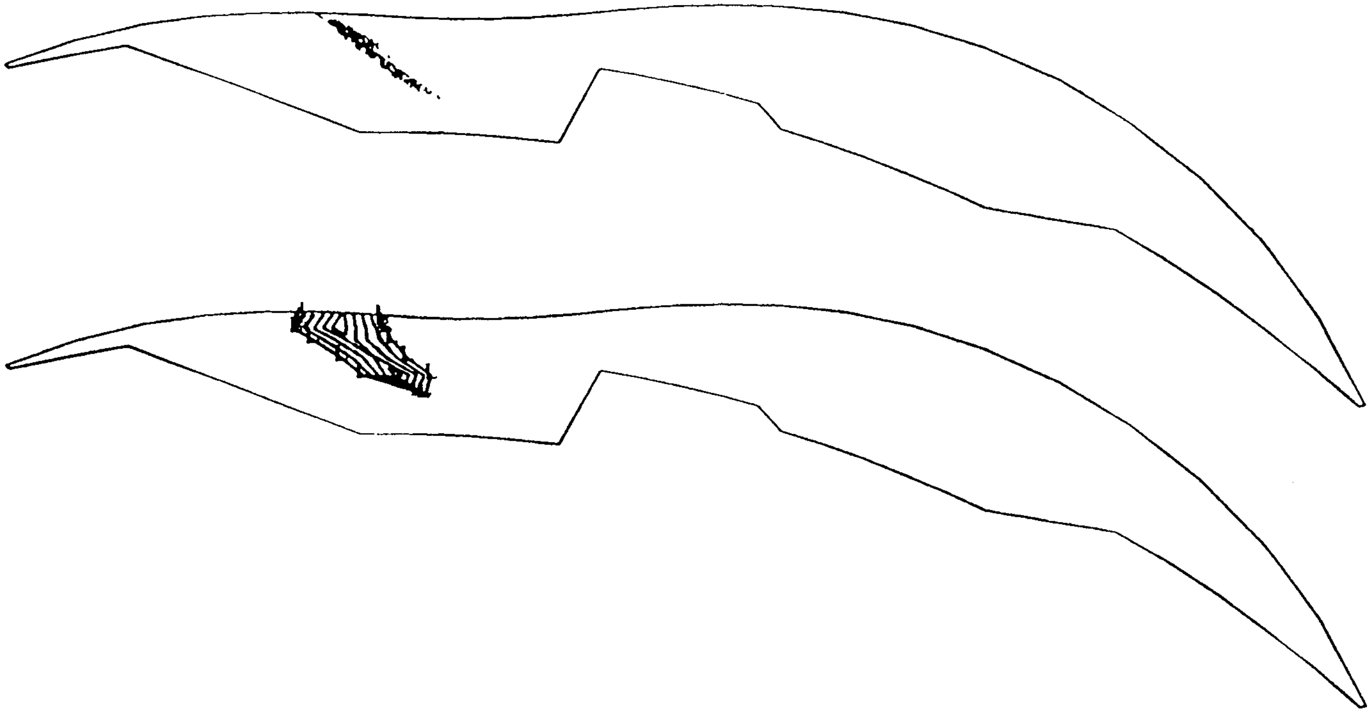

MASS FRACTION OF FUEL, interval = 0.18000E-01
H = 0.12000 ; L = 0.30000E-01
vertex limits of the region: (1, 7, 1) to (25, 7,11)
crank angle = 15.0

Fig.27(a): Particle and fuel/air distribution in the chamber at 1135 CA

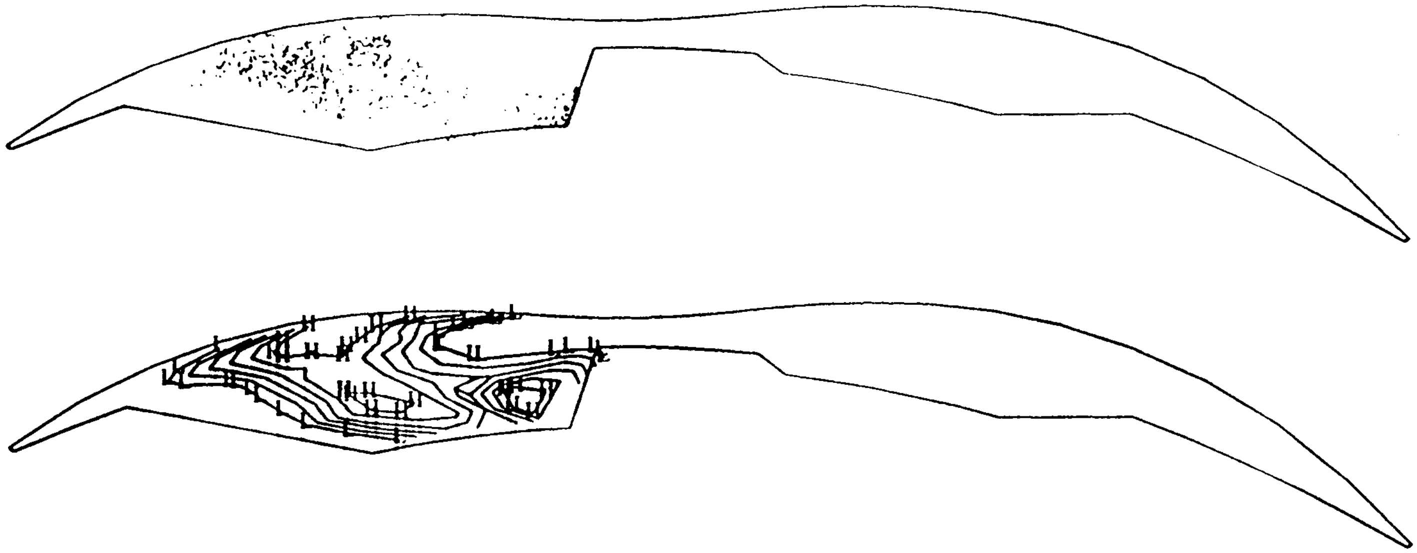

MASS FRACTION OF FUEL, interval = 0.18000E-01
H = 0.12000 ; L = 0.30000E-01
vertex limits of the region: (1, 7, 1) to (25, 7,11)
crank angle = 25.0

Fig.27(b): Particle and fuel/air distribution in the chamber at 1165CA

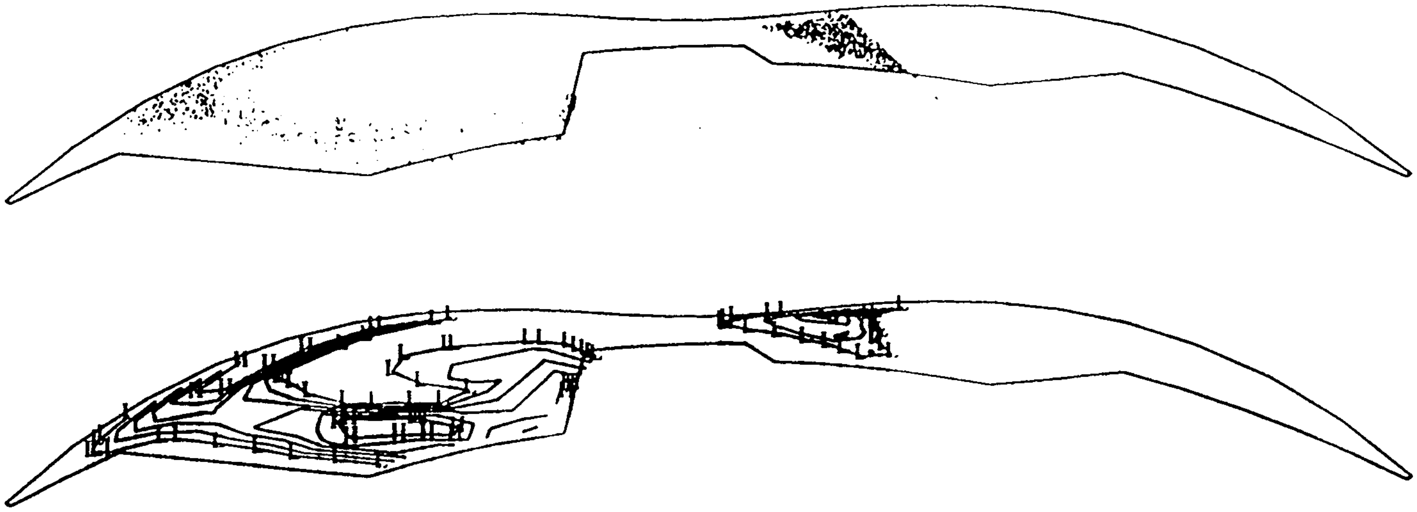

MASS FRACTION OF FUEL, interval = 0.18000E-01
H = 0.12000 ; L = 0.30000E-01
vertex limits of the region: (1, 7, 1) to (25, 7,11)
crank angle = 30.1

Fig.27(c): Particle and fuel/air distribution in the chamber at 1170CA

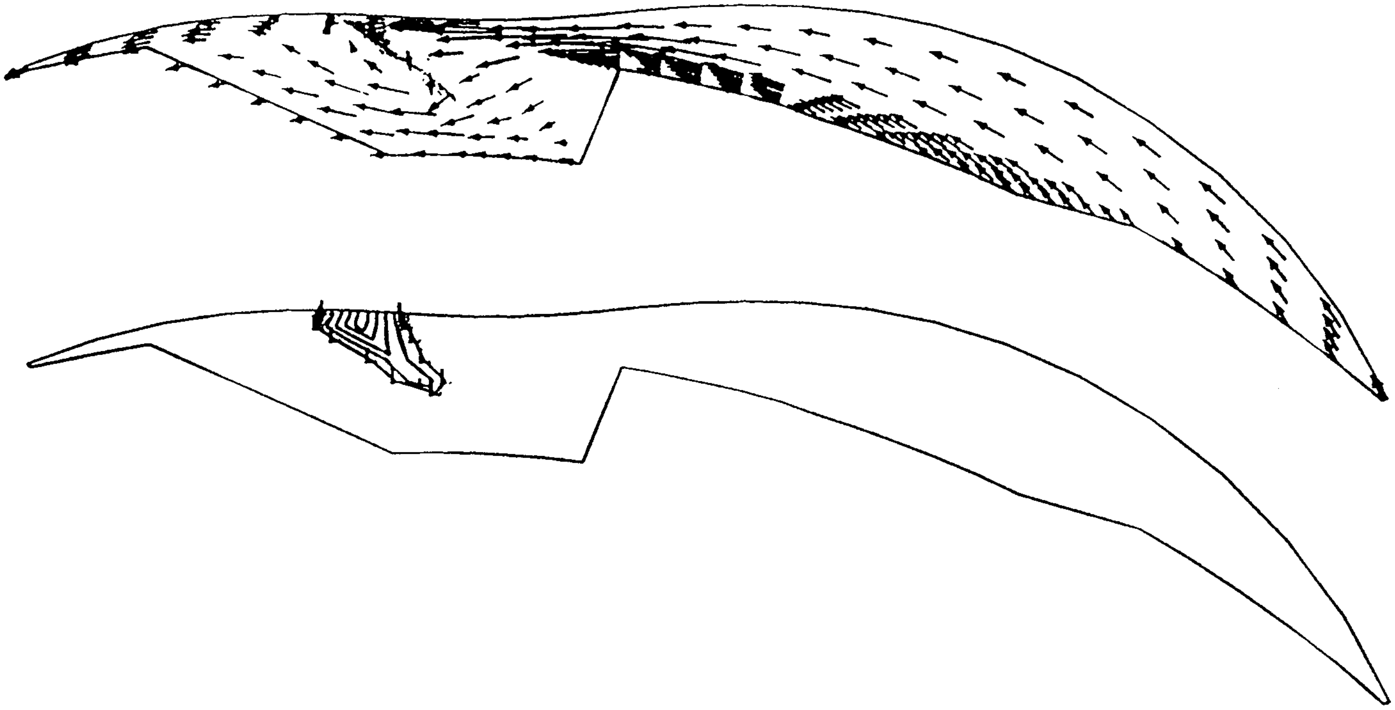

100 m/s
MASS FRACTION OF FUEL, interval = 0.18000E-01
H = 0.12000 ; L = 0.30000E-01
vertex limits of the region: (1, 7, 1) to (25, 7,11)
crank angle = 15.0

Fig 28(a): Velocity particle and fuel/air distribution at 1135 CA

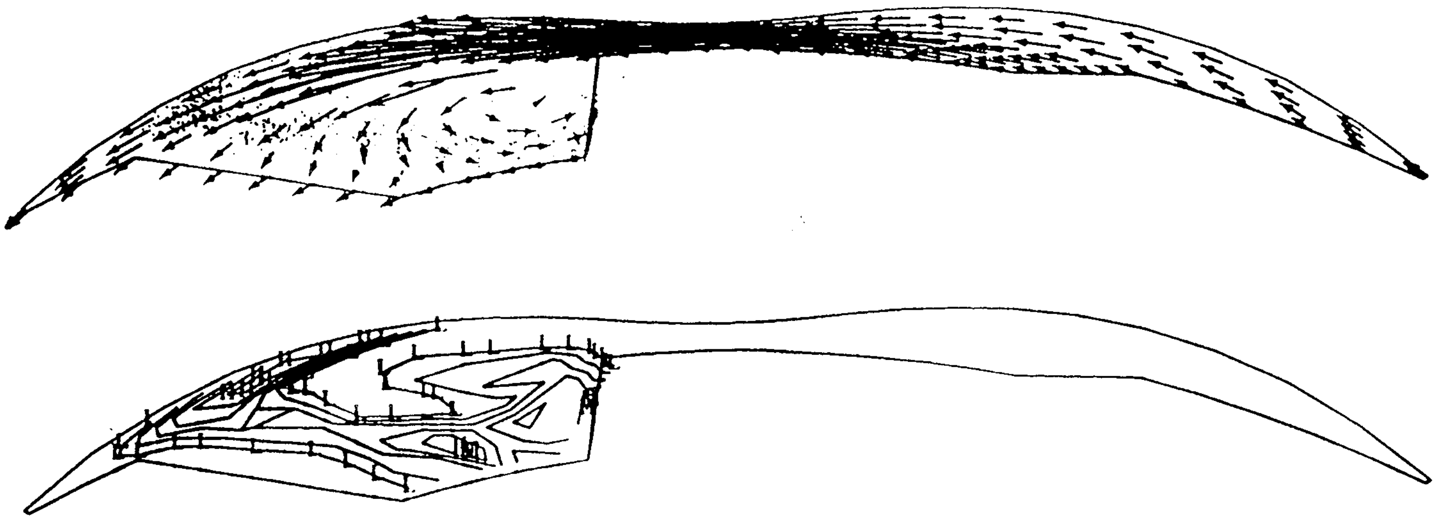

100 m/s
MASS FRACTION OF FUEL, interval = 0.18000E-01
H = 0.12000 ; L = 0.30000E-01
vertex limits of the region: (1, 7, 1) to (25, 7,11)
crank angle = 30.1

Fig 28(b): Velocity particle and fuel/air distribution at 1170 CA

2-D

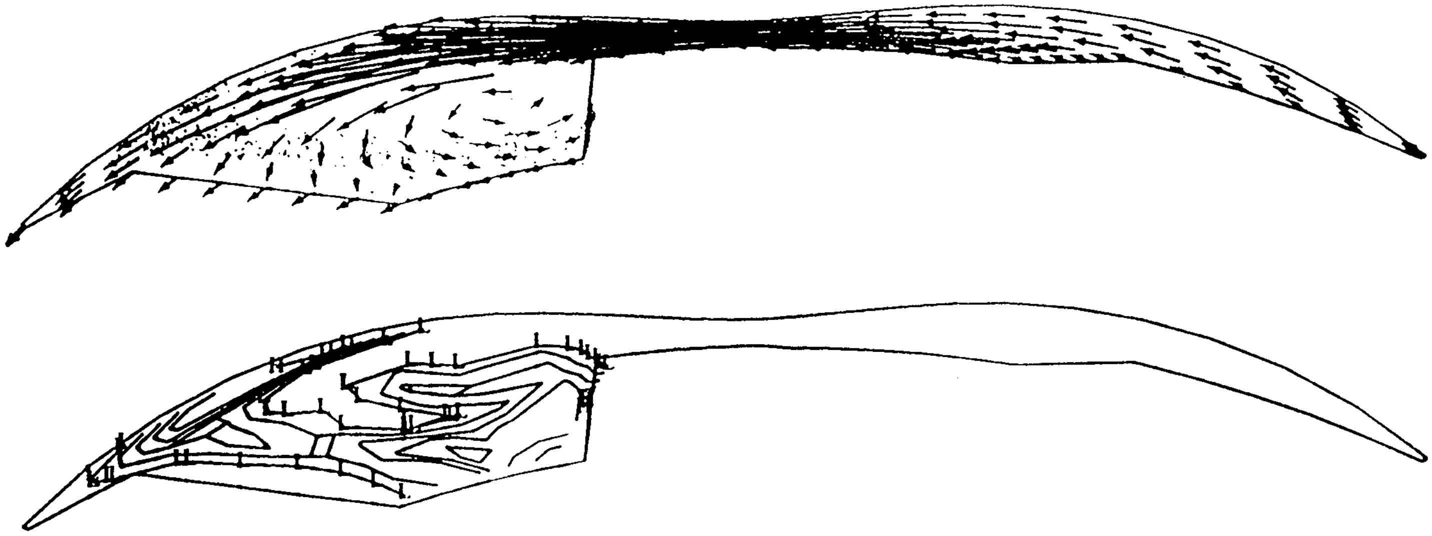

100 m/s

MASS FRACTION OF FUEL, interval = 0.18000E-01

H = 0.12000 ; L = 0.30000E-01

vertex limits of the region: (1, 7, 1) to (25, 7, 11)

crank angle = 31.6

Fig.28(c): Velocity,particle and fuel/air distribution at 15 CA

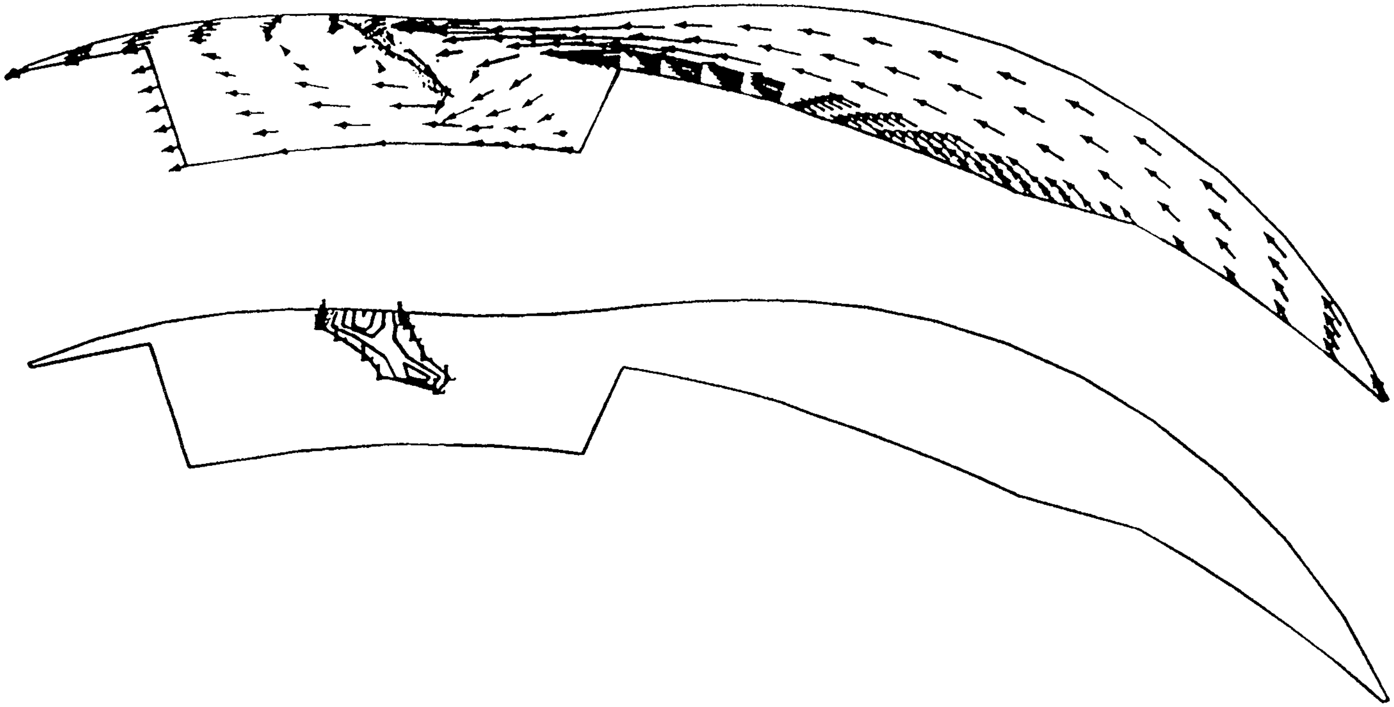

100 m/s
MASS FRACTION OF FUEL, interval = 0.18000E-01
H = 0.12000 ; L = 0.30000E-01
vertex limits of the region: (1, 7, 1) to (25, 7,11)
crank angle = 15.0

Fig.29(a): Velocity,particle and fuel/air distribution at 1135 CA

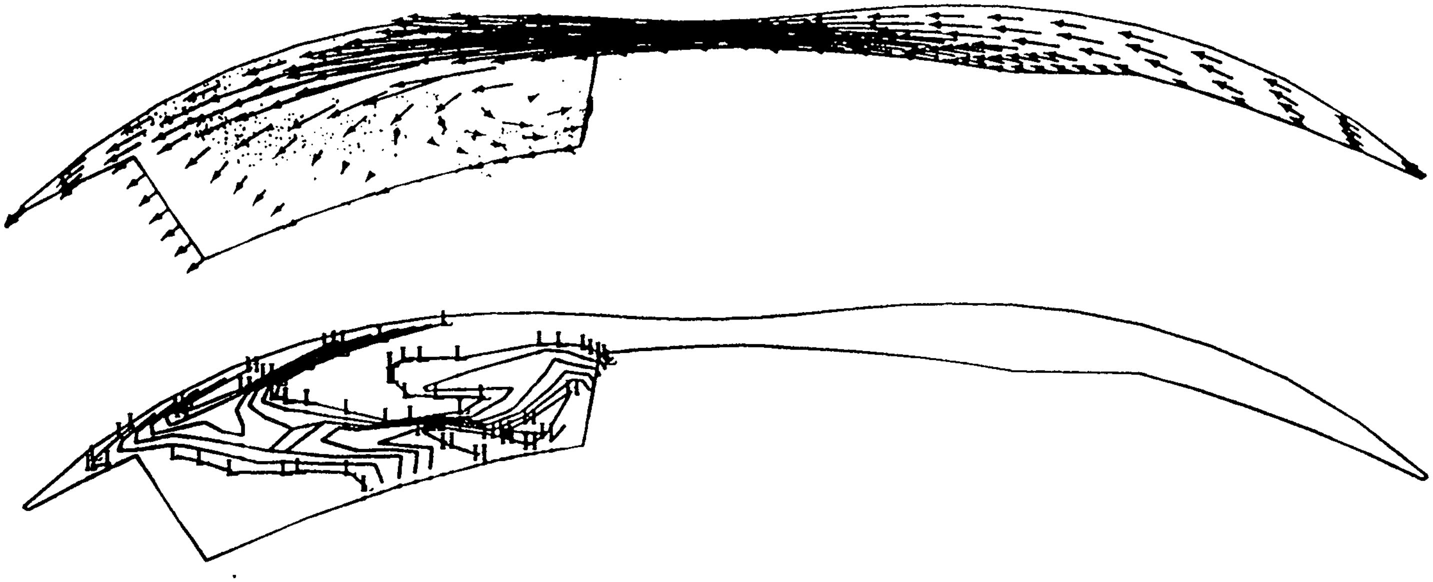

100 m/s

MASS FRACTION OF FUEL, interval = 0.18000E-01

H = 0.12000 ; L = 0.30000E-01

vertex limits of the region: (1, 7, 1) to (25, 7,11)

crank angle = 30.1

Fig.29(b): Velocity,particle and fuel/air distribution at 1165 CA

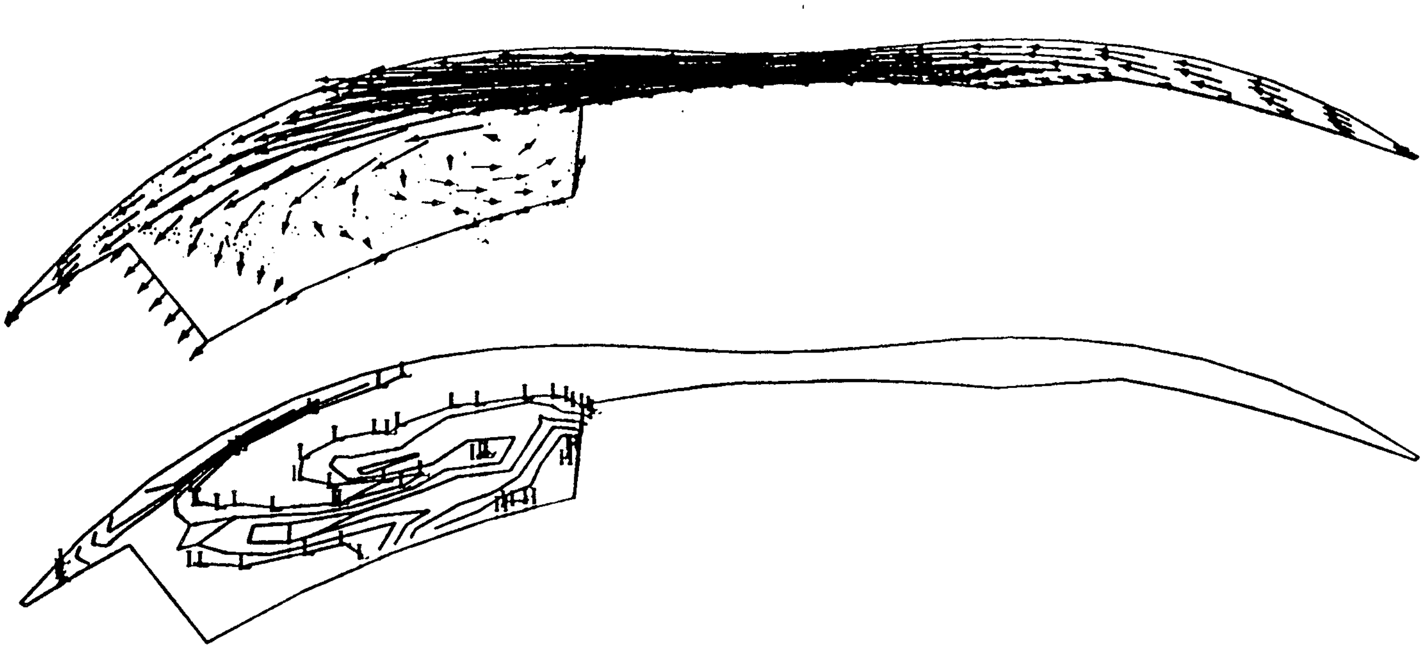

100 m/s

MASS FRACTION OF FUEL, interval = 0.18000E-01

H = 0.12000 ; L = 0.30000E-01

vertex limits of the region: (1, 7, 1) to (25, 7,11)

crank angle = 35.1

ORIGINAL PAGE IS
OF POOR QUALITY

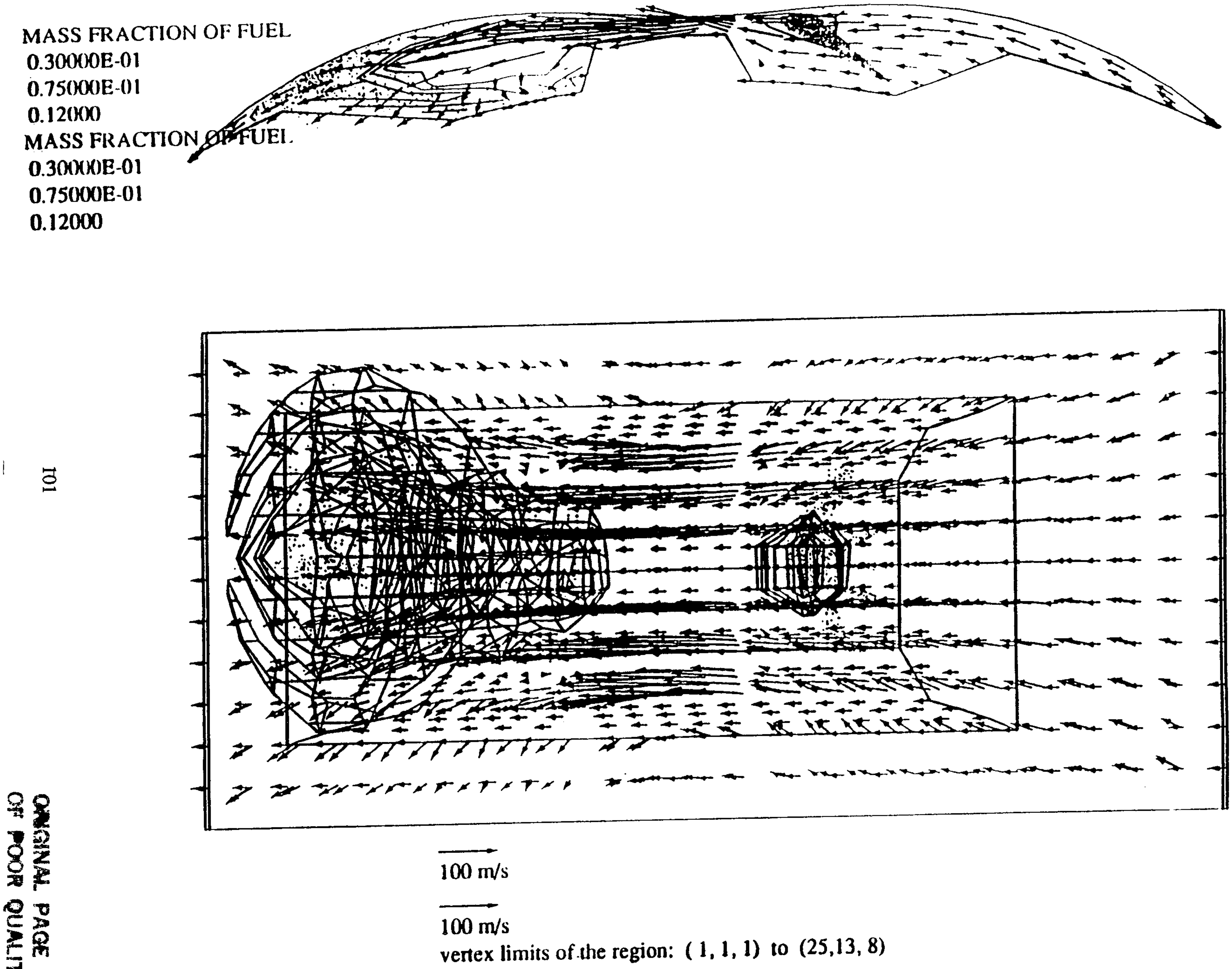

Fig 30: Computed velocity, liquid fuel and vaporized fuel distribution in the

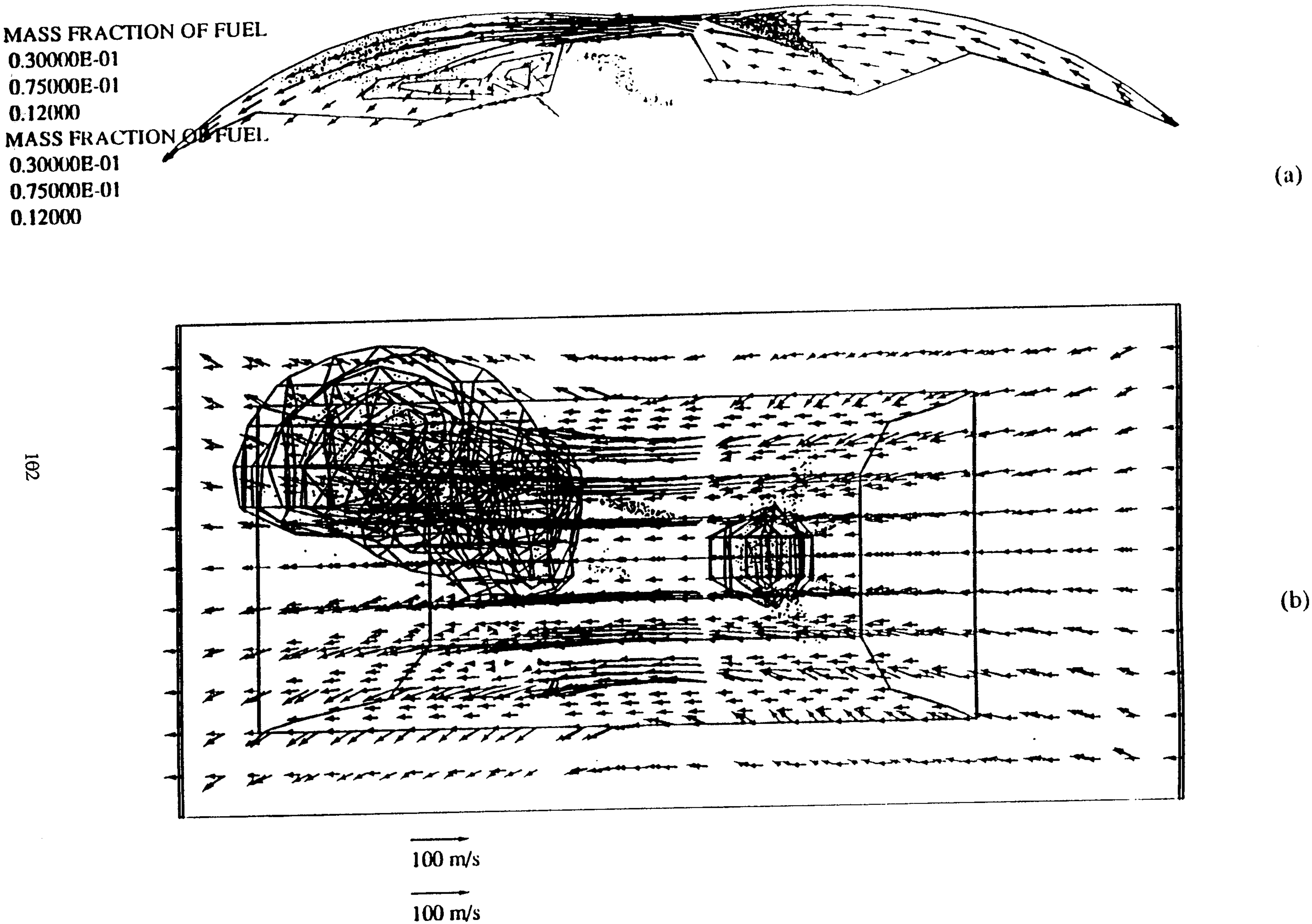

vertex limits of the region: (1, 1, 1) to (25,13, 8)

crank angle = 0.2

[illegible] fuel distribution in the combustion

Fig.32 DUAL POCKET ROTOR HOUSING

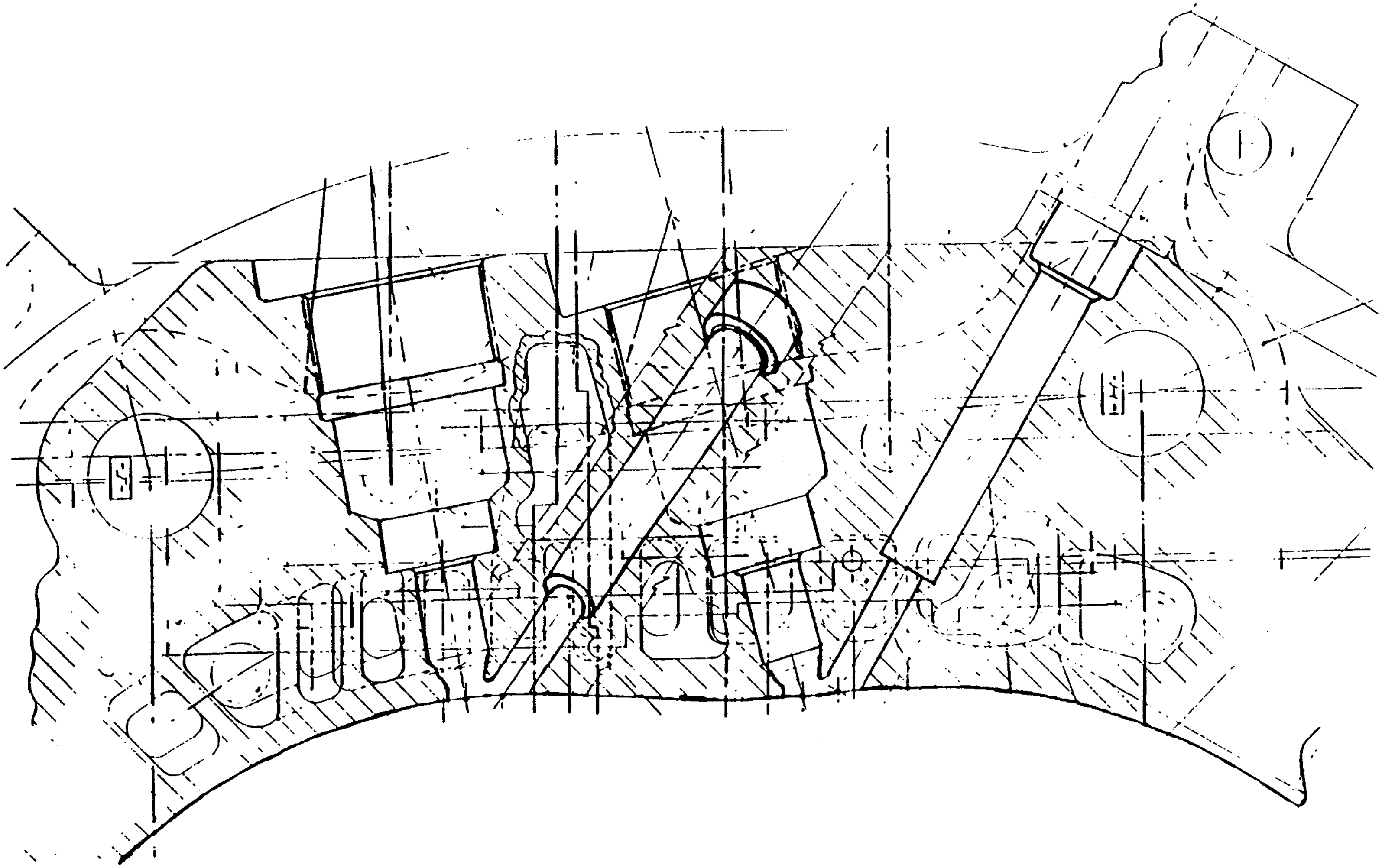

ORIGINAL PAGE IS
OF POOR QUALITY

Fig.33: : Pressure in Dual Pocket Combustion Chamber

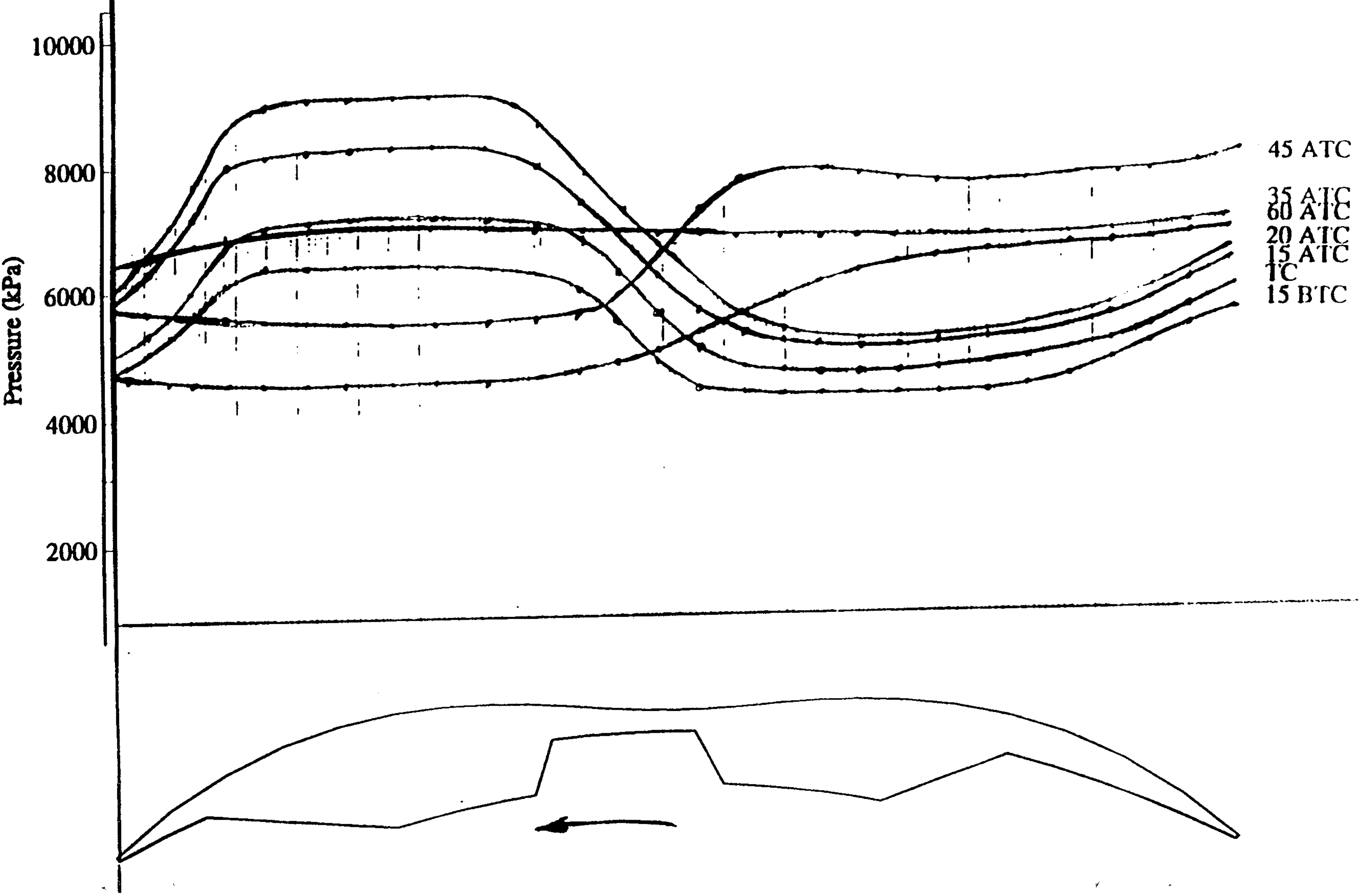

Fig.34

Injection rate comparison
Stanadyne DM and AUI systems

8000 Rpm, 80 mm^3

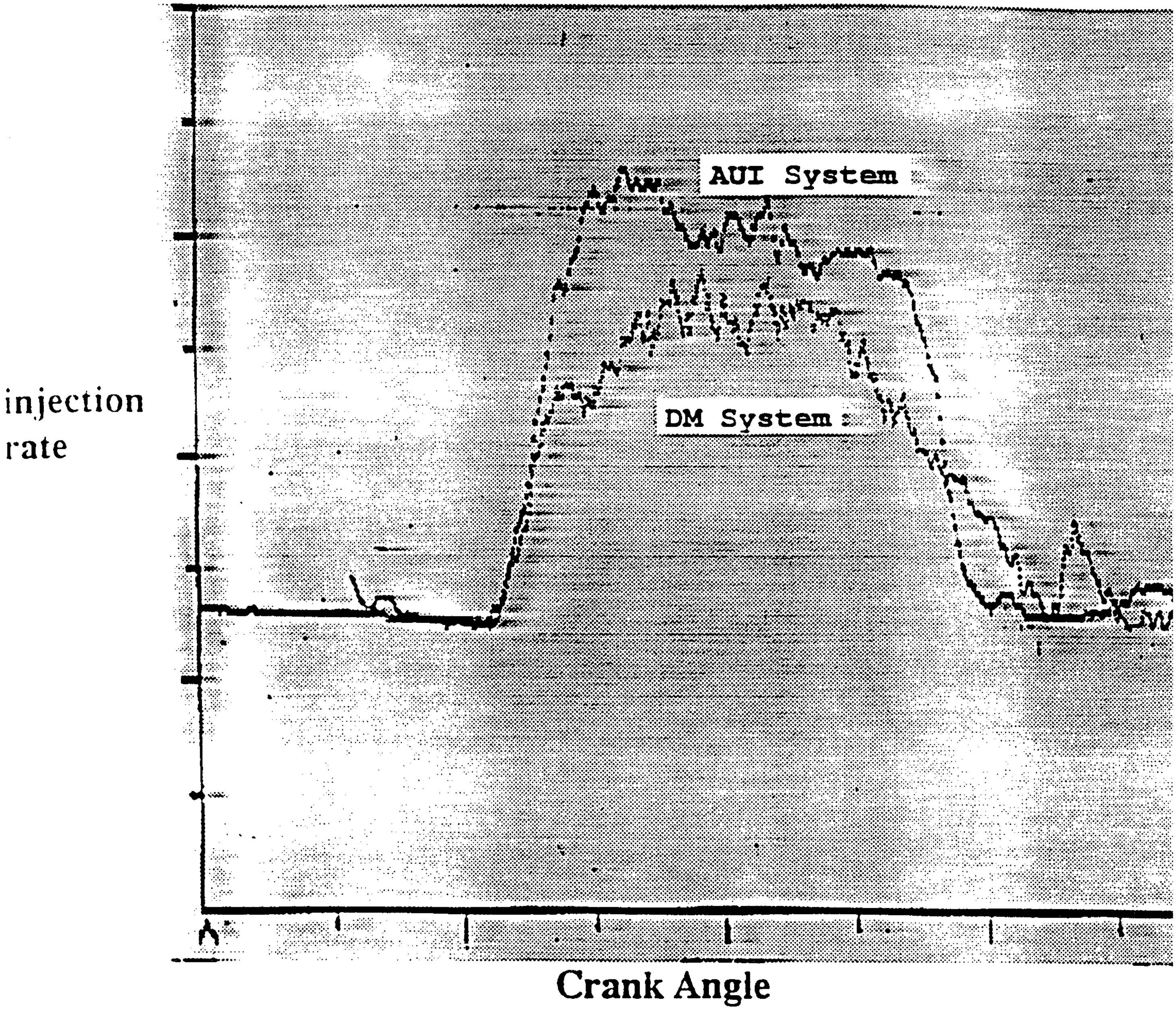

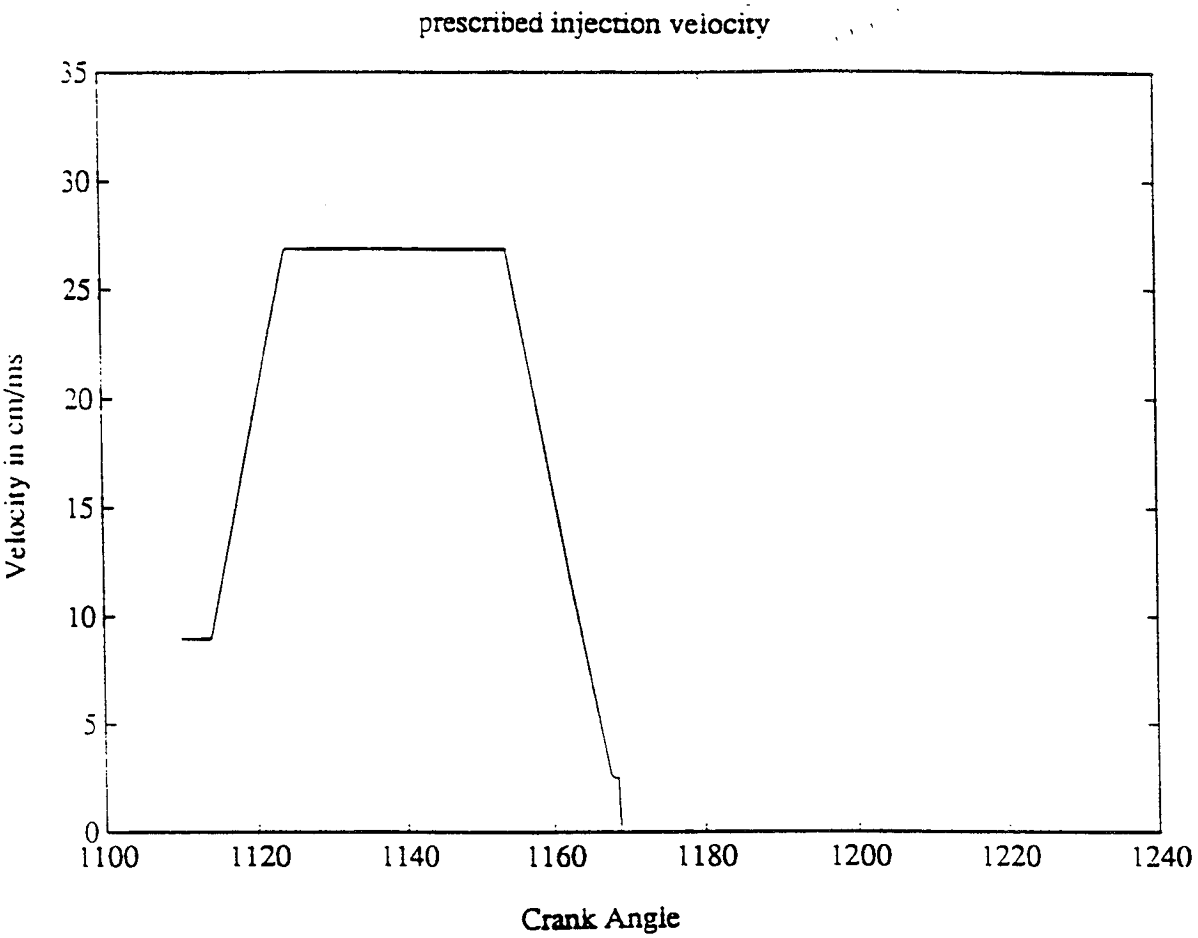

Fig. 35(a): Prescribed injection velocity for the AUI injection system

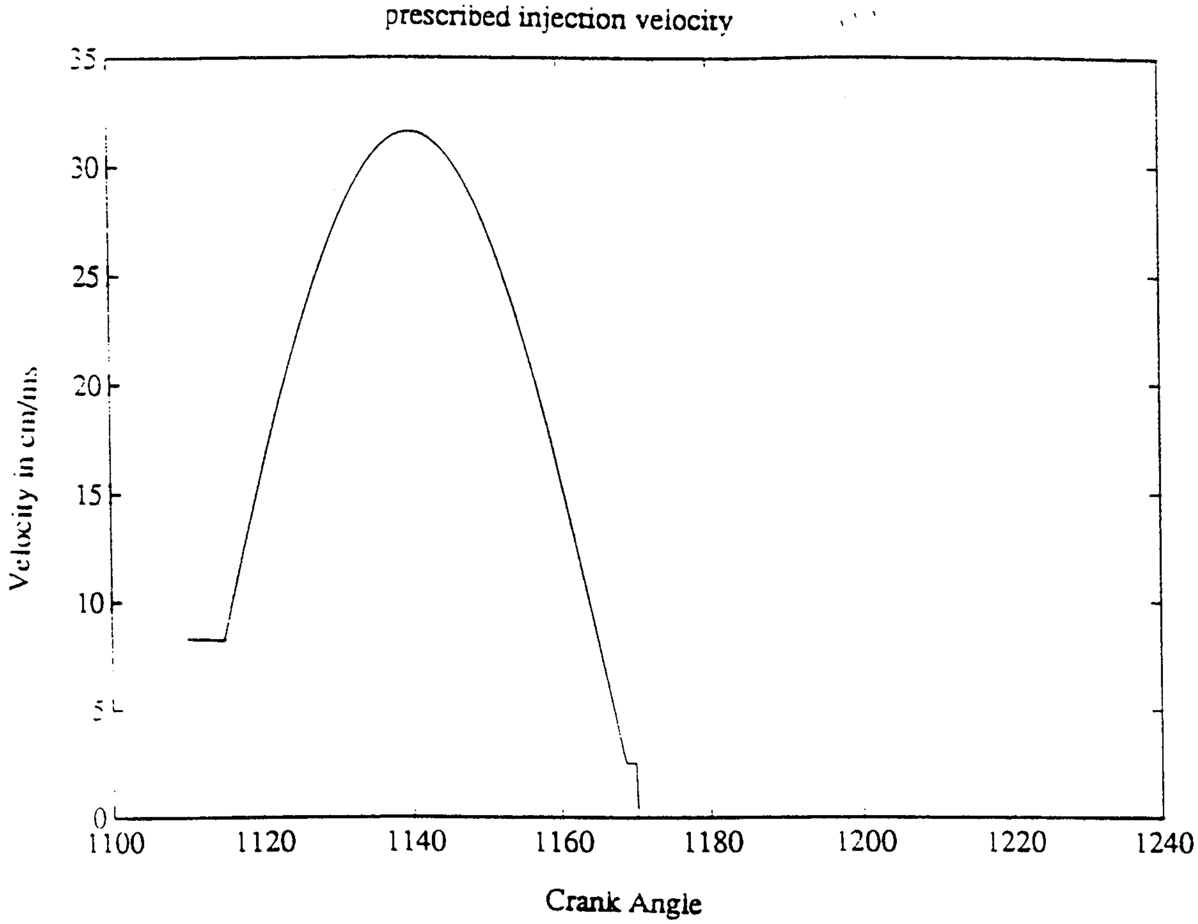

Fig. 35(b): Prescribed injection velocity for the DM pump system

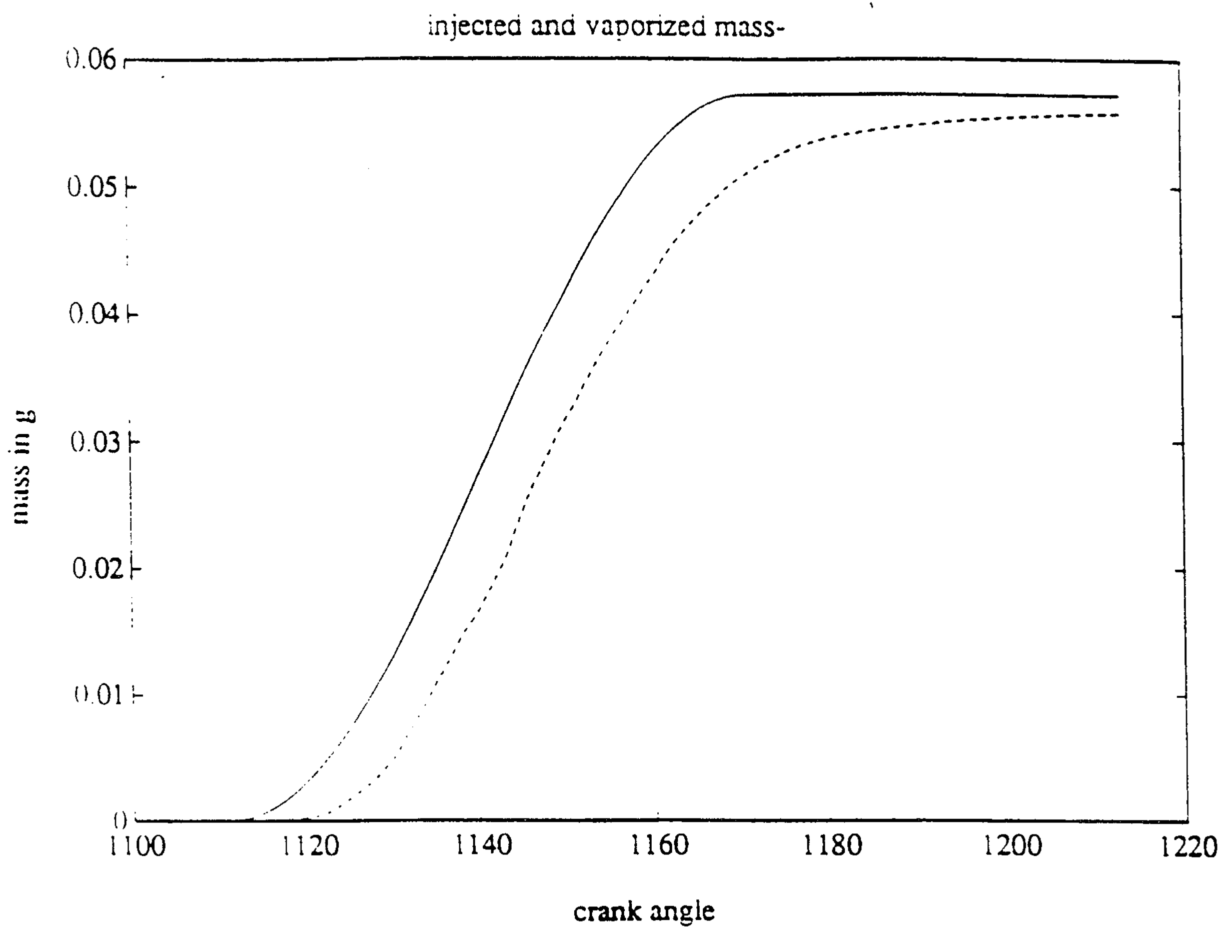

Fig. 36(a): Injected (------) and vaporized(-----) mass of fuel for the AUI system

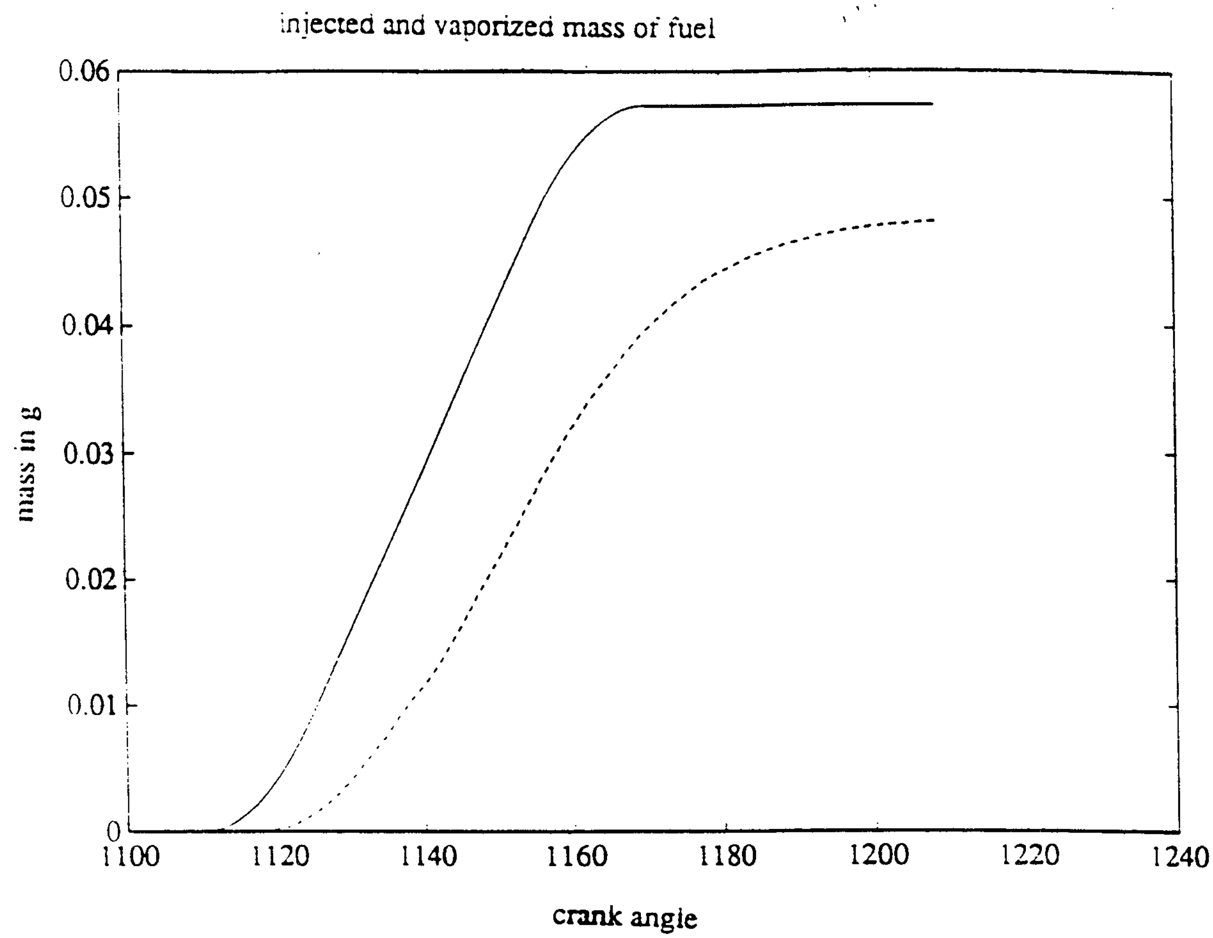

Fig. 36(b): Injected (------) and vaporized(-----) mass of fuel for the DM pump system

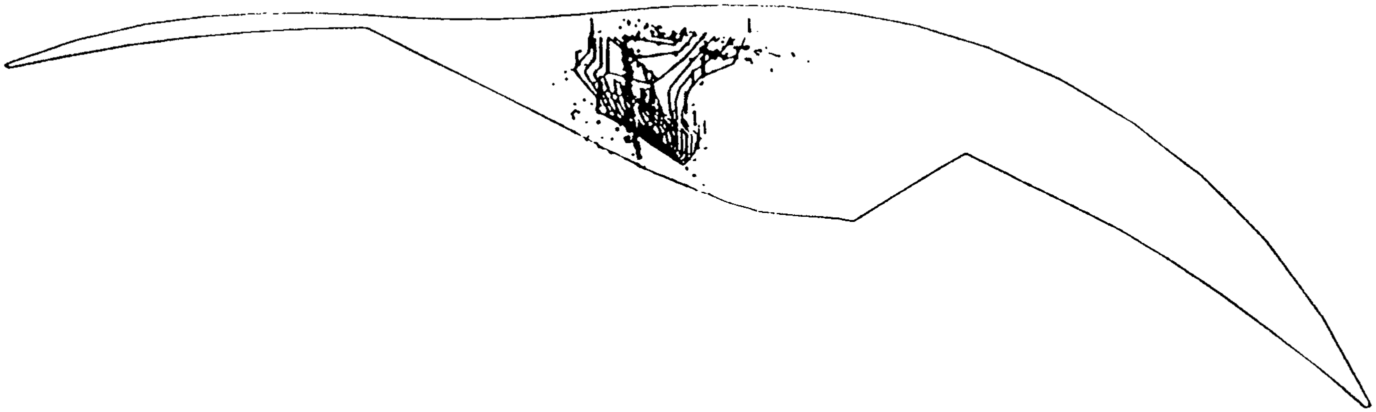

FUEL/AIR RATIO, interval = 0.1286E-01
H = .1200 ; L = .3000E-01
J = 7
crank angle = 1035.0

Fig. 37(a): Cross-section view of combustion chamber along symmetry plane showing the distribution of liquid fuel and vaporized fuel 15 CA after injection for the AUI system.

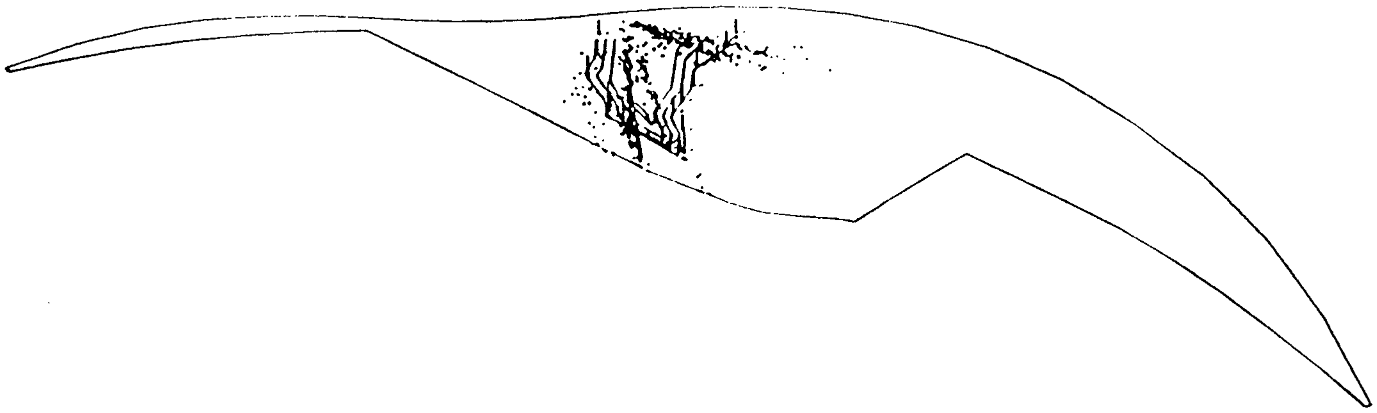

FUEL/AIR RATIO, interval = 0.1286E-01
H = .1200 ; L = .3000E-01
J = 7
crank angle = 1035.0

Fig. 37(b): Cross-section view of combustion chamber along symmetry plane showing the distribution of liquid fuel and vaporized fuel 15 CA after injection for the DM pump system.

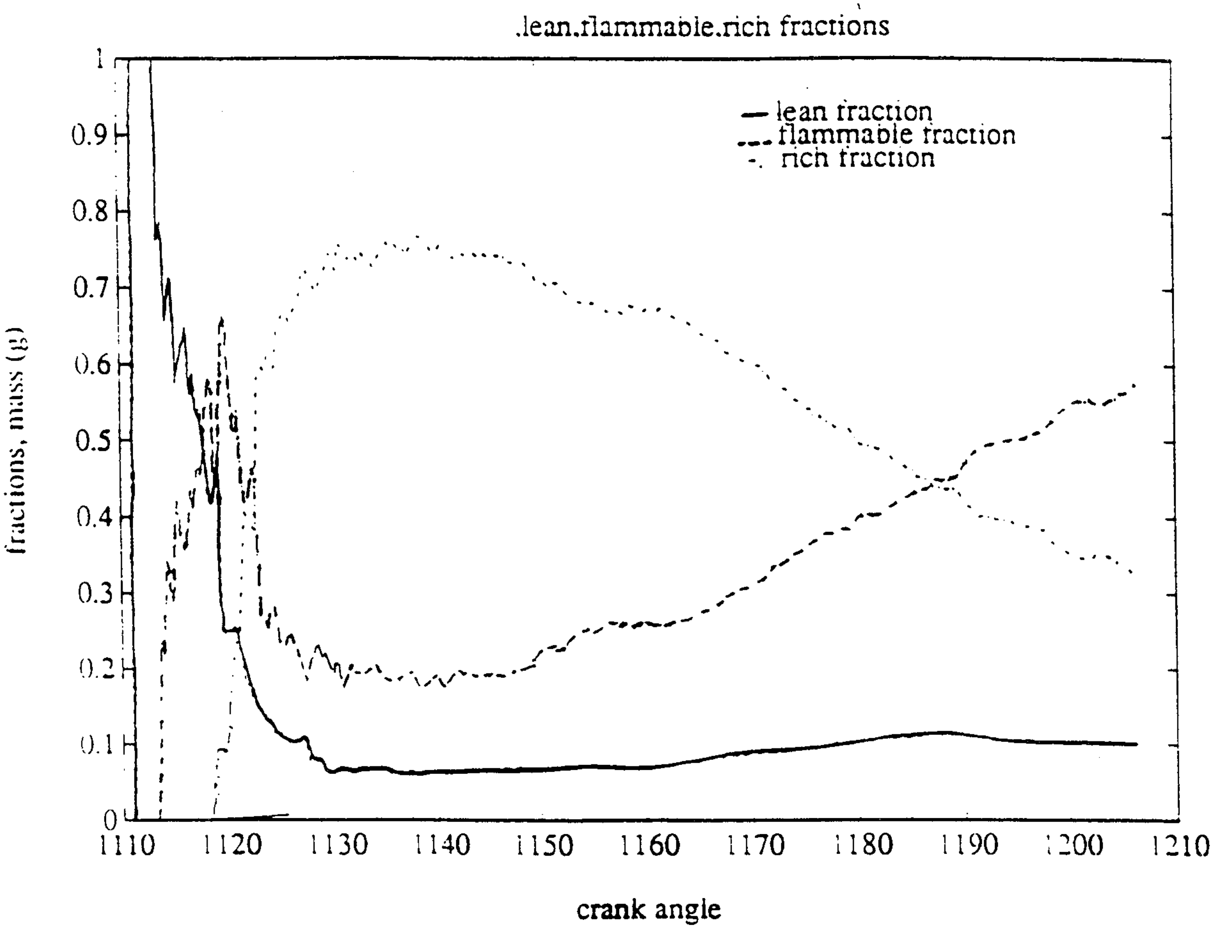

Fig. 38(a): Lean,Rich and Flammable fractions of vaporized fuel as a function of crank angle for the AUI system

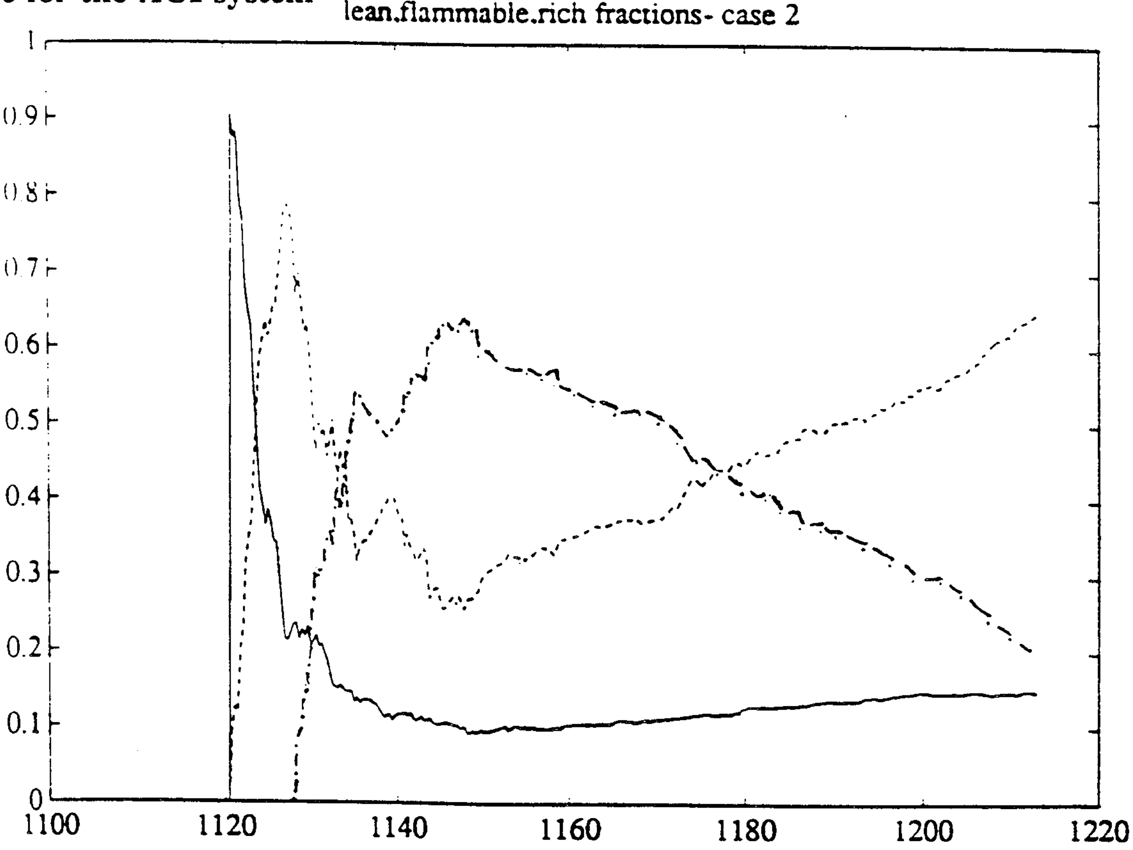

Fig. 38(b): Lean,Rich and Flammable fractions of vaporized fuel as a function of crank angle for the AUI system

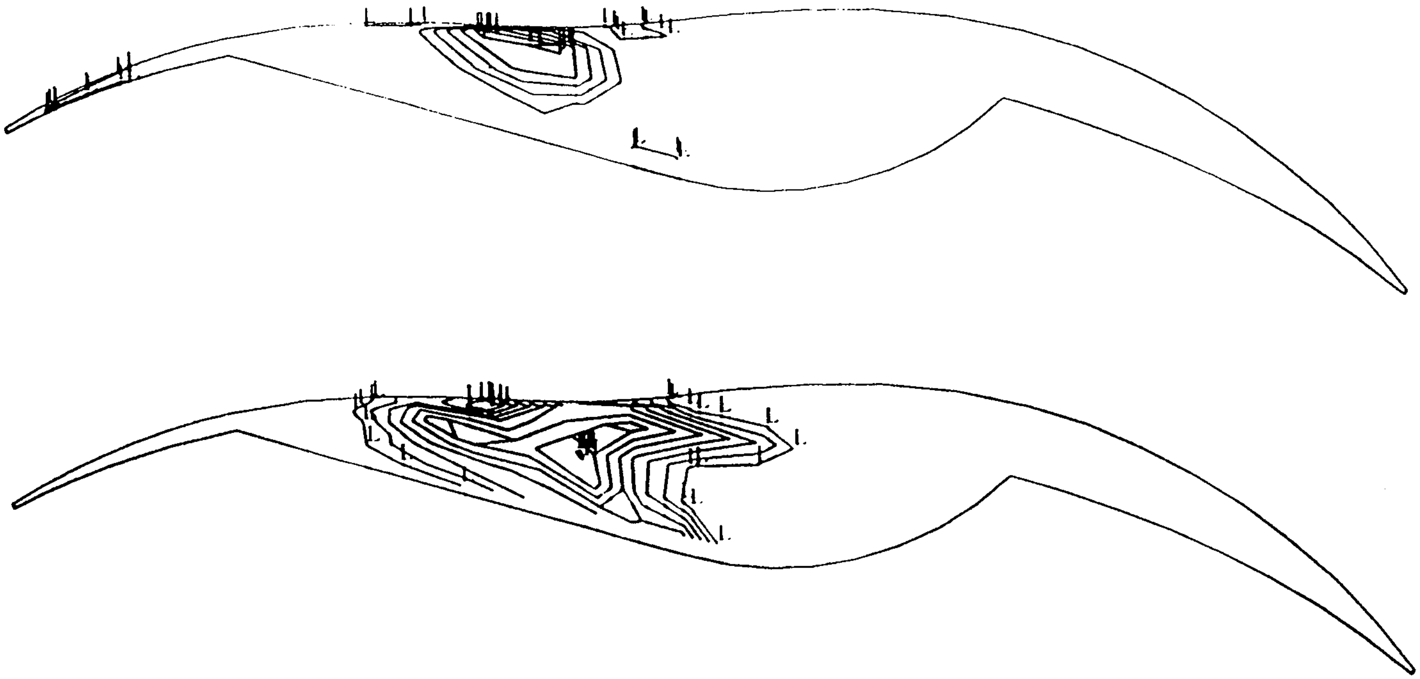

Fig. 39(a): Cross-section view of combustion chamber along symmetry plane showing temperature contours and vaporized fuel contours at 25 CA BTC for the AUI system

TEMPERATURE, interval = 280.0 K
H = 2000. ; L = 600.0
MASS FRACTION OF FUEL, interval = 0.1286E-01
H = .1200 ; L = .3000E-01
vertex limits of the region: (1, 8, 1) to (27, 8, 9)
crank angle = 1145.0

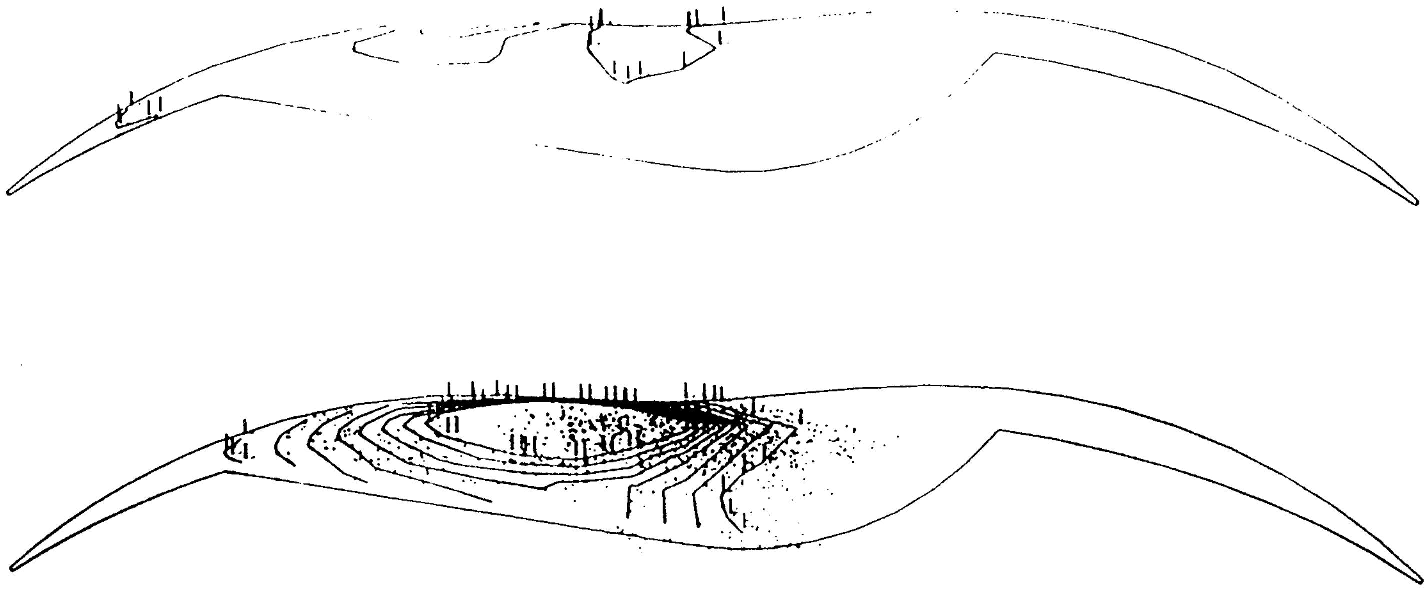

Fig. 39(b): Cross-section view of combustion chamber along symmetry plane showing temperature contours and vaporized fuel contours at 5 CA BTC for the AUI system

TEMPERATURE, interval = 200.0 K
H = 1600. ; L = 600.0
MASS FRACTION OF FUEL, interval = 0.1286E-01
H = .1200 ; L = .3000E-01
vertex limits of the region: (1, 8, 1) to (27, 8, 9)
crank angle = 1165.0

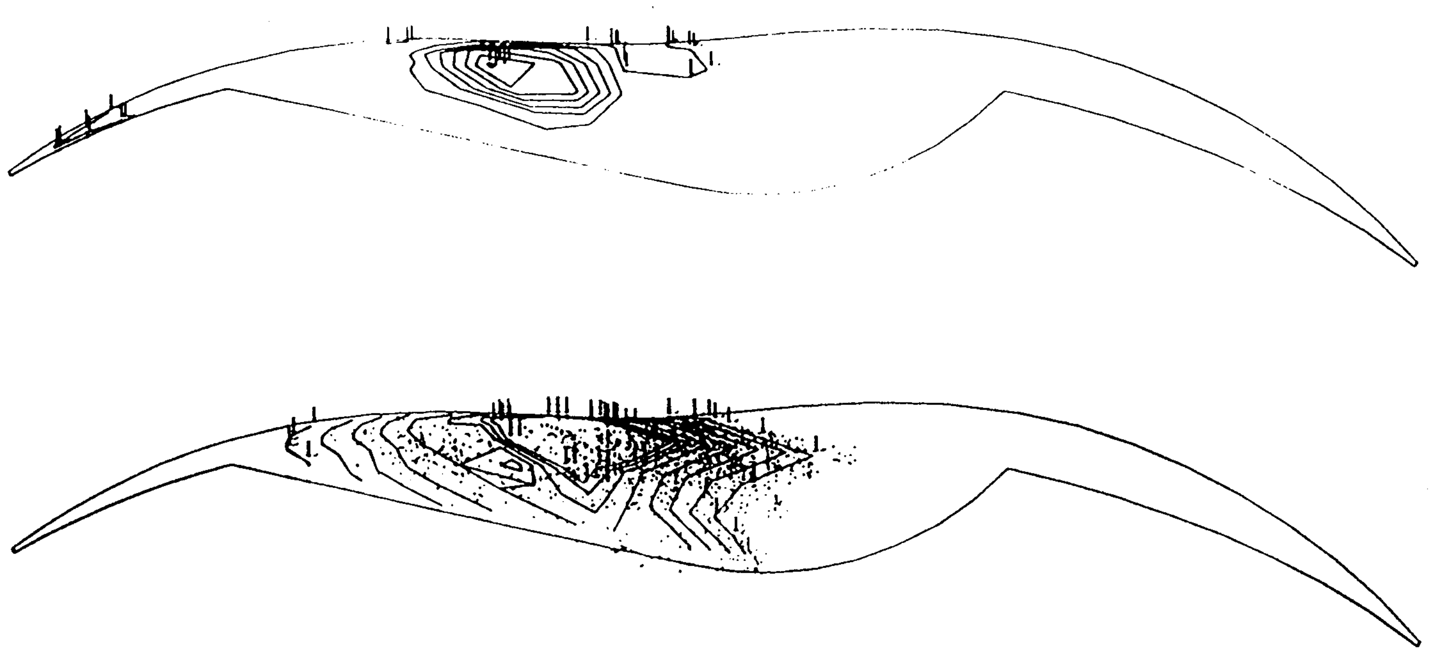

Fig. 40(a): Cross-section view of combustion chamber along symmetry plane showing temperature contours and liquid fuel and vaporized fuel contours at 15 CA BTC for the DM pump system

TEMPERATURE, interval = 192.9 K
H = 1950. ; L = 600.0
MASS FRACTION OF FUEL, interval = 0.1286E-01
H = .1200 ; L = .3000E-01
vertex limits of the region: (1, 8, 1) to (27, 8, 9)
crank angle = 1155.0

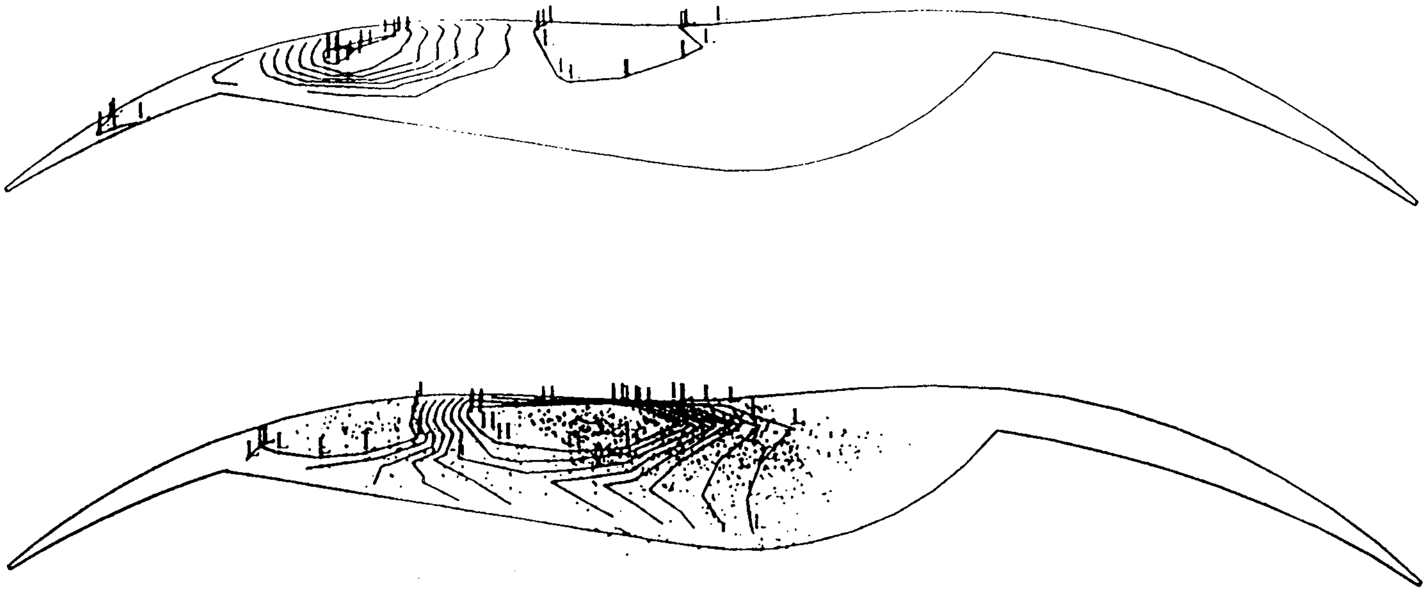

Fig. 40(b): Cross-section view of combustion chamber along symmetry plane showing temperature contours and liquid fuel and vaporized fuel contours at 5 CA BTC for the DM pump system

TEMPERATURE, interval = 228.6 K
H = 2200. ; L = 600.0
MASS FRACTION OF FUEL, interval = 0.1286E-01
H = .1200 ; L = .3000E-01
vertex limits of the region: (1, 8, 1) to (27, 8, 9)
crank angle = 1165.0

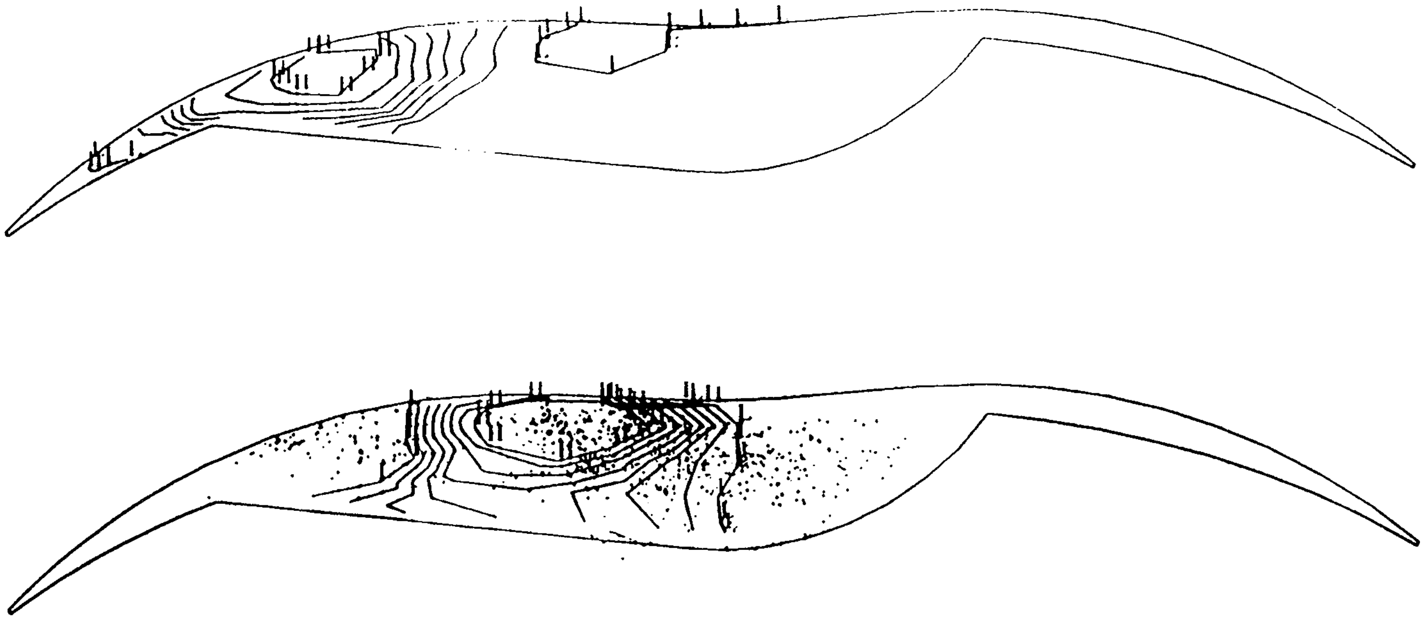

Fig. 40(c): Cross-section view of combustion chamber along symmetry plane showing temperature contours and liquid fuel and vaporized fuel contours at 5 CA ATC for the DM pump system

TEMPERATURE, interval = 228.6 K
H = 2200. ; L = 600.0
MASS FRACTION OF FUEL, interval = 0.1286E-01
H = .1200 ; L = .3000E-01
vertex limits of the region: (1, 8, 1) to (27, 8, 9)
crank angle = 1175.0

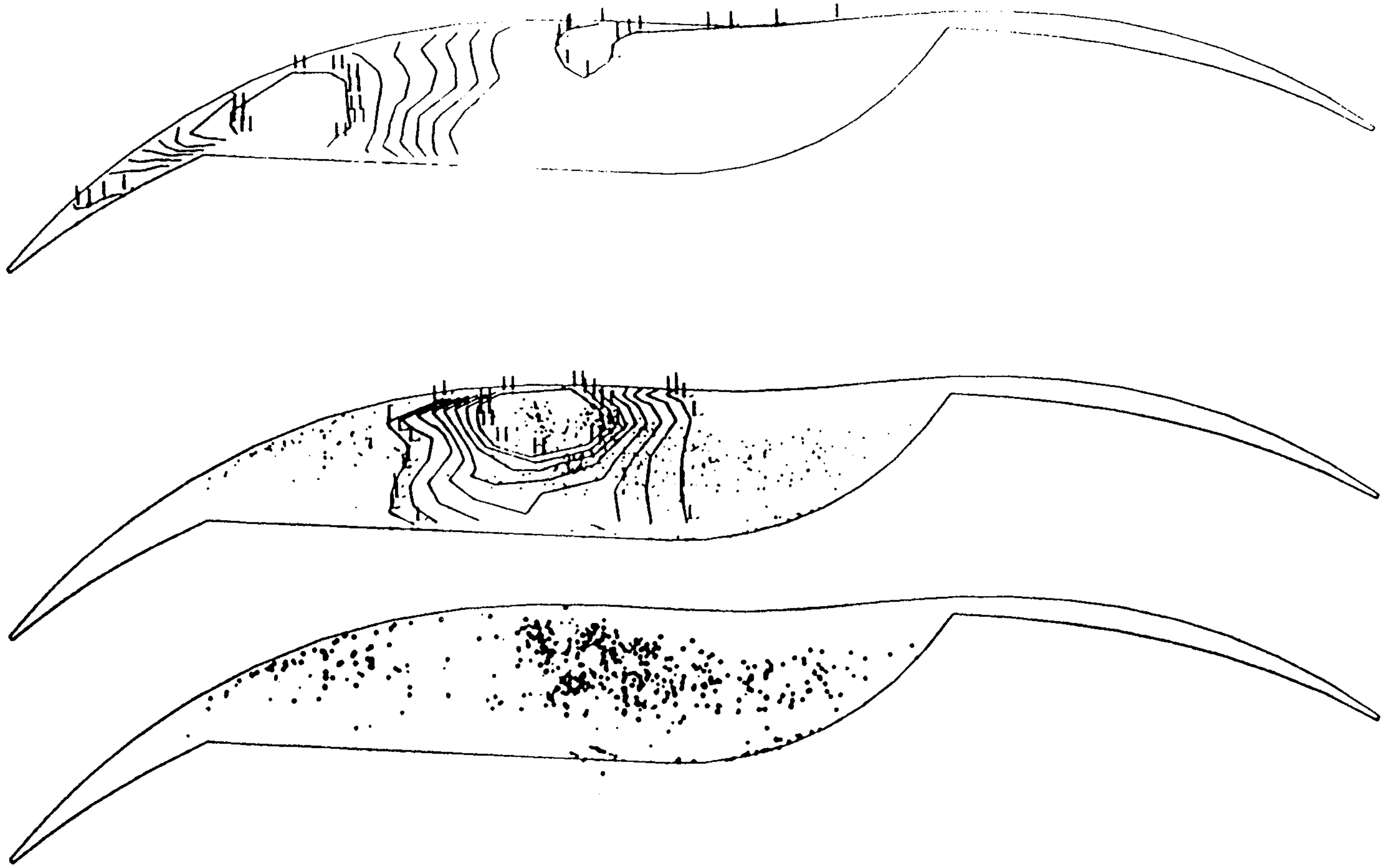

Fig. 40(d): Cross-section view of combustion chamber along symmetry plane showing temperature contours and liquid fuel and vaporized fuel contours at 15 CA ATC for the DM pump system

TEMPERATURE, interval = 228.6 K
H = 2200. ; L = 600.0
MASS FRACTION OF FUEL, interval = 0.1286E-01
H = .1200 ; L = .3000E-01
vertex limits of the region: (1, 8, 1) to (27, 8, 9)
crank angle = 1185.0

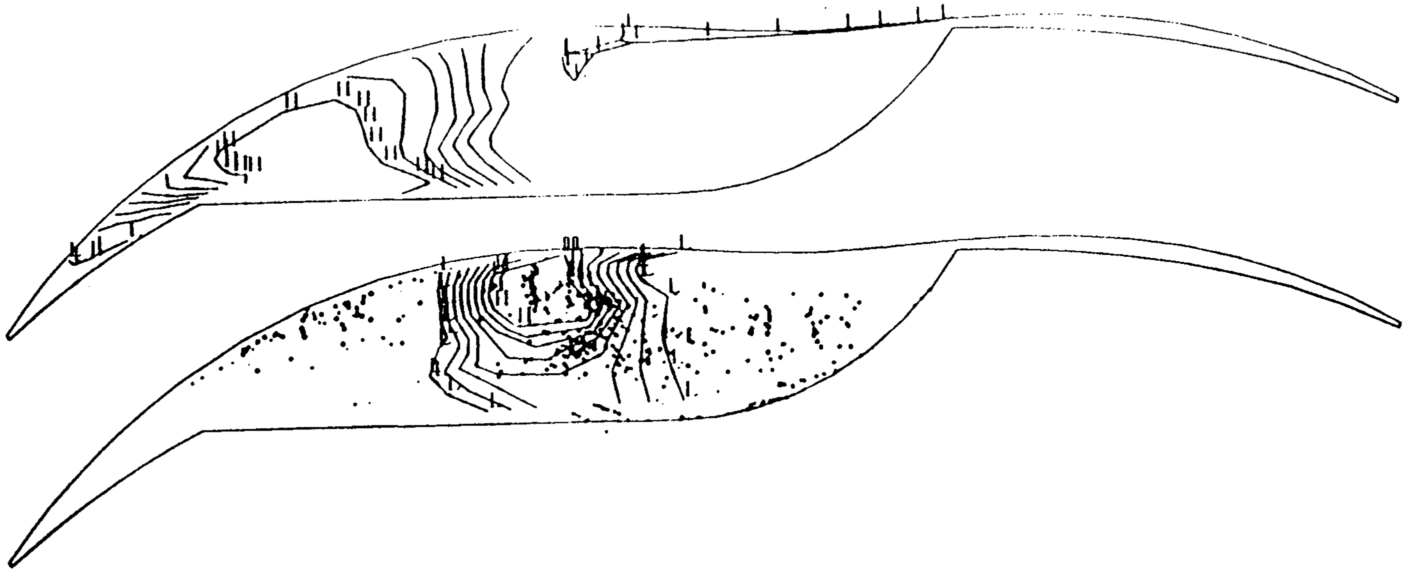

Fig. 40(e): Cross-section view of combustion chamber along symmetry plane showing temperature contours and liquid fuel and vaporized fuel contours at 25 CA ATC for the DM pump system

TEMPERATURE, interval = 228.6 K
H = 2200. ; L = 600.0
MASS FRACTION OF FUEL, interval = 0.1286E-01
H = .1200 ; L = .3000E-01
vertex limits of the region: (1, 8, 1) to (27, 8, 9)
crank angle = 1195.0

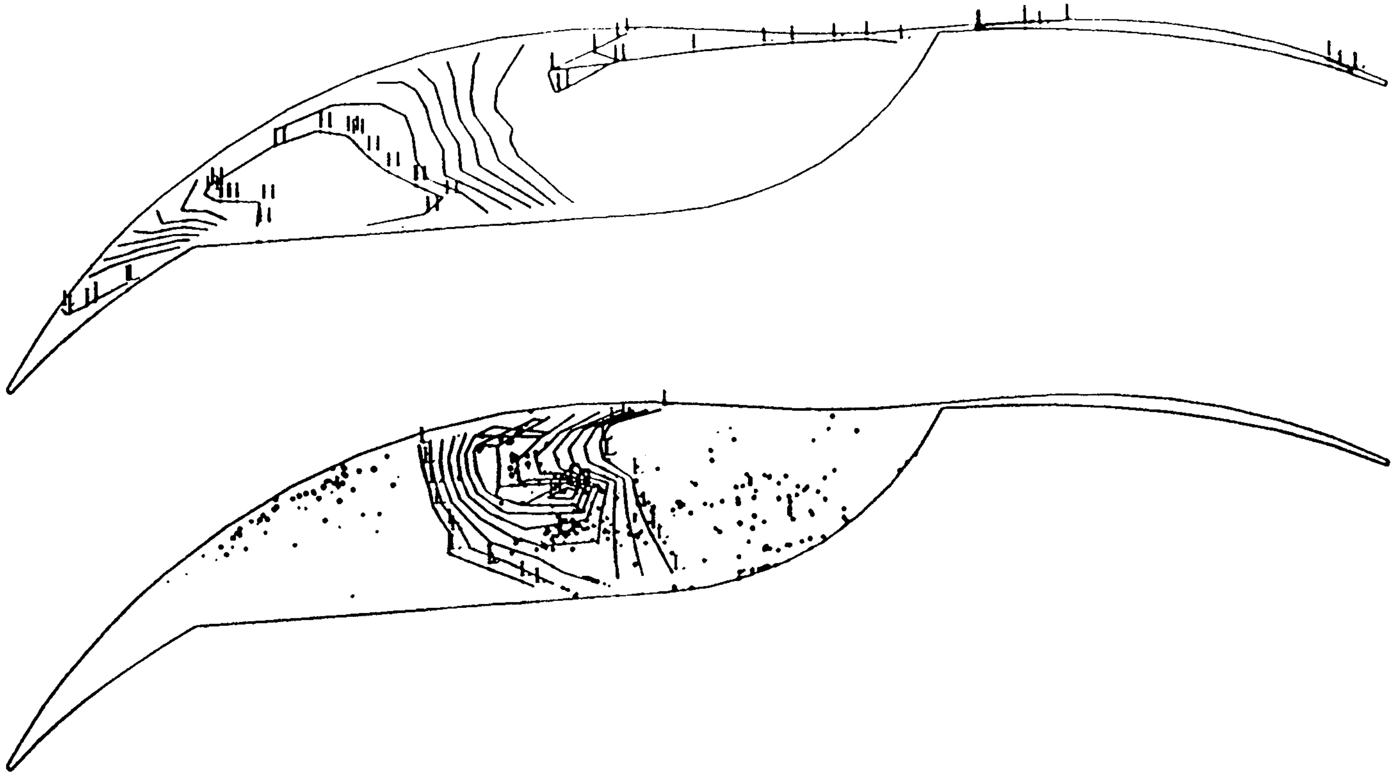

Fig. 40(f): Cross-section view of combustion chamber along symmetry plane showing temperature contours and liquid fuel and vaporized fuel contours at 35 CA ATC for the DM pump system

TEMPERATURE, interval = 228.6 K
H = 2200. ; L = 600.0
MASS FRACTION OF FUEL, interval = 0.1286E-01
H = .1200 ; L = .3000E-01
vertex limits of the region: (1, 8, 1) to (27, 8, 9)
crank angle = 1205.0

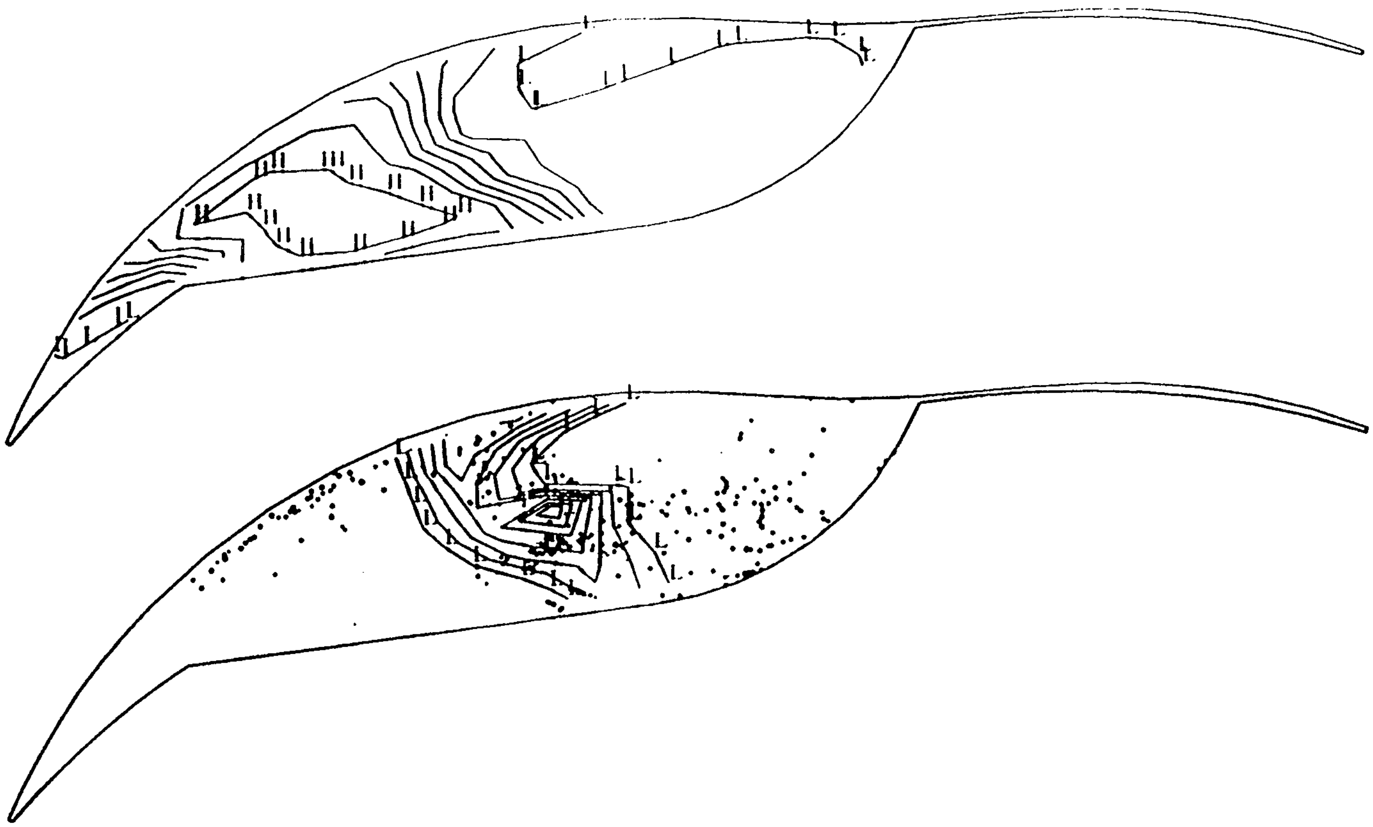

Fig. 40(g): Cross-section view of combustion chamber along symmetry plane showing temperature contours and liquid fuel and vaporized fuel contours at 45 CA ATC for the DM pump system

TEMPERATURE, interval = 228.6 K
H = 2200. ; L = 600.0
MASS FRACTION OF FUEL, interval = 0.1286E-01
H = .1200 ; L = .3000E-01
vertex limits of the region: (1, 8, 1) to (27, 8, 9)
crank angle = 1215.0

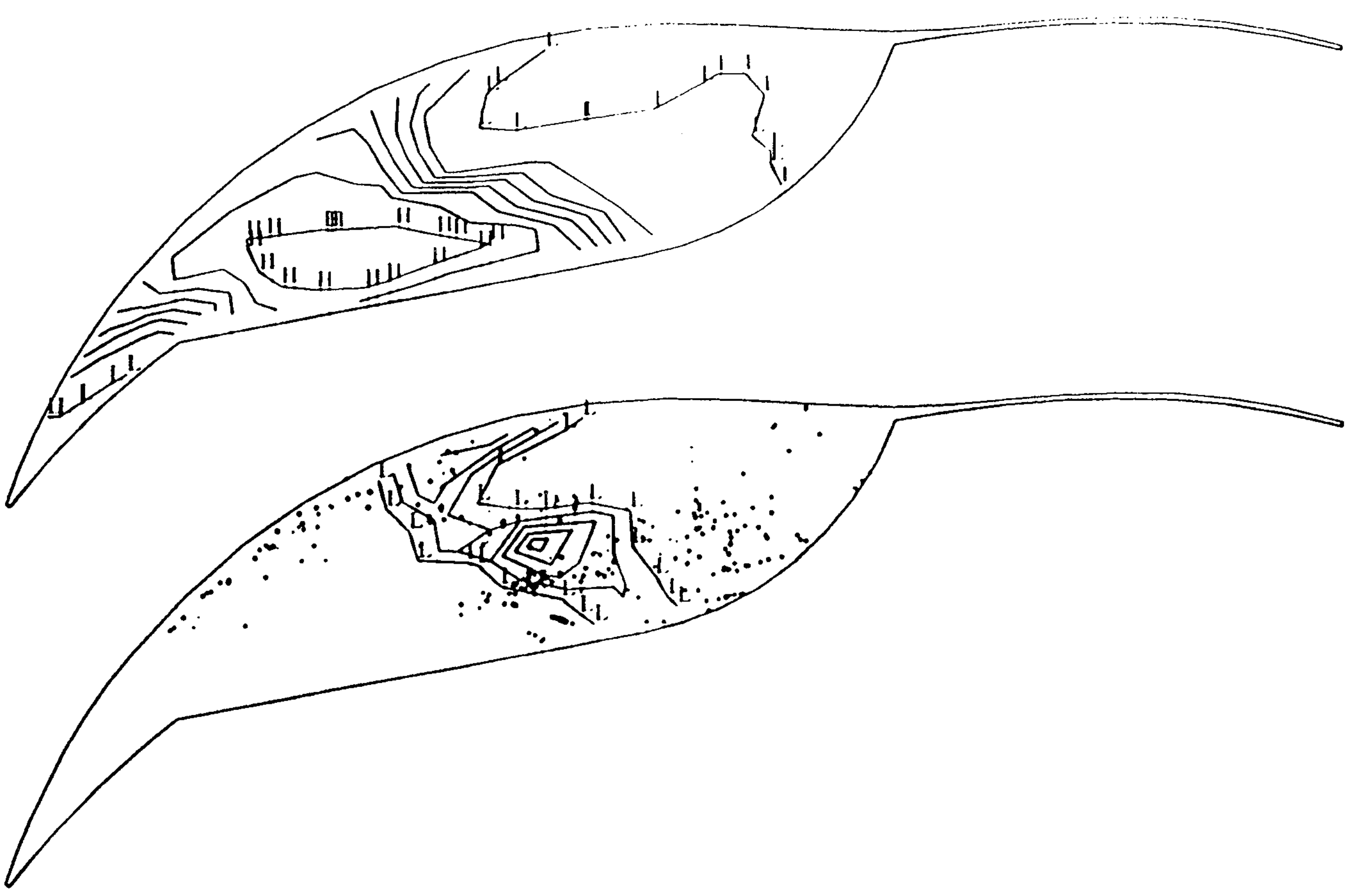

Fig. 40(h): Cross-section view of combustion chamber along symmetry plane showing temperature contours and liquid fuel and vaporized fuel contours at 55 CA BTC for the DM pump system

TEMPERATURE, interval = 228.6 K
H = 2200. ; L = 600.0
MASS FRACTION OF FUEL, interval = 0.1286E-01
H = .1200 ; L = .3000E-01
vertex limits of the region: (1, 8, 1) to (27, 8, 9)
crank angle = 1225.0

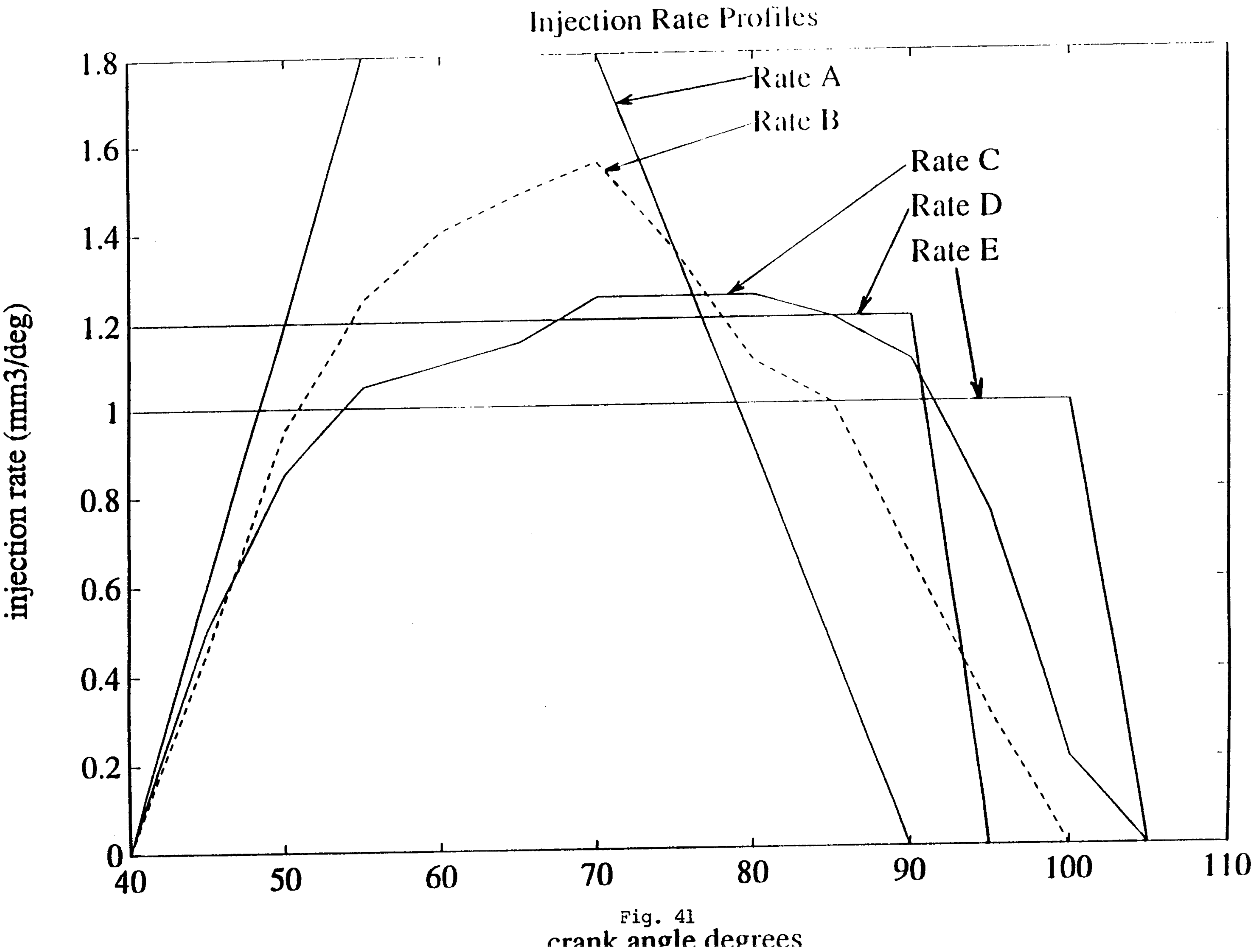
Injection Rate Profiles
Rate A
Rate B
Rate C
Rate D
Rate E
injection rate (mm3/deg)
1.8
1.6
1.4
1.2
1
0.8
0.6
0.4
0.2
0
40
50
60
70
80
90
100
110
crank angle degrees

Fig. 41

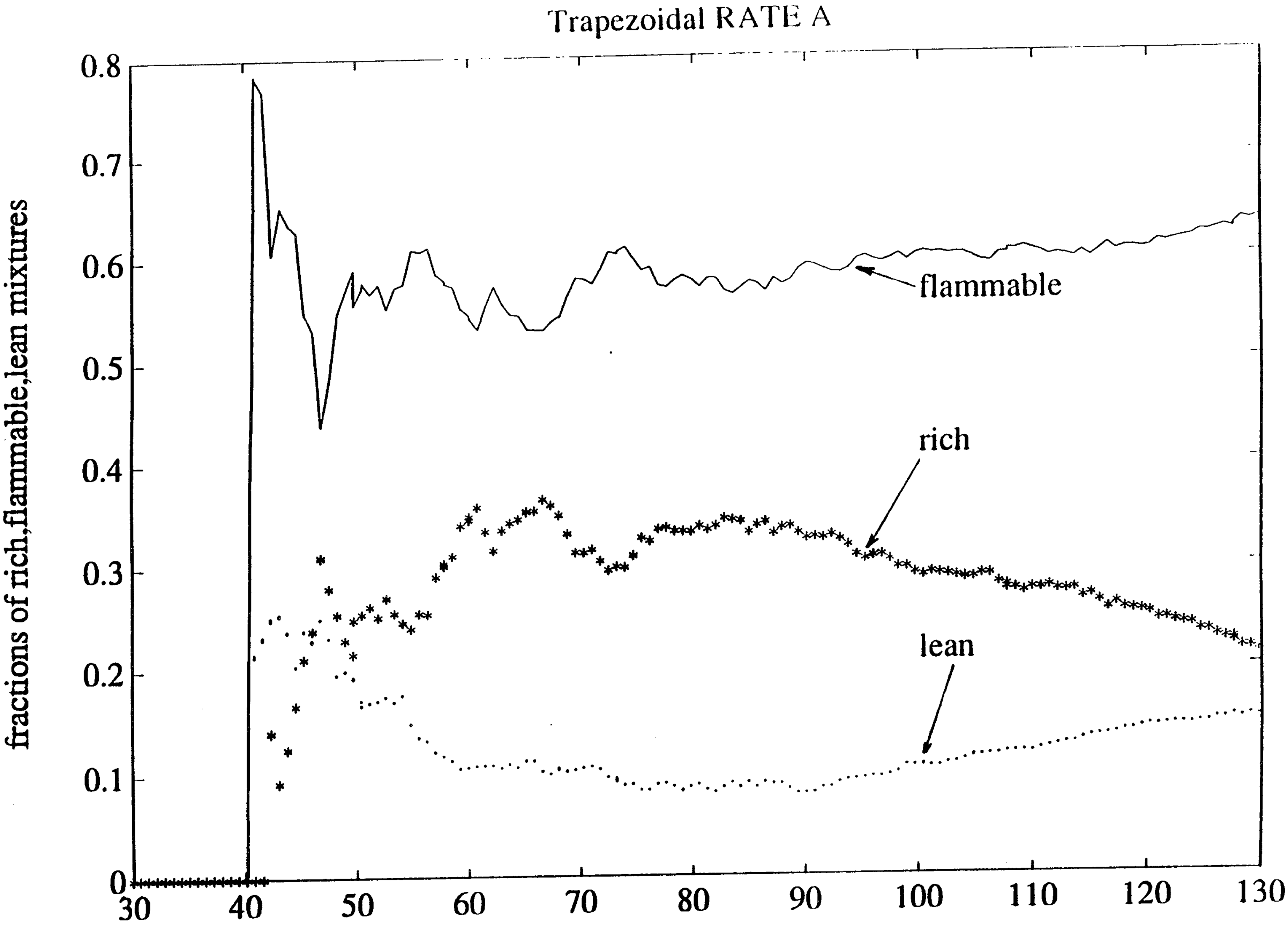
Trapezoidal RATE A
fractions of rich,flammable,lean mixtures
0
0.1
0.2
0.3
0.4
0.5
0.6
0.7
0.8
30
40
50
60
70
80
90
100
110
120
130
flammable
rich
lean
crank angle degrees

Fig. 42

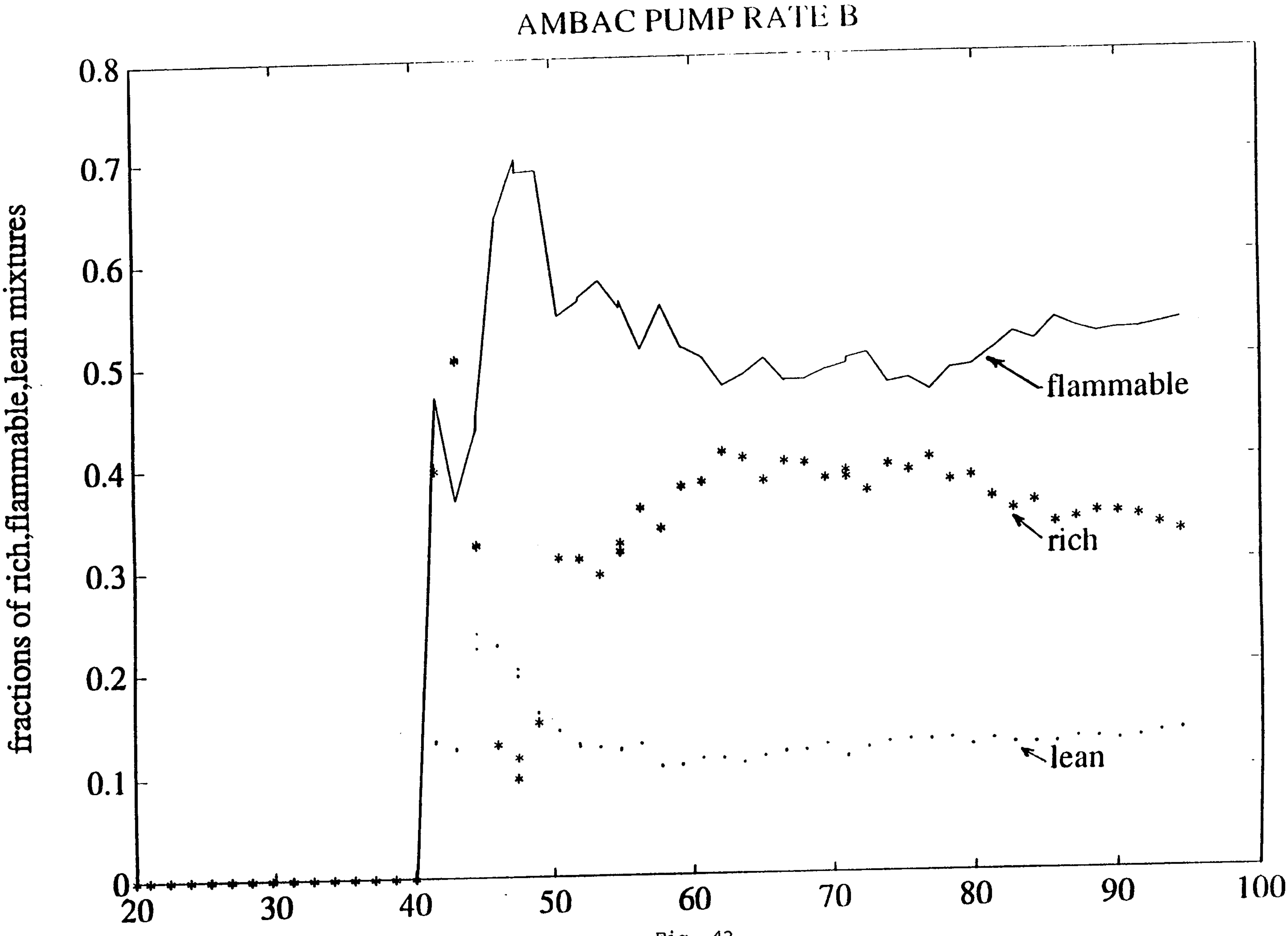
AMBAC PUMP RATE B
fractions of rich,flammable,lean mixtures
0.8
0.7
0.6
0.5
0.4
0.3
0.2
0.1
0
20
30
40
50
60
70
80
90
100
flammable
rich
lean
crank angle degrees

Fig. 43

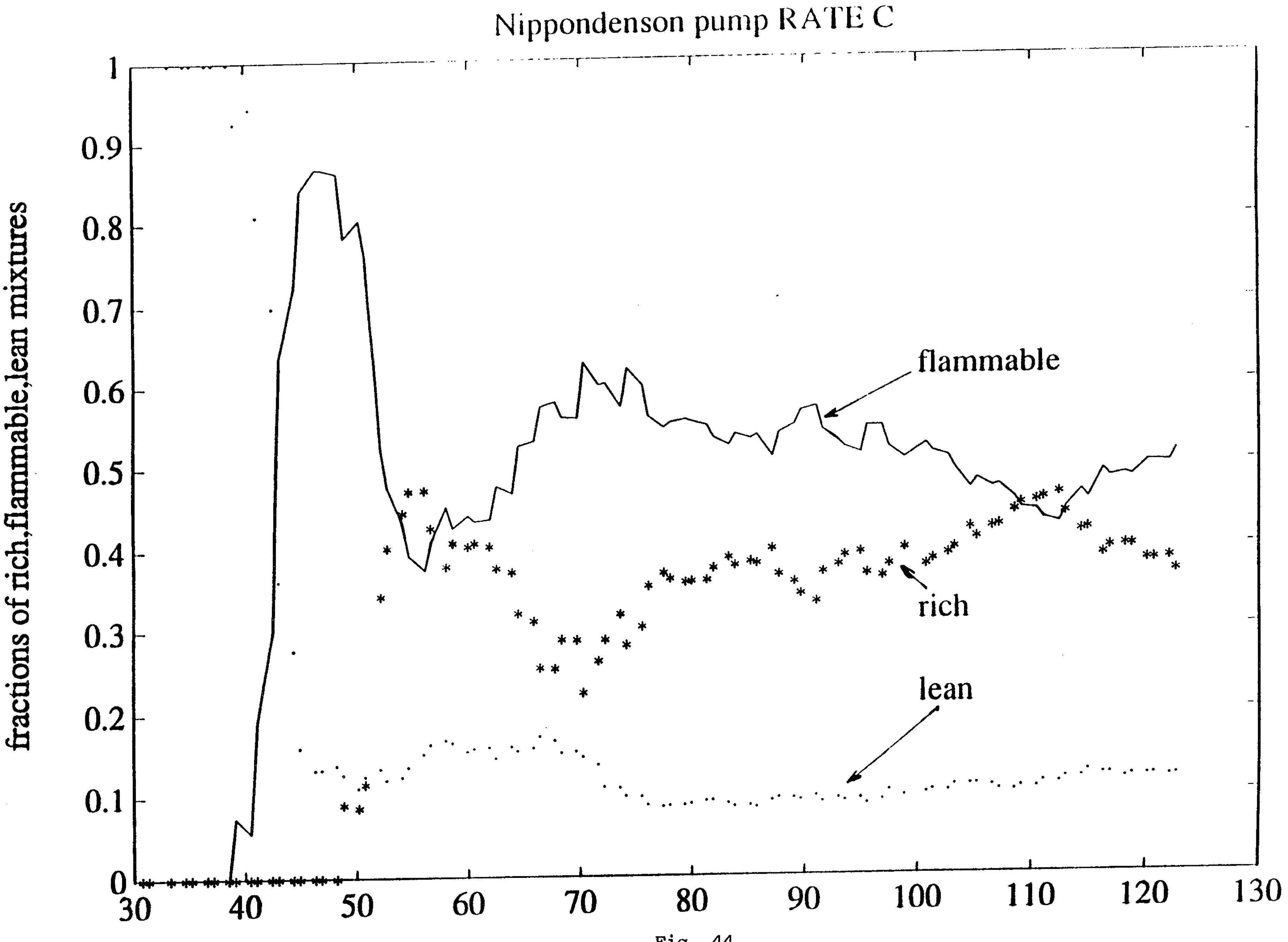
Nippondenson pump RATE C
fractions of rich,flammable,lean mixtures
0
0.1
0.2
0.3
0.4
0.5
0.6
0.7
0.8
0.9
1
30
40
50
60
70
80
90
100
110
120
130
flammable
rich
lean
crank angle degrees

Fig. 44

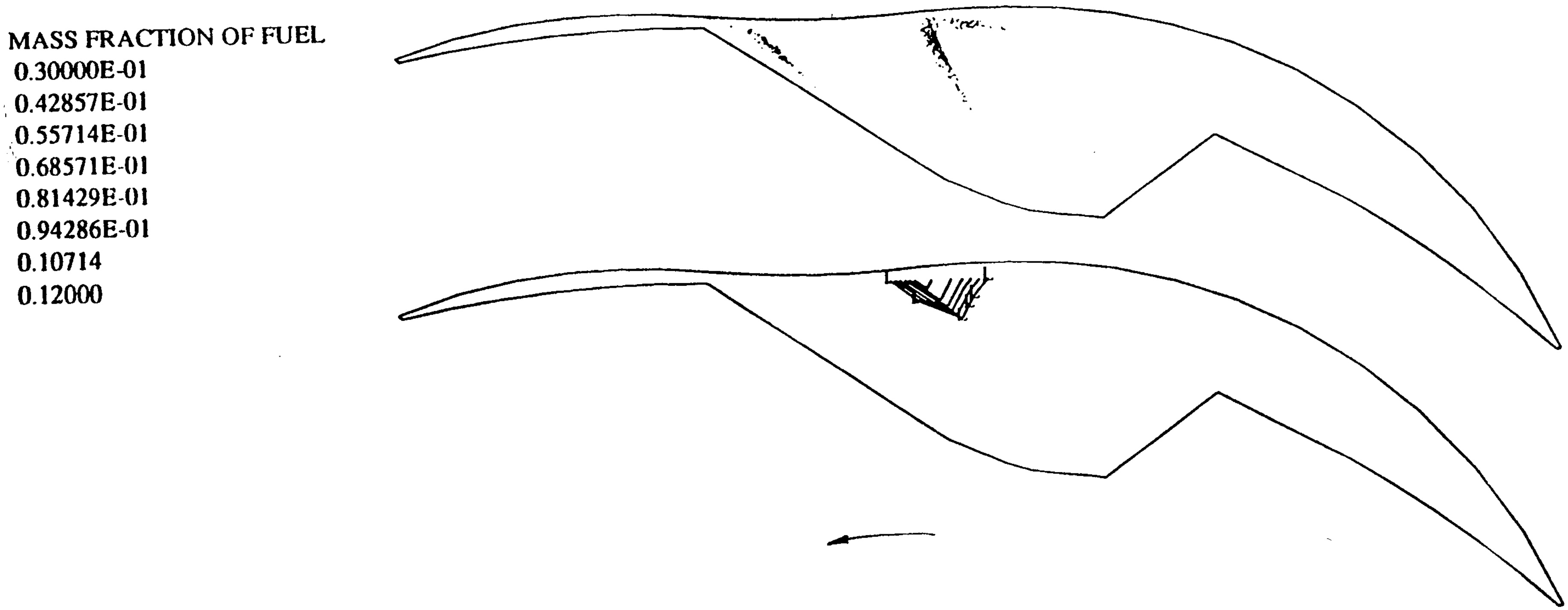

Fig.45(1): Liquid and vaporized fuel distribution at 45 BTC; reference case.

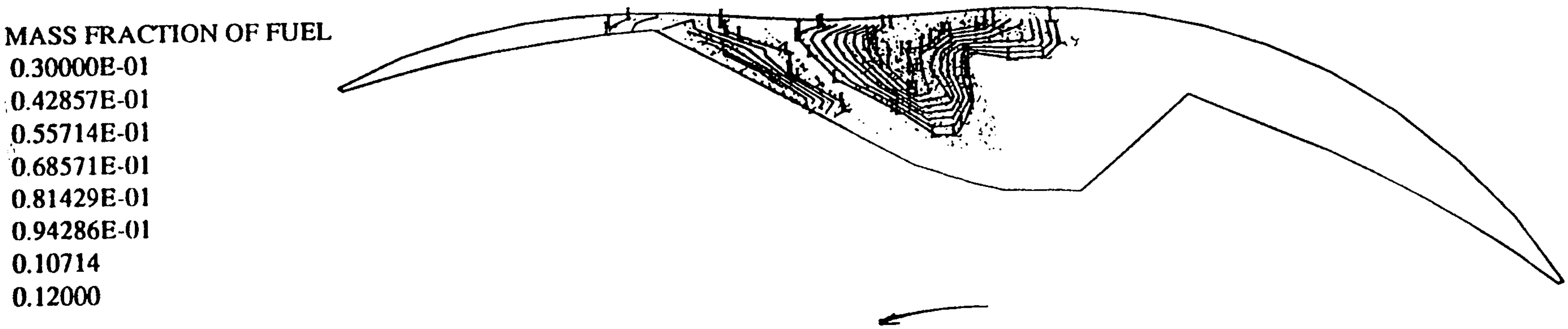

Fig.45(2): Liquid and vaporized fuel distribution at 30 BTC; reference case.

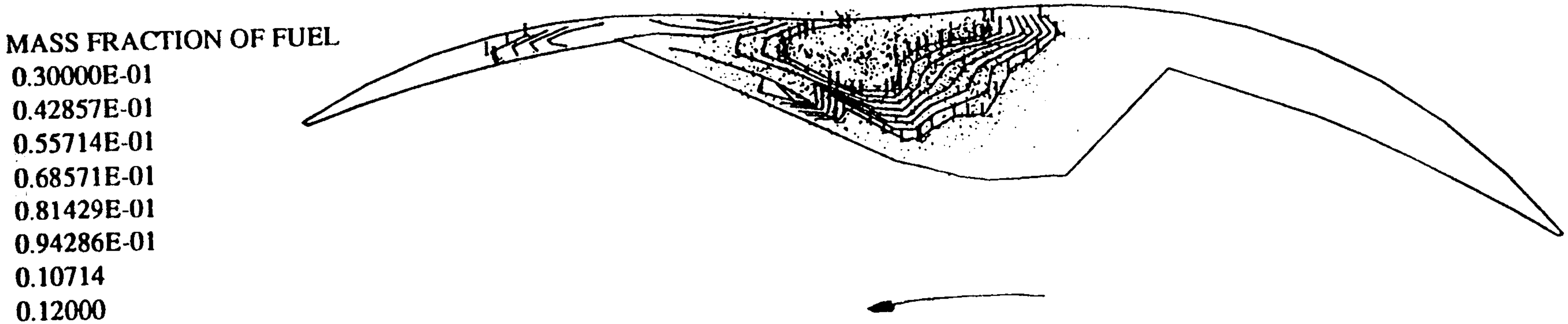

Fig.45(3): Liquid and vaporized fuel distribution at 15 BTC; reference case.

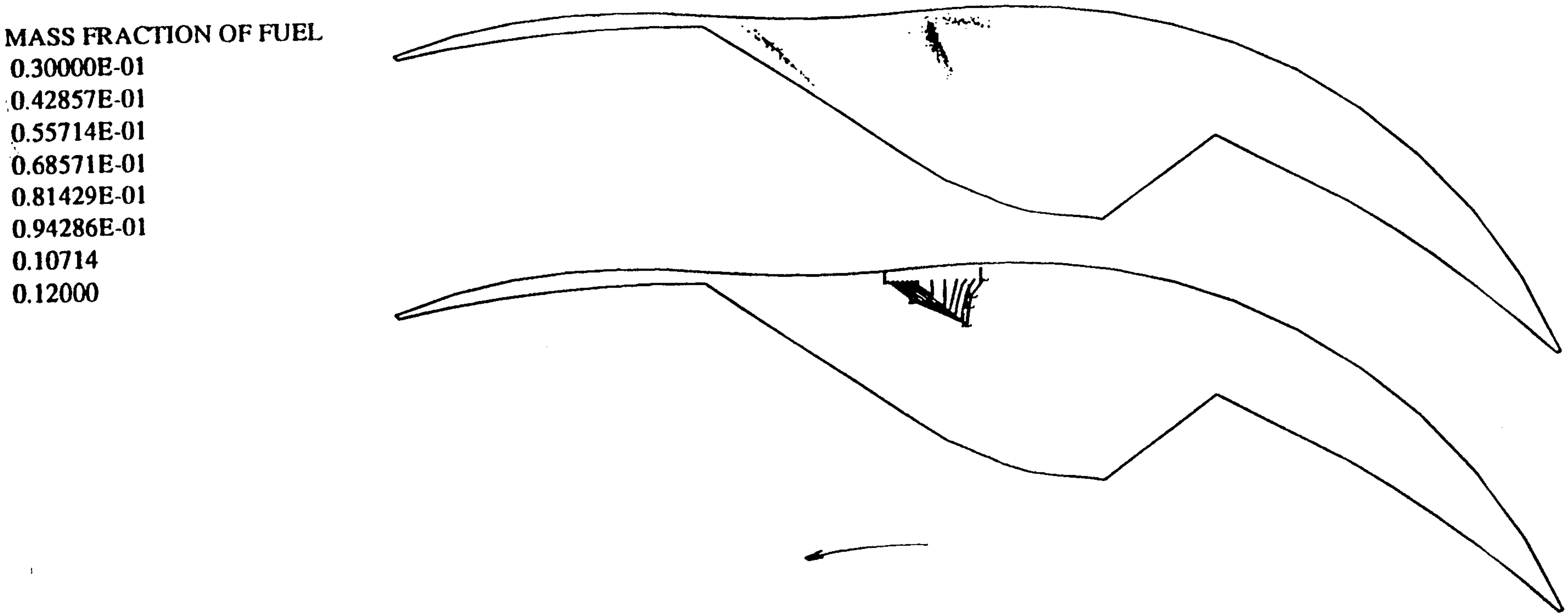

Fig.46(1): Liquid and vaporized fuel distribution at 45 BTC; modified case.

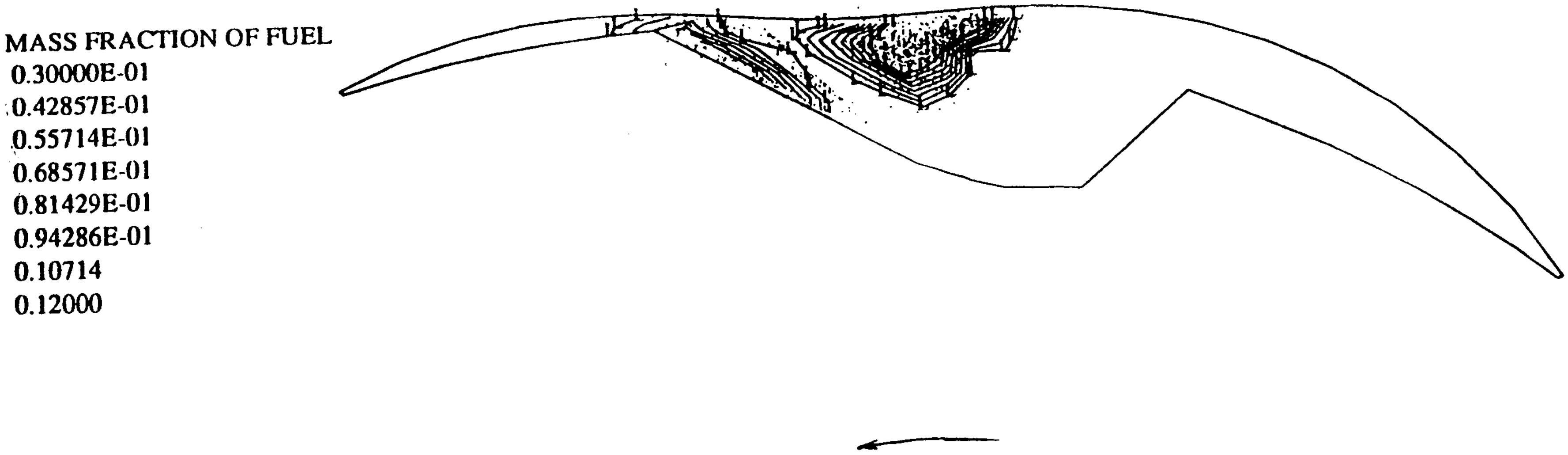

Fig.46(2): Liquid and vaporized fuel distribution at 30 BTC; modified case.

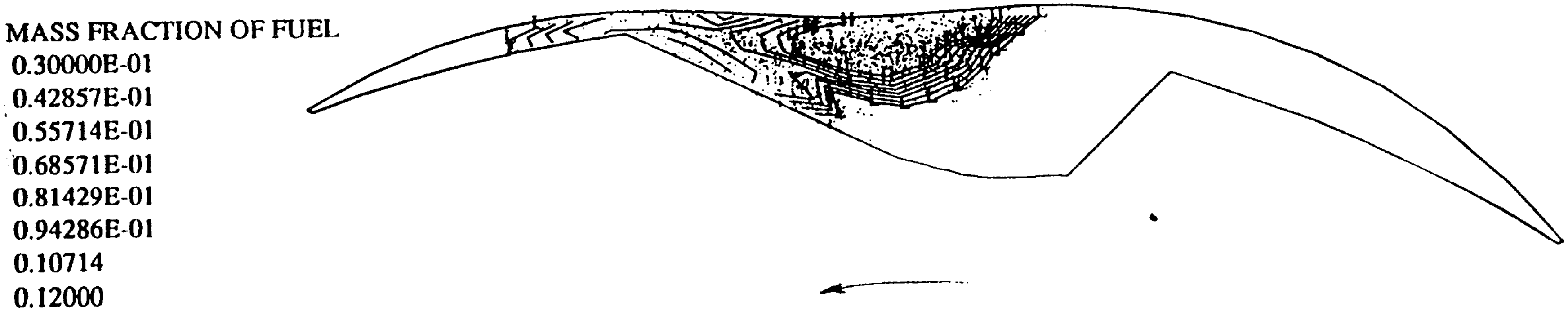

Fig.46(3): Liquid and vaporized fuel distribution at 15 BTC; modified case.

Fig.47: : Study of Effect of L/D ,reference case 1

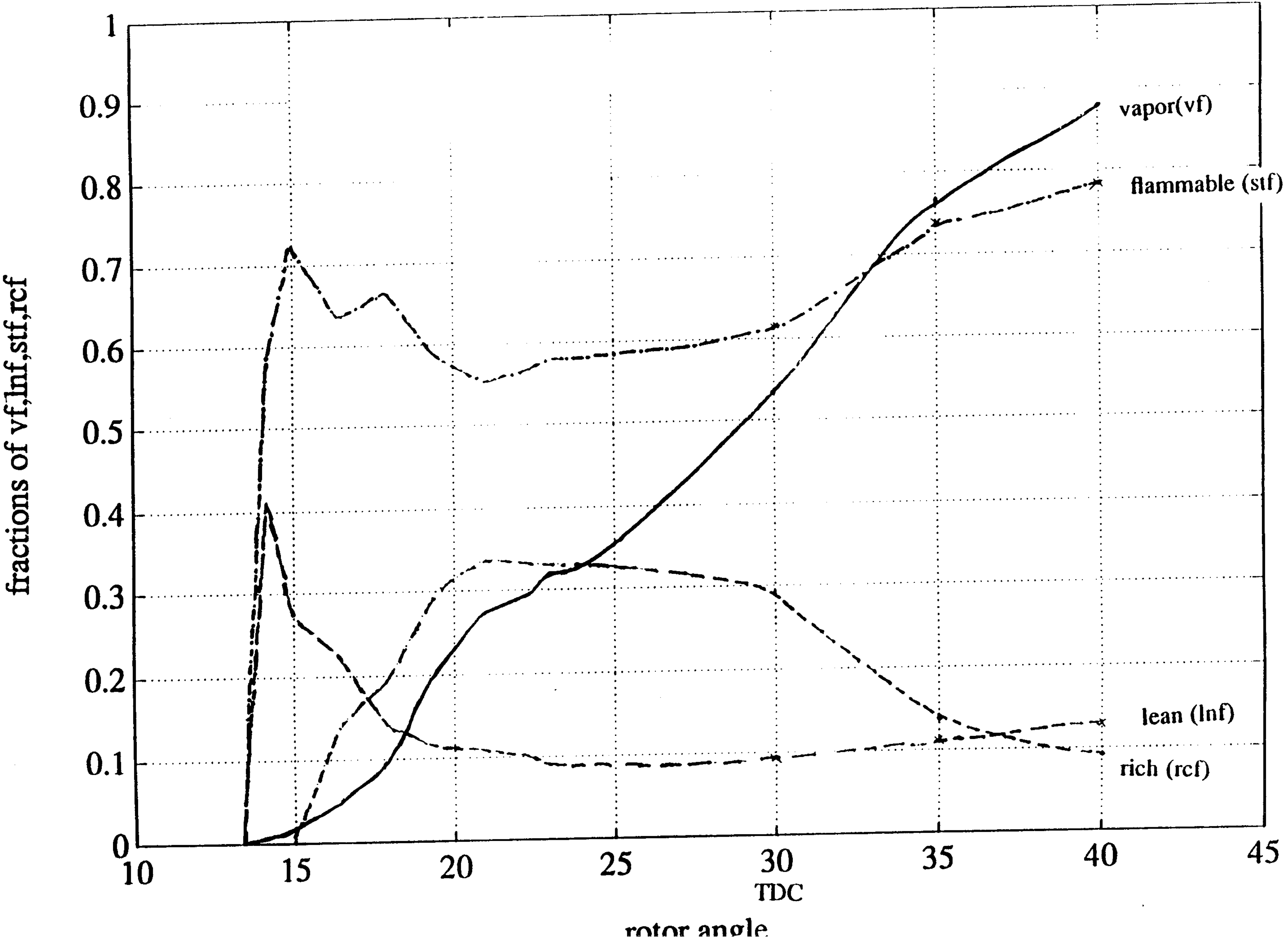

Fig.48: Study of Effect of L/D , Case 2

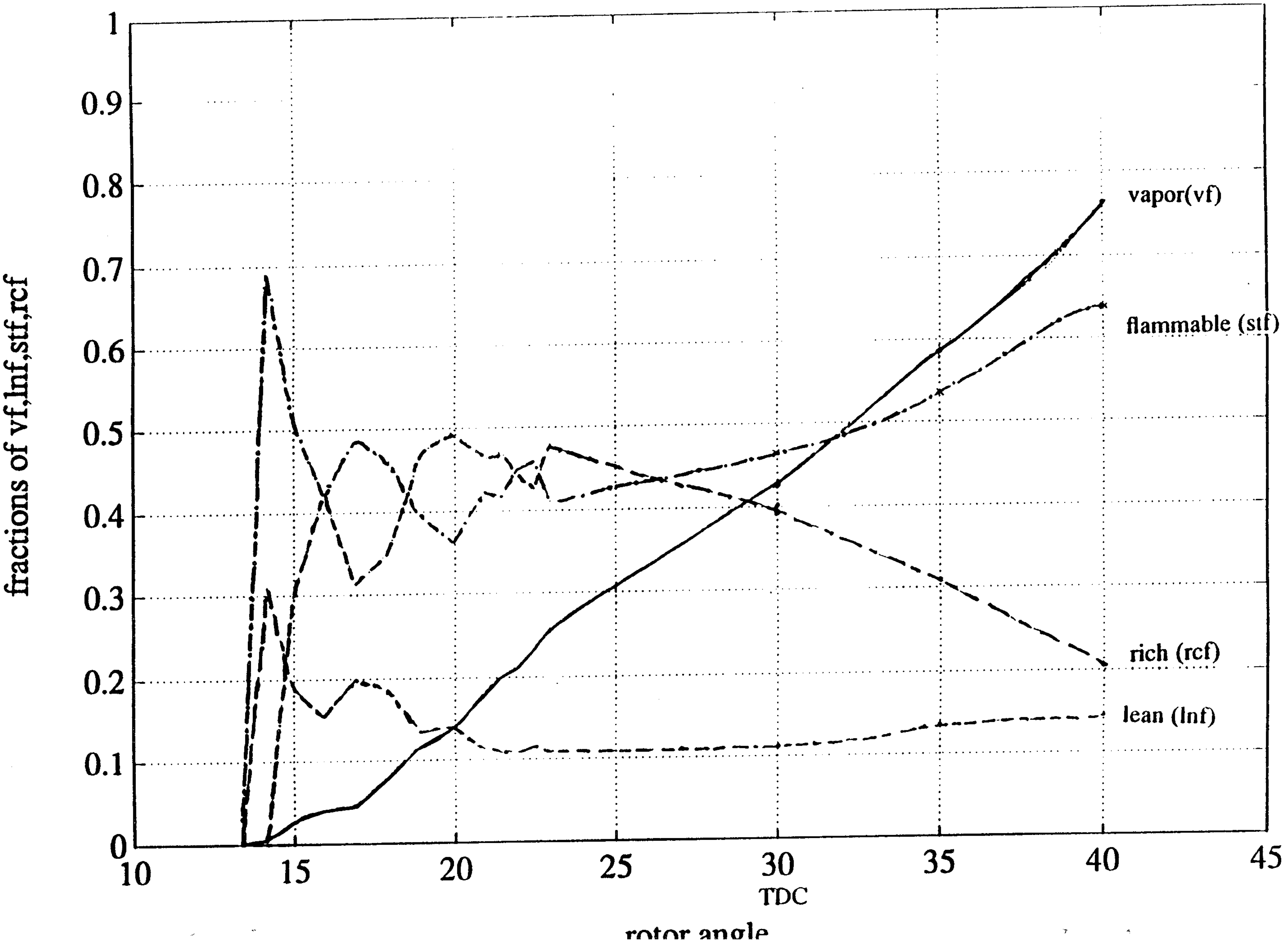

APPENDIX B

FEASIBILITY ANALYSIS--ROTATING VALVE HIGH PRESSURE COMMON RAIL SYSTEM

PRECEDING PAGE BLANK NOT FILMED

APPENDIX B

FEASIBILITY ANALYSIS--ROTATING VALVE HIGH PRESSURE COMMON RAIL SYSTEM

ABSTRACT

This report considers the feasibility of making a high pressure common rail system in which the start, stop, and rate of injection are controlled by a rotating valve. The rotating valve is timed to the engine, either by mechanically driving the valve off of the engine output shaft or by an electronic control system and an electric motor. The system is believed to be capable of operation at 10000 injections per minute at 15000 psi (103.35 mPa) injection pressures. The system should provide accurate injection repeatability, control of fuel delivery and injection rate shaping capability.

PRECEDING PAGE BLANK NOT FILMED

PAGE 136 INTENTIONALLY BLANK

INTRODUCTION

The Stratified Charge rotary engine requires direct chamber fuel injection at a much higher injection frequency than conventional diesel engines. The injection timing range required is somewhat larger than the range required for diesel engines. There are indications that the shape of the injection rate for the rotary engine may be an important tuning parameter. In order to obtain best performance at light loads it may be desirable to operate the engines with one bank, a technique similar to turning off several cylinders of a diesel engine in order to reduce white smoke at light loads.

Additional requirements such as small size and light weight become important when dealing with a rotary engine designed to operate an aircraft. Reliability and controllability become extremely important.

A proposed means of meeting the fuel injection requirements of the rotary engine is to utilize a high pressure common rail system in which a rotating valve provides metering of the fuel.

Figure 1 shows a schematic of the rotary valve concept. In this study we performed design calculations and tests to ascertain the feasibility of this concept. Major areas of concern were:

a) can the valve operate at 10,000 injections/minute without seizing?

b) can the valve operate at the required 15000 (103.35 mPa) psi pressures?

c) can fuel delivery be adequately controlled throughout the speed and load range?

d) can the valves be made accurately enough to guarantee repeatability from one injection to the next and from one injector to the next?

e) can rate shaping be performed by controlling the slot depth?

In the remainder of this report we will address these questions.

TECHNICAL APPROACH

The approach taken was to analyze each required fuel system characteristic individually. Where tractable, analytical tools were used. If a simple analysis was sufficient to bracket the problem (as in fuel leakage between injections), no more detailed calculations were performed.

In the case of valve operating speed, the physical problem is very complex. It was more expeditious to perform an experiment with readily available production hardware to demonstrate the feasibility of operating a rotating valve with very small clearances at high speed.

A) Operating Speed

In order to run at high speeds without seizure of the valve the device must operate in the hydrodynamic lubrication region. Unfortunately the operating characteristics are difficult to predict by calculation because the operating clearance is of the same order of magnitude as the elastic deformation of the bearing elements. This situation is common in fuel injection systems, where the clearance must be kept very small in order to prevent excessive leakage of fuel through it. Any changes in operating temperature of the two pieces also changes the clearance, as do any changes in the pressure of the injected fuel.

We decided that it was less costly and more accurate to determine the feasibility of operating a valve in this regime by a laboratory test. Our test vehicle was a Stanadyne DB4 fuel injection pump shown in Figure 2. The geometry of the rotor (2) operating in the hydraulic head (6) is similar to that of the proposed rotating valve.

Before the test was started the pump was modified by removing four of the six governor flyweights and all of the transfer pump vanes. The transfer pump vanes were removed to prevent excessive side forces on the rotor because experience has shown that Stanadyne distributor pumps seize when the supply pressure exceeds 125 to 130 psi (0.86-0.896 mPa). At the high speeds desired the vane type supply pump will supply far more pressure than that. The governor flyweights were removed as a precaution to avoid excessive loading of the thrust washers, which could cause premature failure of the assembly at a location not critical to the test.

After these precautions the pump was run up in speed starting at 2000 rpm and increasing by 100 rpm increments every 15 minutes. Fuel delivery was controlled to keep injection pressure around 5000 psi (34.45 mPa) in order not to exceed the normal operating limits of the pump. The test was purposely structured to avoid thermal growth problems by allowing the temperature to stabilize at each point. The result was that the pump survived all speeds up to 3800 RPM and failed after only a few seconds at 3900 rpm.

A rotary metering valve can be designed to operate at any desired integral fraction of engine speed up to half engine speed. Two options which would have lower surface speeds than those experienced in the DB4 speed test are a 15 mm valve operating at half engine speed and a 21 mm valve operating at 1/3 engine speed. Since two reasonable rotary valve systems can be designed with lower surface speeds this evidence is sufficient to prove feasibility of the design from a bearing capability standpoint. We will have to pay careful attention to the clearance changes expected during thermal transients.

HIGH PRESSURE COMMON RAIL

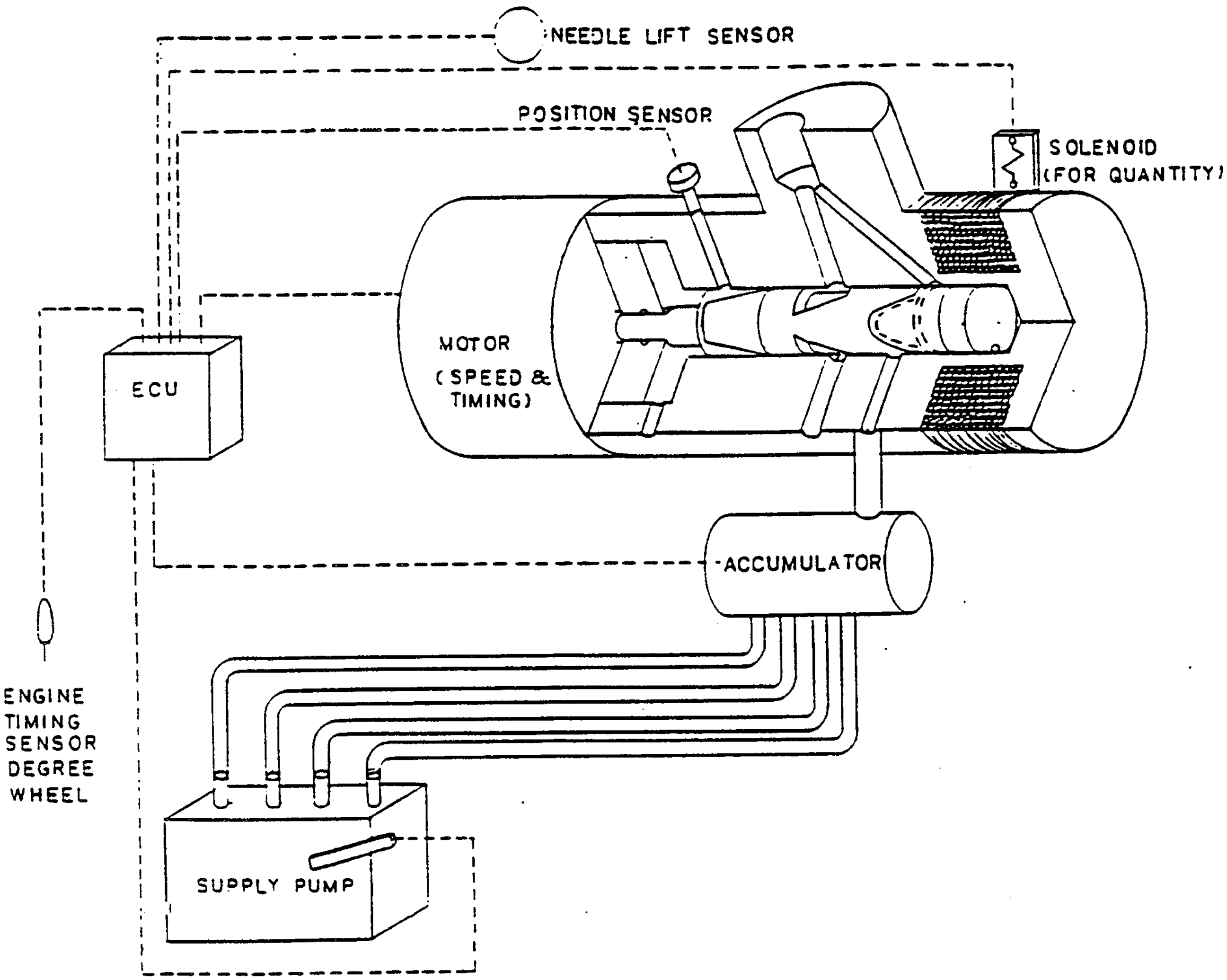
NEEDLE LIFT SENSOR
POSITION SENSOR
SOLENOID (FOR QUANTITY)
MOTOR (SPEED & TIMING)
ECU
ACCUMULATOR
ENGINE TIMING SENSOR DEGREE WHEEL
SUPPLY PUMP

ROTARY VALVE SCHEMATIC

Figure No. 1

10000 INJECTIONS/MINUTE

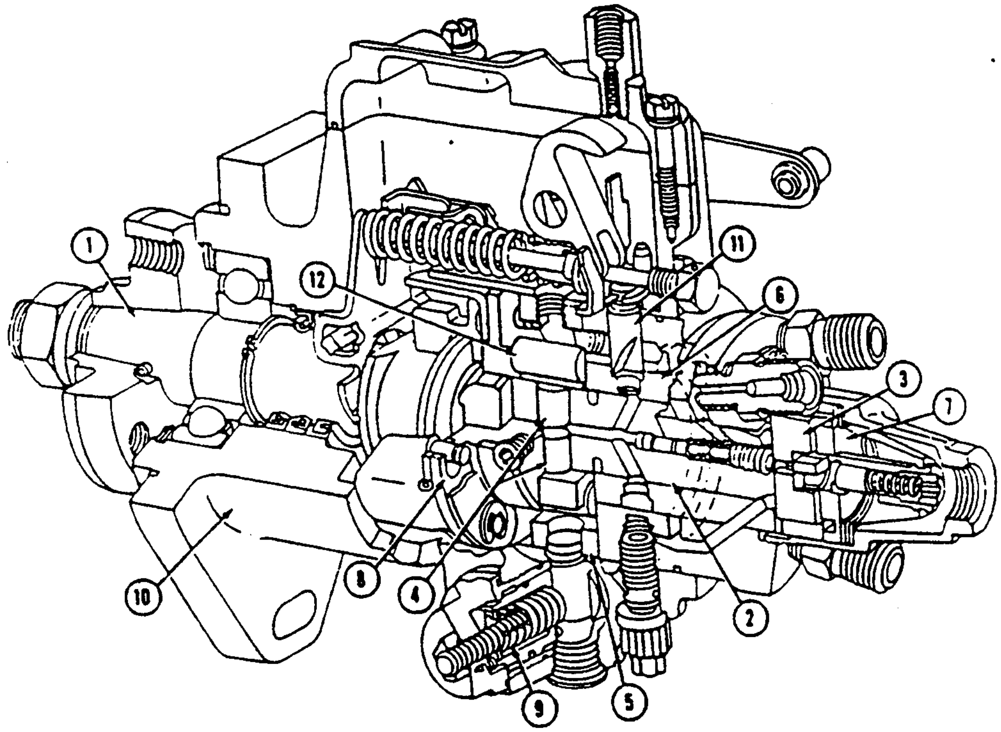

STANADYNE DB4 PUMP WITH 21MM DIAMETER ROTOR WAS RUN TO 3800RPM (SURFACE SPEED 822 FT/MIN, 250 M/MIN)

OPTION 1) RUN 21 MM SHAFT AT 3300RPM WITH 3 SLOTS (9900 ENGINE RPM, SURFACE SPEED 713 FT/MIN, 217 M/MIN)

OPTION 2) RUN 15 MM SHAFT AT 5000RPM WITH 2 SLOTS (10,000 ENGINE RPM, SURFACE SPEED 772 FT/MIN, 235 M/MIN)

THE PREFERRED OPTION IS OPTION 2 BECAUSE OF SMALLER PRESSURE AND THERMAL GROWTH PROBLEMS

STANADYNE DM PUMP

Figure No. 2

B) Operation at 15000 psi (103.35 mPa)

The second major question is whether such a system can operate at 15000 psi (103.35 mPa) injection pressures. As Figure 3 shows the pressures are balanced in all directions. The maximum unbalanced pressure forces expected from manufacturing tolerances in the metering slots are expected to be around 120 lbf (534N).

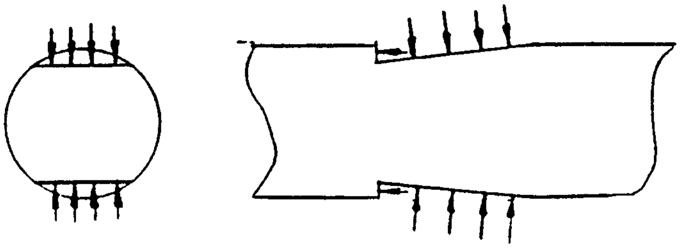

FIGURE 3

BALANCED PRESSURE IN ROTARY VALVE

Further investigation shows that leakage through the valve clearances is the major difficulty with the rotating valve idea. From finite element stress analysis we see that 15000 psi (103.35 mPa) of fluid pressure causes around .0002" (.005mm) of radial growth on a 15 mm barrel. Increasing the thickness of the barrel wall is of little assistance in reducing this growth because the barrel is already so thick that the growth of the external radius is quite small. The standard un-pressurized diametral clearance for this type of device is around .00015" (.0038mm), indicating an operating radial clearance with pressure applied of around .000275". (.007mm) Figure 4 shows the leakage rate through this clearance for one design configuration. The horizontal line is 10% of the injected fuel flow rate. It is apparent that under these conditions the leakage flow will be about 30% of the injected flow at 15000 psi (103.35mm mPa) injection pressures.

A more severe problem may be the leakage from the metering orifice between injections. Figure 5 shows the worst case leakage during the time between injections. The calculation used was orifice flow through the curtain area around the metering orifice; the true case will be bearing flow between flat plates and will be lower. This time the horizontal line represents rated fuel delivery. It can be seen that at the worst case clearance of .000275" (.007mm) the loss in efficiency due to leakage will be about 50% at 5000 rpm. The overall efficiency after accounting for leakage during the injection will be on the order of 43%. When we factor in the efficiency of the high pressure pump at around 70% we obtain a system overall efficiency of 30%, which is slightly better than that obtained with conventional fuel injection systems.

LIMITING FACTOR - LEAKAGE THROUGH THE CLEARANCE

DURING INJECTION

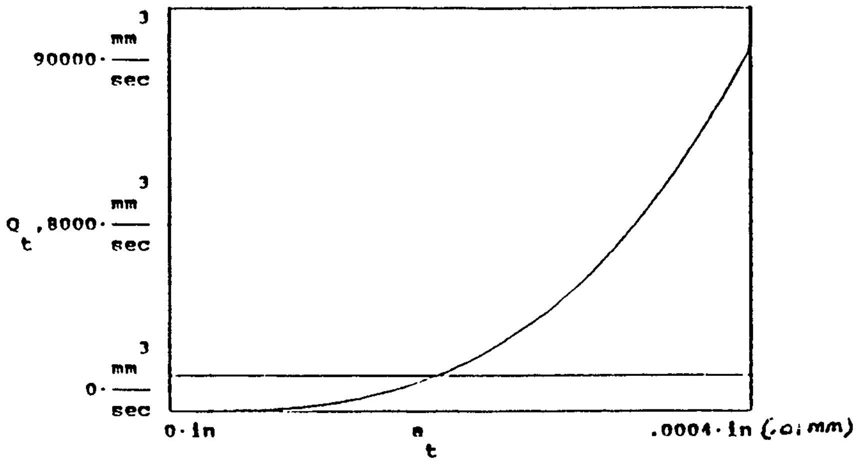

Flow through clearance vs clearance

PRESSURE GROWTH OF OPERATING CLEARANCE = .0002 INCHES (.005mm)
FIGURE 4

BETWEEN INJECTONS

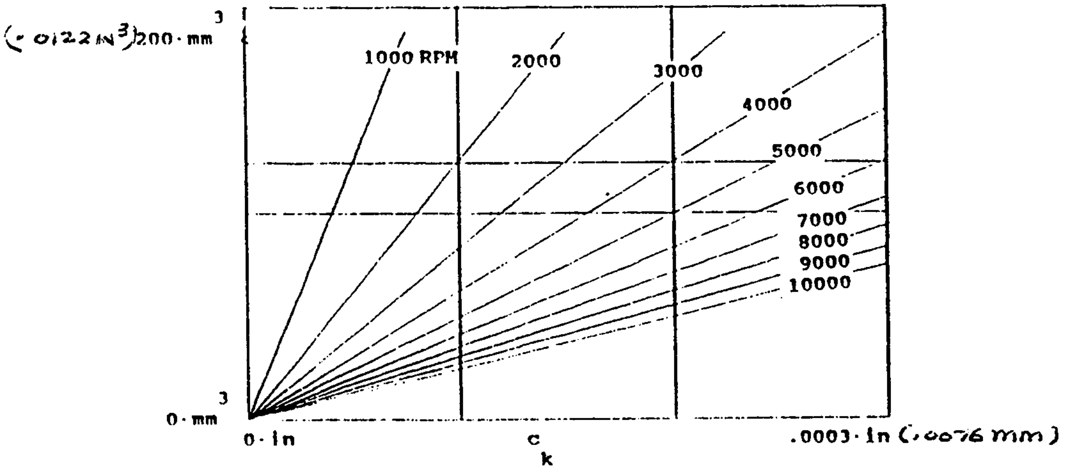

Leakage through curtain area of shut valve

FIGURE 5

LEAKAGE RATE THROUGH THE VALVE

FIGURES 4 AND 5

The losses caused by valve leakage are tolerable when operating a rotary engine at moderate to high speeds. Leakage between injections causes greater difficulty when trying to operate the injection system at low injection frequencies. Some techniques for reducing this leakage will be required in the unlikely event that we desire to operate at low speed and high injection pressures. One relatively simple technique for reducing the leakage would be to run the rotating valve at an intermediate pressure (say 5000 psi/34.45 mPa) and use a hydraulic amplifier in the injection nozzle to boost the pressure to 15000 or even 20000 psi (103.35-137.88 mPa). The necessity for incorporating leakage reduction techniques can best evaluated experimentally.

C) Fuel Delivery Control

Since the flow rate is constant for a given valve position and injection pressure, the quantity of fuel delivered decreases as the engine speed increases. Figure 6 shows the calculated fuel delivery at a constant 15000 psi (103.35 mPa) rail pressure as a function of valve speed and axial position. In our test case we assumed a simple angled flat cut for the metering slot. The cut is .427 mm deep at the deepest end and angled to be 0 mm deep at a point 8mm away. The falling fuel delivery characteristic seen in Figure 6 is good from an engine control standpoint because it means that the engine will be inherently stable. The constant axial position fuel delivery curves become further apart as the engine speed is decreased. This means that the control system will have to account for increasing mechanical fuel delivery gain as the engine speed is decreased.

Control of fuel delivery at cranking speeds will be difficult. We believe that we can obtain acceptably low fuel deliveries by setting the rail pressure slightly higher than nozzle opening pressure and restricting the fuel flow at the metering orifice of the valve. This will cause the nozzle to chatter as it does with conventional systems.

Two concepts have been considered for controlling this fuel system. The first is purely mechanical, with the metering valve driven from the engine eccentric shaft through cogged belts. Timing is changed by increasing or decreasing the engagement of a helical spline which is placed in the drive linkage between the cogged belt and the rotating shaft. The quantity of fuel delivered is set by a push-rod which positions the valve axially. All aspects of this mechanical control system are well within the current state of the art; the system could be made with very little risk. It does, however, place undesirable restrictions on the engine design. Compensation for increased low speed gain can be partially achieved by proper configuration of the metering slot in the valve.

The second concept is for electronic control of the valve. The pressure forces on the valve rotor are balanced so that it is free floating. The torque required to drive the valve and the forces required to change the axial position of the valve are small enough to be handled by conventional DC motors and solenoids. Figure 7 is a conceptual diagram of a control system which would provide synchronization of the rotary valve with the engine eccentric shaft,

FLOW RANGES AND SPEEDS

Estimated Fuel Delivery as a function of engine speed and valve position

R = 7.5·mm metering valve diameter
r = 0.729·mm metering orifice radius
h0 = 0.427·mm max. metering slot depth
L = 8·mm metering slot length
D_n = 0.26·mm nozzle orifice diameter
Ph = 15500·psi rail pressure
Pc = 1000·psi combustion pressure
$\rho = 0.84 \cdot \frac{gm}{cm^3}$ fuel density

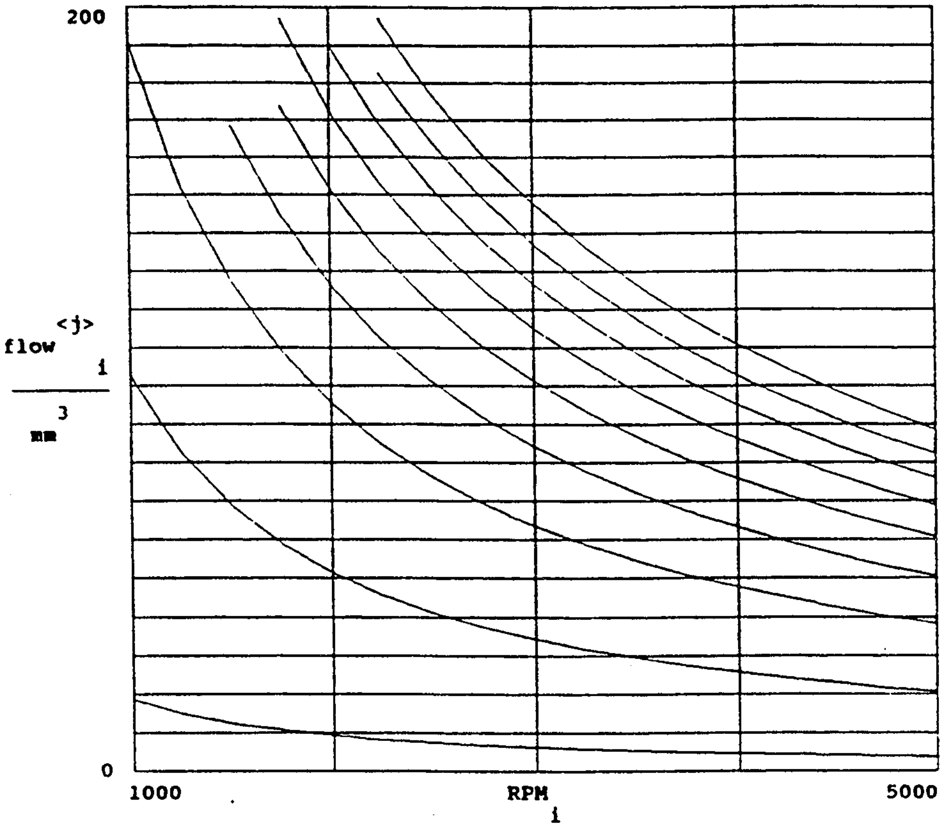

LOW QUANTITIES OF STARTING FUEL FLOW ARE DIFFICULT TO OBTAIN

REDUCE RAIL PRESSURE TO JUST ABOVE NOZZLE OPENING PRESSURE

RESTRICT FUEL FLOW AT METERING ORIFICE

FUEL DELIVERY VS SPEED AND AXIAL POSITION

FIGURE 6

—ROTARY VALVE DRIVE MOTOR CONTROL SYSTEM—

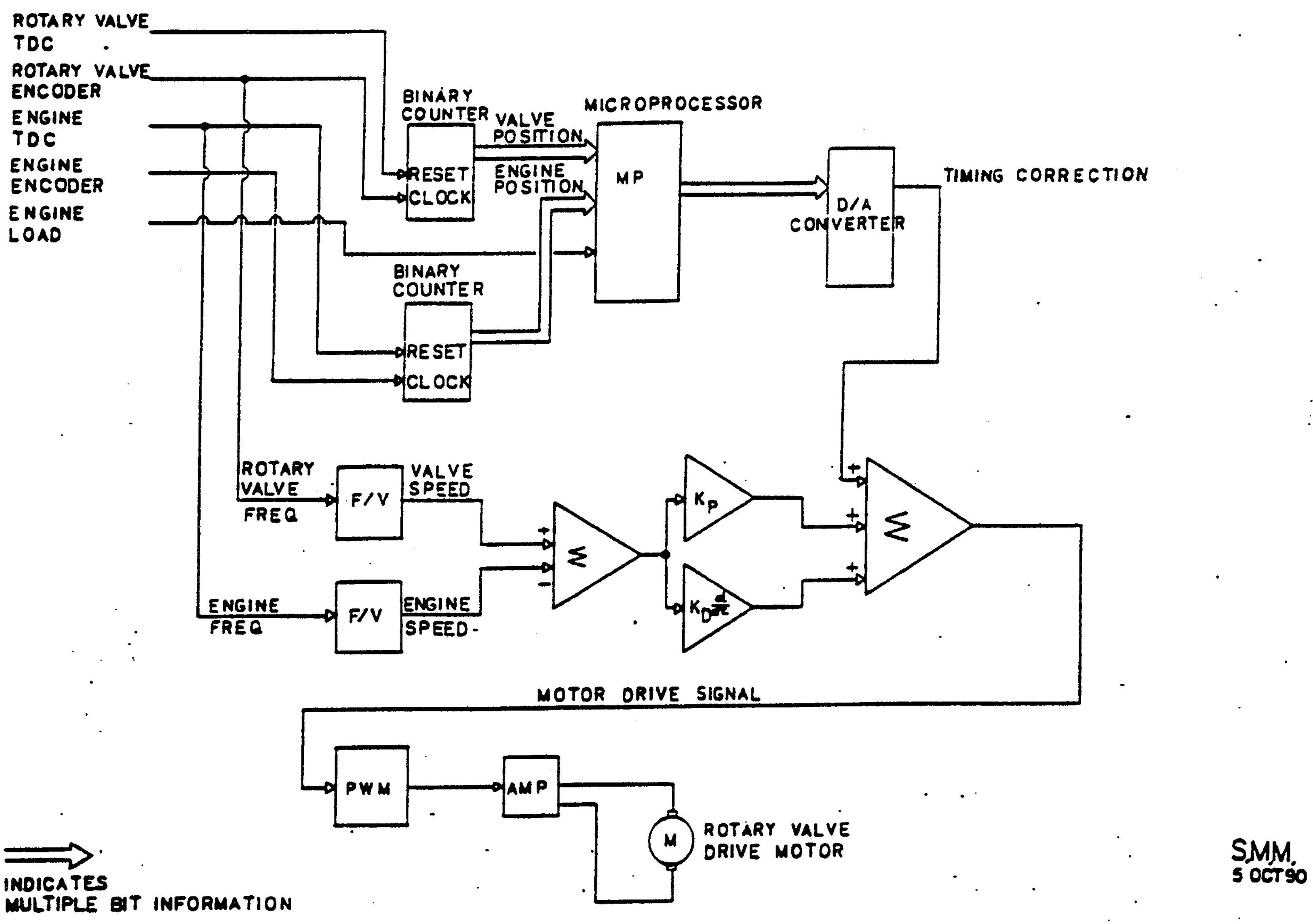
ROTARY VALVE TDC
ROTARY VALVE ENCODER
ENGINE TDC
ENGINE ENCODER
ENGINE LOAD
BINARY COUNTER
RESET
CLOCK
VALVE POSITION
ENGINE POSITION
MICROPROCESSOR
MP
D/A CONVERTER
TIMING CORRECTION
BINARY COUNTER
RESET
CLOCK
ROTARY VALVE FREQ
F/V
VALVE SPEED
ENGINE FREQ
F/V
ENGINE SPEED
+
-
Σ
K_P
$K_D\frac{d}{dt}$
+
+
+
Σ
MOTOR DRIVE SIGNAL
PWM
AMP
M
ROTARY VALVE DRIVE MOTOR
INDICATES MULTIPLE BIT INFORMATION
SMM
5 OCT90

ELECTRONIC CONTROL OF VALVE ROTATION

FIGURE 7

thereby reducing the mechanical connections to some wires, a fuel inlet and a fuel outlet and vastly reducing packaging difficulty. A second circuit as shown in Figure 8 would be required to control the engine power and the high pressure pump output. With this system we gain all the advantages of electronic control; independent control of injectors, complete timing flexibility as a function of speed and load, and the ability to change governing characteristics with engine speed and load.

The rotary valve concept can control fuel delivery adequately throughout the very wide speed range of the rotary engine. Even though more work and some additional risk are involved in developing an electronic control system, we recommend this approach for the aircraft application because of the added flexibility in function and packaging. Using the electronic approach will allow us to avoid procuring a separate test facility for rotary valve development, since all necessary input signals can be generated by a computer.

D) Repeatability from Injection to Injection

If there is wide variation between the injections there will be wide cycle to cycle variation in peak engine firing pressure. Since the engine must be designed to withstand the highest pressure peaks, It will be larger and heavier for a given power output if the injections are not consistent. The rotary valve scheme benefits from the short distance between the controlling mechanism and the injection nozzle, which reduces the hydraulic difficulties usually inherent in fuel injection systems. In addition, the rotary valve scheme allows for very accurate control of the residual pressure in the injection system, which further improves control of the hydraulics. The remaining difficulty is control of the manufacturing tolerances on the metering slot. A study of sensitivity to slot geometry changes shows that a .0002" (.005mm) difference in depth between the two metering slots allows 2.5 mm^3/injection (roughly 2% of full load quantity) difference in delivery at 15000 psi (103.35 mPa) and 10000 injections/minute. This difference is increased to 6.8 mm^3/injection (roughly 5% of full load quantity) when the speed is reduced to 2000 RPM without reducing the rail pressure. The .0002" (.005mm) tolerance band is in the normal realm of fuel injection manufacturing capabilities.

In conjunction with obtaining repeatability from one injection to the next of the same injector, it is also important to be able to obtain repeatable fuel delivery from one injector to the next. Since this system is orifice controlled and not positive displacement, we expect somewhat more sensitivity to nozzle orifice area and nozzle opening pressure than will occur with more conventional systems. The design has the advantage that the metering device is part of the injection nozzle, so that the whole system can be calibrated at manufacture if necessary. At this time we see no insolvable difficulties with injector to injector repeatability.

E) Rate Shaping

ROTARY VALVE INJECTION -
ENGINE SPEED/LOAD CONTROL

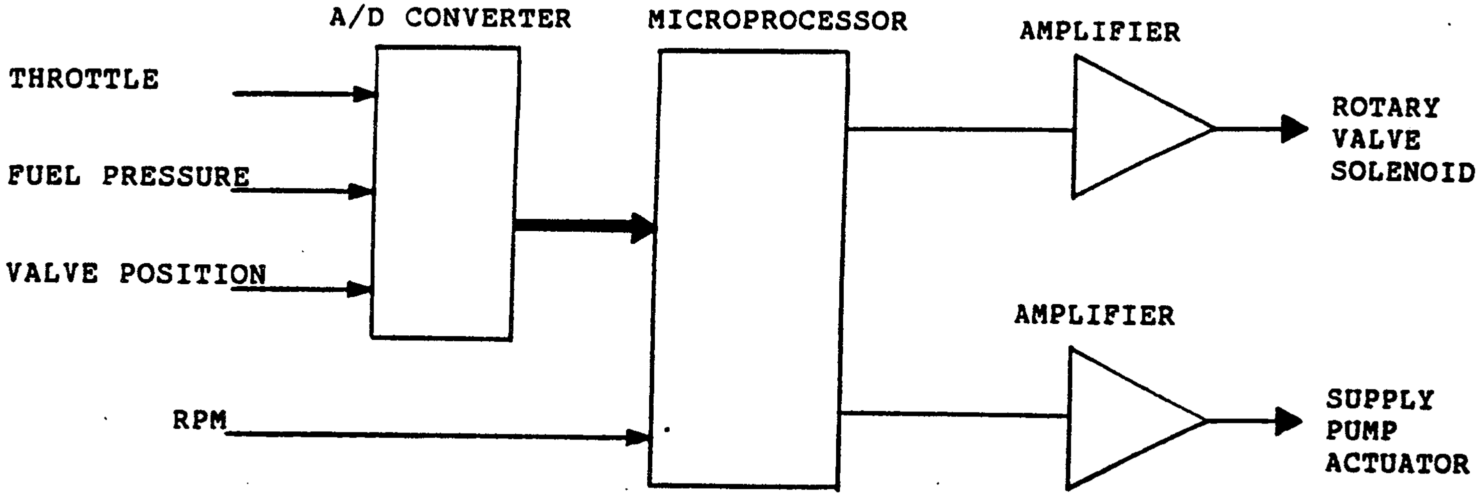
A/D CONVERTER
MICROPROCESSOR
AMPLIFIER
THROTTLE
FUEL PRESSURE
VALVE POSITION
RPM
ROTARY VALVE SOLENOID
AMPLIFIER
SUPPLY PUMP ACTUATOR

ELECTRONIC CONTROL OF FUEL DELIVERY

FIGURE 8

S.M.M.
24 OCT 90

A major advantage the rotary valve device has over more conventional systems is the capability of shaping the injection rate curve. This is accomplished by restricting flow into the metering valve at the metering orifice. The size of the effective orifice is varied by controlling the depth of the metering slot and thereby limiting the curtain area through which the delivered fuel must flow. Figure 9 shows the sensitivity of injection pressure to clearance height. The metering orifice size is selected to obtain peak injection pressure (wide open orifice) of 15000 psi (103.35 mPa) with the selected rail pressure. We can see that the control band is on the order of .008 inches (0.203mm), which is sufficient to allow precise control over the injection rate.

Restricting the fuel at the inlet to the valve will create heat. Since the amount of flow restriction will vary as a function of engine load, the temperature of the fuel going into the valve can be expected to change very rapidly. With operating clearances as low as .00015" (.0038mm) diameter, any difference in thermal growth between the valve body and the valve rotor can cause the valve to seize. Figure 10 shows the temperature rise in Jet A fuel as a function of initial temperature and pressure. We see that a worst case load transient might change the fuel temperature by as much as 80° F (26.7° C).

We have therefore performed a set of transient thermodynamic analysis of the valve in order to evaluate this effect. Figure 11 shows the minimum valve clearance as a function of time from application of an 80° F (26.7° C) change in fuel temperature. We have also considered manufacturing the valve from materials with dissimilar thermal properties in order to design in appropriate transient thermal growth. If the rotor were manufactured out of stainless steel its thermal growth would be slowed down because of the lower conductivity and higher heat capacity of stainless. Figure 11 also shows the clearance change in a transient where the rotor is made from stainless steel.

CONCLUSIONS:

1. The rotary valve high pressure common rail fuel injection system shows great promise for use with the rotary engine. All of the characteristics we investigated showed that the rotary valve could be made to work well provided proper care was taken in design and manufacture of the system.

2. Great care must be taken in selecting the materials for the rotary valve in order to avoid problems with thermal transients.

3. The most difficult control problem with the rotary valve system is limiting the fuel quantity during starting.

4. Manufacturing tolerances for the metering slot must be held quite tightly in order to provide accurate fuel metering from one injection to the next. The required tolerance is within the realm of current fuel injection practice.

INJECTION RATE SHAPE CONTROL--RAIL PRESSURE SELECTION

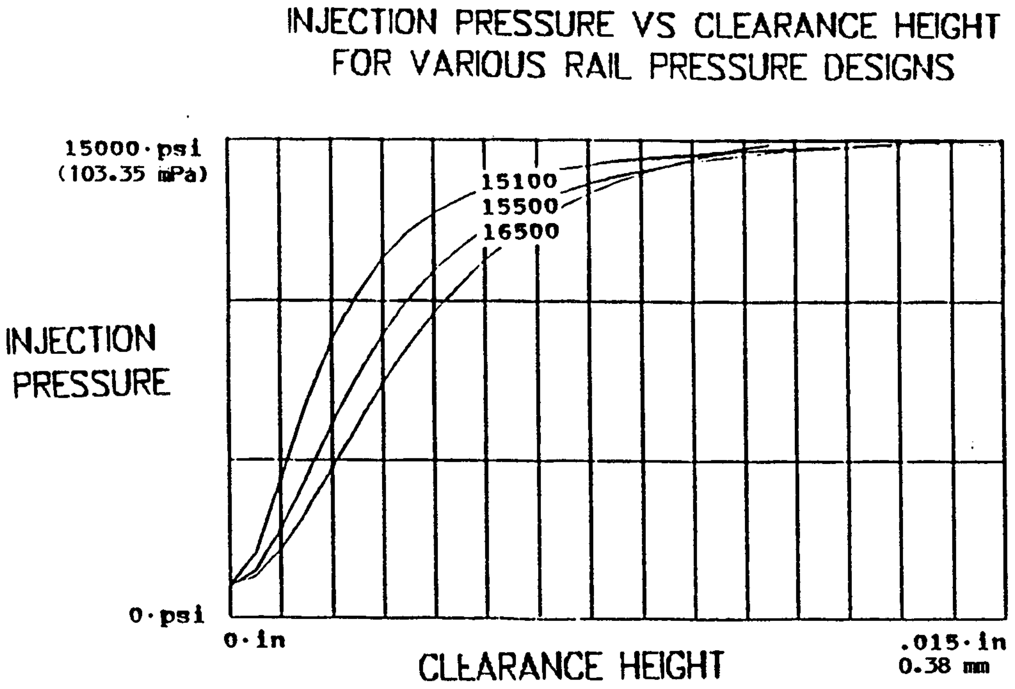

REQUIRED RAIL PRESSURE FOR RATE SHAPING--15500 PSI (106.79 mPa)

SLOT DEPTH OVER WHICH RATE CONTROL IS OBTAINED -- .008" (.203 mm)

INJECTION PRESSURE VS CLEARANCE HEIGHT

FIGURE 9

INJECTION RATE SHAPE CONTROL--TEMPERATURE RISE

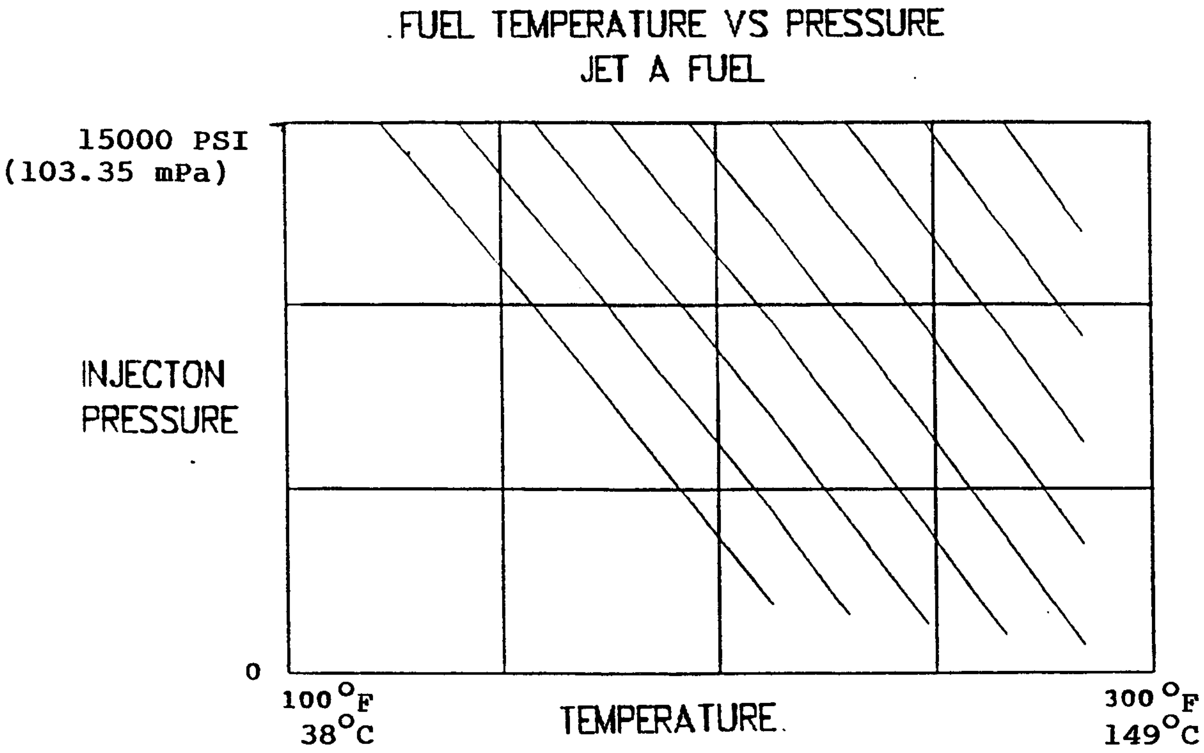

CONCERN--THE TEMPERATURE RISE WHEN THE FUEL IS THROTTLED FOR RATE SHAPING MAY CAUSE THE VALVE TO SEIZE.

FUEL TEMPERATURE RISE VS PRESSURE DROP

FIGURE 10

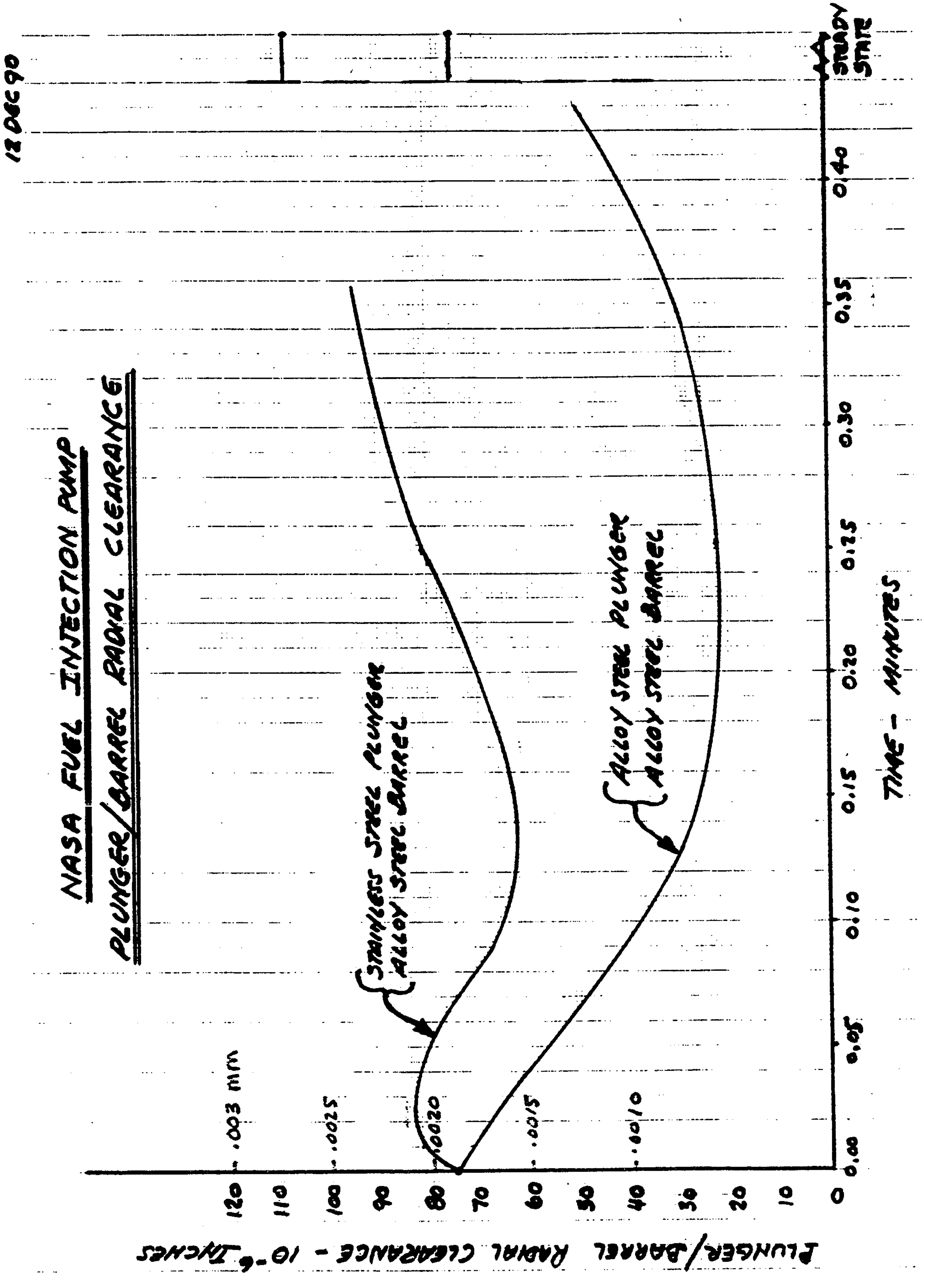

VALVE CLEARANCE VS TIME IN THERMAL TRANSIENT

FIGURE 11

APPENDIX C

TURBOMACHINERY SYSTEM ANALYSIS FOR STRATIFIED CHARGE ROTARY ENGINE CRITICAL TECHNOLOGY/ENABLEMENT

SUNDSTRAND AEROSPACE

☐ ELECTRIC POWER SYSTEMS
☐ MECHANICAL SYSTEMS
☐ FLUID SYSTEMS
☐ POWER SYSTEMS
☐ TECHNICAL SERVICES OPERATIONS
☐ MANUFACTURING OPERATIONS
☒ RESEARCH

REPORT NO. AER 3485
DATE 10/04/91
REVISION ___ DATE ___
FILE REF. RM91/1980.RDG

ENGINEERING REPORT

Turbomachinery System Analysis For Stratified Charge Rotary Engine Critical Technology Enablement

CONTROLLED DISTRIBUTION COPY
FOR John Deere Technologies Inc
APPROVED C. L. Jernor 10/8/91
CONTRACT DATA MANAGER DATE

APPROVAL AND CLASSIFICATION
BY DIR. OR MANAGER OF ENG.
SPECIAL DATE ___
DIST. ONLY ___

CONTROLLED DIST. (SEE EN10.07) DATE 10-4-91

INTERNAL DIST. ONLY ___ DATE ___

DISTRIBUTION PROHIBITED DATE

MILITARY CONTRACT NUMBER ___

WITNESSED BY ME OR BY ONE UNDER MY SUPERVISION ___
QAR DPRO ROCKFORD
DATE

Robert D. Grennan .... PREPARED BY .... 4 October 1991 DATE

.... ENGINEER .... DATE

.... ENGINEERING MANAGER .... DATE

.... MANAGER OF ENGINEERING .... 10/4/91 DATE

.... QUALITY ASSURANCE MANAGER .... DATE

.... CONTRACT ADMINISTRATOR .... DATE

101554/

PAGE 154 INTENTIONALLY BLANK

PRECEDING PAGE BLANK NOT FILMED

TABLE OF CONTENTS

Page Number

ABSTRACT 1

KEYWORDS 2

1.0 INTRODUCTION 3

2.0 ANALYTICAL MODELS 4

2.1 System Model 4
2.2 Turbines and Compressors 4
2.3 Heat Exchangers 8
2.4 Ducts 8
2.5 Exhaust Pulses 10
2.6 Gearboxes 10

3.0 SYSTEM EVALUATION 13

3.1 Design Conditions 13
3.2 Candidate System 16
3.3 Optimization Criteria 21
3.4 Parametric Evaluations 23

4.0 RESULTS AND RECOMMENDATIONS 29

4.1 Results 29
4.2 Recommendations 42

5.0 REFERENCES 42

ABSTRACT

Analytical studies of turbomachinery systems to enhance the performance of stratified charge rotary engines were conducted under subcontract to John Deere Technologies International, Inc. (JDTI). JDTI was under contract with NASA Lewis Research Center (NAS3-25945) to demonstrate critical technologies for a general aviation aircraft engine in the Stratified Charge Rotary Engine Critical Technologies Enablement (SCRECTE) program. The design objective is an engine suitable for a high performance twin-engine light aircraft. To obtain adequate power density in high altitude cruise, as well as for stratified charge operation, turbocharging is mandatory. The turbomachinery analytical studies were conducted to determine the optimum system configuration. The Sundstrand effort included assembly of component sizing and performance prediction models into a system analysis model for evaluation of candidate systems. Evaluation criteria were developed, and an optimization routine used to find the preferred configurations. The best turbomachinery configuration included a compounding turbine, which converts some of the exhaust energy to shaft power, as well as a turbocharger having two compressor stages driven by a single-stage turbine. The intake charge was intercooled between compressor stages and between the second compressor and the engine intake port. Intake manifold pressure control was effected by exhaust wastegate operation.

KEYWORDS

Keywords or phrases for computerized technical information data base: SCRECTE, rotary engine turbocharger, turbochargers, general aviation, and turbocompound engine.

1.0 SUMMARY

The NASA Lewis Research Center contracted with John Deere Technologies International, Inc. (JDTI), under the Stratified Charge Rotary Engine Critical Technologies Enablement (SCRECTE) program, to demonstrate a competitive general aviation engine. The demonstrator was based on previous JDTI designs but required significant development in fuel economy and power density at cruise altitude. The engine specification required 40 percent thermal efficiency (brake specific fuel consumption, BSFC, of 0.34 lbs/hp/hr on Jet-A fuel) at cruise conditions and specified full power to be available from sea level to 25,000 feet altitude and 75 percent power for cruise up to 33,000 feet. In order to meet the power requirement at altitude, intake port air density needed to be as high as previously demonstrated at sea level. The compressor could not use shaft power, because this would increase BSFC, which needed to be lowered. The source of energy available to improve the BSFC and provide intake pressurization is the engine exhaust. The flow rates, pressures, and temperatures involved strongly suggest the use of turbomachines for these processes. JDTI employed Sundstrand to analyze the turbomachinery system for the engine.

Sundstrand originally planned, in a multiphase program, to provide system analysis, including component sizing and performance predictions; to design the turbomachinery and ancillary equipment; to procure, assemble, and test the turbomachinery system; and, finally, to support engine testing with the turbomachinery system. The program was subsequently descoped due to alterations in the contractual agreements between JDTI and NASA, and the Sundstrand effort was terminated before the design hardware effort was begun.

The system analysis process leading to system configuration selection, essentially complete at program termination, consisted of several tasks.

- Creation of candidate system configurations. Many suggestions were compiled from various sources, including Sundstrand, JDTI, and consultants.
- Assembly of component models. Each element of the system, including turbines, compressors, heat exchangers, ducts, and gearboxes, needed to be characterized in terms of weight, performance, and volume. Most of the component models were available or easily adapted from existing Sundstrand models.
- Define the parameters of interest in assessing the candidate systems, in order to be able to select the "best" configuration.
- Encode a computer program, including an optimization algorithm, to find the best implementation of each of the candidate system configurations, to estimate the characteristics of the components, and to calculate the system selection parameters.

The design/sizing analysis was essentially complete at program termination, and a recommended system configuration was selected. Some additional detailed analysis was needed to confirm estimated exhaust pulse recovery benefits, which were expected to provide significant improvements in exhaust energy recovery and, therefore, engine BSFC.

The selected turbomachinery system configuration incorporates a turbocharger consisting of two compressor stages and one turbine stage on a single shaft, intercooling after each compressor stage, and a compounding turbine upstream of the turbocharger (at the engine exhaust). The system is estimated to weigh 206.50 lbm, to impose a net ram drag of 5.05 lbf on the aircraft, and to produce 49.4 hp of shaft power through turbocompounding (increasing engine output). The following sections of the report describe the above activities in more detail.

2.0 ANALYTICAL MODELS

In order to rapidly evaluate a number of candidate system configurations, computer models were constructed to estimate and optimize characteristics of components. These were combined into a system thermodynamic analysis computer program which balances component functions and computes system parameters. An optimization function, called equivalent power, was defined to enable the "best" system to be selected (the optimization function derivations are given in Section 3.3).

2.1 System Model

A typical turbomachinery system for a rotary engine is shown in Figure 1. This system, like all the systems evaluated, employs various turbine and compressor stages, heat exchangers for rejection of charge air heat of compression to ambient air, charge air lines and ram air ducts. A gearbox is employed for the power turbine options. Each of these component types is modelled by unique component sizing subroutines which predict component size and weight. Most of the routines perform heat transfer and thermodynamic analysis and some use empirically derived sizing relationships. The line sizing subroutine was adapted for this contract; the remaining subroutines existed before the contract began and are Sundstrand proprietary.

The system analysis computer program can be adapted to model various system configurations by altering input flags. A system schematic with various configuration options is shown in Figure 2. The program calculates system state points (temperature, pressure and flow rate) at the numbered locations, based on the input design conditions, constraints and the current values of the optimization parameters (defined in Section 3.4) and calls the various component sizing models to size the components based on the calculated state points. The equivalent power function is evaluated for the resultant values of engine exit pressure, power turbine power, incurred drag and fixed weight. An optimization routine is included in the system analysis computer program (flow chart provided in Figure 3). The optimization routine varies the system optimization parameters until the equivalent power is maximized.

2.2 Turbines and Compressors

The turbomachinery models incorporated in the system model use specific speed curves and empirical relations to determine wheel diameters which are then used with scaling functions to estimate component weight. For the turbomachines which include more than one wheel on a shaft (i.e. one turbocharging spool), the shaft speed is selected such that

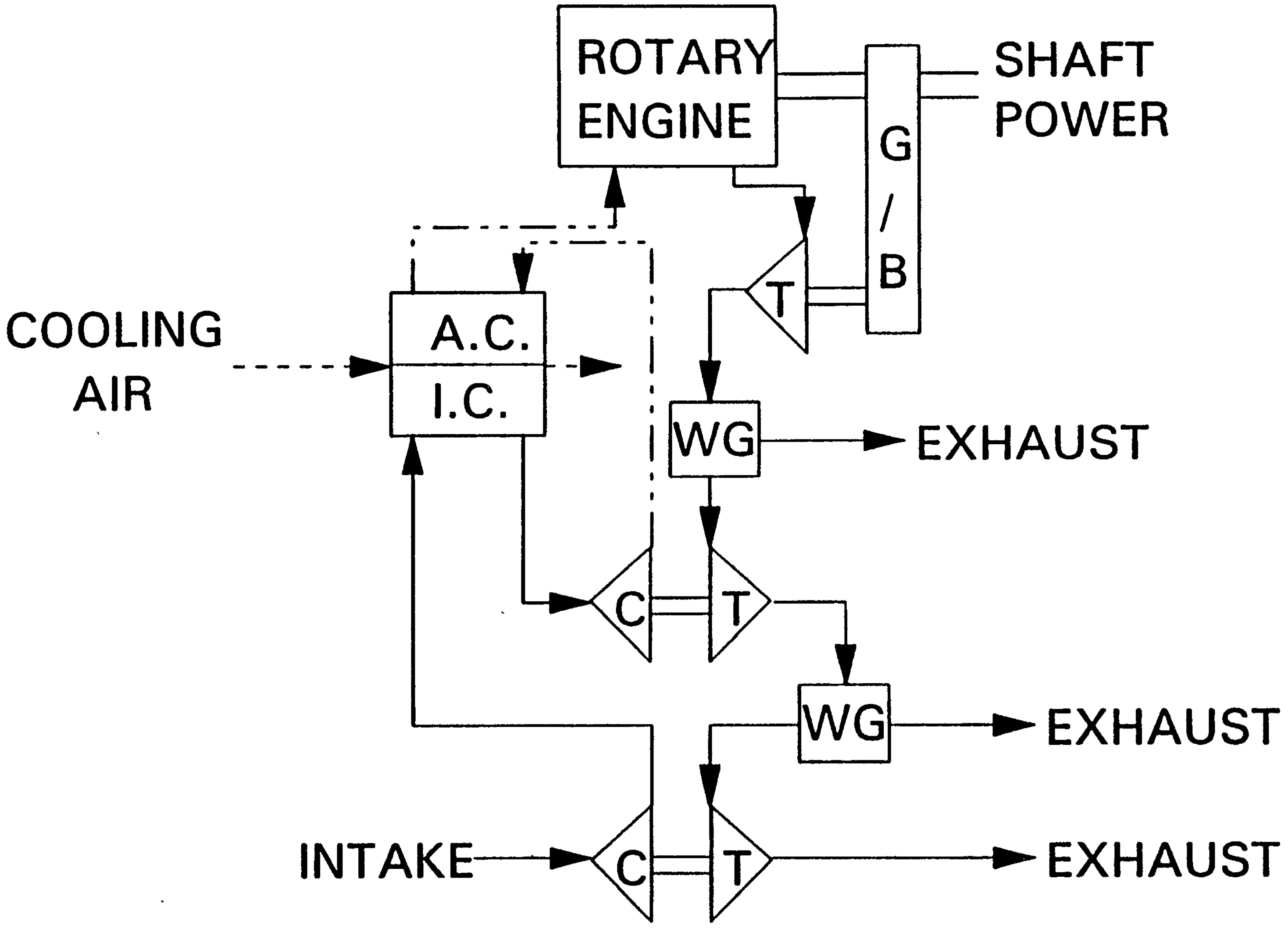
ROTARY ENGINE
SHAFT POWER
G / B
T
COOLING AIR
A.C.
I.C.
WG
EXHAUST
C
T
WG
EXHAUST
INTAKE
C
T
EXHAUST

FIGURE 1. TURBOCOMPOUND ENGINE

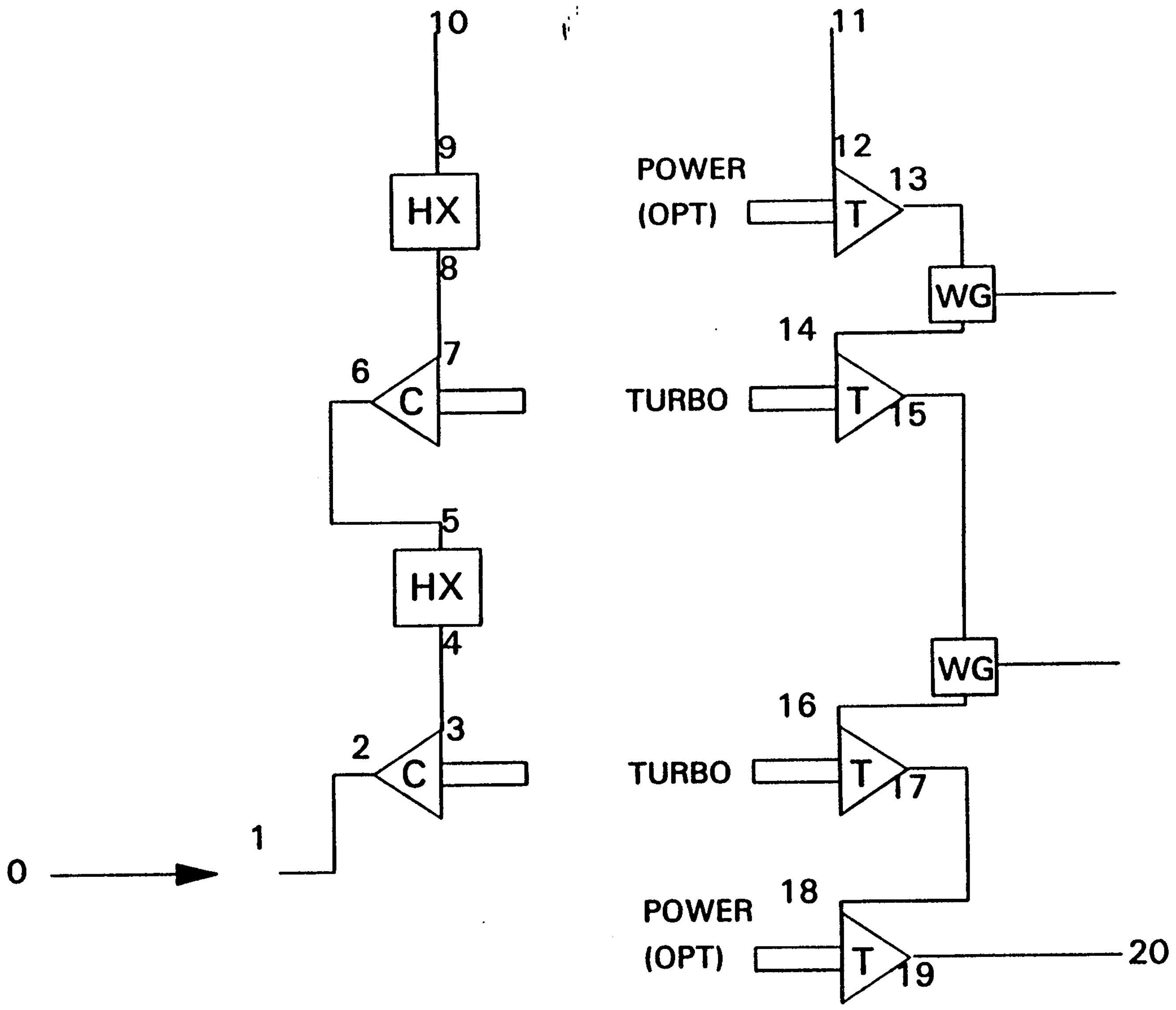
10
11
9
12
POWER
(OPT)
13
HX
T
8
WG
14
7
6
C
TURBO
T
15
5
HX
4
WG
16
3
2
C
TURBO
T
17
1
0
18
POWER
(OPT)
T
19
20

FIGURE 2 TURBOMACHINERY SYSTEM STATE POINTS

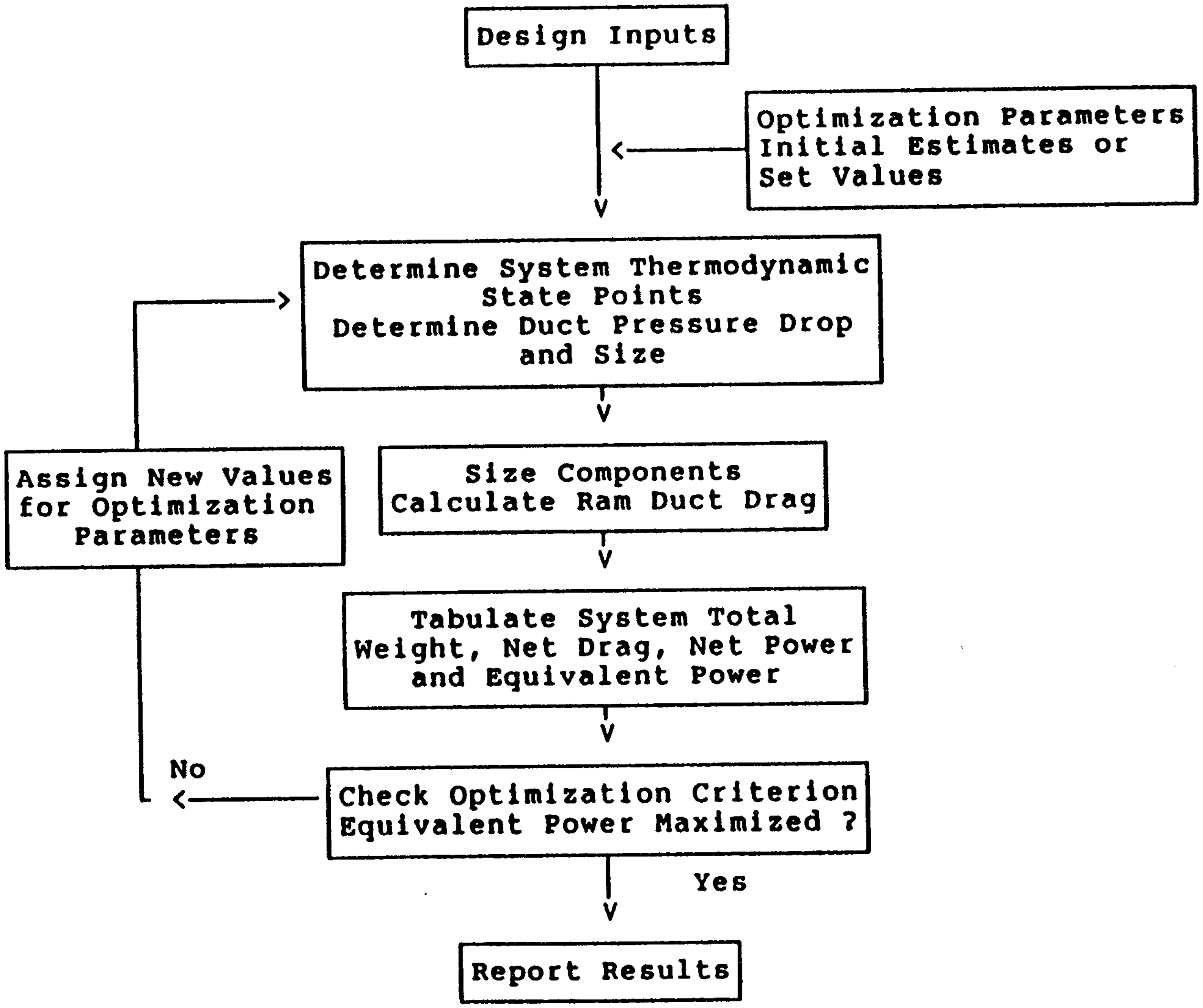
Design Inputs
Optimization Parameters Initial Estimates or Set Values
Determine System Thermodynamic State Points
Determine Duct Pressure Drop and Size
Assign New Values for Optimization Parameters
Size Components
Calculate Ram Duct Drag
Tabulate System Total Weight, Net Drag, Net Power and Equivalent Power
No
Check Optimization Criterion
Equivalent Power Maximized ?
Yes
Report Results

FIGURE 3. SYSTEM ANALYSIS PROGRAM FLOW CHART

all of the wheels on that shaft operate at near-optimum specific speeds. The acceptable specific speed ranges are set such that efficiencies range between 0.7 and 0.85. For turbomachines with only one wheel on a shaft (i.e. a power turbine on a gearbox), the shaft speed is determined such that the specific speed is optimal for maximum efficiency.

Compressor and turbines sizes are determined by somewhat different techniques. For compressors, the tip speed, determined by the head coefficient, and shaft speed are used to determine wheel diameter. For turbines, a specific speed/specific diameter correlation for peak efficiencies is used to determine the optimum specific diameter; the wheel diameter is calculated from the specific diameter. In either case, the wheel diameter is used in an empirical correlation to determine wheel and housing weight. The weight correlation has been calibrated using turbocharger data supplied by Beech Aircraft.

Turbine and compressor designs generated by the system models have been checked using more detailed Sundstrand proprietary computer programs to assure reasonable accuracy. The results of these check runs provided the efficiency predictions input to the system program. Turbomachinery inlet conditions and isentropic head rise are input to the design routine, which then calculates shaft speed, turbomachine weight, and volume.

2.3 Heat Exchangers

The heat exchangers are modelled as crossflow plate fin devices. Alternating layers of fin stock and parting plates make up the heat exchanger core as illustrated in Figure 4. Aluminum fins with aluminum parting plates are used for heat exchangers with service temperature below 350°F while nickel fins with stainless steel parting plates are used for service temperatures above 350°F. Typical values of fin height, spacing and thickness, parting plate thickness, etc. are assigned to each side of the heat exchanger based on the whether the fluid is liquid or gas. The required heat exchanger UA is determined by the effectiveness-NTU method. An iterative approach (outlined in Kays and London [1]) where the hot and cold side mass fluxes are iterated until the desired pressure drop on each side is met, is used to determine heat exchanger geometry. Plate fin correlations for friction factor and Colburn J factor are used to determine friction factor and heat transfer coefficient. The design routine takes hot and cold side inlet and exit temperature, pressure drop and flow rate as input and calculates heat exchanger weight, volume and face area.

2.4 Ducts

The duct model determines duct pressure drop, heat loss, and weight for a specified inlet Mach number. The duct area is determined which yields the specified inlet Mach number for the required duct flow rate. The duct pressure drop is calculated based on a friction factor correlation and the determined duct diameter. Insulation properties, local ambient conditions, and duct diameter are used to determine the duct heat loss. Finally, weight and volume are determined based on the duct diameter and wall thickness and the insulation properties. Duct inlet conditions, duct and insulation length, thickness, density and conductivity, and local ambient conditions are input to the routine and duct pressure drop, temperature drop, weight and volume are calculated.

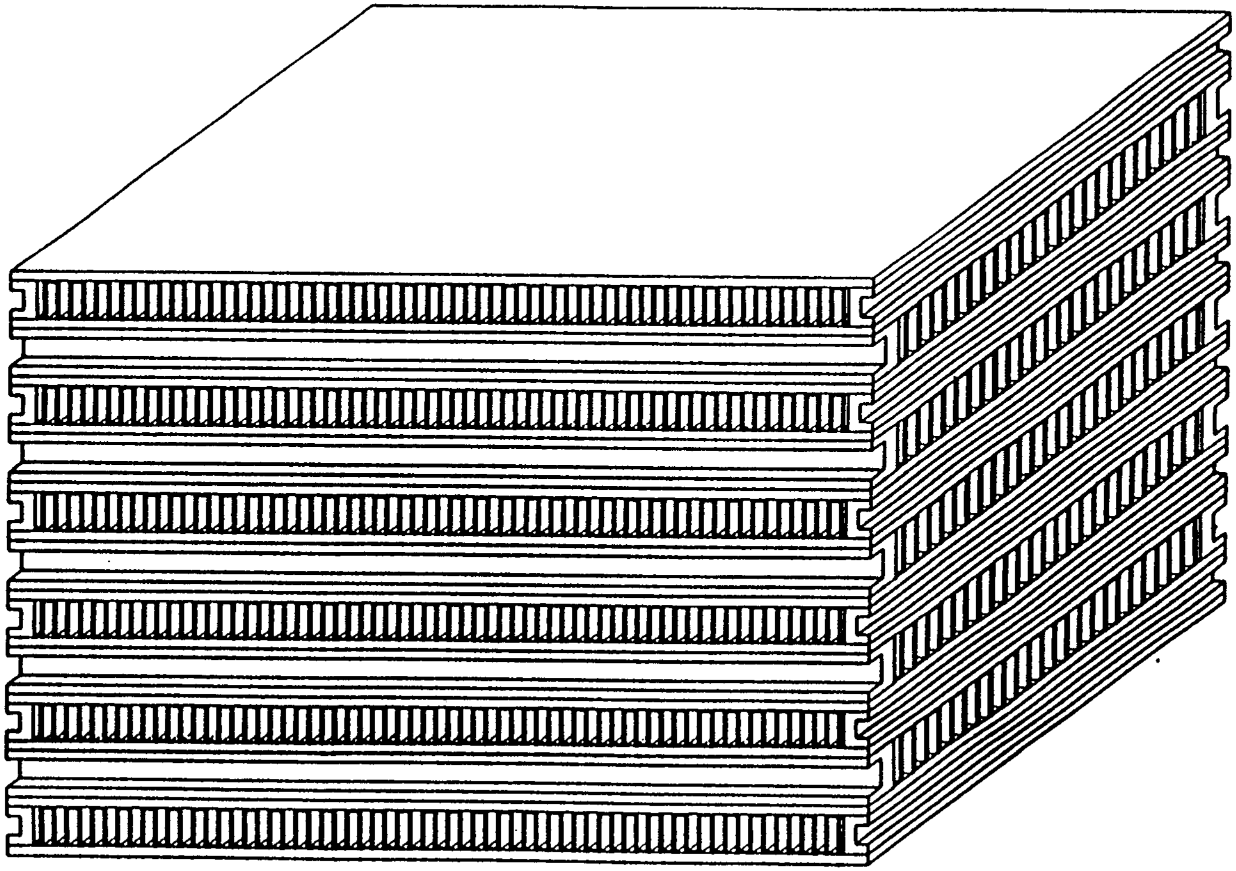

FIGURE 4. CROSSFLOW HEAT EXCHANGER CORE

A ram air circuit model calculates the duct losses and drag incurred by the ram air ducts. This routine tracks total pressure and accounts for frictional losses through an assumed duct geometry. The duct configuration, shown in Figure 5, includes a flush inlet, an inlet diffuser, a heat exchanger, a 90° bend section leading to a fan, the fan, a section of duct leading to an exit nozzle, and an exit nozzle. The SCRECTE system does not require a ram air fan, so the fan and the upstream 90° bend duct are deleted from the ram air duct analysis by a flag in the subroutine. Friction factor correlations and diffuser and nozzle loss correlations are used to model the pressure drops in the circuit. Ambient conditions, heat exchanger flow area and pressure drop, ram air flow rate, and fan pressure rise are input to the model and duct drag and fan power are calculated. If the inlet area is not specified (and usually it should not be) it is determined such that the inlet Mach number is 76 percent of the free stream Mach number. Inlet Mach numbers lower than this could cause boundary layer separation, causing flow instability and large losses at the inlet. Due to the many possible ram air duct installations the weight of the ram air duct is not estimated.

2.5 Exhaust Pulses

All of the component models, as well as the system model, predict performance and size of components on the basis of steady state flow conditions. It is well known, however, that the intermittent flow in the exhaust of an internal combustion causes pressure and flow pulses which greatly alter the distribution of energy with time and affect turbomachine size and performance. In order to assess these effects, a model of the exhaust system was created to calculate correction factors to be used in the system model. The transient model integrates the engine exhaust port and turbine inlet flows to determine the rate of change of mass in the exhaust duct and the resulting exhaust duct pressure. Wave dynamics have been ignored. Figure 6 shows some sample calculations of one exhaust cycle of one rotor; the variations shown are due to changes in the exhaust duct exit pressure and in exhaust duct length (volume). The taller pulses contain more energy, indicating the need for low volume exhaust systems. The pressures shown are not high enough to affect engine internal flow processes. The pulse modelling was not completed, but clearly indicates that care should be taken in the sizing of the exhaust system to preserve the power potential of the pulses. Preliminary results also indicate that the pulsed flow can contain 50 to 100 percent more power than a steady flow, and that up to 50 percent larger turbine and duct flow areas are required than for steady flow. Turbine average efficiency is lower than for steady flow by a few percentage points, but this is a small effect compared to the extra available energy, which greatly increases turbine power.

2.6 Gearboxes

Gearbox weight is determined from a correlation of weight versus power. Weights were estimated for several gearbox designs over a range of power turbine powers and speeds to derive this correlation. An allowance for unsteady shaft dynamics was included by sizing all gearbox elements for three times the rated power. Engine rotor accelerations and decelerations, due to intermittent combustion, are amplified through the power turbine gear train and can result in large loads and/or shaft deflections. It is recognized that a much more rigorous shaft dynamics analysis is needed for actual gearbox design.

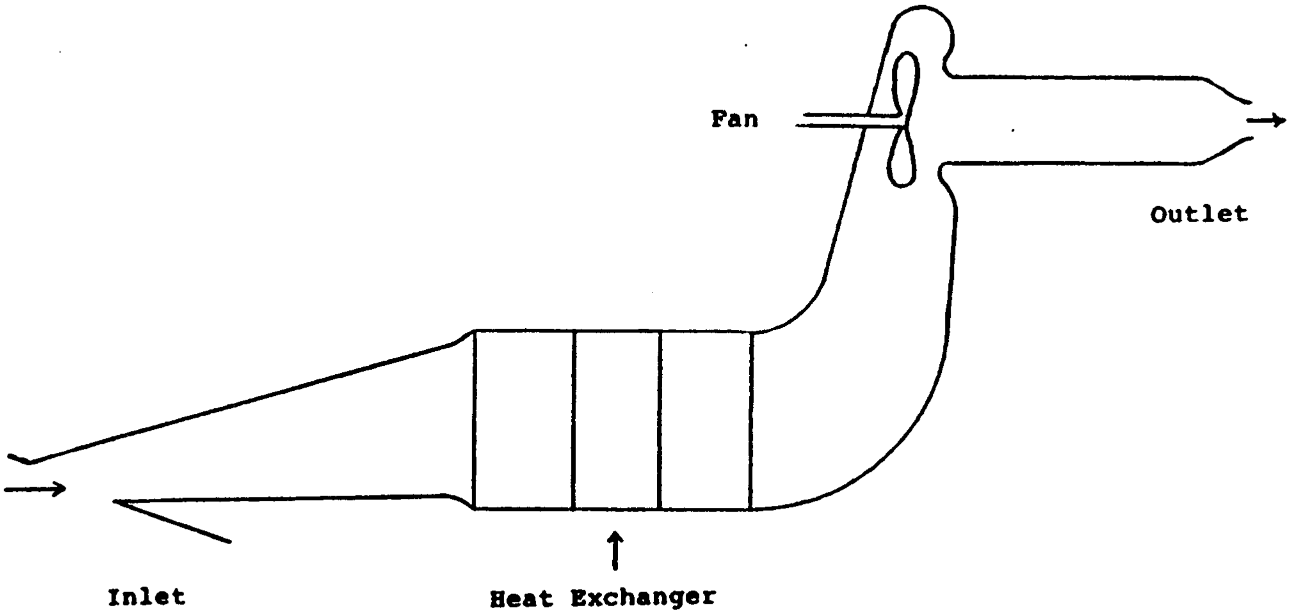
Fan
Outlet
Inlet
Heat Exchanger

FIGURE 5. RAM AIR DUCT SYSTEM

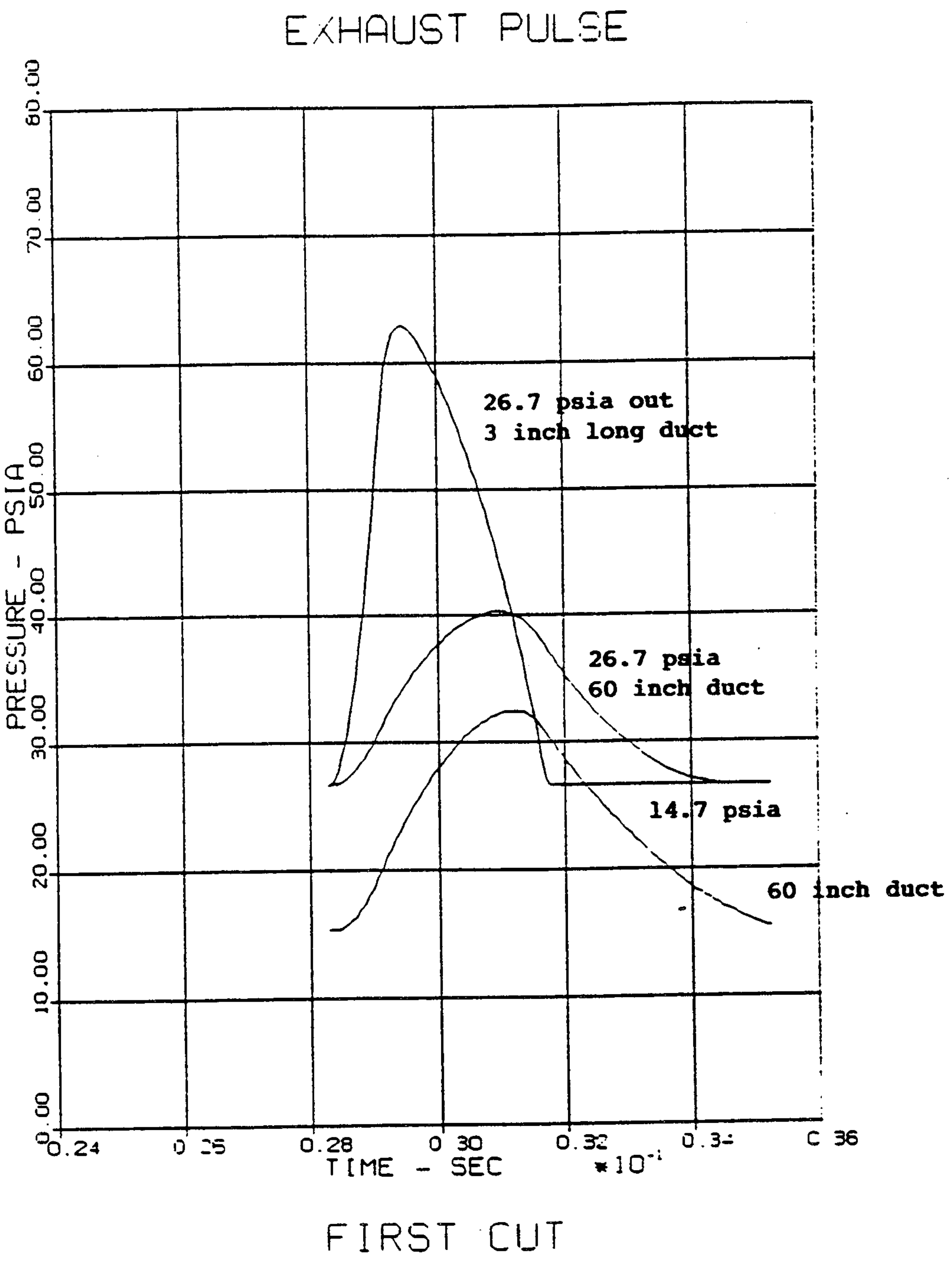

FIGURE 6. EXHAUST PULSES

3.0 SYSTEM EVALUATION

The functional requirements for the turbomachinery system are described in Section 3.1. These form the boundary conditions for analysis of any proposed system. The comparative evaluation of candidate turbomachinery systems required several steps subsequent to development of the system analysis computer program. Initially, an array of candidate system configurations was identified by brainstorming and extraction from publications or other experienced sources on turbocharging. Some sorting of these schematics was done based on operational considerations, the rest using the system analysis program. The candidate systems are discussed in Section 3.2. Secondly, it became clear that there was no clear definition of what constituted the "best" turbomachinery system; significant effort was expended in defining and encoding the optimization parameters. These are discussed in Section 3.3. Finally, the system analysis/optimization computer program was used to calculate comparative values of the system criteria for the most promising system configurations. Results are given in Section 3.4.

3.1 Design Conditions

A list of design conditions for 25 kft climb, which constrain each turbocharger system design, is given in Table 1. These values are either taken or calculated from information given to Sundstrand by John Deere and Beech Aircraft. Table 2 lists the assumed design constraints which depend on installation.

The total pressure and temperature of the flow entering the heat exchanger cooling circuit ram air scoop are affected by the engine propeller. An analysis at the propeller, based on propeller information supplied by Beech Aircraft, has been performed to determine these conditions . The thrust developed by the propeller and the power required to supply this thrust can be expressed as:

$$T = W * (V_2 - V_1) / g_c$$
$$W = \rho_1 * V_1 * A_1$$
$$A_1 = A_p$$
$$T = \rho_1 * V_1 * A_p * (V_2 - V_1) / g_c$$

$$HP = T * V_1 / \eta_p / 550$$
$$T = HP * \eta_p * 550 / V_1$$

Definitions:

T - thrust
W - air flow rate
V_2 - air velocity downstream of propeller
V_1 - air velocity upstream of propeller (true air speed)
ρ_1 - upstream density
A_p - propeller diameter
HP - engine power
η_p - propeller efficiency

So V_2 can be expressed as:

$$V_2 = V_1 + HP*\eta_p*550*g_c / (\rho_1*V_1^{2}* A_p)$$

Table 2
Assumed Design Constraints

Charge Air Ducts	
Compression side	
Length (ft)	5.0
Material	Al
Wall thickness (in)	0.03125
Density (lbm/ft^3)	172.8
Conductivity (Btu/hr ft °F)	110.0
Expansion side	
Length (ft)	3.0
Material	Steel
Wall thickness (in)	0.03125
Density (lbm/ft^3)	499.5
Conductivity (Btu/hr ft °F)	8.67
Insulation	
Density (lbm/ft^3)	11.9
Conductivity (BTU/hr ft °F)	0.10
Inlet and Exit	
Inlet diffuser half angle (deg)	10.0
Exit nozzle half angle (deg)	10.0
Ratio of nozzle exit to freestream momentum	1.0
Heat loss to surroundings	
Heat transfer coefficient (Btu/hr ft^2 °F)	2.0
Ram air heat exchanger cooling duct	
Inlet diffuser half angle (deg)	10.0
Angle of exit flow relative to free stream	0.0

Table 1
Design Conditions
25000 ft climb

Ambient	
Pressure (psia)	5.46
Temperature (°F)	6.71
Mach number	0.267
Downstream of Propeller	
Pressure (psia)	5.84
Total Temperature (°F)	16.14
Mach number	0.311
Engine air requirements	
Inlet temperature (°F)	140.0
Inlet flow rate (lbm/min)	70.55
Inlet Pressure (psia)	34.9
Exit temperature (°F)	1154.0
Exit flow rate (lbm/min)	72.84
Engine parameters	
Propeller efficiency	0.83
Displaced volume (in^3)	80.0
Engine Speed (rpm)	8500.0
Exit pressure for 400 HP (psia)	30.6
Aircraft lift over drag	11.2

The total temperature and Mach number downstream of the propeller

$$T_{T2} = T_{T1} + HP*550/778/(c_p*W)$$

$$M_2 = V_2 / (\gamma*R*T_{T2} - (\gamma-1)/2*V_2^2)^{.5}$$

T_{T1} - upstream (ambient) total temperature
T_{T2} - downstream total temperature
c_p - specific heat
M_2 -downstream Mach number
γ - specific heat ratio
R - gas constant

The total pressure downstream of the propeller is then:

$$P_{T2} = P_{S1}*(1 + (\gamma-1)/2*M_2^2)^{\gamma/(\gamma-1)}$$

P_{T2} - downstream total temperature
P_{S1} - upstream (ambient) static temperature

The heat transfer coefficient between the hot expansion side ducts and the surrounding air in the engine cowl has been determined based on a simple free convection correlation. The correlation applies to free convection around a heated circular duct.

3.2 Candidate Systems

Several types and arrangements of equipment have been considered for the turbomachinery system. These are shown and discussed below.

The turbocharger system consists of six characteristic functions, which are illustrated in Figure 7. The turbocharger extracts power from the exhaust stream and uses it to compress the intake charge. The intercooler (I.C.) and aftercooler (A.C.) reduce the temperature of the compressed air to increase the intake charge density. A power turbine can be used to extract additional exhaust energy for use as engine output shaft power. A gearbox is needed to connect the power turbine to the engine shaft. The exhaust wastegates bypass exhaust gas around the turbocharger to limit intake pressurization. Ducts provide the interface connections among the system components and between the system and the engine and airframe.

The system shown as an example in Figure 7 is a simple, thermodynamically complete turbomachinery system for a turbocompounded, turbocharged engine system. Many different candidate system arrangements can be devised from this system by varying the number of compression stages, the number of turbine stages, the order in which the exhaust gases pass through the turbines, and the presence or absence of the power turbine which provides the turbocompounding. A few of these possible configurations are shown in Figures 8 through 10.

Figure 8 shows three system configurations without turbocompounding. The first is composed of two conventional turbochargers (multiple spool system), each having a single compressor stage and a single turbine stage, with intercooling after each compressor stage. Intake manifold pressure is limited by sequential operation of the wastegates, starting with the low pressure spool. The second configuration combines the two compressors on a single shaft driven by a single turbine. This multistage turbocharger system promises to

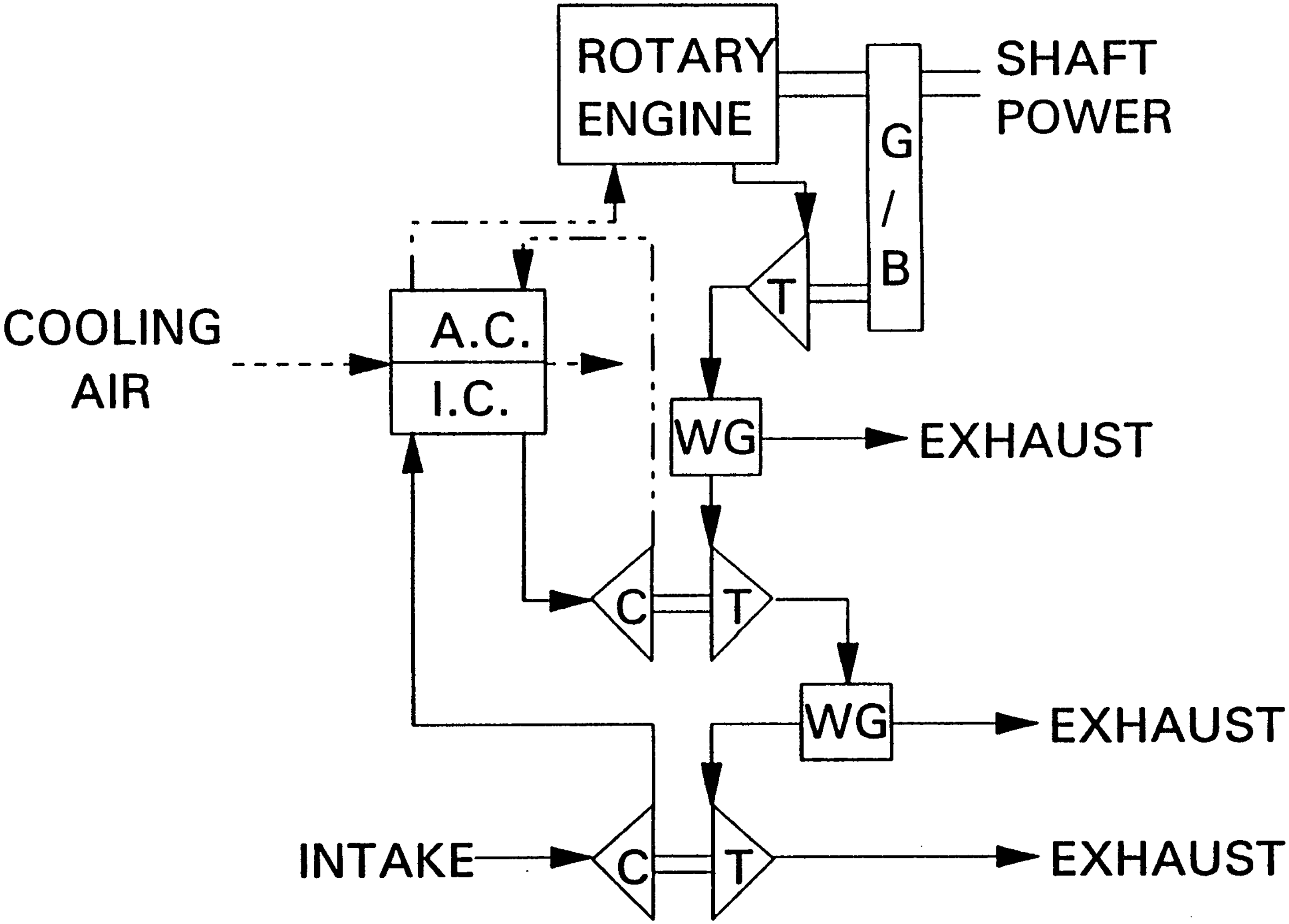
ROTARY ENGINE
SHAFT POWER
G / B
T
COOLING AIR
A.C.
I.C.
WG
EXHAUST
C
T
WG
EXHAUST
INTAKE
C
T
EXHAUST

FIGURE 7. TURBOCOMPOUND ENGINE

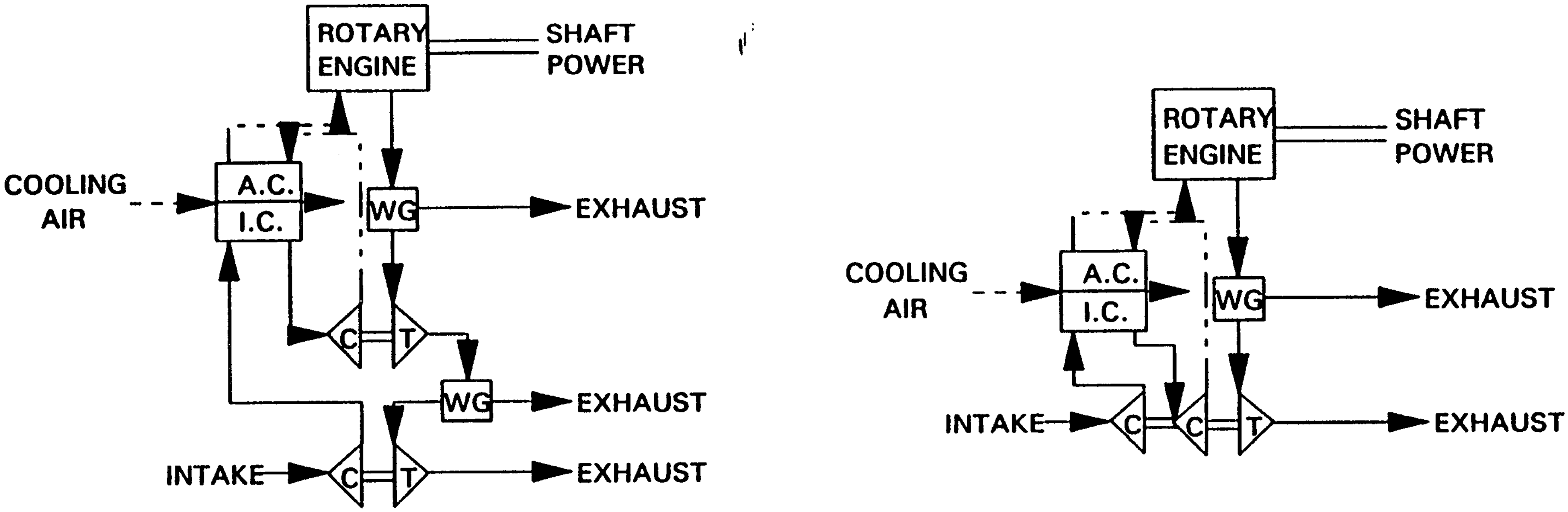
ROTARY ENGINE
SHAFT POWER
COOLING AIR
A.C.
I.C.
WG
EXHAUST
C
T
WG
EXHAUST
INTAKE
C
T
EXHAUST
ROTARY ENGINE
SHAFT POWER
COOLING AIR
A.C.
I.C.
WG
EXHAUST
INTAKE
C
C
T
EXHAUST

MULTIPLE SPOOL TURBOCHARGER

MULTIPLE STAGE TURBOCHARGER

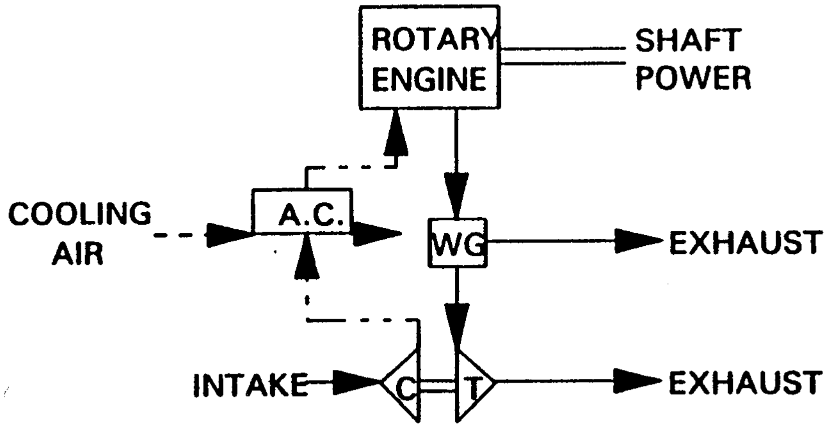
ROTARY ENGINE
SHAFT POWER
COOLING AIR
A.C.
WG
EXHAUST
INTAKE
C
T
EXHAUST

SINGLE STAGE TURBOCHARGER

FIGURE 8. CANDIDATE SYSTEMS (NO COMPOUNDING)

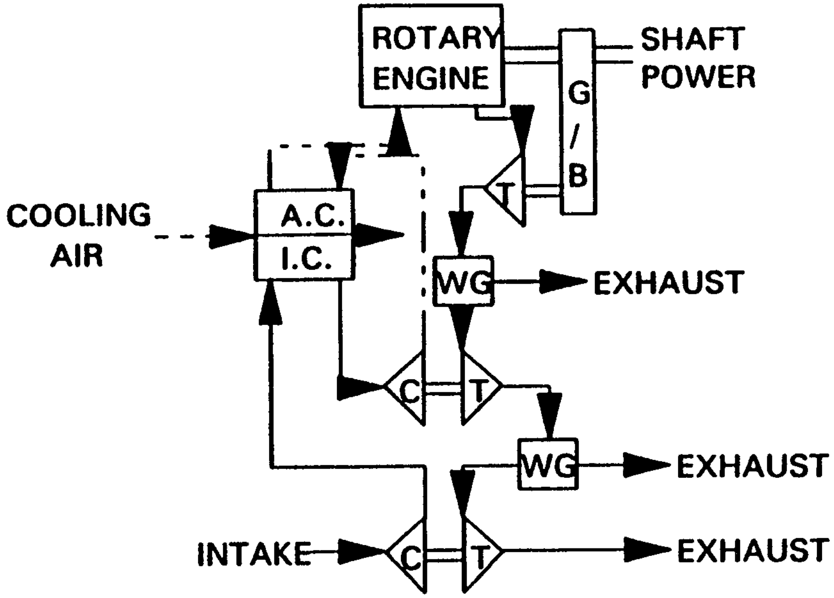
ROTARY ENGINE
SHAFT POWER
G / B
T
COOLING AIR
A.C.
I.C.
WG
EXHAUST
C
T
WG
EXHAUST
INTAKE
C
T
EXHAUST

TURBOCOMPOUND
MULTIPLE SPOOL TURBOCHARGER

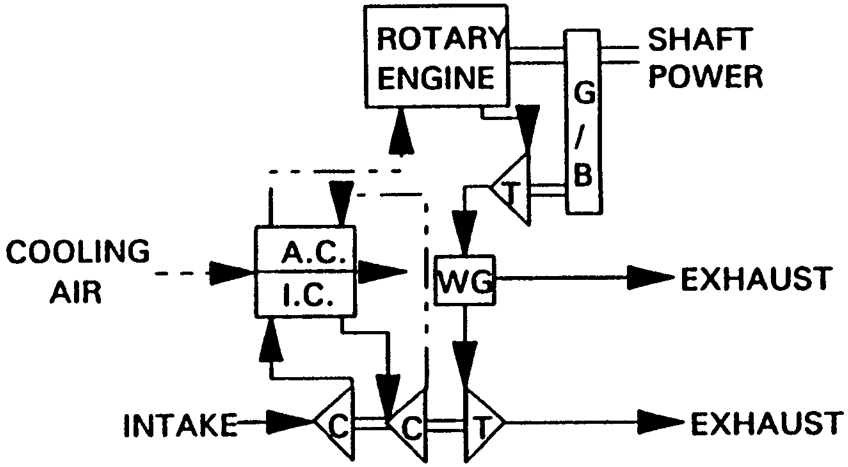
ROTARY ENGINE
SHAFT POWER
G / B
T
COOLING AIR
A.C.
I.C.
WG
EXHAUST
INTAKE
C
C
T
EXHAUST

TURBOCOMPOUND
MULTIPLE STAGE TURBOCHARGER

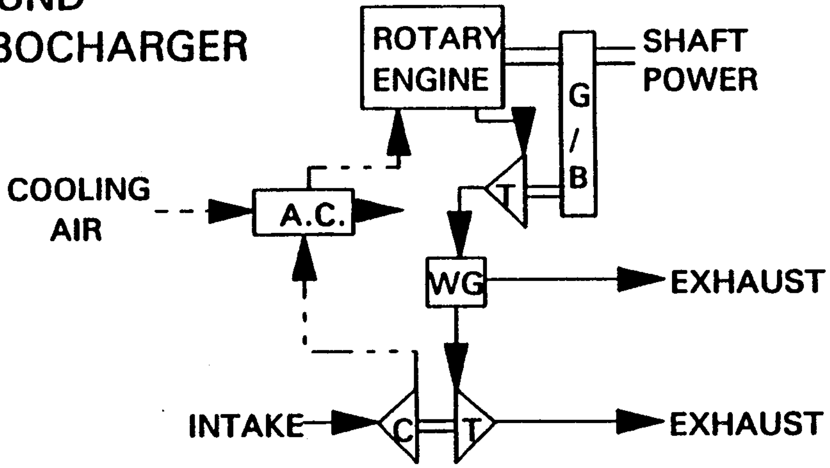
ROTARY ENGINE
SHAFT POWER
G / B
T
COOLING AIR
A.C.
WG
EXHAUST
INTAKE
C
T
EXHAUST

TURBOCOMPOUND
SINGLE STAGE TURBOCHARGER

FIGURE 9. TURBOCOMPOUND CANDIDATE SYSTEMS

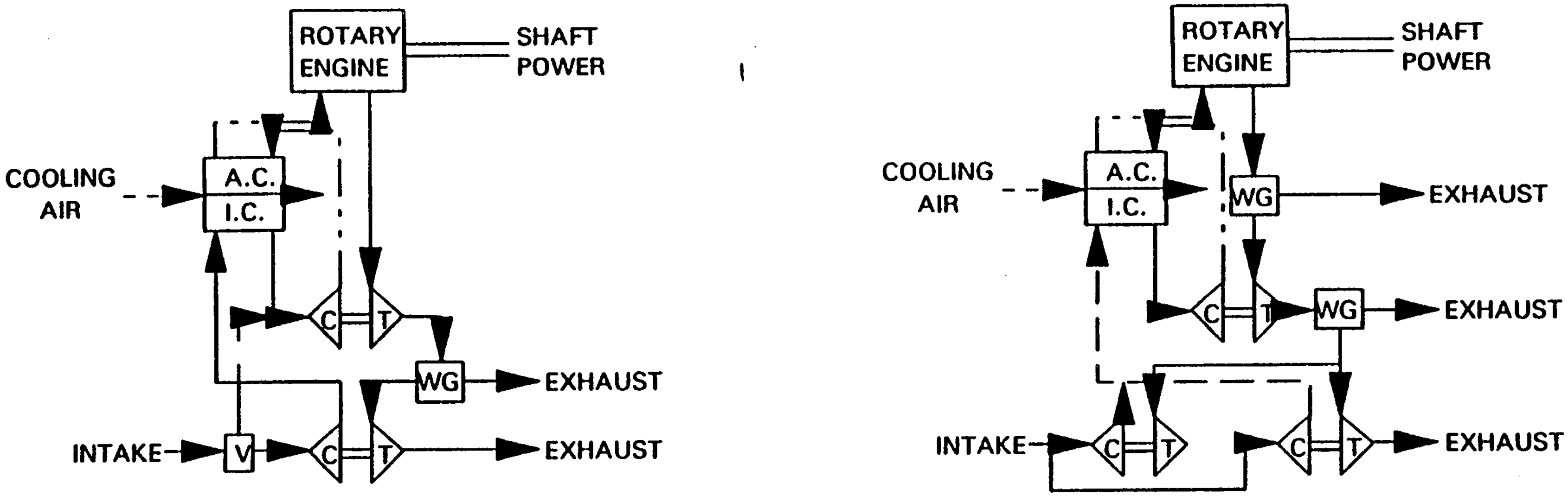
ROTARY ENGINE
SHAFT POWER
COOLING AIR
A.C.
I.C.
C
T
WG
EXHAUST
INTAKE
V
EXHAUST
ROTARY ENGINE
SHAFT POWER
COOLING AIR
A.C.
I.C.
WG
EXHAUST
C
T
WG
EXHAUST
INTAKE
C
T
C
T
EXHAUST

REDIV ALTERNATE 1

3 EQUAL TURBOCHARGERS

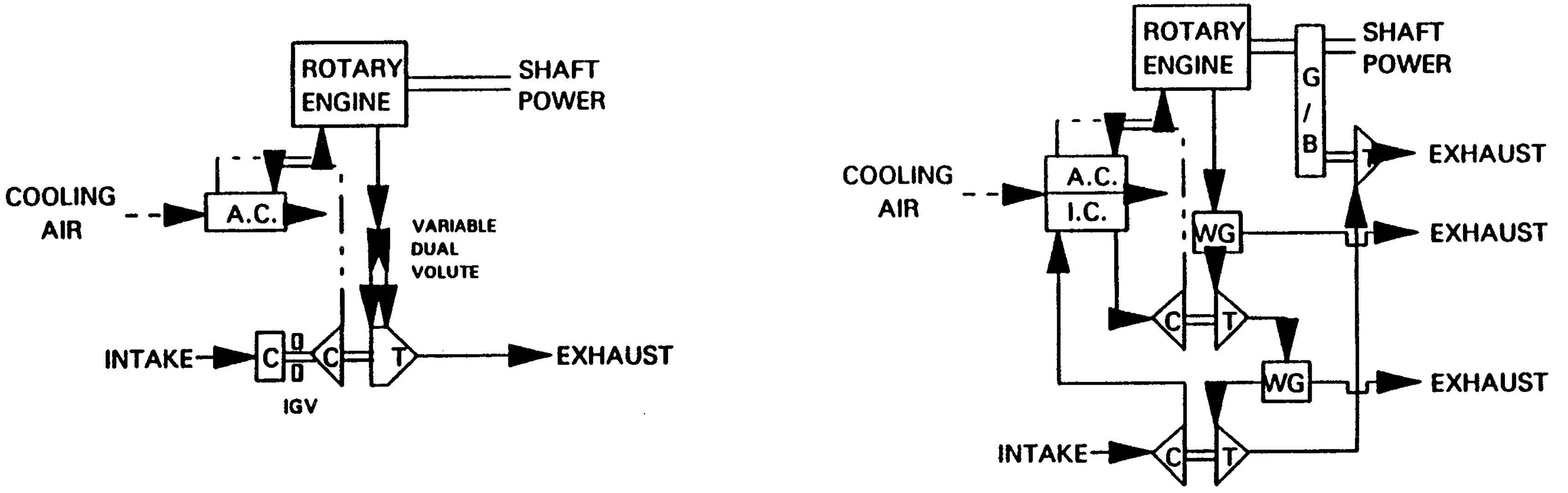
ROTARY ENGINE
SHAFT POWER
COOLING AIR
A.C.
VARIABLE DUAL VOLUTE
INTAKE
C
C
T
EXHAUST
IGV
ROTARY ENGINE
SHAFT POWER
G/B
EXHAUST
COOLING AIR
A.C.
I.C.
WG
EXHAUST
C
T
WG
EXHAUST
INTAKE
C
T

REDIV ALTERNATE 2

ALTERNATE TURBOCOMPOUND ENGINE

FIGURE 10. ALTERNATE CANDIDATE SYSTEMS

be more compact than the multispool system, while delivering similar thermodynamic performance. The third system achieves the required compression in a single stage. The single stage turbocharger appears to provide the simplest system, but was determined to have thermodynamic disadvantages and to be a more risky approach.

The three systems in Figure 9 are similar to those in the previous figure, except that each has a power turbine in the exhaust stream preceding the turbocharger(s). This turbine provides the "turbocompounding" effect, extracting excess power from the exhaust to add to the engine output shaft power. The analysis shows that there is significant gas power available for turbocompounding, and that this function may be necessary to achieve the engine BSFC goal.

In Figure 10 are shown four other schematics which were proposed but discarded for various reasons. The first configuration is like the basic multiple spool configuration, but uses an additional valve to control the compressor flow split. This causes additional compressor matching problems without adding any performance to the system. The second schematic, REDIV Alternate 2, suggests using a variable geometry turbine instead of wastegate control and an axial/centrifugal compressor. This is thermodynamically equivalent to the multistage turbocharger at design operation, which is the only operating condition analyzed to date. Some operational (off-design) advantages may accrue from using variable geometry instead of wastegate control. Controls would be more complex, and development would be necessary. The three equal turbochargers were proposed as a potential approach for constructing a ground test article to demonstrate thermodynamic performance. The additional pieces of hardware and plumbing would make it impractical for aircraft installation. The alternate turbocompound schematic illustrates the potential for positioning the power turbine last in the exhaust, instead of first. This is suggested in the literature as a technique for improving engine throttle response, because it tends to maintain turbocharger turbine pressure ratios at a more constant level. However, it also eliminates the increase in turbocharger output with increasing altitude, which is an absolute must for the aircraft engine.

3.3 Optimization Criteria

A mathematical optimization process, such as included in the system analysis, requires an objective function which smoothly varies with the independent parameters of the problem. The NASA contract for this engine development set goals for power, weight, and fuel consumption of the entire system; however, the allotments for the turbomachinery were not known, nor was there any guidance given for tradeoffs. In order to proceed with the system optimization, it was necessary to develop optimization functions.

The turbocharger system imposes three penalties on the airframe and engine. These are the system fixed weight, the drag incurred by the ram air cooled heat exchangers, and the back pressure imposed at the engine exhaust. The formulated penalty function relates the relative impact on the airframe and engine of these three factors. The optimization parameters are varied (or optimized) by an optimization algorithm to minimize this penalty function and thus maximize the benefits of the turbomachinery system to the aircraft.

The approach taken to formulate the penalty function recognizes that the purpose of the rotary engine and its turbomachinery system is to provide propulsive power to the airframe. Benefits and penalties to the aircraft performance which are generated by the turbomachinery system can be accounted as a combination of thrusts and drags (or the equivalent powers). Thus, the ram drag of the system, drag due to lift incurred by system weight, engine power changes due to exhaust pressure changes, and power turbine contributions can all be combined into a single expression for net output power due to the turbomachinery system. (The "best" turbomachinery, by this definition, is the one which maximizes installed thrust-minus-drag.)

Drag:

The system fixed weight and incurred drag can be combined into the net drag imposed on the airframe by the turbomachinery system. The weight results in a drag penalty on the airframe due to additional lift required; this can be expressed by dividing the weight by the lift over drag (LOD) ratio. The net drag function takes the form:

net drag = incurred drag + fixed weight/LOD

Power:

The engine exhaust pressure can be converted into a net power change from the baseline power, produced by the engine and power turbine pair. The pumping loop contribution to engine power can be expressed as:

$$Pw_{pl} = \Delta V \times N \times (Pe_{in} - Pe_{out})$$

Pw_{pl} - pumping loop power
N - engine speed
ΔV - swept volume
Pe_{in} - engine inlet pressure
Pe_{out} - engine exhaust pressure

The power at some reference engine exhaust pressure has been given by the engine manufacturer. The pumping loop power portion of total engine power at this reference exhaust pressure ($Pe_{out,ref}$) is given by:

$$Pw_{pl,ref} = \Delta V \times N \times (Pe_{in} - Pe_{out,ref})$$

Assuming that a change in the exit pressure effects only the pumping loop power, the change in the engine power (which is just the change in pumping loop power) for this exit pressure is given by:

$$\Delta Pw = Pw_{pl} - Pw_{pl,ref}$$
$$\Delta Pw = \Delta V \times N \times (Pe_{out,ref} - Pe_{out})$$

The net power change from the engine power baseline also includes the power turbine contribution. The net power change is given by:

$$\Delta Pw_{net} = \Delta Pw + Pw_{pt}$$

Pw_{pt} - power to propeller shaft from power turbine

Equivalent Power:

The net effect of the turbomachinery system on engine shaft power available for propulsion is obtained by converting the net drag to a (negative) thrust power and adding to the net power. The "equivalent power" optimization function for the turbocharging system has the form:

$$Pw_{eq} = \Delta Pw_{net} + V_{free} \text{ x net drag } / \eta_{prop}$$

V_{free} - free stream velocity

η_{prop} - propeller efficiency

or,

$$Pw_{eq} = \Delta V \text{ x } N \text{ x } (Pe_{out,ref} - Pe_{out}) + Pw_{pt} - V_{free} \text{ x (incurred drag + fixed weight/LOD)}$$

3.4 Parametric Evaluations

Optimization Parameters:

Nine parameters have been identified which affect the optimization function, as well as weight, drag, and engine exhaust pressure. Some affect only one or two of these. The optimization parameters are listed below along with a description of the penalty factors they affect.

1.	First stage compression ratio	affects system weight and engine exit pressure (net power), affects heat exchanger size which has only slight effect on incurred drag
2.	Intercooler charge air exit temperature	same effects as above
3.	Inter/aftercooler charge air side pressure drop	trades heat exchanger weight against engine exit pressure (net power), affects heat exchanger size which has only slight effect on incurred drag
4.	Duct mach number	trades duct weight against engine exit pressure (net power), no effect on incurred drag
5.	Power supplied to prop shaft from power turbine	affects power turbine weight (and system weight slightly) and engine exit pressure (net power), no effect on incurred drag
6.	Expansion side duct insulation thickness	trades weight of insulation against engine exit pressure (net power), no effect on incurred drag
7.	Inter/aftercooler air side pressure drop	trades weight of heat exchangers against ram air drag, no effect on engine exit pressure (net power)
8.	Intercooler air flow rate	trades weight of heat exchangers against ram air drag, no effect on engine exit pressure (net power)

9. Aftercooler air flow rate	trades weight of heat exchangers against ram air drag, no effect on engine exit pressure (net power)

Results:

The effects of each of the optimization parameters was examined individually. Several were found to have optima which fell into narrow ranges and could be fixed for system optimization studies.

The dual stage turbocharger system (two compressor stages driven by one turbine stage) was used for evaluating the effects of insulation thickness, pressure ratio split, intercooler charge air exit temperature, and air side pressure drop and flow rate through the intercooler and aftercooler on net drag, net power and equivalent power. Turbocompounding was not included, inter/aftercooler charge air side pressure drop was set to 0.125 psid, and duct Mach number was set to 0.175 for this set of optimization studies.

Insulation Thickness:

As insulation is added to the exhaust ducts, less thermal energy is lost and lower engine back pressure is required to drive the turbines, resulting in a net power increase. However, duct weight and net drag increase. The net effect is for equivalent power to drop as insulation thickness is increased. Therefore, insulation thickness is set to zero since this leads to maximum equivalent power.

Compressor Pressure Ratio Split:

Over a wide range of the other optimization parameters, the first stage compression ratio (Pr) is optimal between 3.6 and 3.8 for maximum equivalent power. Pressure ratio was, therefore, fixed at 3.7.

Ram Air Heat Exchanger Pressure Drop:

As intercooler and aftercooler air side pressure drop (ΔPc) increases, heat exchanger weight decreases but ram air drag increases. Only net drag is effected. A value of ΔPc of 0.1 psid was found to be optimal for minimum net drag.

Intercooling:

Figure 11 shows the effect of intercooler charge air exit temperature (Tic_o) on net power, net drag and equivalent power. For each value of Tic_o, inter/aftercooler ram air flow rate (Wc_{ic} and Wc_{ac}) are optimized for minimum net drag (they have no effect on net power). Over a range of Tic_o from 140.0 °F to 210.0 °F the equivalent power is constant within 0.7%. Net drag decreases from 21.71 to 20.11 and net power decreases from 28.19 to 27.74 over this range. Tic_o is set to 150.0 °F since it yields high net power. The values of Wc_{ic} and Wc_{ac} for which net drag is minimum for this temperature are 53.3 and 54.7 lbm/min.

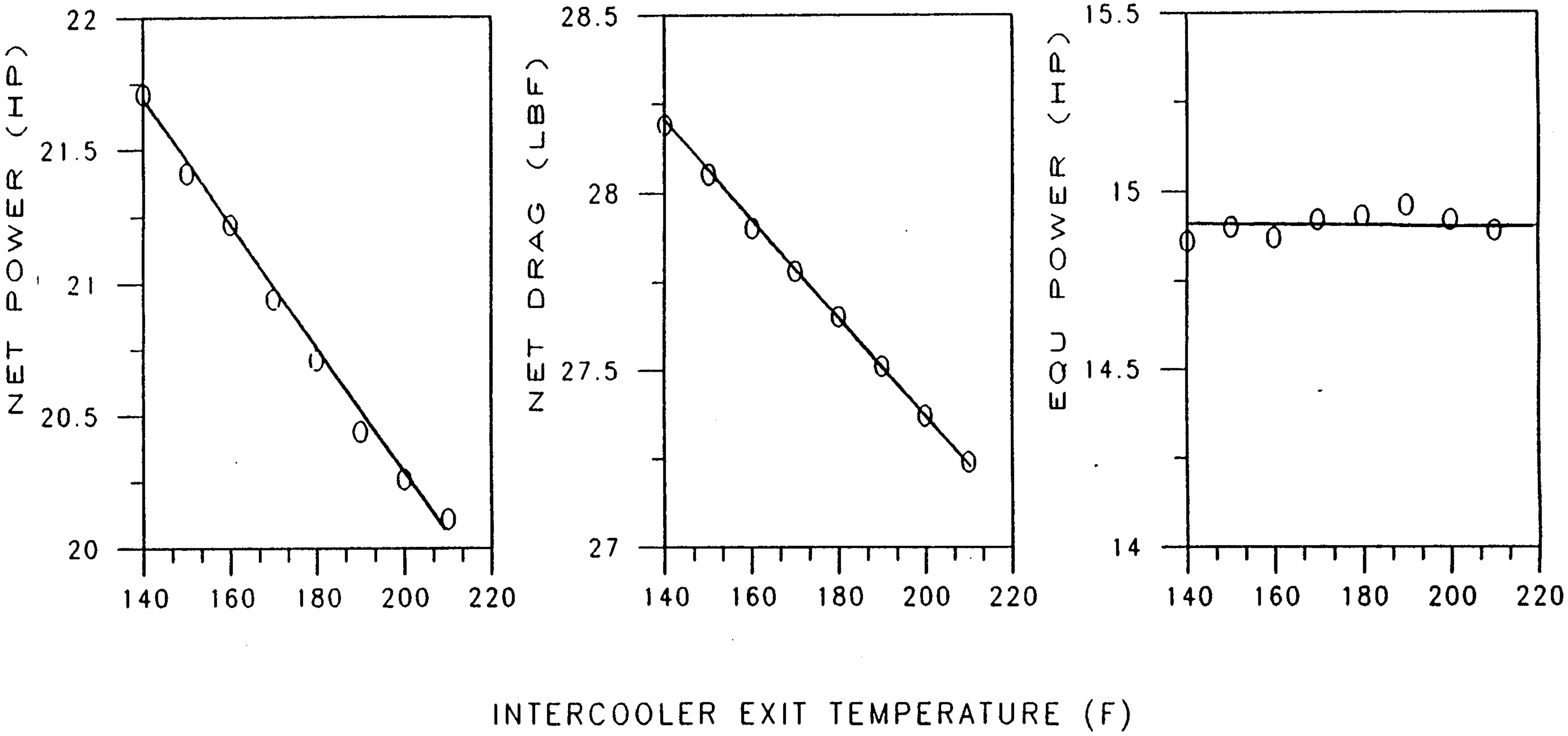

FIGURE 11. EFFECT OF INTERCOOLING

Charge Air Heat Exchanger/Duct Pressure Drop:

With the previously discussed optimization parameters fixed, the optimal values of intercooler/aftercooler charge air pressure drop (ΔP_{hx}), duct Mach number (M_d), and turbocompounding power remain to be determined. The power turbine is placed upstream of the turbocharger as this results in the lowest weight power turbine, with little effect on the turbocharger. Figure 12 shows the effect of heat exchanger pressure drop and duct Mach number, at various levels of power turbine output power, on net power, net drag, and equivalent power. (The analysis is for steady state flow, analysis with pressure pulse effects is discussed below.) The heat exchanger pressure drop, ΔP_{hx}, and duct Mach number, M_d, together characterize the charge air pressure drop. In order to vary them together systematically, normalized parameters are used:

normalized pressure drop, $(\Delta P_{hx} - \Delta P_{hx,min})/(\Delta P_{hx,max} - \Delta P_{hx,min})$

and

normalized duct Mach number, $(M_d - M_{d,min})/(M_{d,max} - M_{d,min})$

The normalized pressure drop and Mach number are increased together along the x-axis of the three plots, from $\Delta P_{hx,min}$ of 0.05 psid to $\Delta P_{hx,max}$ of 0.25 psid, and $M_{d,min}$ of 0.10 to $M_{d,max}$ of 0.30. As the pressure drop and Mach number increase, the heat exchangers and duct weights decrease, which results in a net drag decrease, but power must be expended to overcome the increased charge air pressure drops, and thus net power is decreased. The resultant equivalent power curves are nearly flat with a slight maximum between 25 percent and 50 percent of the pressure drop range, and decrease at higher pressure drops. Values of 0.125 psid and 0.175 Mach number are selected for ΔP_{hx} and M_d.

Power Turbine Power:

Power turbine power is indicated by the coding numbers on the curves, in tens of horsepower (e.g., the curve having the numeral "4" embedded in it indicates a fixed power turbine power of 40 horsepower). With increasing power turbine power, net power increases. Net drag at first increases; there is a jump in weight, and thus in net drag from zero power (no turbine or gearbox) to finite power output. Then net drag decreases as increasing power turbine pressure ratios (at fixed flow) result in faster, smaller turbines. Equivalent power decreases with the initial addition of hardware between zero and non-zero turbine power, then increases. Net and equivalent power increase monotonically with increasing power turbine power, seemingly indicating very large power availability. However, there is probably a practical limit at back pressures sufficiently high (exhaust pressures near engine inlet pressure) to cause engine scavenging difficulties. The inlet and exhaust pressures specified by REDIV (34.9 and 30.6 psia, respectively) are shown on the net power plot. They show a practical power turbine maximum design power to be in the 50-60 horsepower range (with NO pulse effects), with resulting equivalent power of 35-40 horsepower.

Figure 13 shows the effect of ΔP_{hx} and M_d, again using the parameter k, at various levels of turbocompounding power, on net drag, net power, and equivalent power with initial

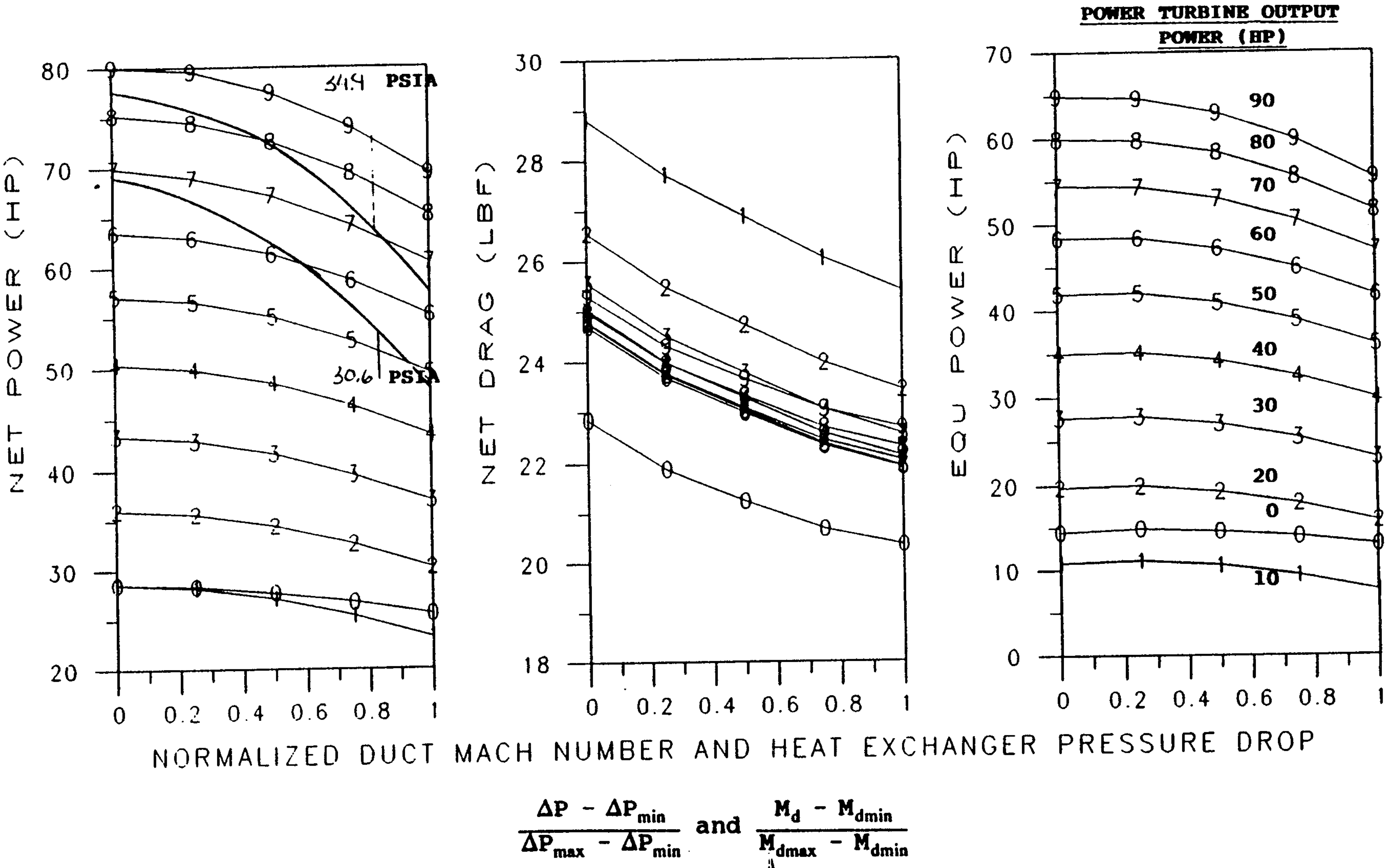

FIGURE 13. EFFECT OF CHARGE AIR PRESSURE DROP (WITH PULSE EFFECT)

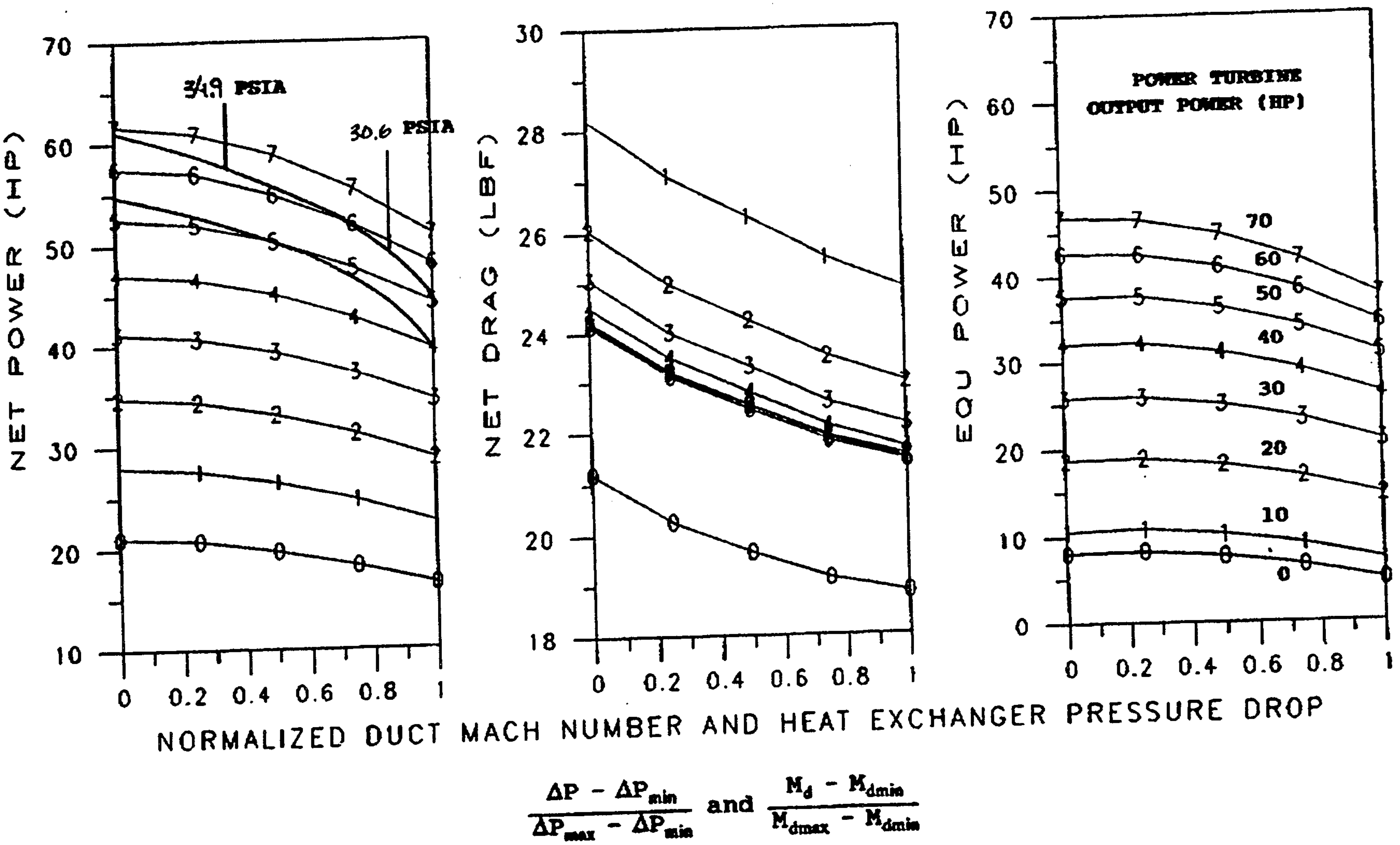

FIGURE 12. EFFECT OF CHARGE AIR PRESSURE DROP (NO PULSE EFFECTS)

estimates of pressure pulse effects included. The trends are the same as those with pressure pulse effects neglected, however the levels of available power turbine power are increased to 65-80 horsepower. Both net power and equivalent power are increased by 15-20 horsepower by pulse effects. (Although incomplete, the pressure pulse analysis indicated that even higher turbine powers should be available with pulse recovery.)

In summary, the power turbine analysis shows equivalent power gains of 35 horsepower (minimum, steady flow) to 60 horsepower (maximum, initial pulse analysis), or more. These gains represent recovery of 12-20 percent of the rotary engine shaft power from its wasted exhaust energy; inclusion of the power turbine in the optimum system would seem to be mandatory. Some further pulse analysis, in conjunction with installation design, is needed to quantify the achievable turbocompounding benefit.

4.0 RESULTS AND RECOMMENDATIONS

4.1 Results

With the optimization parameter ranges characterized, the system analysis program was used to characterize the three candidate systems previously shown in Figure 9. These are the multiple spool, multistage, and single stage turbochargers, each in a system having a power turbine upstream of the turbocharger for turbocompounding. The calculated equivalent powers for the three optimized systems are shown in Figure 14. Power turbine power was fixed at a conservative 40 HP (at the engine output shaft). The dual spool configuration (two turbines driving one compressor each) is thermodynamically equivalent to the dual stage configuration (one turbine driving two compressors) on the compression side so the optimization parameters are optimal at the same values for both. For the single stage configuration (one turbine driving one stage of compression), there is no compressor ratio split to optimize, nor is there an intercooler (only an aftercooler). As in the study with the dual stage turbocharger, the insulation thickness and ΔPc optimize to 0.0 and 0.10 respectively, and ΔP_{hx} and M_d have optimal values of 0.125 psid and 0.175 Mach number. Wc_{ac} is optimized for minimum drag at 99.0 lbm/min.

The dual stage configuration leads to the highest value of equivalent power by a modest amount (16 percent higher than that of the dual spool). The single stage system, expected to be potentially the best, falls midway between the others. Relative to the dual stage configuration, the single stage system suffers from somewhat poorer thermodynamic performance (no intercooling) as well as high aftercooler weight resulting from the need to use steel materials at the high compressor outlet temperature. Data from the turbomachinery system sizing computer program are shown in Tables 3, 4, and 5 for the dual spool, dual stage, and single stage systems, respectively. Figure 15 shows the dual stage configuration system state points.

Since the equivalent power does not indicate a clear advantage for one of the configurations, other factors, such as reliability, cost, off design performance, should be considered. Table 6 lists some of the other advantages and disadvantages of the three configurations.

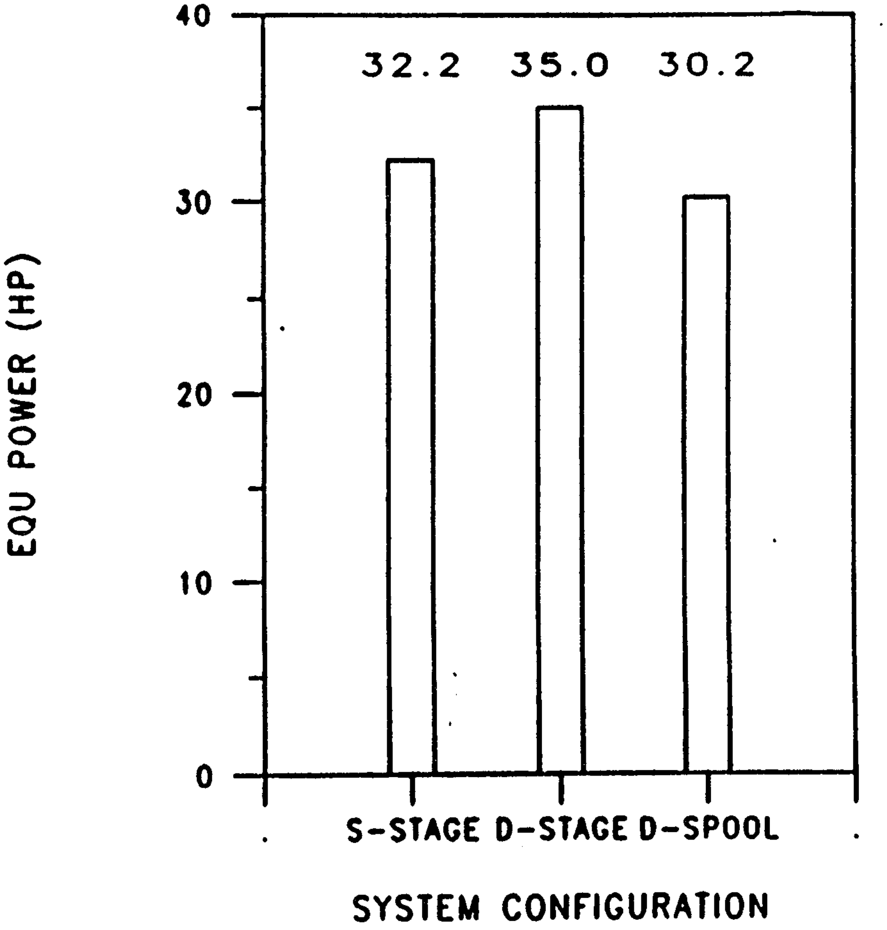

FIGURE 14. SYSTEM COMPARISON

TABLE 3. DUAL SPOOL, 40 HP POWER TURBINE (25 KFT)

SYSTEM STATE POINTS

STATION	FLOW LB/MIN	PRESSURE PSIA	TEMP DEG F	MACH	AREA SQ.IN.
AMBIENT		5.46	6.71	0.2670	
INLET	70.55	5.71	12.99	0.2029	0.1721
COMPRESSOR 1 IN		5.70	12.99	0.1748	0.1983
COMPRESSOR 1 OUT		21.08	282.58	0.1750	0.0669
INTERCOOLER IN		20.97	282.58	0.1751	0.0669
INTERCOOLER OUT		20.85	150.00	0.1750	0.0612
COMPRESSOR 2 IN		20.74	150.00	0.1752	0.0612
COMPRESSOR 2 OUT		35.47	278.36	0.1750	0.0396
AFTERCOOLER IN		35.24	278.36	0.1754	0.0396
AFTERCOOLER OUT		35.12	140.00	0.1750	0.0360
ENGINE IN		34.89	140.00	0.1755	0.0360
ENGINE OUT		25.00	1154.00	0.1750	0.0877
TURBINE 4 IN		24.92	1148.11	0.1747	0.0877
TURBINE 4 OUT		20.10	1074.87	0.1750	0.1062
TURBINE 3 IN		19.98	1068.86	0.1746	0.1062
TURBINE 3 OUT		13.85	951.35	0.1750	0.1474
TURBINE 2 IN		13.78	945.17	0.1745	0.1474
TURBINE 2 OUT		5.58	690.68	0.1750	0.0000
TURBINE 1 OUT		5.58	690.68	0.1750	0.3286
EXIT	72.84	5.57	684.43	0.1743	0.3286
AMBIENT		5.46	6.71	0.0000	

DUCT CONDITIONS AND SIZE

SECTION	MACH IN	LENGTH FT.	DIA IN.	DP PSI	DT DEG R	WEIGHT LBM	VOLUME CU IN
1 TO 2	0.1748	3.000	6.030	0.013	0.101	2.229	1081.5
3 TO 4	0.1750	5.000	3.501	0.110	2.446	2.106	598.6
5 TO 6	0.1750	5.000	3.350	0.110	1.253	2.020	548.8
7 TO 8	0.1750	5.000	2.695	0.228	1.905	1.631	358.4
9 TO 10	0.1750	5.000	2.571	0.228	0.920	1.561	326.7
11 TO 12	0.1750	3.000	4.010	0.074	5.888	4.139	468.9
13 TO 14	0.1750	3.000	4.413	0.055	6.007	4.552	566.3
15 TO 16	0.1750	3.000	5.199	0.033	6.183	5.355	782.7
19 TO 20	0.1750	3.000	7.762	0.010	6.250	7.974	1730.8

HEAT EXCHANGER CONDITIONS AND SIZE

INTERCOOLER

	SINK	CHARGE AIR
INLET TEMPERATURE (F)	15.23	282.58
OUTLET TEMPERATURE (F)	190.40	150.00
PRESSURE DROP SPECIFIED (PSIA)	0.10	0.13
PRESSURE DROP ACTUAL (PSIA)	0.10	0.12
FLOW RATE (LBM/MIN)	53.30	70.55
EFFECTIVENESS / LOAD (BTU/MIN)	0.4959	2239.
WEIGHT (LBM) / VOLUME (IN3)	19.93	770.2

TABLE 3. DUAL SPOOL (continued)

AFTERCOOLER

	SINK	CHARGE AIR
INLET TEMPERATURE (F)	15.23	278.36
OUTLET TEMPERATURE (F)	193.36	140.00
PRESSURE DROP SPECIFIED (PSIA)	0.10	0.13
PRESSURE DROP ACTUAL (PSIA)	0.10	0.13
FLOW RATE (LBM/MIN)	54.70	70.55
EFFECTIVENESS / LOAD (BTU/MIN)	0.5258	2336.
WEIGHT (LBM) / VOLUME (IN3)	22.46	900.4

COMPRESSOR/TURBINE CONDITIONS AND SIZE

COMPRESSION STAGES = 2

STAGE	1	2	3	4
SHAFT POWER, BTU/MIN	0.00	4556.22	2154.31	1696.67
COMPRESSOR CP, BTU/LBM F	0.0000	0.2410	0.2394	0.0000
COMP DELTA H, BTU/MIN	0.00	64.58	30.54	0.00

EXPANSION STAGES = 3

STAGE	1	2	3	4
TURBINE CP, BTU/LBM F	0.0000	0.2602	0.2663	0.2692
TURB DELTA H, BTU/MIN	0.00	65.84	31.13	24.52
AVG PRESS DH, BTU/MIN	0.00	65.84	31.13	19.62

POWER TURBINE SHAFT 4

	TURBINE
PRESSURE RATIO	1.24
SPEED (RPM)	23295.
SPECIFIC SPEED	0.6000
DIAMETER (IN)	7.879
WEIGHT (LBM)	34.89
VOLUME (IN3)	2569.

TURBOCHARGER SHAFT 2 WITH SINGLE STAGE COMPRESSOR

	TURBINE	COMPRESSOR
PRESSURE RATIO	2.47	3.70
SPEED (RPM)	30918.	
SPECIFIC SPEED	0.6000	0.5099
DIAMETER (IN)	9.728	11.430
WEIGHT (LBM)	53.18	52.26
VOLUME (IN3)	5969.	11380.

TURBOCHARGER SHAFT 3 WITH SINGLE STAGE COMPRESSOR

	TURBINE	COMPRESSOR
PRESSURE RATIO	1.44	1.71
SPEED (RPM)	29041.	
SPECIFIC SPEED	0.6947	0.5000
DIAMETER (IN)	7.342	8.368
WEIGHT (LBM)	30.29	28.01
VOLUME (IN3)	1937.	3268.

TABLE 3. DUAL SPOOL (continued)

```
WASTE GATE SIZING

WASTE GATE 3         CORRECTED FLOW         0.9860
                     WEIGHT (LBM)             6.06

WASTE GATE 2         CORRECTED FLOW         1.3717
                     WEIGHT (LBM)             9.95

GEAR BOX SIZING
PROP POWER              40.00
WEIGHT (LBM)            9.880

SYSTEM SUMMARY

TURBOMACHINERY SYSTEM NET DELIVERED POWER
  PEOUT   ENG DELTA  POWER TRB   NET
   25.00      9.62     40.00     49.62

SYSTEM WEIGHT, DRAG AND NET DRAG
  WEIGHT     DRAG    NET DRAG    VAMB
  298.47     5.05     31.70    280.38

NET EQUIVALENT POWER = 30.16
```

TABLE 4. DUAL STAGE, 40 HP POWER TURBINE (25 KFT)

SYSTEM STATE POINTS

STATION	FLOW LB/MIN	PRESSURE PSIA	TEMP DEG F	MACH	AREA SQ.IN.
AMBIENT		5.46	6.71	0.2670	
INLET	70.55	5.71	12.99	0.2029	0.1721
COMPRESSOR 1 IN		5.70	12.99	0.1748	0.1983
COMPRESSOR 1 OUT		21.08	282.58	0.1750	0.0669
INTERCOOLER IN		20.97	282.58	0.1751	0.0669
INTERCOOLER OUT		20.85	150.00	0.1750	0.0612
COMPRESSOR 2 IN		20.74	150.00	0.1752	0.0612
COMPRESSOR 2 OUT		35.47	278.36	0.1750	0.0396
AFTERCOOLER IN		35.24	278.36	0.1754	0.0396
AFTERCOOLER OUT		35.12	140.00	0.1750	0.0360
ENGINE IN		34.89	140.00	0.1755	0.0360
ENGINE OUT		25.14	1154.00	0.1750	0.0872
TURBINE 4 IN		25.07	1148.13	0.1747	0.0872
TURBINE 4 OUT		20.22	1074.89	0.1750	0.0000
TURBINE 3 OUT		20.22	1074.89	0.1750	0.1056
TURBINE 2 IN		20.10	1068.89	0.1746	0.1056
TURBINE 2 OUT		5.58	697.11	0.1750	0.0000
TURBINE 1 OUT		5.58	697.11	0.1750	0.3295
EXIT	72.84	5.57	690.80	0.1743	0.3295
AMBIENT		5.46	6.71	0.0000	

DUCT CONDITIONS AND SIZE

SECTION	MACH IN	LENGTH FT.	DIA IN.	DP PSI	DT DEG R	WEIGHT LBM	VOLUME CU IN
1 TO 2	0.1748	3.000	6.030	0.013	0.101	2.229	1081.5
3 TO 4	0.1750	5.000	3.501	0.110	2.446	2.106	598.6
5 TO 6	0.1750	5.000	3.350	0.110	1.253	2.020	548.8
7 TO 8	0.1750	5.000	2.695	0.228	1.905	1.631	358.4
9 TO 10	0.1750	5.000	2.571	0.228	0.920	1.561	326.7
11 TO 12	0.1750	3.000	3.998	0.075	5.873	4.127	466.1
15 TO 16	0.1750	3.000	4.400	0.055	5.992	4.538	563.1
19 TO 20	0.1750	3.000	7.772	0.010	6.309	7.985	1735.5

HEAT EXCHANGER CONDITIONS AND SIZE

INTERCOOLER

	SINK	CHARGE AIR
INLET TEMPERATURE (F)	15.23	282.58
OUTLET TEMPERATURE (F)	190.40	150.00
PRESSURE DROP SPECIFIED (PSIA)	0.10	0.13
PRESSURE DROP ACTUAL (PSIA)	0.10	0.12
FLOW RATE (LBM/MIN)	53.30	70.55
EFFECTIVENESS / LOAD (BTU/MIN)	0.4959	2239.
WEIGHT (LBM) / VOLUME (IN3)	19.93	770.2

TABLE 4. DUAL STAGE (continued)

AFTERCOOLER

	SINK	CHARGE AIR
INLET TEMPERATURE (F)	15.23	278.36
OUTLET TEMPERATURE (F)	193.36	140.00
PRESSURE DROP SPECIFIED (PSIA)	0.10	0.13
PRESSURE DROP ACTUAL (PSIA)	0.10	0.13
FLOW RATE (LBM/MIN)	54.70	70.55
EFFECTIVENESS / LOAD (BTU/MIN)	0.5258	2336.
WEIGHT (LBM) / VOLUME (IN3)	22.46	900.4

COMPRESSOR/TURBINE CONDITIONS AND SIZE

COMPRESSION STAGES = 2

STAGE	1	2	3	4
SHAFT POWER, BTU/MIN	0.00	6710.53	0.00	1696.67
COMPRESSOR CP, BTU/LBM F	0.0000	0.2410	0.2394	0.0000
COMPR DELTA H, BTU/MIN	0.00	64.58	30.54	0.00

EXPANSION STAGES = 2

STAGE	1	2	3	4
TURBINE CP, BTU/LBM F	0.0000	0.2623	0.0000	0.2692
TURB DELTA H, BTU/MIN	0.00	96.98	0.00	24.52
AVG PRESS DH, BTU/MIN	0.00	96.98	0.00	19.62

POWER TURBINE SHAFT 4

	TURBINE
PRESSURE RATIO	1.24
SPEED (RPM)	23363.
SPECIFIC SPEED	0.6000
DIAMETER (IN)	7.856
WEIGHT (LBM)	34.68
VOLUME (IN3)	2539.

TURBOCHARGER SHAFT 2 WITH DUAL STAGE COMPRESSOR

	TURBINE	COMP 1	COMP 2
PRESSURE RATIO	3.60	3.70	1.71
SPEED (RPM)	41226.		
SPECIFIC SPEED	0.6000	0.6798	0.7098
DIAMETER (IN)	8.854	8.572	5.895
WEIGHT (LBM)	44.05		43.29
VOLUME (IN3)	4097.	3600.	805.

WASTE GATE SIZING

WASTE GATE 2	CORRECTED FLOW	0.9802
	WEIGHT (LBM)	6.01

GEAR BOX SIZING

PROP POWER	40.00
WEIGHT (LBM)	9.880

TABLE 4. DUAL STAGE (continued)

```
SYSTEM SUMMARY

TURBOMACHINERY SYSTEM NET DELIVERED POWER
  PEOUT    ENG DELTA  POWER TRB    NET
   25.14       9.37     40.00     49.37

SYSTEM WEIGHT, DRAG AND NET DRAG
  WEIGHT      DRAG    NET DRAG    VAMB
  206.50       5.05     23.48    280.38

NET EQUIVALENT POWER = 34.95
```

TABLE 5. SINGLE STAGE, 40 HP POWER TURBINE (25 KFT)

SYSTEM STATE POINTS

STATION	FLOW LB/MIN	PRESSURE PSIA	TEMP DEG F	MACH	AREA SQ.IN.
AMBIENT		5.46	6.71	0.2670	
INLET	70.55	5.71	12.99	0.2029	0.1721
COMPRESSOR 1 IN		5.70	12.99	0.1748	0.1983
COMPRESSOR 1 OUT		35.47	427.71	0.1750	0.0436
INTERCOOLER IN		35.24	427.71	0.1753	0.0436
INTERCOOLER OUT		35.12	140.00	0.1750	0.0360
ENGINE IN		34.89	140.00	0.1755	0.0360
ENGINE OUT		27.04	1154.00	0.1750	0.0811
TURBINE 4 IN		26.96	1148.31	0.1747	0.0811
TURBINE 4 OUT		21.74	1075.07	0.1750	0.0000
TURBINE 3 OUT		21.74	1075.07	0.1750	0.0982
TURBINE 2 IN		21.61	1069.27	0.1746	0.0982
TURBINE 2 OUT		5.58	679.47	0.1750	0.0000
TURBINE 1 OUT		5.58	679.47	0.1750	0.3268
EXIT	72.84	5.57	673.32	0.1743	0.3268
AMBIENT		5.46	6.71	0.0000	

DUCT CONDITIONS AND SIZE

SECTION	MACH IN	LENGTH FT.	DIA IN.	DP PSI	DT DEG R	WEIGHT LBM	VOLUME CU IN
1 TO 2	0.1748	3.000	6.030	0.013	0.101	2.229	1081.5
3 TO 4	0.1750	5.000	2.828	0.223	3.001	1.708	393.8
5 TO 6	0.1750	5.000	2.571	0.228	0.920	1.561	326.7
11 TO 12	0.1750	3.000	3.855	0.083	5.686	3.981	433.9
15 TO 16	0.1750	3.000	4.243	0.061	5.807	4.378	524.1
19 TO 20	0.1750	3.000	7.740	0.010	6.146	7.952	1721.4

HEAT EXCHANGER CONDITIONS AND SIZE

HIGH TEMP AFTERCOOLER

	SINK	CHARGE AIR
INLET TEMPERATURE (F)	15.23	427.71
OUTLET TEMPERATURE (F)	221.72	349.99
PRESSURE DROP SPECIFIED (PSIA)	0.10	0.03
PRESSURE DROP ACTUAL (PSIA)	0.10	0.03
FLOW RATE (LBM/MIN)	26.74	70.55
EFFECTIVENESS / LOAD (BTU/MIN)	0.1884	1322.
WEIGHT (LBM) / VOLUME (IN3)	20.82	416.1

TABLE 5. SINGLE STAGE (continued)

LOW TEMP AFTERCOOLER

	SINK	CHARGE AIR
INLET TEMPERATURE (F)	15.23	349.99
OUTLET TEMPERATURE (F)	221.72	140.00
PRESSURE DROP SPECIFIED (PSIA)	0.10	0.09
PRESSURE DROP ACTUAL (PSIA)	0.10	0.09
FLOW RATE (LBM/MIN)	72.26	70.55
EFFECTIVENESS / LOAD (BTU/MIN)	0.6273	3572.
WEIGHT (LBM) / VOLUME (IN3)	30.55	1233.4

COMPRESSOR/TURBINE CONDITIONS AND SIZE

COMPRESSION STAGES = 1

STAGE	1	2	3	4
SHAFT POWER, BTU/MIN	0.00	7027.64	0.00	1696.67
COMPRESSOR CP, BTU/LBM F	0.0000	0.2417	0.0000	0.0000
COMPR DELTA H, BTU/MIN	0.00	99.61	0.00	0.00

EXPANSION STAGES = 2

STAGE	1	2	3	4
TURBINE CP, BTU/LBM F	0.0000	0.2620	0.0000	0.2692
TURB DELTA H, BTU/MIN	0.00	101.56	0.00	24.52
AVG PRESS DH, BTU/MIN	0.00	101.56	0.00	19.62

POWER TURBINE SHAFT 4

	TURBINE
PRESSURE RATIO	1.24
SPEED (RPM)	24227.
SPECIFIC SPEED	0.6000
DIAMETER (IN)	7.576
WEIGHT (LBM)	32.25
VOLUME (IN3)	2196.

TURBOCHARGER SHAFT 2 WITH SINGLE STAGE COMPRESSOR

	TURBINE	COMPRESSOR
PRESSURE RATIO	3.87	6.22
SPEED (RPM)	43010.	
SPECIFIC SPEED	0.6000	0.5198
DIAMETER (IN)	8.685	10.205
WEIGHT (LBM)	42.39	41.65
VOLUME (IN3)	3792.	7230.

WASTE GATE SIZING

WASTE GATE 2	CORRECTED FLOW	0.9115
	WEIGHT (LBM)	5.39

GEAR BOX SIZING

PROP POWER	40.00
WEIGHT (LBM)	9.88

TABLE 5. SINGLE STAGE (continued)

```
SYSTEM SUMMARY

TURBOMACHINERY SYSTEM NET DELIVERED POWER
  PEOUT    ENG DELTA  POWER TRB    NET
   27.04      6.11      40.00     46.11

SYSTEM WEIGHT, DRAG AND NET DRAG
  WEIGHT      DRAG     NET DRAG    VAMB
  204.74      4.37      22.65    280.38

NET EQUIVALENT POWER = 32.20
```

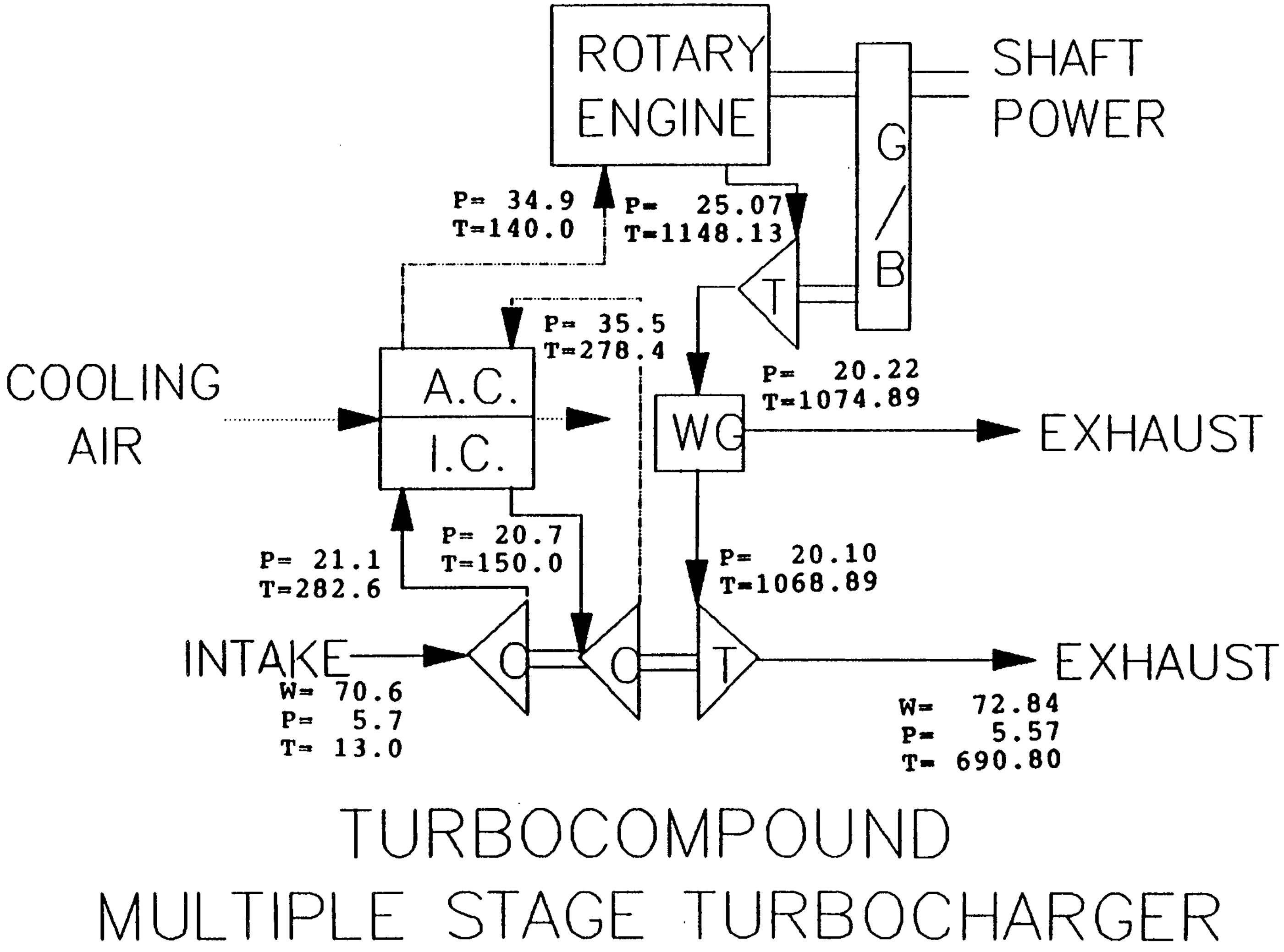
ROTARY ENGINE
SHAFT POWER
G/B
P= 34.9
T=140.0
P= 25.07
T=1148.13
T
P= 35.5
T=278.4
COOLING AIR
A.C.
I.C.
P= 20.22
T=1074.89
WG
EXHAUST
P= 21.1
T=282.6
P= 20.7
T=150.0
P= 20.10
T=1068.89
INTAKE
C
C
T
EXHAUST
W= 70.6
P= 5.7
T= 13.0
W= 72.84
P= 5.57
T= 690.80
TURBOCOMPOUND
MULTIPLE STAGE TURBOCHARGER

FIGURE 15. SYSTEM STATE POINTS

Table 6

Dual spool	- largest region of shaft speed where speed match is possible. Allows each turbine and compressor to be run at near optimal speed for best efficiency - lowest engine back pressure - good performance range for off-design operation - most complex, highest weight
Dual stage	- smaller region of shaft speed where speed match is possible. More difficult to get all turbomachinery elements to optimal speed for best efficiency - good performance range for off-design operation - low engine back pressure - simple and low weight
Single stage	- simple and low weight - high engine back pressure - narrower performance range for off-design operation - very narrow region of shaft speed where speed match is possible. May not be possible to get both wheels to optimal speed for best efficiency - high compressor and turbine tip speeds (high stress)

4.2 Recommendations

The dual stage turbocharging configuration with an upstream turbocompounding (power) turbine is preferred for its high equivalent power, good off-design operating performance range, and reasonable simplicity. The recovery of pulse power leads to substantial increases in power turbine output, so the system should be designed to fully utilize this power. The power turbine can provide at least 60 to 80 hp, while keeping the engine back pressure between 30.6 psia and 34.9 psia.

Additional analytical efforts are needed to better quantify exhaust pulse effects, which apparently will significantly affect turbomachinery sizing and power output. Additionally, an off-design system analysis should be performed to learn how the proposed system configuration(s) perform at lower altitudes and lower throttle settings. These conditions will determine control schedules and may have an impact on proper turbomachinery matching.

5.0 REFERENCES

1. Kays, William M. and London, A. L., Compact Heat Exchangers, Third Edition, (McGraw-Hill Book Company, 1984).

REPORT DOCUMENTATION PAGE	*Form Approved* *OMB No. 0704-0188*

Public reporting burden for this collection of information is estimated to average 1 hour per response, including the time for reviewing instructions, searching existing data sources, gathering and maintaining the data needed, and completing and reviewing the collection of information. Send comments regarding this burden estimate or any other aspect of this collection of information, including suggestions for reducing this burden, to Washington Headquarters Services, Directorate for Information Operations and Reports, 1215 Jefferson Davis Highway, Suite 1204, Arlington, VA 22202-4302, and to the Office of Management and Budget, Paperwork Reduction Project (0704-0188), Washington, DC 20503.

1. AGENCY USE ONLY (*Leave blank*)	**2. REPORT DATE** August 1992	**3. REPORT TYPE AND DATES COVERED** Final Contractor Report

4. TITLE AND SUBTITLE Stratified Charge Rotary Engine Critical Technology Enablement Volume II - Appendixes	**5. FUNDING NUMBERS** WU–505–62–1 C–NAS3–25945
6. AUTHOR(S) C.E. Irion and R.E. Mount	
7. PERFORMING ORGANIZATION NAME(S) AND ADDRESS(ES) Rotary Power International, Inc. P.O. Box 128 Wood-Ridge, New Jersey 07075	**8. PERFORMING ORGANIZATION REPORT NUMBER** E–8831
9. SPONSORING/MONITORING AGENCY NAME(S) AND ADDRESS(ES) National Aeronautics and Space Administration Lewis Research Center Cleveland, Ohio 44135–3191	**10. SPONSORING/MONITORING AGENCY REPORT NUMBER** NASA CR–189106

11. SUPPLEMENTARY NOTES

Project Manager, Paul T. Kerwin, Propulsion Systems Division, NASA Lewis Research Center, organization code 2703, (216) 433–3409.

12a. DISTRIBUTION/AVAILABILITY STATEMENT Unclassified - Unlimited Subject Category 07	**12b. DISTRIBUTION CODE**

13. ABSTRACT ***(Maximum 200 words)***

This report summarizes results of a critical technology enablement effort with the stratified charge rotary engine (SCRE) focusing on a power section of 0.67 liters (40 cu. in.) per rotor in single and two rotor versions. The work is a continuation of prior NASA Contracts NAS3–23056 and NAS3–24628. Technical objectives are multi-fuel capability, including civil and military jet fuel and DF-2, fuel efficiency of 0.355 Lbs/BHP-Hr. at best cruise condition above 50% power, altitude capability of up to 10Km (33,000 ft.) cruise, 2000 hour TBO and reduced coolant heat rejection. Critical technologies for SCREs that have the potential for competitive performance and cost in a representative light-aircraft environment were examined. Objectives were: the development and utilization of advanced analytical tools, i.e. higher speed and enhanced three dimensional combustion modeling; identification of critical technologies; development of improved instrumentation, and to isolate and quantitatively identify the contribution to performance and efficiency of critical components or subsystems.

14. SUBJECT TERMS Stratified charge; Rotary; Engine; Aircraft; Fuel injection; CFD computer codes; Flow visualization; Multi-fuel	**15. NUMBER OF PAGES** 200 **16. PRICE CODE** A09

17. SECURITY CLASSIFICATION OF REPORT Unclassified	**18. SECURITY CLASSIFICATION OF THIS PAGE** Unclassified	**19. SECURITY CLASSIFICATION OF ABSTRACT** Unclassified	**20. LIMITATION OF ABSTRACT**

NSN 7540-01-280-5500

Standard Form 298 (Rev. 2-89)
Prescribed by ANSI Std. Z39-18
298-102